ENVIRONMENTAL DEGRADATION OF GLASS FIBRE REINFORCED POLYMER COMPOSITES

A
Thesis Report

Submitted in partial fulfilment of the requirement for the award of degree

MASTER OF ENGINEERING
IN
CAD/CAM/ROBOTICS

Submitted By
Amit Sharma
Roll No. 80781003

Under Guidance of

Dr. Abhijit Mukherjee
Director
Thapar University, Patiala

Dr. Rahul Chhibber
Lecturer
Deptt. of Mechanical Engg.
Thapar University, Patiala

DEPARTMENT OF MECHANICAL ENGINEERING
THAPAR UNIVERSITY
PATIALA-147004, INDIA

INDEX

INDEX

CERTIFICATE

This is to certify that the work in this Thesis report entitled "**Environmental Degradation of Glass Fibre-Reinforced Polymer Composites**" submitted in partial fulfilment of requirement for the award of **Master Degree in CAD/CAM/Robotics** in the Mechanical Engineering Department at Thapar University, Patiala, is an authentic record of work carried out by me under the guidance of **Dr. Abhijit Mukherjee, Director, Thapar University, Patiala and Dr. Rahul Chhibber, Lecturer, Mechanical Engineering Department, Thapar University, Patiala.**

The matter embodied in this report has not been submitted in part or full to any other university or institute for the award of any degree.

Amit S harma

(Amit Sharma)

Dated: 15/7/09

This is to certify that above declaration made by the student concerned is correct to the best of my knowledge & belief.

Dr. Abhijit Mukherjee
Director
Thapar University, Patiala

Rahul Chhibber

Dr. Rahul Chhibber
Lecturer
Deptt. of Mechanical Engg.
Thapar University, Patiala

Dr. S.K. Mohapatra
Professor & HOD
Deptt. of Mechanical Engg.
Thapar University, Patiala

RK Sharma 22/7/09

Dr. R.K. Sharma
Dean
Deptt. of Academic Affairs
Thapar University, Patiala

ACKNOWLEDGEMENT

I am highly grateful to the authorities of Thapar University, Patiala for providing this opportunity to carry out the thesis work.

I would like to express a deep sense of gratitude and thank profusely to my thesis guide Dr. Abhijit Mukherjee & Dr. Rahul Chhibber for their sincere & invaluable guidance and suggestions which inspired me to submit thesis report in the present form.

I am highly thankful to Dr. Maneek Kumar, H.O.D, Civil Engg. Department for his invaluable guidance & permission to carry out work in his department.

I heartly thanks to Dr. Navneet Arora and Mr. Abhishek Shyte for their help in conducting the tests at I.I.T. Roorkee.

I am also thankful to other faculty members of Mechanical and Civil Engineering Department, Thapar University, Patiala for their intellectual support. My special thanks are due to my family members and friends who constantly encouraged me to complete this work.

Amit Sharma

ABSTRACT

Carbon fibre-reinforced polymer (CFRP) and Glass fibre-reinforced polymer (GFRP) have been used as an alternative to steel in concrete due to high strength-to-weight ratio, high stiffness-to-weight ratio, and corrosion and fatigue resistance.

GFRP's have been found attractive in the Asian region due to their cost competitiveness in comparison to CFRP. Wide-spread use of fibre-reinforced polymers (FRP) in construction is hampered in this part of world due to lack of long-term durability and performance data, especially in a tropical environment.

The main environmental factors for the deterioration of GFRP are temperature, sunshine, water/moisture, alkalinity and load. Most of the early durability tests were carried out with reference to application of FRP (Fibre Reinforced Polymer) in aerospace.

Thus considerable data is available with only one or a combination of some of these parameters. Hence effort is required to fully comprehend the GFRP response under natural and accelerated moisture and temperature conditions.

For the achieving the objective an experimental setup was prepared. The aim of the experiment was to study the combined effect of chosen parameters moisture, alkali and temperature & also to study the rate & magnitude of damage of GFRP composites. This will help in studying the response of the composite to the given hygrothermal load. The changes occurring in the physical composition of the composite material were also studied.

LIST OF FIGURES

LIST OF TABLES

CHAPTER 1 INTRODUCTION

1.1 WHAT IS COMPOSITE?

In a broad sense the word "**composite**" means made of two or more different parts. A composite material consists of assemblage of two materials of different nature competing and allowing us to obtain a material of which the set of performance characteristics is greater than that of the components taken separately.

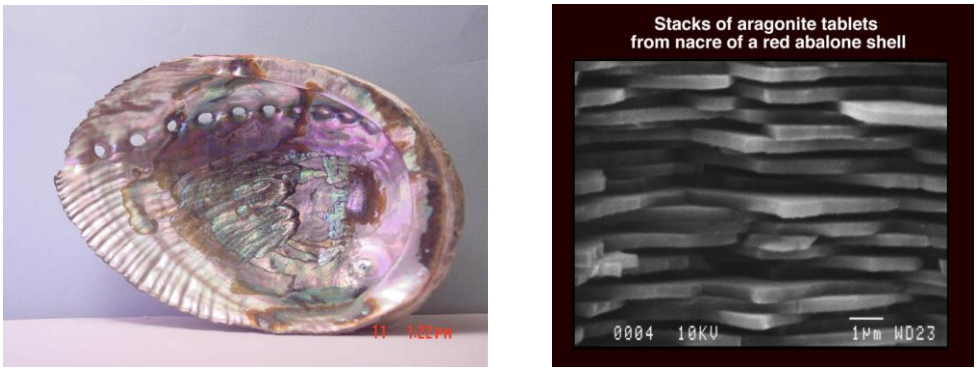

Fig. 1.1 Natural Composite-Abalone shell ($CaCO_3$) with SEM (Scanning Electron Microscope) details in right figure [1]

There are many natural composites such as wood, shells (Fig.1.1), pearlite (steel which is a mixture of a phase and Fe_3C). From a materials engineering standpoint, "composite" is typically used to refer to two (or more) phase systems that are purposely engineered to maximize the benefits of both layers.

1.2 HISTORY OF COMPOSITES

Fig. 1.2 Piece of Plywood [2]

Plywood (Fig.1.2) is a common composite material that many people encounter in their everyday lives. The most primitive composite materials were straw and mud combined to form bricks for building construction; the Biblical book of Exodus speaks of the Israelites being oppressed by Pharaoh, by being forced to make bricks without straw being provided. The ancient brick-making process can still be seen on Egyptian tomb paintings in the Metropolitan Museum of Art.

The most advanced examples perform routinely on spacecraft in demanding environments. The most visible applications pave our roadways in the form of either steel and aggregate reinforced portland cement or asphalt concrete. Those composites closest to our personal hygiene form our shower stalls and bath tubs made of fibreglass. Solid surface, imitation granite and cultured marble sinks and counter tops which are widely used to enhance our living experiences are all composites.

1.3 INTRODUCTION TO THE COMPOSITE MATERIALS

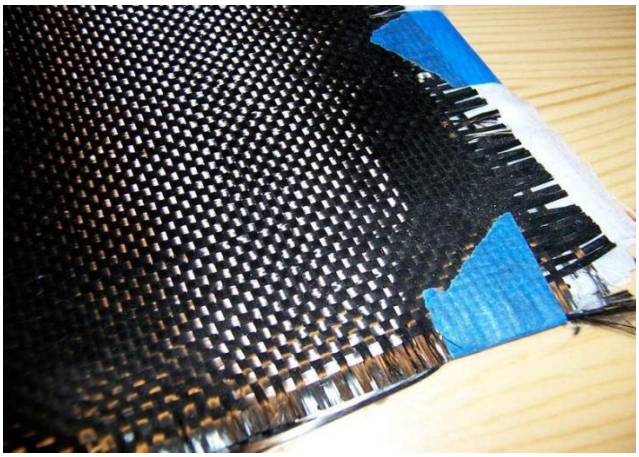

Fig. 1.3 Commercially available Carbon Fibre Sheet used as dispersed phase [2]

Composite material is a material composed of two or more distinct phases (matrix phase and dispersed phase) and having bulk properties significantly different from those of any of the constituents.

- **Matrix phase**

The primary phase, having a continuous character, is called matrix. Matrix is usually more ductile and less hard phase. It holds the dispersed phase and shares a load with it.

- **Dispersed (reinforcing) phase**

The second phase is imbedded in the matrix in a discontinuous form. This secondary phase is called dispersed phase (Fig.1.3). Dispersed phase is usually stronger than the matrix, therefore it is sometimes called reinforcing phase.

Many of common materials (metal alloys, doped Ceramics and Polymers mixed with additives) also have a small amount of dispersed phases in their structures, however they are not considered as composite materials since their properties are similar to those of their base constituents (physical properties of steel are similar to those of pure iron).

The following are some of the reasons why composites are selected for certain applications:

- High strength to weight ratio (low density high tensile strength)
- High creep resistance
- High tensile strength at elevated temperatures
- High toughness

Typically, reinforcing materials are strong with low densities while the matrix is usually a ductile, or tough, material. If the composite is designed and fabricated correctly, it combines the strength of the reinforcement with the toughness of the matrix to achieve a combination of desirable properties not available in any single conventional material. The downside is that such composites are often more

expensive than conventional materials. Examples of some current application of composites include the diesel piston, brake-shoes and pads, tires and the Beechcraft aircraft in which 100% of the structural components are composites.

The strength of the composite depends primarily on the amount, arrangement and type of fibre (or particle) reinforcement in the resin. Typically the higher the reinforcement content, the greater the strength. In some cases, glass fibres are combined with other fibres, such as carbon or aramid (Kevlar29 and Kevlar49) to create a "hybrid" composite that combines the properties of more than one reinforcing material. In addition, the composite is often formulated with fillers and additives that change processing or performance parameters. The complete anatomy of composite (Fig.1.4) is shown below.

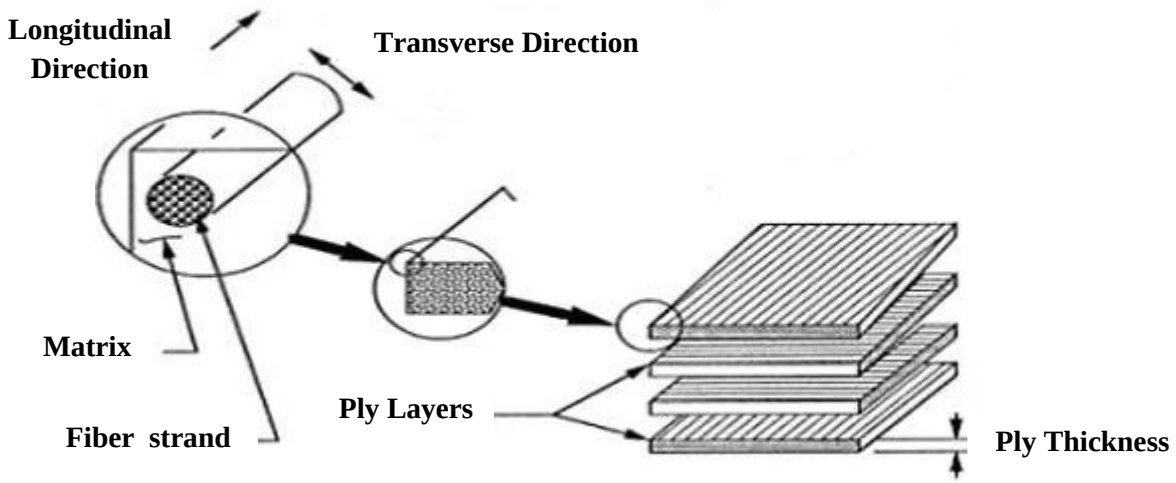

Fig. 1.4 Anatomy of Composite Material (Fibre Reinforced) [3]

1.4 CLASSIFICATION SYSTEMS OF COMPOSITES

There are two classification systems of composite materials. One of them is based on the matrix material (metal, ceramic and polymer) and the second is based on the material structure.

Classification of composites I:

1. Metal Matrix Composites (MMC)

Metal Matrix Composites are composed of a metallic matrix (aluminium, magnesium, iron, cobalt, copper) and a dispersed ceramic (oxides, carbides) or metallic (lead, tungsten, molybdenum) phase.

2. Ceramic Matrix Composites (CMC)

Ceramic Matrix Composites are composed of a ceramic matrix and embedded fibres of other ceramic material (dispersed phase).

3. Polymer Matrix Composites (PMC)

Polymer Matrix Composites are composed of a matrix from thermoset (Unsaturated Polyester (UP), Epoxy (EP)) or thermoplastic (Polycarbonate (PC), Polyvinylchloride, Nylon, Polystyrene) and embedded glass, carbon, steel or Kevlar fibres (dispersed phase).

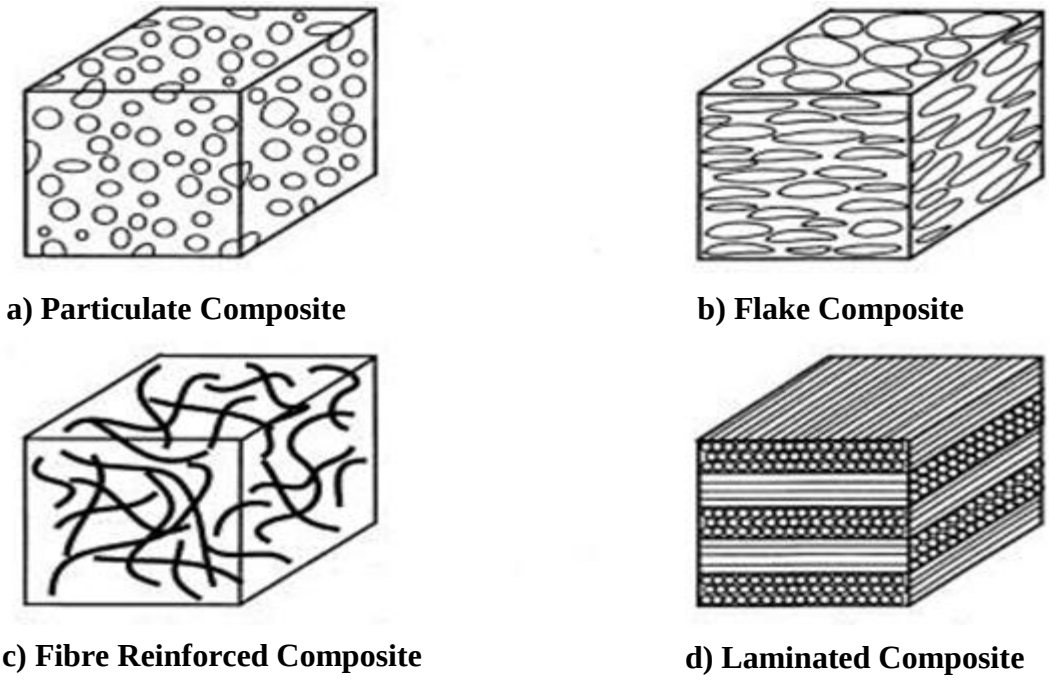

a) Particulate Composite **b) Flake Composite**

c) Fibre Reinforced Composite **d) Laminated Composite**

Fig. 1.5 Figures a, b, c & d shows type of dispersed phase of particles in composites [4]

Classification of composite materials II (Fig.1.5):

1) Particulate Composites

It consists of a matrix reinforced by a dispersed phase in form of particles.

1. Composites with random orientation of *particles*.
2. Composites with preferred orientation of particles. Dispersed phase of these materials consists of two-dimensional *flat platelets (flakes)*, laid parallel to each other.

2) Fibrous Composites

1. Short fibre reinforced composites. Short fibre reinforced composites consist of a matrix reinforced by a dispersed phase in form of discontinuous fibres (length < 100 *diameter).

- Composites with random orientation of fibres.
- Composites with preferred orientation of fibres.

2. Long-fibre reinforced composites. Long-fibre reinforced composites consist of a matrix reinforced by a dispersed phase in form of continuous fibres.

- Unidirectional orientation of fibres.
- Bidirectional orientation of fibres (woven).

3) Laminate Composites

When a fibre reinforced composite consists of several layers with different fibre orientations, it is called multilayer (angle-ply) composite.

1.5 WHY COMPOSITES?

The demands on material performance are so great and diverse that no one material is able to satisfy them, e.g. lightweight yet strong & stiff structure. Composite material systems results in a performance unattainable by the individual constituents. Composite material offer advantage of a flexible design that can be tailored to the design requirements.

We can see in Fig. 1.6 below the comparison of metals like steel & aluminium with composites. The reason for choosing the aluminium and steel is that they are widely used in industry. One can figure out that in comparison by weight composites are much lighter than other two metals. Similarly in comparison of thermal expansion the composites are low which is good for places where high temperature working is required. In case of stiffness & strength the composites are ahead of the aluminium & steel.

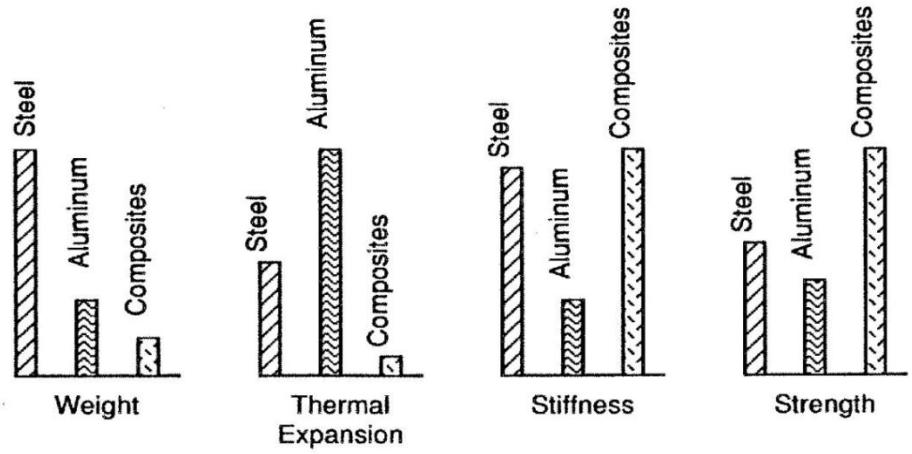

Fig. 1.6 Comparison of performance of composites with other metals [3]

The other advantages of using of composites are:

1. Dimensional stability (e.g. Space based telescope)
2. Low dielectric
3. Corrosion resistance
4. Aero elastic Tailoring
5. Weight Saving

1.6 METHODS OF MOULDING OF COMPOSITES:

In general, the reinforcing and matrix materials are combined, compacted and processed to undergo a melding event. After the melding event, the part shape is essentially set, although it can deform under certain process conditions. For **a thermoset polymeric matrix** material, the melding event is a curing reaction that is initiated by the application of additional heat or chemical reactivity such as organic peroxide. For a thermoplastic polymeric matrix material, the melding event is solidification from the melted state. For a metal matrix material such as titanium foil, the melding event is a fusing at high pressure and a temperature near the melt point.

For many moulding methods, it is convenient to refer to one mould piece as a "lower" mould and another mould piece as an "upper" mould. Lower and upper refer to the different faces of the moulded panel, not the mould's configuration in space. In this convention, there is always a lower mould, and sometimes an upper mould. Part construction begins by applying materials to the lower mould. Lower mould and upper mould are more generalized descriptors than more common and specific terms such as male side, female side, a-side, b-side, tool side, bowl, hat, mandrel, etc. Continuous manufacturing processes use a different nomenclature.

The moulded product is often referred to as a panel. For certain geometries and material combinations, it can be referred to as a casting. For certain continuous processes, it can be referred to as a profile. Applied with a pressure roller, a spray device or manually. This process is generally done at ambient temperature and atmospheric pressure. Two variations of open moulding are Hand Layup and Spray-up.

Vacuum bag moulding

A process using a two-sided mould set that shapes both surfaces of the panel. On the lower side is a rigid mould and on the upper side is a flexible membrane or vacuum bag. The flexible membrane can be a reusable silicone material or an extruded polymer film. Then, vacuum is applied to the mould cavity. This process can be performed at either ambient or elevated temperature with ambient atmospheric pressure acting upon the vacuum bag. Most economical way is using a venturi vacuum and air compressor or a vacuum pump.

Pressure bag moulding

This process is related to vacuum bag moulding in exactly the same way as it sounds. A solid female mould is used along with a flexible male mould. The reinforcement is place inside the female mould with just enough resin to allow the fabric to stick in place. A measured amount of resin is then liberally brushed indiscriminately into the mould and the mould is then clamped to a machine that contains the male flexible mould. The flexible male membrane is then inflated with heated compressed air or possibly steam. The female mould can also be heated. Excess resin is forced out along with trapped air. This process is extensively used in the production of composite helmets due to the lower cost of unskilled labour. Cycle times for a helmet bag moulding machine vary from 20 to 45 minutes, but the finished shells require no further curing if the moulds are heated.

Autoclave moulding

A process using a two-sided mould set that forms both surfaces of the panel. On the lower side is a rigid mould and on the upper side is a flexible membrane made from silicone or an extruded polymer film such as nylon. Reinforcement materials can be placed manually or robotically. They include continuous fibre forms fashioned into textile constructions. Most often, they are pre-impregnated with the resin in the form of prepreg fabrics or unidirectional tapes. In some instances, a resin film is placed upon the lower mould and dry reinforcement is placed above. The upper mould is installed and vacuum is applied to the mould cavity. The assembly is placed into an autoclave pressure vessel. This process is generally performed at both elevated pressure and elevated temperature. The use of elevated pressure facilitates a high fibre volume fraction and low void content for maximum structural efficiency.

Resin transfer moulding (RTM)

A process using a two-sided mould set that forms both surfaces of the panel. The lower side is a rigid mould. The upper side can be a rigid or flexible mould. Flexible moulds can be made from composite materials, silicone or extruded polymer films such as nylon. The two sides fit together to produce a mould cavity. The distinguishing feature of resin transfer moulding is that the reinforcement materials are placed into this cavity and the mould set is closed prior to the introduction of matrix material. Resin transfer moulding includes numerous varieties which differ in the mechanics of how the resin is introduced to the reinforcement in the mould cavity. These variations include everything from vacuum infusion (see also resin infusion) to vacuum assisted resin transfer moulding. This process can be performed at either ambient or elevated temperature.

Other

Other types of moulding include press moulding, transfer moulding, pultrusion moulding, filament winding, casting, centrifugal casting and continuous casting.

TYPICAL PRODUCTS:

Composite materials have gained popularity (despite their generally high cost) in high-performance products that need to be lightweight, yet strong enough to take harsh loading.

1. *Aerospace components* (tails, wings, fuselages, propellers), boat and scull hulls, bicycle frames and racing car bodies.
2. Carbon composite is a key material in today's *launch vehicles and spacecraft*. It is widely used in solar panel substrates, antenna reflectors and yokes of spacecraft. It is also used in payload adapters, inter-stage structures and heat shields of launch vehicles.
3. The shell composed of CosmoLite, a thermoplastic fibre-reinforced composite and the exterior surface SpectraLite which incorporates DuPont Surlyn, an impact-resistant coating found on *golf balls*.

1.7 INTRODUCTION TO FRP

A **fibre-reinforced polymer** (**FRP**) (also *fibre-reinforced plastic*) is a composite material comprising a polymer matrix reinforced with fibres. The fibres are usually fibreglass, carbon, or aramid, while the polymer is usually an epoxy, vinyl ester or polyester thermosetting plastic. FRP's are commonly used in the aerospace, automotive, marine, and construction industries. Fig. 1.7 shows the application of FRP to a concrete bridge.

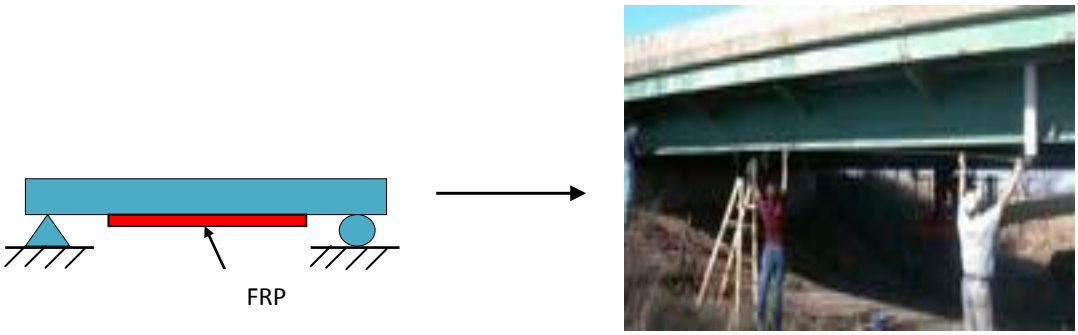

Fig. 1.7 Application of FRP to a Bridge [5]

The strength properties of FRP collectively make up one of the primary reasons for which civil engineers select them in the design of structures. A material's strength is governed by its ability to sustain a load without excessive deformation or failure. When an FRP specimen is tested in axial tension, the applied force per unit cross-sectional area (stress) is proportional to the ratio of change in a specimen's length to its original length (strain). When the applied load is removed, FRP returns to its original shape or length. In other words, FRP responds linear-elastically to axial stress. The response of FRP to axial compression is reliant on the relative proportion in volume of fibres, the properties of the fibre and resin, and the interface bond strength.

FRP composite compression failure occurs when the fibres exhibit extreme (often sudden and dramatic) lateral or sides-way deflection called fibre buckling. FRP's response to transverse tensile stress is very much dependent on the properties of the fibre and matrix, the interaction between the fibre and matrix, and the strength of the fibre-matrix interface. Generally, however, tensile strength in this direction is very poor. Shear stress is induced in the plane of an area when external loads tend to cause two segments of a body to slide over one another. The shear strength of FRP is difficult to quantify. Generally, failure will occur within the matrix material parallel to the fibres.

According to orientation of fibre (Fig.1.8) they can be categorized as:

1. Unidirectional
2. Bidirectional
   - Cross Ply
   - Angle Ply

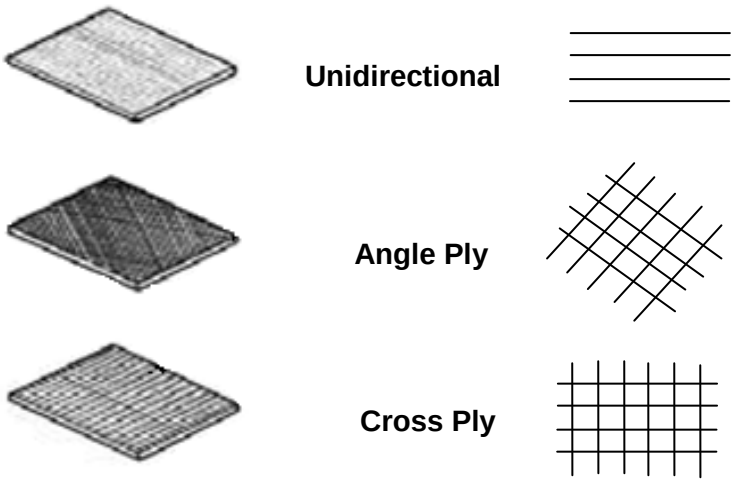

Fig. 1.8 Ways of Fibre orientation in FRP [5]

ADVANTAGES OF FRP:

1. High strength to weight ratio
2. Corrosion resistant
3. Can be tailored for the application (both shape and type of FRP)
4. FRP has a low cost considering other materials
5. Cost of installation versus replacement is low
6. Cost of installation time (both direct and indirect) is also low.

1.8 PROPERTIES OF REINFORCED FIBRES:

The mechanical properties of most reinforcing fibres are considerably higher than those of un-reinforced resin systems. The mechanical properties of the fibre/resin composite are therefore dominated by the contribution of the fibre to the composite. The four main factors that govern the fibre's contribution are:

1. The basic mechanical properties of the fibre itself.

2. The surface interaction of fibre and resin (the interface).

3. The amount of fibre in the composite (Fibre Volume Fraction).

4. The orientation of the fibres in the composite.

1.9 FIBRE TYPES:


(a)

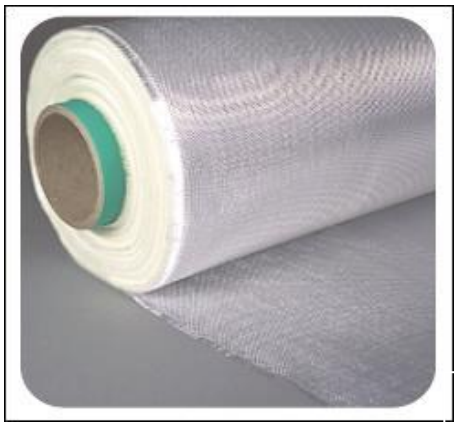
(b)

Fig. 1.9 (a) Roll of Glass Fibre, (b) Woven Fabric of Glass Fibre [6]

a) Glass Fibre (Fig. 1.9)

By blending quarry products (sand, kaolin, limestone etc.) at 1,600^{o}C, liquid glass is formed. The liquid is passed through micro-fine bushings and simultaneously cooled to produce glass fibre filaments from 5-24µm in diameter. The filaments are drawn together into a strand (closely associated) or roving (loosely associated), and coated with a "size" to provide filament cohesion and protect the glass from abrasion. By variation of the recipe, different types of glass can be produced.

The types of glasses used for structural reinforcements are as follows:

1) **E-glass** (electrical) - lower alkali content and stronger than A glass (alkali). Good tensile and compressive strength and stiffness, good electrical properties and relatively low cost, but impact resistance relatively poor. E-glass is the most common form of reinforcing fibre used in polymer matrix composites.

2) **C-glass** (chemical) - best resistance to chemical attack. Mainly used in the form of surface tissue in the outer layer of laminates used in chemical and water pipes and tanks.

3) **R, S or T-glass** – manufacturers' trade names for equivalent fibres having higher tensile strength and modulus than E glass, with better wet strength retention. Higher I.L.S.S (inter laminate shear strength) and wet out properties are achieved through smaller filament diameter. S-glass is produced in the USA by OCF, R-glass in Europe by Vetrotex and T-glass by Nittobo in Japan. Developed for aerospace and defence industries, and used in some hard ballistic armour applications. This factor and low production volumes mean relatively high price.

Glass fibre is available in the following forms (Fig.1.10):

1. Continuous Fibre
2. Chopped strands
3. Woven Fabric.

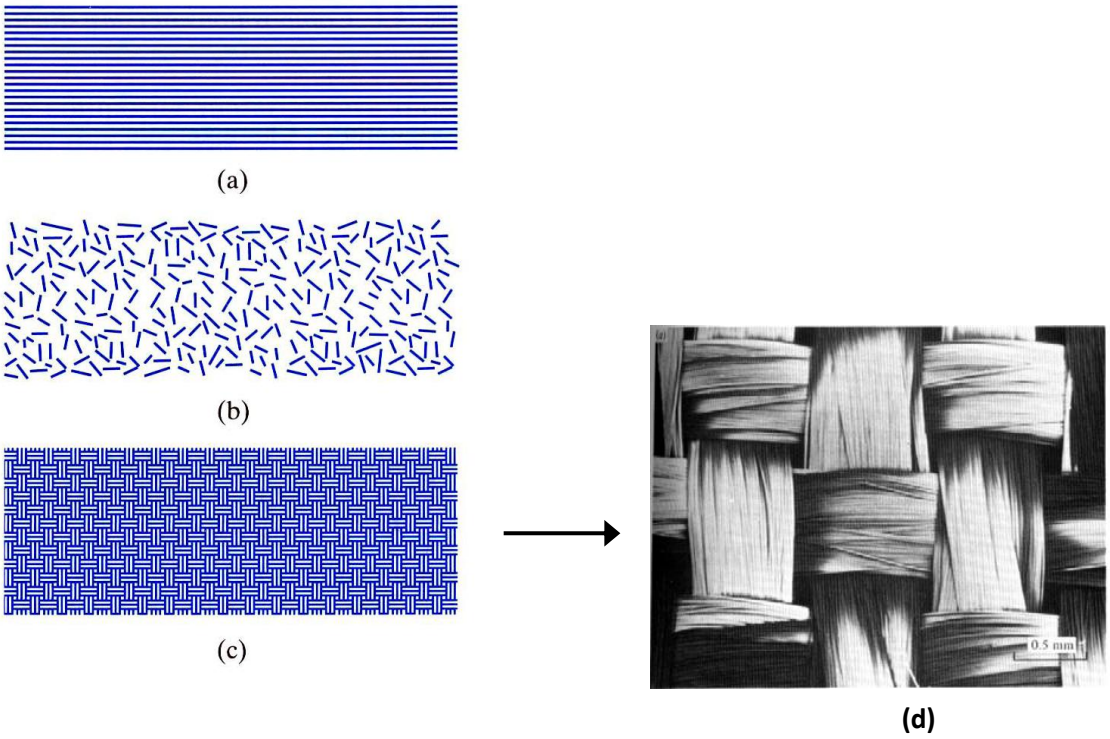

Fig. 1.10 (a) Continuous Fibres (b) Chopped Fibres (c) Woven Fabric (d) Enlarged detail of Woven Fibre [7]

Glass Fibre Designation:

Glass fibres are designated as per table T1 as internationally recognised terminology:

Table T1: Designation of Glass Fibre [6]

Glass Type (example)	Yarn Type	Filament Diameter (μ)	Strand Weight (tex)	Single Strand Twist	No. Of Strands	Multi Strand Twit	No. of turns per metre
E	C	9	34	Z	X2	S	150
E = Electrical C = Continuous				Z = Clockwise S = Anticlockwise			

b) Aramid (Kevlar) Fibre

Fig. 1.11 Roll of Aramid Fibre [6]

Aramid fibre (Fig.1.11) is a man-made organic polymer (an aromatic polyamide) produced by spinning a solid fibre from a liquid chemical blend. The bright golden yellow filaments produced can have a range of properties, but all have high strength and low density giving very high specific strength. All grades have good resistance to impact, and lower modulus grades are used extensively in ballistic applications. Compressive strength, however, is only similar to that of E glass.

Although most commonly known under its Dupont trade name 'Kevlar', there are now a number of suppliers of the fibre, most notably Akzo Nobel with 'Twaron'. Each supplier offers several grades of aramid with various combinations of modulus and surface finish to suit various applications. As well as the high strength properties, the fibres also offer good resistance to abrasion, and chemical and thermal degradation. However, the fibre can degrade slowly when exposed to ultraviolet light. Aramid fibres are usually available in the form of rovings, with texes ranging from about 20 to 800.

c) Carbon Fibre

Fig. 1.12 Roll of Carbon Fibre [6]

Carbon fibre (Fig.1.12) is produced by the controlled oxidation, carbonisation and graphitisation of carbon-rich organic precursors which are already in fibre form. The most common precursor is polyacrylonitrile (PAN), because it gives the best carbon fibre properties, but fibres can also be made

from pitch or cellulose. Once formed, the carbon fibre has a surface treatment applied to improve matrix bonding and chemical sizing which serves to protect it during handling.

Carbon fibres are usually grouped according to the Young's modulus in which their properties fall. These bands are commonly referred to as: high strength (HS), intermediate modulus (IM), high modulus (HM) and ultra high modulus (UHM). The filament diameter of most types is about 5-7um. Carbon fibre has the highest specific stiffness of any commercially available fibre, very high strength in both tension and compression and a high resistance to corrosion creep and fatigue. Their impact strength, however, is lower than either glass or aramid, with particularly brittle characteristics being exhibited by HM and UHM fibres.

FIBRE TYPE COMPARISONS:

Comparing the properties of all of the fibre types (Table T2) with each other, shows that they all have distinct advantages and disadvantages. This makes different fibre types more suitable for some applications than others.

The following table provides a basic comparison between the main desirable features of generic fibre types.

'A' indicates a feature where the fibre scores well

'C' indicates a feature where the fibre is not so good.

Table T2: Comparison of Fibre Types [6]

Property	Aramid	Carbon	Glass
High Tensile Strength	B	A	B
High Tensile Modulus	B	A	C
High Compressive Strength	C	A	B
High Compressive Modulus	B	A	C
High Flexural Strength	C	A	B
High Flexural Modulus	B	A	C
High Impact Strength	A	C	B
High Interlaminar Shear Strength	B	A	A
High in-plane Shear Strength	B	A	A
Low density	A	B	C
High Fatigue Resistance	B	A	C
High Fire Resistance	A	C	A
High Thermal Insulation	A	C	B
High Electrical Insulation	B	C	A
Low Thermal Expansion	A	A	A
Low Cost	C	C	A

1.10 TYPES OF FIBRE REINFORCED POLYMERS:

- Carbon Fibre Reinforced Polymer (CFRP)
- Glass Fibre Reinforced Polymer (GFRP)
- Boron Fibre Reinforced Polymer (BFRP)
- Aramid Fibre Reinforced Polymer (AFRP) etc.

Glass Fibre Reinforced Polymer (GFRP):

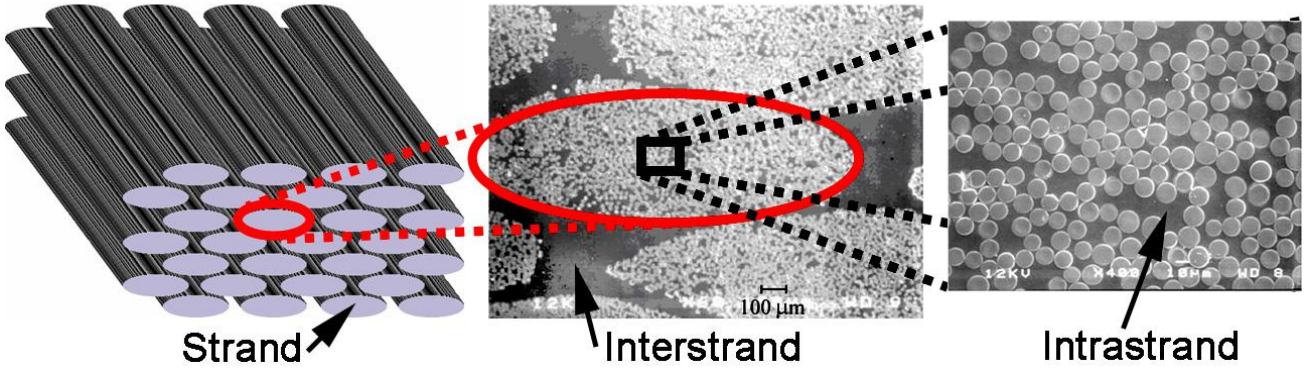

Fig. 1.13 Micrograph showing internal details of Glass Fibre Reinforced Polymer sheets [8]

Glass fibre reinforced polymers sheets (Fig.1.13 & Fig.1.14) are being increasingly used in rehabilitation and retrofitting of concrete structures as an alternative to steel in concrete due to their high strength-to-weight ratio and corrosion and fatigue resistance. Ease of handling and application at site are its added advantage.

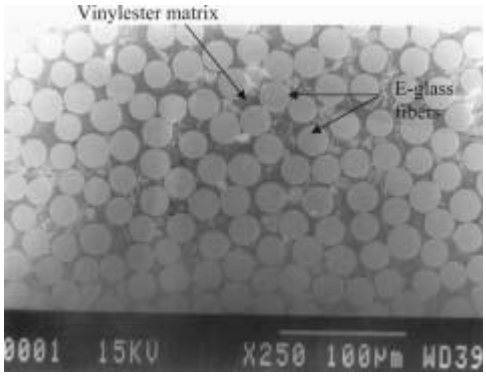

Fig. 1.14 Micrograph showing distribution of glass fibres in a GFRP reinforcing bar [9]

Of the different types of glass fibres, E-Glass is mostly used for reinforcement due to its high strength and electrical resistivity. Glass fibres have high strength and temperature resistance, but it is the low cost that makes GFRP the most popular FRP reinforcement in civil engineering applications. GFRP's have been found attractive in Asian region due to their cost competitiveness over carbon fibre composites.

The FRP sheets are being used for repair, strengthening and retrofitting of structural components. Degradation of steel reinforcements due to corrosion, cracking of concrete due to weathering, rapidly changing traffic needs (both in terms of intensity and load levels) and recent earthquake damages have necessitated the use of strengthening of basic structural components such as slabs, panels, walls, beams and columns. Tests carried on concrete beams reinforced externally with FRP plates indicate substantial increase in the strength of the beams and decks. Wrapping of columns with FRP have been studied for enhanced performance and are found suitable for seismic column retrofitting. Wide spread utilization of FRP's in construction is hampered by lack of long-term durability and performance data in tropical environment. The main environmental factors for the deterioration of GFRP are temperature, sunshine, water/moisture, alkalinity resulting from hydration of cement in concrete and stress due to service loads. Most of the early durability tests carried out on GFRP was for applications in auto and aerospace industries. The durability data with reference to one or combinations of some of these parameters is presently available. Beams bonded externally with GFRP sheet and subjected to wet and dry exposure under sea water resulted in 33% reduction in strength.

Accelerated testing for long-term durability of GFRP laminates for marine use was done and it was found that the methodology is applicable to the plain woven cloth GFRP laminates for conventional marine use. It was characterized from the experimental results that the flexural fatigue strength of GFRP laminates decreases strongly with increasing time and temperature as well as the number of load cycles to failure. The capacity of beams exposed to 100 wet/dry cycles dropped by 36%. This drop in capacity is directly related to a drop in tensile capacity of the fabric. GFRP's are susceptible to alkali attack and a loss up to 100% has been reported. From the review of literature it is observed that there is no standardisation of test procedures for durability of concrete-GFRP hybrid systems. The performance of such a system must be evaluated under actual environmental conditions. The Table T3 show the comparison of different fibre reinforced composite material.

Table T3: Comparison of different fibre reinforced Composite materials [10]

Property	Composite Material		
	GFRP	**BFRP**	**CFRP**
Major Young's Modulus, E_L (msi)	6.8	30.0	30.0
Minor Young's Modulus, E_T (msi)	2.6	3.0	0.75
Major Poisson's Ratio, V_{LT}	0.25	0.30	0.25
Shear Modulus, G_{LT} (msi)	1.3	1.0	0.375
Specific Weight, γ (Pci)	0.072	0.068	0.055
The unit msi denotes millions of psi			
It is assumed that minor Poisson's ratio is given by $V_{TL} = (E_T / E_L) * V_{LT}$			

COMMERCIALLY AVAILABLE GLASS FIBRE SPECIFICATIONS:

The table T4 shows the technical data detail of the glass fibre sheet.

Table T4: Detail of Commercially Available Fibre Glass Sheet (EU 900 & EU 750) [11]

MBrace G Sheet EU 900 & EU 750 – Unidirectional Glass fibre sheet		
Technical data of fibre	E-Glass, 900 gsm	E-Glass, 750 gsm
Modulus of elasticity	73 kN/mm²	73 kN/mm²
Tensile strength	3400 N/mm²	3400 N/mm²
Total weight of sheet	900 g/m² in main directions	750 g/m² in main directions
Density	2.6 g/cm³	2.6 g/cm³
ε Ultimate %	4.5	4.5
Thickness for static design weight / density	0.342 mm	0.285 mm
Safety factor for static design (manual lamination / woven product)	1.5 (recommended)	1.5 (recommended)

COMMERCIALLY AVAILABLE MATRIX RESIN SPECIFICATIONS:

MBrace Saturant resin (Table T5) is the easy-to-apply, 100% solids material that permits adhesion of a lightweight sheet, within the MBrace Composite Strengthening System. When cured with the tow sheet, MBrace Saturant resin produces a high performance composite system for use in external structural repair or upgrade applications.

Table T5: Details of commercially available MBrace Matrix Resin [11]

Aspect	Translucent blue liquid
Mixed density	1.13 ± 0.03 kg/litre
Volume solids	100 %
Mixing ratio, by weight	100 (Base): 40 (Hardener)
Mixed viscosity	3500 ± 500 cps at 25°C
Coverage	
200 ~ 350 gsm fibre sheet	0.8 to 1.0 kg/m^2
350 ~ 450 gsm fibre sheet	0.9 to 1.2 kg/m^2
750 ~ 900 gsm fibre sheet	1.5 to 1.8 kg/m^2
Setting time	5 Hours at 25°C
Over coating time	On setting
Full cure	7 Days
Compressive strength (ASTM C579)	> 40 MPa at 1 Day
	> 60 MPa at 7 Days
Tensile strength (BS:6319, pt 7)	> 23 MPa
Flexural strength(BS:6319, pt 3)	> 43 MPa

1.11 ENVIRONMENTAL EFFECTS ON FIBRE COMPOSITES:

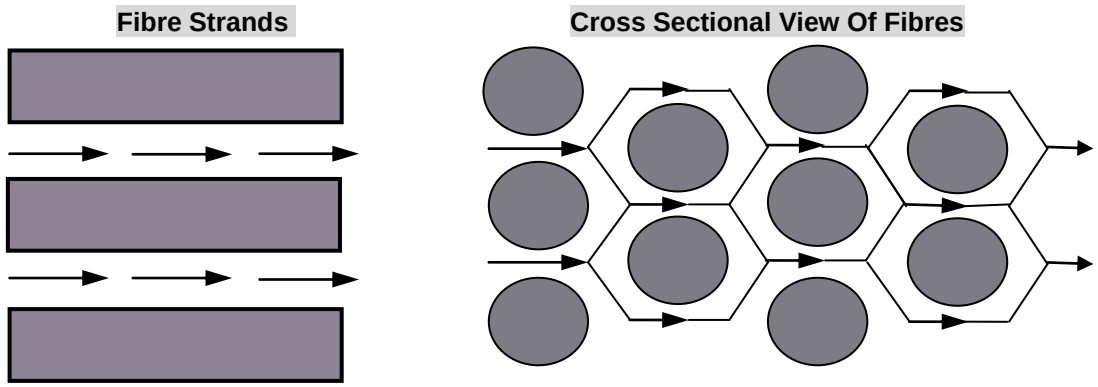

Fig. 1.15 Diffusion path of moisture into composite thickness direction [24]

Fibrous composites, especially carbon fibre reinforced epoxy are increasingly being used in military and aerospace applications owing to several desirable properties including high specific strength, high specific stiffness and controlled anisotropy. Despite these advantages over conventional structural materials such as metals, composites are susceptible to heat and moisture when operating in harsh and changing environmental conditions. When exposed to humid environments, carbon–epoxy composites absorb moisture (Fig. 1.15) and undergo dilatational expansion.

The presence of moisture and the stresses associated with moisture induced expansion can result in lowered damage tolerance, with an adverse effect on long-term structural durability. The amount of moisture absorbed by the epoxy matrix is significantly greater than that by the carbon fibres, which absorb very little or no moisture. This result in a significant mismatch in the moisture induced volumetric expansion between the matrix and the fibres, and thus leads to the evolution of localized stress and strain fields in the composite.

Additionally, moisture absorption leads to changes in the thermo physical, mechanical and chemical characteristics of the epoxy matrix by plasticization and hydrolysis. These changes in the polymer structure lower both the elastic modulus and the glass transition temperature. At the same time, moisture wicking along the fibre matrix interface degrades the fibre matrix bond, resulting in loss of micro structural integrity. The net effect of moisture absorption is the deterioration of matrix-dominated properties such as compressive strength, interlaminar shear strength, fatigue resistance and impact tolerance .These factors lead to reduced damage tolerance and lack of long-term durability.

In homogeneous materials, the kinetics of moisture diffusion is governed by the maximum moisture content and the diffusivity. The maximum moisture content is defined by the net amount of moisture that a fully saturated material contains under steady state equilibrium when exposed to a given environmental condition. It is usually expressed as the ratio of the increase in weight per unit dry weight at the point of saturation. The relative weight gain approaches the maximum moisture content of composite at infinite time. It has been shown that the maximum moisture content strongly depends on the relative humidity of the exposure environment. Usually the maximum moisture content is determined by exposing the material to a humid environment for a long duration of time until steady state equilibrium is attained. This process often takes several months, which makes the procedure cumbersome and time consuming.

Also the rate of moisture diffusion is governed by the diffusivity. In general, the diffusivity is a strong function of the ambient temperature and a weak function of the relative humidity. In the case of composites, the diffusion process is more complex. It depends on the diffusivities of the individual constituents, their relative volume fractions, constituent arrangement and morphology. Traditionally, effective diffusivity has been used to predict the amount of moisture content. The figure 1.16 shows the various effects of moisture diffusion on a composite sample.

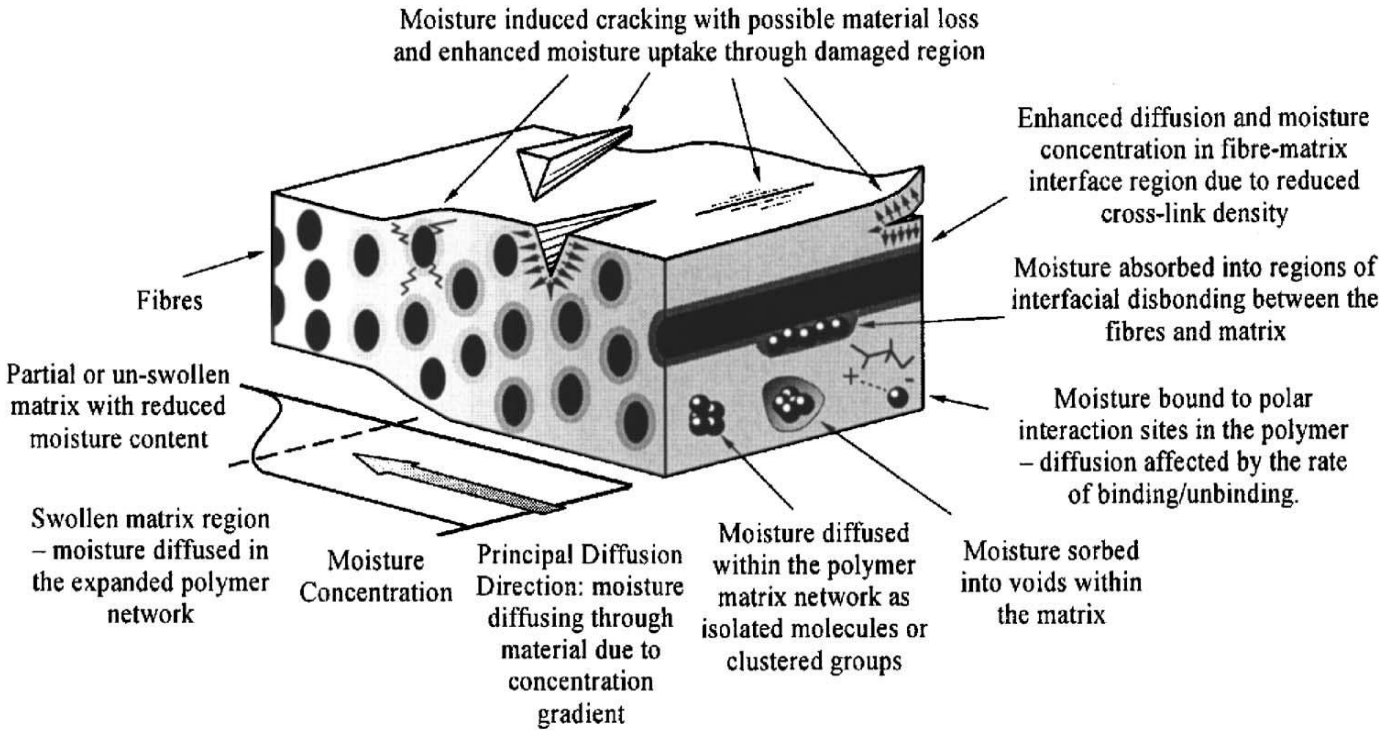

Fig. 1.16 A piece of Composite different effects of moisture diffusion [12]

When a fibre-reinforced composite material is exposed to a hygrothermal environment and mechanical loads, changes in material properties are expected. These changes in material properties are connected to an irreversible material degradation. The moisture may affect the laminates through chemical changes such as relaxation and oxidation of the matrix material. A cyclic moisture environment exposed to a laminate may cause damage such as *debonding* at fibre/matrix interfaces and continuous cracks.

Other damage modes that can occur in a fibre-composite laminate are transverse matrix cracks, delamination and fibre fracture. The results of chemical changes and mechanical damage in general affect the overall material properties, e.g. elastic modulus, hygrothermal expansion coefficients, diffusion coefficients.

Usually one of the first observed damage modes in a laminated composite is *matrix cracking*. These cracks are in general not critical for final failure, but if they are connected to a surrounding moisture environment more rapid moisture absorption may be expected for the cracked laminate. The accelerated moisture absorption in a cracked material exposed to humid air is a result of the faster diffusion in air compared to the diffusion speed in the composite material. Faster moisture uptake may also develop a faster material degradation. This makes it important to know the moisture absorption behaviour in a cracked laminate.

For an undamaged material, well-accepted moisture transportation models are available. The most common models for the transportation of moisture in undamaged polymeric composite materials are Fickian diffusion and Langmuir diffusion. If the material contains cracks that significantly affect the moisture uptake, then the original laws of Fickian and Langmuir are no longer valid for the whole laminate, but locally they still work. The influences of matrix cracks on moisture uptake in glass-fibre/epoxy laminates have been studied. Experiments, finite-element calculations and analytical calculations have been performed and the results are compared. The experimental results show that crack closure may occur early in the absorption process and that the crack closure is significantly influencing the moisture absorption.

CHAPTER 2 LITERATURE REVIEW

[9] A. Mukherjee, S.J. Arwikar-Part2 [2006]

In the first part of the paper the structural scale tests on the synergistic effects of moisture, temperature, alkalinity and stress level on the performance and durability of GFRP sheet bonded externally on concrete have been discussed. This part describes the micro structural studies to find out the nature, quantum and mechanism of deterioration in the conditioned sheets. Micrographic investigations were carried out using a scanning electron microscope (SEM) to visualize the changes in the microstructure. The other tests are energy dispersive X-ray analysis (EDX) and inductively coupled plasma mass spectrometry (ICP-MS) to determine the chemical changes in the composite.

[13] A. Mukherjee, S.J. Arwikar-Part1 [2006]

A set of accelerated aging and natural environment tests has been carried out to evaluate performance of glass fibres reinforced polymer (GFRP) sheets bonded on concrete in tropical environment. Plain concrete beams were cast and externally reinforced by bonding with E-glass GFRP sheets. The beams were immersed in a 60^{o}C water bath for varying durations. The novelty of the experiment was that the environmental exposure was given while they were subjected to service loads. This load helped in seeping sheet exposed to hot water under stressed condition. Thus field environment very similar to tropical climate was simulated. The loaded specimens were also subjected to natural weathering for 6 and 12 months duration. The sheets were removed from the specimens and the tensile strength and modulus were determined to assess the degradation, if any. In the first part of the paper the structural level studies are discussed. In Part 2 [9] the micro structural investigation is reported.

[14] Abhijit Mukherjee and S. J. Arwikar-Part1 [2007]

A set of accelerated aging and natural environment tests has been carried out to evaluate performance of glass fibre-reinforced polymer (GFRP) reinforcing bar in a tropical environment. Beams were cast with the GFRP reinforcing bars as internal reinforcement. They were immersed in a 60 °C water bath for varying durations. The novelty of the experiment was that the environmental exposure was given to the beams while they were subjected to service loads. These loads kept the cracks open for reinforcing bars to remain exposed to hot water. Thus, a field environment very similar to a tropical climate was created. The loaded specimens were also subjected to natural weathering for 18 and 30 months duration. The reinforcing bars were removed from the specimens and investigated at both structural and micro structural scale to assess the degradation, if any.

[15] Abhijit Mukherjee and S. J. Arwikar-Part 2 [2007]

In the first part of this study, the structural scale tests on the synergistic effects of moisture, temperature, alkalinity, and stress level on the performance and durability of glass fibre-reinforced polymer (GFRP) reinforcing bars in concrete have been discussed. In this part, investigations on micro structural studies, carried out to find out the nature, quantum, and mechanism of deterioration in the conditioned reinforcing bars, are reported. Microstructural investigations were carried out using a scanning electron microscope (SEM) to visualize the changes in the microstructure. The other tests that have been carried out are

energy-dispersive x-ray analysis (EDX) and inductively coupled plasma mass spectrometry (ICPMS) to determine the chemical changes in the composite.

[16] Pavankiran Vaddadi, Toshio Nakamura, Raman P. Singh [2003]

Transient hygrothermal stresses induced in fibre-reinforced composites are studied in detail by adopting a novel heterogeneous characterization approach. This approach incorporates two distinct features: transient moisture absorption analysis of actual composite materials exposed to a humid environment, and highly detailed computational analyses that capture the actual heterogeneous microstructure of the composite. The latter feature is carried out by modelling a uniaxial laminate having more than one thousand individual carbon fibres that are randomly distributed within an epoxy matrix. Results indicate that these computational models are essential in capturing the accurate moisture absorption process of the actual specimen. In the analysis, the evolutions of thermal residual stresses and moisture-induced stresses within the humidity and thermal exposed composites have been analyzed. It was observed that high stress concentration develops in the epoxy phase where high fibre density or fibre clustering exists and its magnitude increases as the moisture content saturates. Large stresses can potentially initiate epoxy damage or delamination of epoxy and fibres. Furthermore, due to opposing effects of thermal and moisture exposure, lower stresses are found in the laminate when both are considered simultaneously.

[17] Pavankiran Vaddadi, Toshio Nakamura , Raman P. Singh [2002]

A new approach has been developed, based on an inverse analysis technique, to determine critical moisture diffusion parameters for a fibre-reinforced composite. This technique incorporates two distinct features: direct experimental observations of the weight gained by a composite material exposed to a humid environment, and highly detailed computational analyses that capture the actual heterogeneous microstructure of the composite. The latter feature was carried out by modelling more than 1000 individual carbon fibres that are randomly distributed within an epoxy matrix. The verification and efficacy of this technique was established by conducting an experiment on a high-grade IM7/997 carbon fibre-reinforced epoxy to determine the maximum moisture content at saturation and the diffusivity of epoxy. With the inverse analysis, the time duration required to estimate these moisture diffusion parameters could be drastically reduced as compared to conventional procedures. Subsequently, the established models were employed to characterize transient moisture absorption process within the composite. Here, it was demonstrated that modelling the heterogeneous microstructure of the composite is critical for obtaining accurate diffusion parameters, and an analytical model with effective properties does not produce correct transient moisture absorption behaviour. Furthermore, the evolution of stress fields due to moisture induced volumetric expansion was quantified. It was observed that high stress concentrations develop in regions of fibre concentration. These regions then act as potential failure initiation sites that can lead to lower damage tolerance.

[18] Samit Roy , K. Vengadassalam , Yong Wang , Soojae Park , Kenneth M. Liechti [2005]

In this paper a coupled model for strain-assisted diffusion is derived from the basic principles of continuum mechanics and thermodynamics, and material properties characterized using diffusion experiments. The proposed methodology constitutes a significant step toward modelling the synergistic bond degradation mechanism at the bonded interface between a Fibre Reinforced Polymer (FRP) and a substrate, and for predicting debond initiation and propagation along the interface in the presence of a

diffusing penetrant at the crack tip and at elevated temperatures. It is now well-known that Fick's law is frequently inadequate for describing moisture diffusion in polymers and polymer composites. Non-Fickian or anomalous diffusion is likely to occur when a polymer is subjected to external stresses and strains, as well as elevated temperatures and humidity. In this paper, a modelling methodology based on the basic principles of continuum mechanics and thermodynamics is developed which allows characterization of the combined effects of temperature, humidity, and strain on diffusion coefficients as well as on moisture saturation level, from moisture weight gain data.

[19] Narayanan Ramanujam , Pavankiran Vaddadi , Toshio Nakamura, Raman P. Singh [2007]

The fatigue growth of a fibre reinforced composite laminate was characterized under thermal cycling using a combined experimental and computational investigation. The inspection of fracture surfaces, after completion of the fatigue tests, reveals an angled or kinked crack front growth with greater propagation distances near the free-surfaces/edges. Due to the non-uniform crack growth across the specimen thickness, three-dimensional finite element analyses are performed to investigate the fatigue growth mechanisms under thermal load. From the analysis, the energy release rate as well as the mixed-mode stress intensity factors is calculated and the variations of these fracture parameters are found to be consistent with the observed crack front configuration. Using the computed results, the experimentally measured crack growth rates are also correlated with the amplitude of energy release rate, and a power law form of the fatigue law is established. The relevant coefficients as well as the threshold energy release rate are also determined. The present analysis is useful for not only understanding the fatigue delamination mechanisms under thermal cycling but also for estimating the threshold temperature variation that is needed to drive crack growth.

[20] E. Ahci , R. Talreja [2006]

This paper describes a thermodynamics based model for viscoelastic composites with damage and illustrates its use in characterization of viscoelastic response of polymer matrix woven fabric composites subjected to loading at high temperatures. The characterization is conducted by an experimental method aided by finite element (FE) modelling. The experimental characterization is based on creep data obtained under constant loads of different magnitudes and at different temperatures, and on recovery data collected after unloading. A carbon fibre/polyamide resin woven composite with glass transition temperature of around 380^{o}C was used in the experimental program. A FE model was developed to determine the non-linear viscoelastic response by implementing incremental constitutive relations into an ABAQUS code. The laminate viscoelastic properties were obtained by finite element micromechanics analysis using the neat resin data as input. Comparing its results with creep-recovery test data at different temperature and stress levels validated the FE model. There are several factors affecting the viscoelastic behaviour of polymer matrix composites such as temperature, moisture and stress level. Accordingly, a large number of tests need to be performed to characterize the viscoelastic response experimentally for each fibre matrix combination. For this purpose an efficient and systematic experimental procedure was used to understand the effects of temperature and stress level on the viscoelastic response, to clarify the damage-viscoelasticity coupling and to determine the viscoelastic properties of the material system.

[21] Zheng-Ming Huang[2000] The overall thermal–mechanical properties of a fibrous composite out of an elastic deformation range can be simply simulated using a recently developed micromechanics model, the Bridging Model. Only the in situ constituent fibre and matrix properties of the composite and the fibre volume fraction are required in the simulation. This general yet easy-to-implement micromechanics model is reviewed and summarized in the present paper. Application of the model to predict various properties of unidirectional laminate and multidirectional laminates, including thermo elastic behaviour, elasto-plastic response, ultimate failure strength, strength at elevated temperature, and fatigue strength and *S–N* curve, is demonstrated. It is suggested that use of the bridging model, appropriately calibrated with experimental data, can therefore inform composite design by identifying suitable constituent materials, their contents, and their geometrical arrangements. Some technical issues regarding applications of the bridging model are also addressed.

[22] Ashcroft et al [2003] In this paper, a method of predicting failure in bonded composite joints subjected to combined mechanical loading and environmental degradation is described. The technique is based on a coupled mechanical-diffusion finite-element analysis combined with an appropriate failure criterion. The method is evaluated by predicting the fatigue thresholds of epoxy-CFRP lap-strap joints preconditioned and tested in dry and wet environments. The coupled stress-diffusion method was shown to be capable of predicting correctly the effect that different environments would have on the fatigue resistance of the joints. Both elastic and elasto-plastic fracture criteria were then used to quantitatively predict the fatigue thresholds. The elasto-plastic fracture criterion was the most suitable when moisture was encountered at elevated temperatures and was capable of predicting fatigue thresholds within the experimental scatter range. It is concluded that the technique described is a powerful and flexible way to predict failure in bonded joints subjected to a wide variety of loads and environmental conditions. The method does, however, rely on material data not commonly available, and reasonable simplifying assumptions should be made to make the method cost effective.

[23] Asp L.E. - HTA/6376C [1998] composites has been investigated for influence of temperature and moisture content on the interlaminar delamination toughness in mode I, mode II and mixed mode conditions. Dry and moisture-saturated specimens were tested over the temperature range -50°C to 100°C. Evaluation methods based on load/displacement and load measurements were employed. In pure mode II the critical strain-energy release rate drops with moisture content and increase in temperature. In mixed mode the critical strain energy release rate also decreases with moisture content, but no general trends in the dependence on temperature is observed. The critical strain-energy release rate in pure mode is unaffected by changes in moisture content and was found to increase slightly at elevated temperatures. During crack propagation, enhanced fibre bridging due to increase in temperature and moisture content promotes R-curve behaviour in the pure mode I tests. The resulting mode mixity of the mixed-mode bending (MMB) tests is found to be severely affected by the evaluation methods. Methods based on load measurements only are considered to give unreliable strain-energy release rates as the measured compliance/displacement relationships were found to be non-linear even prior to crack growth. Further studies are needed to assess the mixed-mode ratio in the MMB test.

[24] V.Alvarez & A.Vazquez [2005] In this work, the cycling diffusion behaviour of glass-fibre/VE matrix composites was studied. It was shown that glass fibres act as inert in the water absorption process of VE matrix and their main effect is the loss of the interfacial adhesion. Composites absorb less water than matrix and, for both, the amount of water increased with the temperature increase and cycle. On the other hand, diffusion coefficients were similar for composites and matrix. Temperature affects the diffusion coefficient values and the obtained values were fitted by an exponential equation. It was possible to observe, from SEM micrographs, that the adhesion at the fibre–matrix interface decreased as temperature increased. The cycle affects the composites exposed at a high temperature more when loss of adhesion was observed at the fibre–matrix interface. The flexural modulus did not change after water exposure, but the loss of strength was related to the poorer interface. The diffusion coefficients are calculated by using the simplest Fick's equation.

[25] Benkhedda et al. [2007] Polymer matrix composites are relevant materials for future supersonic aircraft due to their high specific properties. However, in such aeronautical applications, the material is exposed to severe environmental conditions. The present paper aims at assessing an approximate model to evaluate hygrothermoelastic stress in composite laminated plates during moisture desorption taking into account the change of mechanical characteristics induced by the variation of temperature and moisture. The developed method permits us to calculate such stresses during desorption phase without the computation of the moisture concentration, through laminated plates. It observed through this study that the variation of elasticity modulus due to the temperature causes a stress relaxation. These stresses have to be taken into account for the design of composite structures submitted to a moist environment. Through the presented study, we hope to contribute to the understanding of hygrothermal behaviour of composite laminated plates.

[26] Botelho et al [2006] The environmental factors, such as humidity and temperature, can limit the applications of composites by deteriorating the mechanical properties over a period of time. Environmental factors play an important role during the manufacture step and during composite's life cycle. The degradation of composites due to environmental effects is mainly caused by chemical and/or physical damages in the polymer matrix, loss of adhesion at the fibre/matrix interface, and/or reduction of fibre strength and stiffness. Composite's degradation can be measure by shear tests because shear failure is a matrix dominated property. In this work, the influence of moisture in shear properties of carbon fibre/epoxy composites (laminates [0/0]s and [0/90]s) have been investigated. The interlaminar shear strength (ILSS) was measured by using the short beam shear test, and Iosipescu shear strength and modulus (G12) have been determinated by using the Iosipescu test. Results for laminates [0/0]s and [0/90]s, after hygrothermal conditioning, exhibited a reduction of 21% and 18% on the interlaminar shear strength, respectively, when compared to the unconditioned samples. Shear modulus follows the same trend. A reduction of 14.1 and 16.6% was found for [0/0]s and [0/90]s, respectively, when compared to the unconditioned samples. Micro structural observations of the fracture surfaces by optical and scanning electron microscopes showed typical damage mechanisms for laminates [0/0]s and [0/90]s.

[27] Leon L. Mishnaevsky Jr and Siegfried Schmauder [2001] In this paper advanced finite element techniques in simulation of the materials behaviour under mechanical loading are reviewed. Advantages, limitations and perspectives of different approaches to the simulation of deformation, damage and

fracture of materials taking into account their micro and mesostructure are analyzed. Development of the methods of simulation of different aspects of the materials behaviour (such as the unit cell approach, real structure simulation, cohesive zone model, etc) is described from initial simplest versions of the methods to advanced, highly efficient models. Possibilities of using of the finite element method in the development of new materials are analyzed.

[28] **Leon L. Mishnaevsky Jr. [2004]** Three-dimensional finite element (FE) simulations of the deformation and damage evolution of SiC particle reinforced Al composites are carried out for different microstructures of the composites. A program for the automatic generation and the design of FE meshes for different 3D microstructures of composites is developed. Numerical testing of composites with random, regular, clustered and gradient arrangements of spherical particles is carried out. The fraction of failed particles and the tensile stress–strain curves were determined numerically for each of the microstructures. It was found that the strain hardening coefficient increases with varying the particle arrangement in the following order: gradient<random<clustered<regular microstructure. The variations of the particle sizes causes strong decrease in the strain hardening rate of the composite, and leads to the quicker and earlier damage growth in the composites.

[29] **Leon Mishnaevsky Jr. and Povl Brøndsted [2007]** A 3D FE (finite element) simulations of deformation and damage evolution in fibre reinforced aluminium matrix composites are carried out. The fibre/matrix interface damage is modelled as a finite element weakening in the interphase layers. The fibre cracking is simulated as the damage evolution in the randomly placed damageable layers in the fibres, using the ABAQUS subroutine User Defined Field. The effect of matrix cracks and the interface strength on the fibre failure is investigated numerically. It is demonstrated that the interface properties influence the bearing capacity and damage resistance of fibres in the case of the weak fibre/matrix interface, fibre failure begins at much lower applied strains than in the case of the strong interface.

CHAPTER 3 PROBLEM FORMULATION

Glass fibre-reinforced polymer (GFRP) have been used as an alternative to steel in concrete due to high strength-to-weight ratio, high stiffness-to-weight ratio, and corrosion and fatigue resistance. GFRP have been found attractive in the Asian region due to their cost competitiveness in comparison to CFRP.

Wide-spread use of fibre-reinforced polymers (FRP) in construction is hampered in this part of world due to lack of long-term durability and performance data, especially in a tropical environment. Hence effort is required to fully comprehend the GFRP response under natural and accelerated moisture and temperature conditions.
The presented work was an attempt to study the effect of moisture, alkali & heat on **Glass Fibre Reinforced Polymer (GFRP) woven fabric (E Glass)**. The changes occurring in the physical composition & mechanical properties of the composite material under natural and accelerated conditions had been studied.

For the achieving the objective an experimental setup was prepared. The aim of the experiment was to study the combined effect of parameters moisture, alkalinity and temperature & study *the rate & magnitude of damage* of the chosen composite material which further helped in studying the response of the composite to the given hygrothermal load.

The natural degradation of material takes long time to show appreciable results so we had chosen accelerated degradation condition to have results in short duration of time. The material was pre-stretched in order to form some cracks so as to allow water to seep at a faster rate,

The samples were held in experimentation for pre-decided time periods & then tested for their tensile strength by loading in tension. The presented work was mainly carried out on the first two sets of samples i.e. holding time of 1 & 2 months (refer Table T6).

The modelling work was done using the unit cell approach which helped to model a unit volume of fibre including matrix. Both geometric modelling and analysis were carried out using the ABAQUS software to determine damage done by the hygrothermal load. This further helped in simulating the results which experimentally otherwise were not possible to measure.

The work provided some insight into the performance and durability of composite material under tropical environment and this laboratory scale data might be useful to model the performance and durability of real time components under similar environmental conditions.

3.1 FLOWCHART FOR SUMMARY OF THE WORK DONE

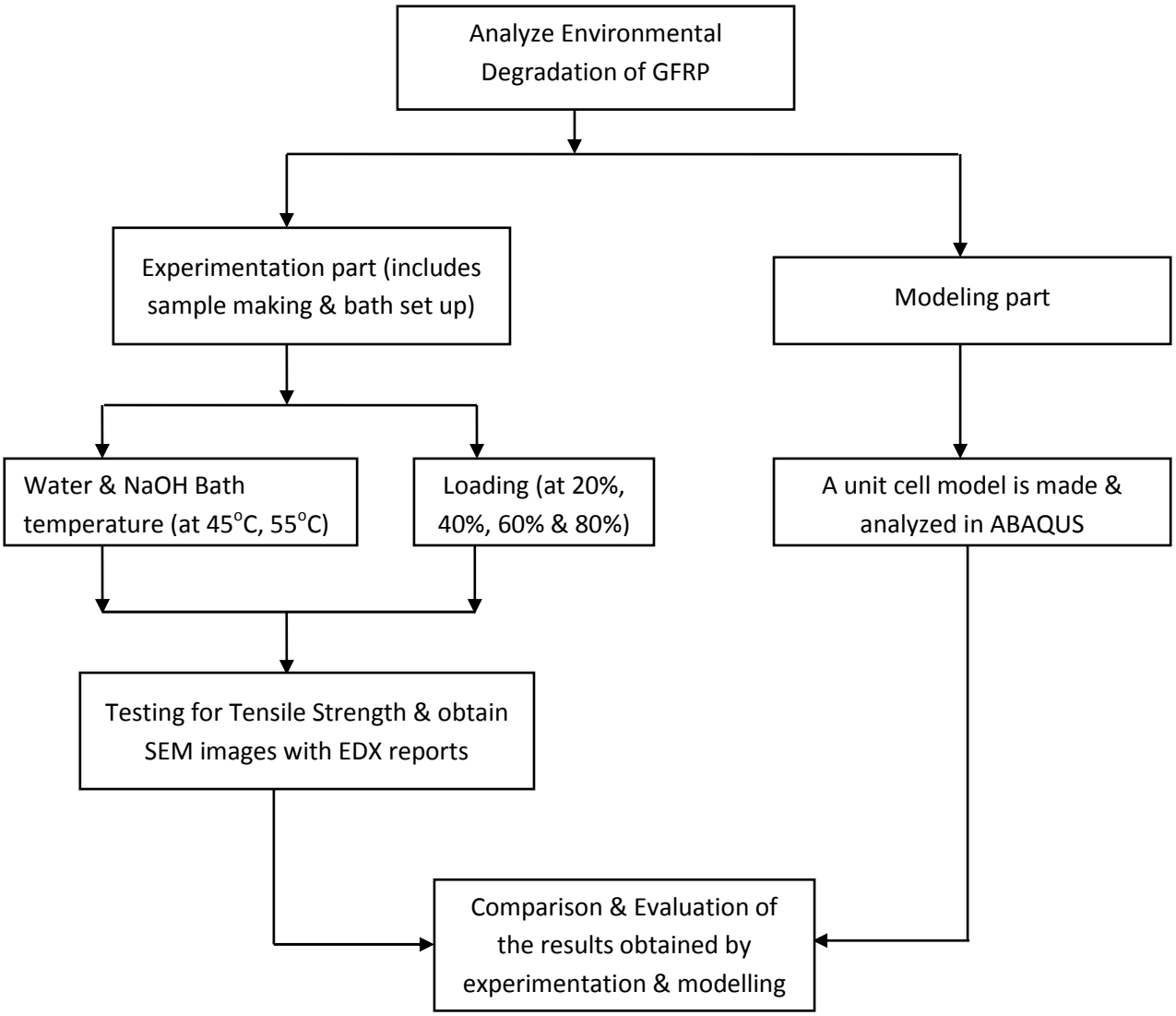

CHAPTER 4 EXPERIMENTATION

4.1 EXPERIMENTAL SETUP:

A set of accelerated aging tests had been carried out to evaluate performance of pre-stretched glass fibres reinforced polymer (GFRP) sheets embedded in epoxy matrix. The field environment very similar to that of tropical climate had been simulated.

The samples were immersed in various baths for different time durations. The novelty of the experiment was that the accelerated environmental exposure had been given to samples while they were pre-stretched to different service loads. The specimens were removed from the bath after decided time period. The tensile strength is measured and a SEM (Scanning Electron Microscope) image was obtained to check the condition of composite material.

Fig. 4.1 Full setup view

4.2 SETUP FABRICATION:

The setup (Fig.4.1) basically consists of following main items:

	ITEM NAME	QTY.
1	Water Tanks	- 04
2	Samples	- 64
3	Heating Elements	- 04
4	RTD Sensors	- 04
5	Temperature Controllers	- 04
6	Solid State Relays	- 04

1) Water Tanks:

The experimental setup consists of four well insulated tanks (Fig. 4.2). The tank was of cylindrical shape made out of plastic. The approximate capacity of the tank was 60 litres. Two tanks were filled totally with tap water and other two were having solution of aqueous NaOH solution with 5% strength by weight. One water bath and one aqueous NaOH bath both were kept at same temperature i.e. 45^{o}C and

similarly other two were kept at 55^{o}C (refer Test Matrix -Table T6). The water which evaporated from the tank was replenished on daily basis during experimentation. Each tank was labelled as per details of experimentation (refer Fig. 4.2).

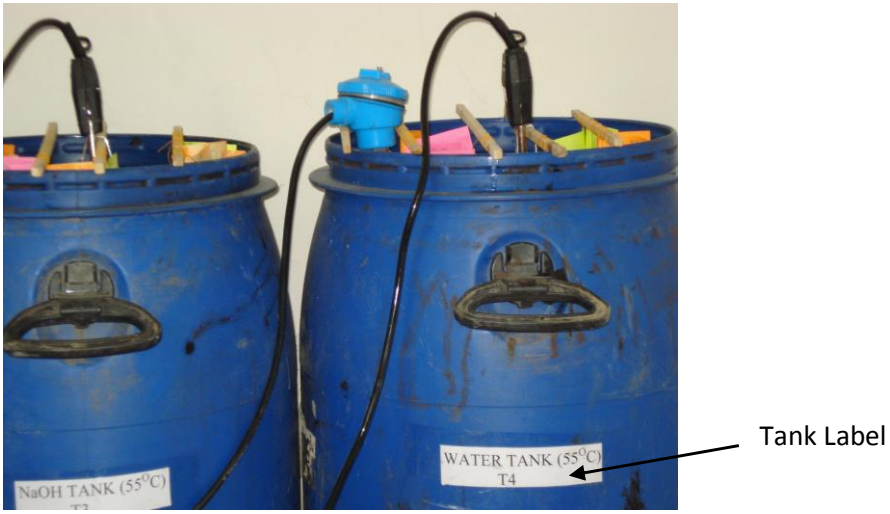

Fig. 4.2 Water Tanks

2) Samples:

Commercially available GFRP sheet had been used for making specimens. The GFRP sheet was placed along the length side (0^{o} orientation) for cutting the samples.

The following were the specifications of the sample (refer Fig. 4.3):

Length of specimen : 500 mm
Breadth of specimen : 10 mm
Thickness of specimen : 0.8 mm (approx.)

The samples were having "tabs" at both sides only upto a length of 150 mm from respective ends. This left an "effective length" of about 200 mm in centre. We had taken the ASTM Standard D-3039 as a reference to decide the shape and specification of the sample.

Fig. 4.3 Dimensions of the Specimen

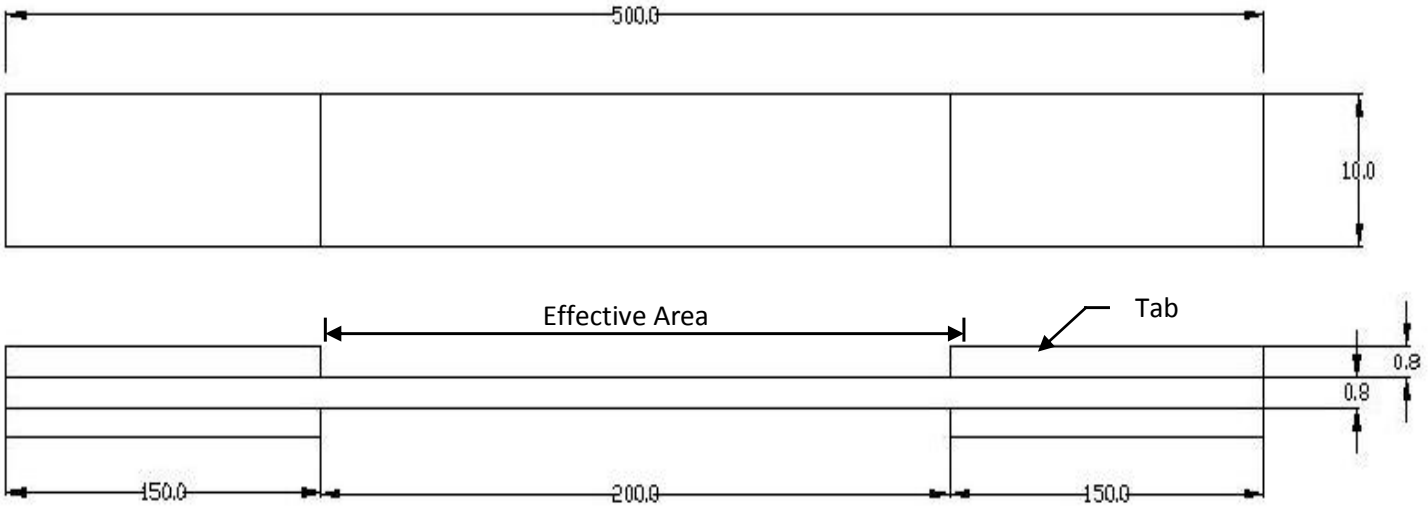

All dimensions are in mm

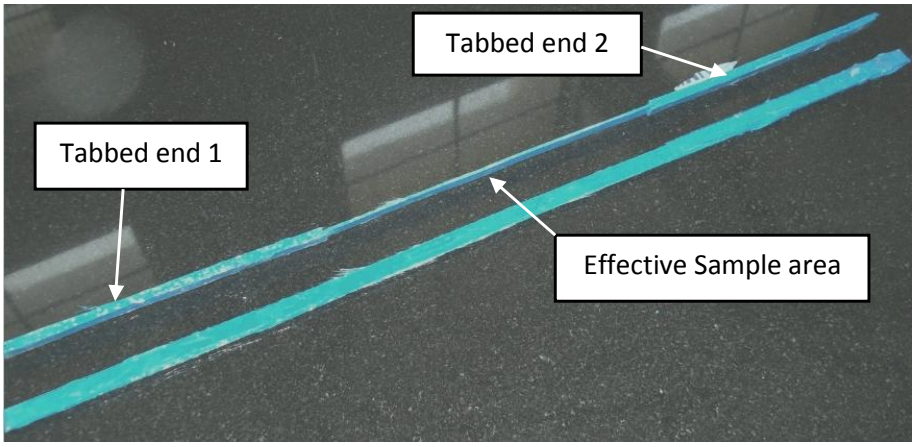

Fig. 4.4 Actual image of the specimen

The actual image of the final sample is shown in Fig.4.4. The samples were hanged fully immersed into the bath over a hanger stick with help of thread. A piece of paper was attached to every sample's thread indicating its details. We had used different colour slips (Fig.4.5) in order to differentiate sample easily with different pre-streched loads. After the time of respective samples were over the sample were taken out & the tensile tests was performed on them in order to check their degradation. A SEM image of the sample was also taken in order to see the actual degradation of fibre.

3) Heating Element:

The setup was heated with help of commercially available heating rod elements (Fig. 4.5). Each bath was having its own heating rod connected via temperature controller (Fig.4.6). The wattage of rod was 1000KW with single phase connection. As the temperature reaches the required value the power supply of rods were cut off by controllers.

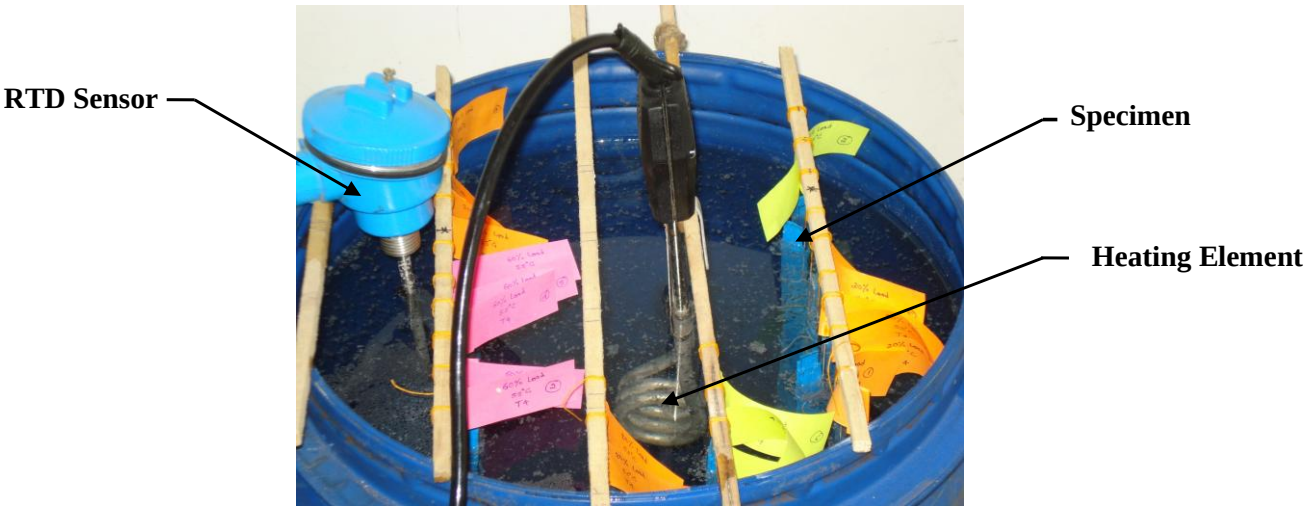

Fig. 4.5 Heating Element and RTD sensor in a tank

4) RTD (Resistance temperature detector) Sensors: Each of the tanks were provided with separate RTD sensors (Fig.4.5). It senses process value of temperature (value at given time) of the bath and input was send to the controller which controlled the system as per set value.

5) Temperature Controller:

The objective of this set up was to maintain the bath temperature at specified value till the duration of experiment for day and night on daily basis. So a temperature controller (Fig.4.6) was connected with each of the bath along with relays cut off.

The controller used the proportional-integral-derivative (PID) control to maintain the temperature. On the controller display we had to feed the "Set Value" of temperature indicated in green and the "Process Value" of temperature would be indicated in the red (refer Fig.4.6), which was the output from the RTD sensor. For the very first time we had to set the controller to auto-tune mode so that it could adjust itself according to the input variables. Once the bath had attained the set value the controller cuts off its supply and after sometime it senses the temperature had gone below set value it again starts heating to obtain set value.

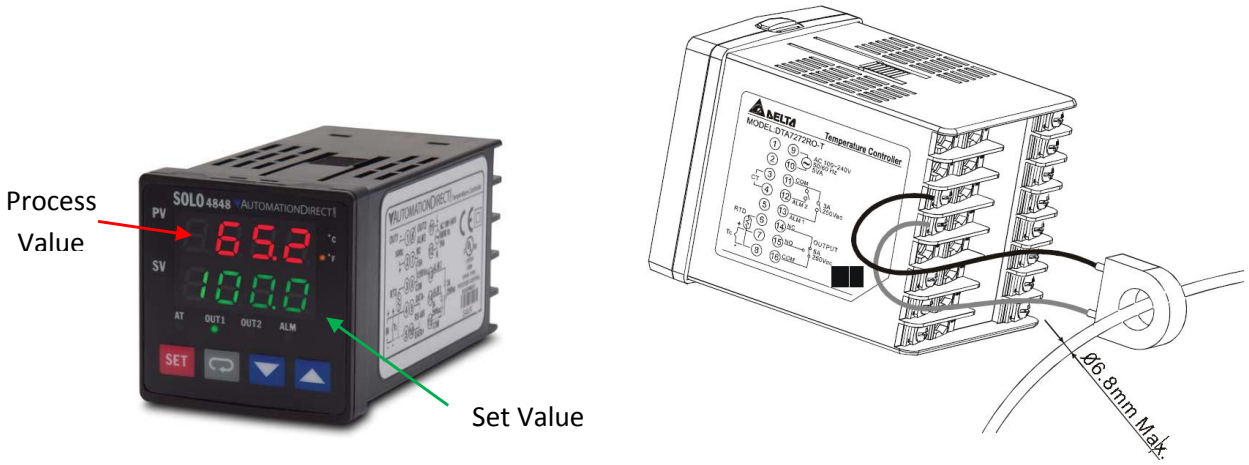

Fig. 4.6 Actual image of the temperature controller showing front and back side of it [30]

The connections of controller are shown below in the Fig.4.7 as given by its maufacturer. It consists of terimanls named with different numbers. Each terminal is having specific input or output requirements. Terminal 1 and 2 here were connected to the power supply of 220Volts with live at 1 and neutral at 2. The relay was connected to the terminals at 3 & 4 with respective positive and negative connections. The live terminal of the heating element was connected to the T1 terminal of the relay and neutral was connected to the power input.The RTD Sensor was connected to the terminals 7, 8 & 9 as shown in circuit diagram (Fig.4.7).

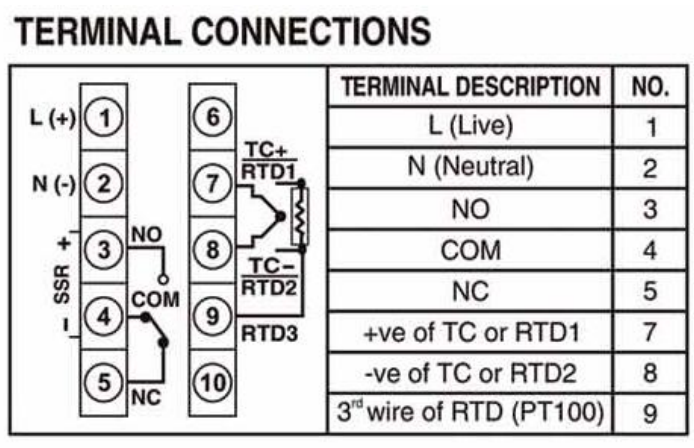

TERMINAL DESCRIPTION	NO.
L (Live)	1
N (Neutral)	2
NO	3
COM	4
NC	5
+ve of TC or RTD1	7
-ve of TC or RTD2	8
3rd wire of RTD (PT100)	9

Fig. 4.7 The circuit diagram of the connections made in the controller [30]

The temperature controller was needed to be secured at some place so we fabricated a display panel out of wood (Fig.4.9). The front face was provided with four holes of the size of the controller outer cover specifications i.e. 48 X 48mm (Fig.4.8). The difference of about 200mm was kept within back of controller and the wall it was attached. The distance was kept more so as to provide accessibility as well as good air circulation to dispose of heat generated.

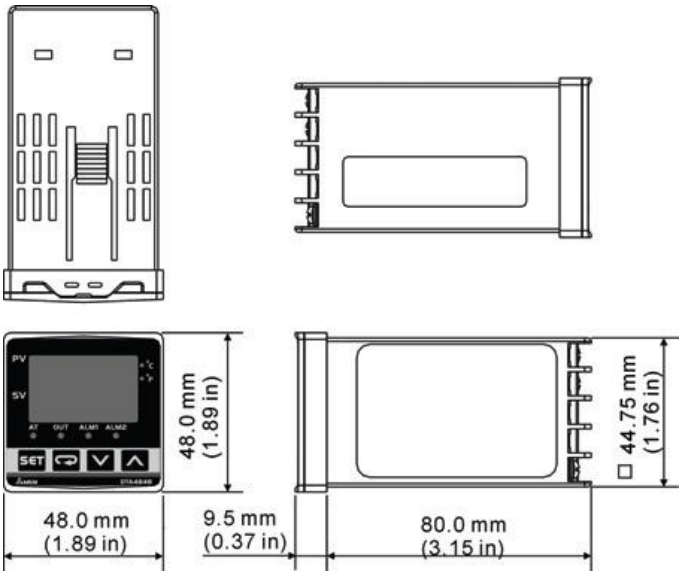

Fig. 4.8 Dimensions of controller [30]

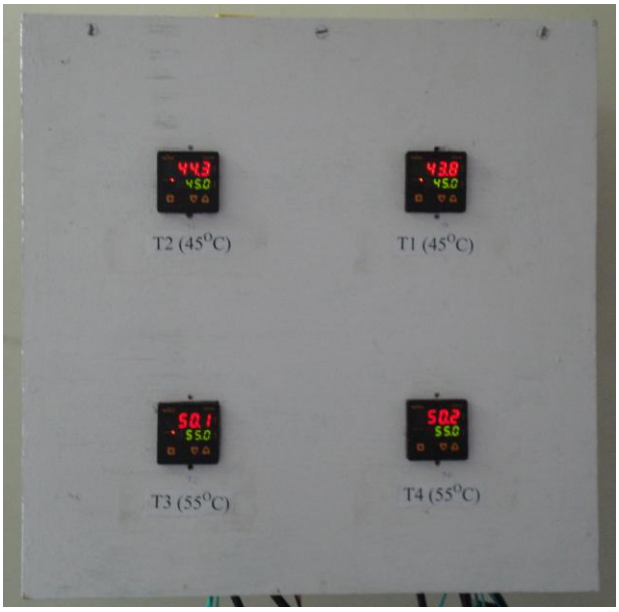

Fig. 4.9 Temperature display panel with controllers

6) Solid State Relays (SSR):

The solid state relay (Fig.4.10) was required to break the circuit in case of overloading. It controlled the switching of the heating element and acted as a switch. It helped in protecting controller for any kind of overload or short circuiting.

Fig. 4.10 Solid State Relay used in setup [31]

4.3 FABRICATION OF SAMPLES:

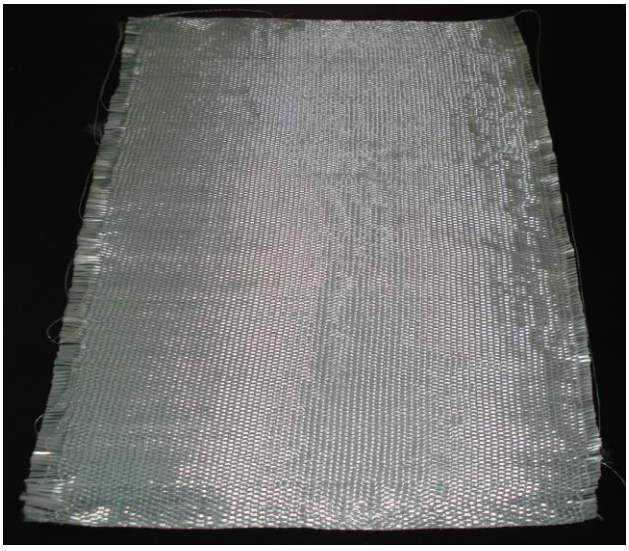

Fig. 4.11 Uncoated GFRP sheet used for making sample

A) Cutting GFRP Sheet

For our experimentation we had purchased the unidirectional woven fabric roll of GFRP (Fig.4.11) of 50cm width having 0^o fibre orientation woven with polymer fibres. The sheets were initially cut from roll in length of 550mm (i.e. 50mm more than actual sample length). The reason for overcutting was that after its curing we had to trim of the edges in order to remove flaws at end.

B) Mixing of Epoxy

The sheets were epoxy coated in order to make a composite material. In our case we had used the epoxy resin (by M Brace) which basically consists of two parts (refer Fig. 4.12):

a) Base

b) Hardener

Base is thick blue liquid which was considered as main ingredient and orangish coloured hardener was added to it to help it in settling down by starting the exothermic reactions. Both base and hardener were mixed (by weight) in a container in ratio of 100: 40 respectively.

Fig. 4.12 Base (blue colour container) and Hardener (white bottle) used for coating

Fig. 4.13 Hand mixing of both base and hardener

After putting the base and hardener in required quantity, the mixture was stirred continuously by manual process (Fig.4.13) so that the mixing takes place in proper manner. If mixing was not done properly the material would not settle well. Also if the ratio of the hardener was more than the pot life of the material would have been lesser. We prepared the amount which was consumed in 20-30 min. otherwise epoxy would have settled in container itself. Approx. 300gms of epoxy was needed to apply to both side of sheet in our case.

C) Applying resin on sheet

The epoxy was applied on sheet using a steel scrapper (Fig. 4.14) by carefully spreading it evenly on all sides of sheet. It was made sure that there is no air bubbles present entrapped inside the epoxy applied on sheet otherwise it would create a flaw there. After applying epoxy the sheet took overnight to dry and now the coat could be applied on other side if required. The full curing of sheet (Fig.4.15) was done by leaving it under ambient temperature for at least seven days before processing further.

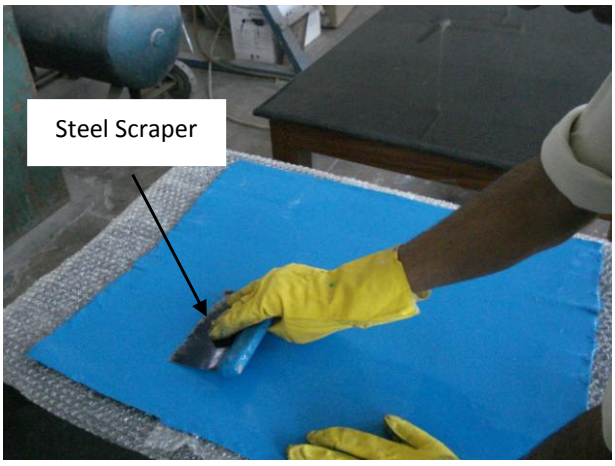

Fig. 4.14 GFRP sheet being resin coated.

Fig. 4.15 The fully cured sheet with epoxy coating

The thing to note here was that we are making two types of sheets here:
One with epoxy coating on both sides - it's used to make actual sample
Other with epoxy coating on one side only - it's used to make Tab

D) Sizing of sheet for samples and tabs

Once the epoxy was fully cured, we cut the sheet to actual sample size using the Treadle shearing machine (Fig.4.16) which would shear it into required size of 10mm x 500mm. After obtaining the long cured strips of the resin coated GFRP sheet, they were further tabbed on each side of either ends. The tabs were cut in size of 150mm x 10mm with same Treadle shearing machine.

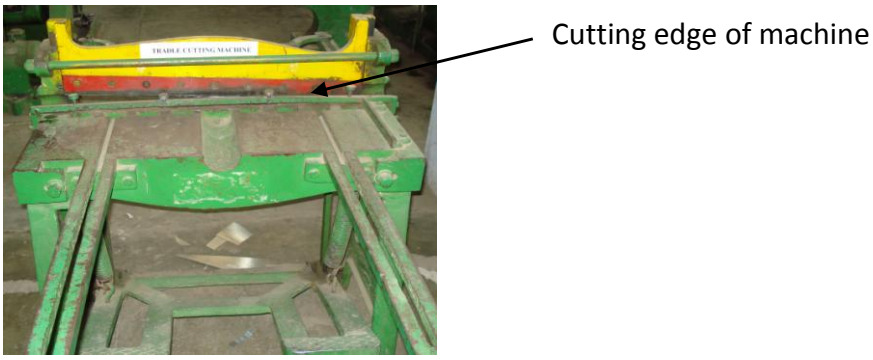

Fig. 4.16 Treadle Shearing Machine

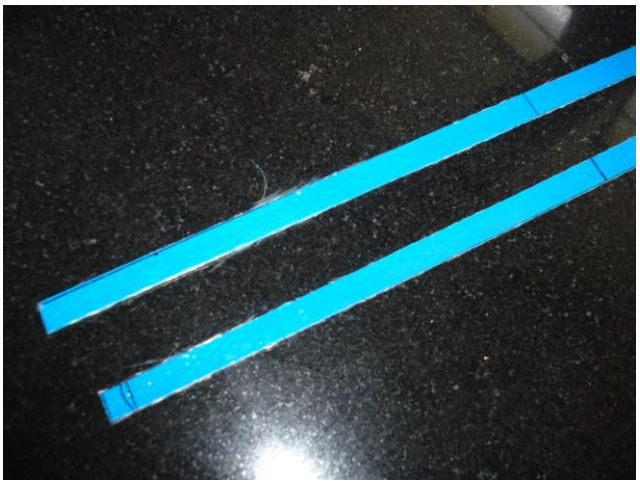

Fig. 4.17 Sample before tabbing

Fig. 4.18 Actual image of "Tab"

The Fig.4.17 shows the actual sample before they were tabbed and correspondingly the "Tab" used to made final sample shown in Fig.4.18.

E) Placing tabs on samples

The samples had to be tabbed on either side on two ends. We had to again prepare the mixture of epoxy as discussed before and carefully apply it on the either side of sample. The tabs were now placed on either side of epoxy pasted sample (with epoxy coated side of tab on upper side). The epoxy would act as binder between tab and actual sample. Two paper clamps (Fig.4.19) were placed on either tabbed side to hold tabs in place and also to apply pressure while epoxy between them was getting dried.

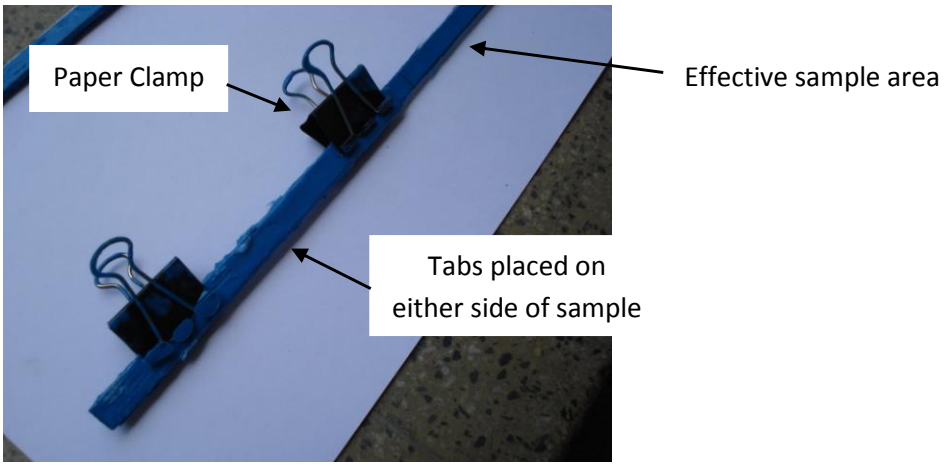

Fig. 4.19 Sample tabbed, Clamped and left for drying

Once the sample was dried, paper clamps used to hold tabs in place were removed. Samples were again cured for 5 days before they were put to any testing. A single sample finally would have four tabs (in total) on either side of both ends (Fig.4.20). This sample was ready now for any kind of further testing.

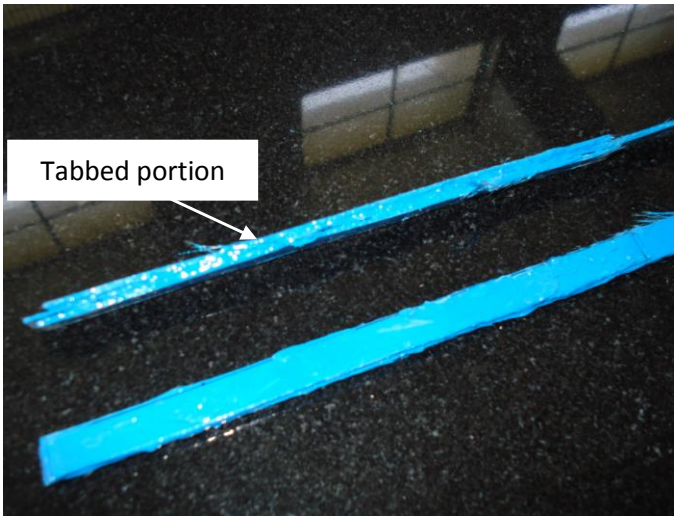

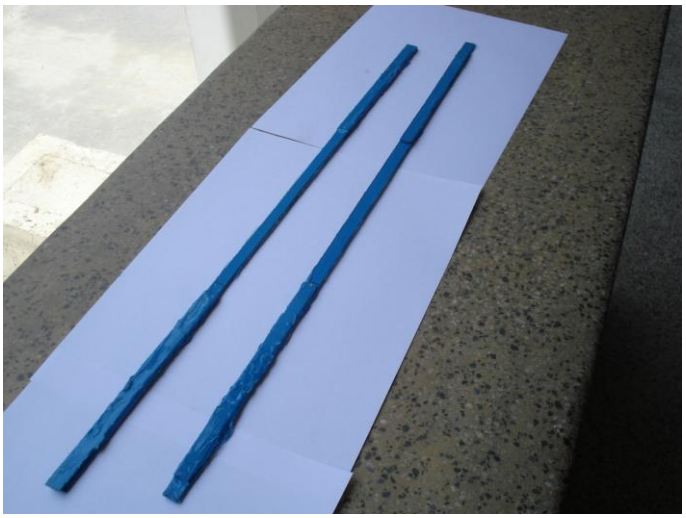

a) **b)**

Fig. 4.20 Sample after tabbing (a) Shows detail at tabbed end (b) Shows final sample tabbed at both ends

- The whole process can be summarised as mentioned below:

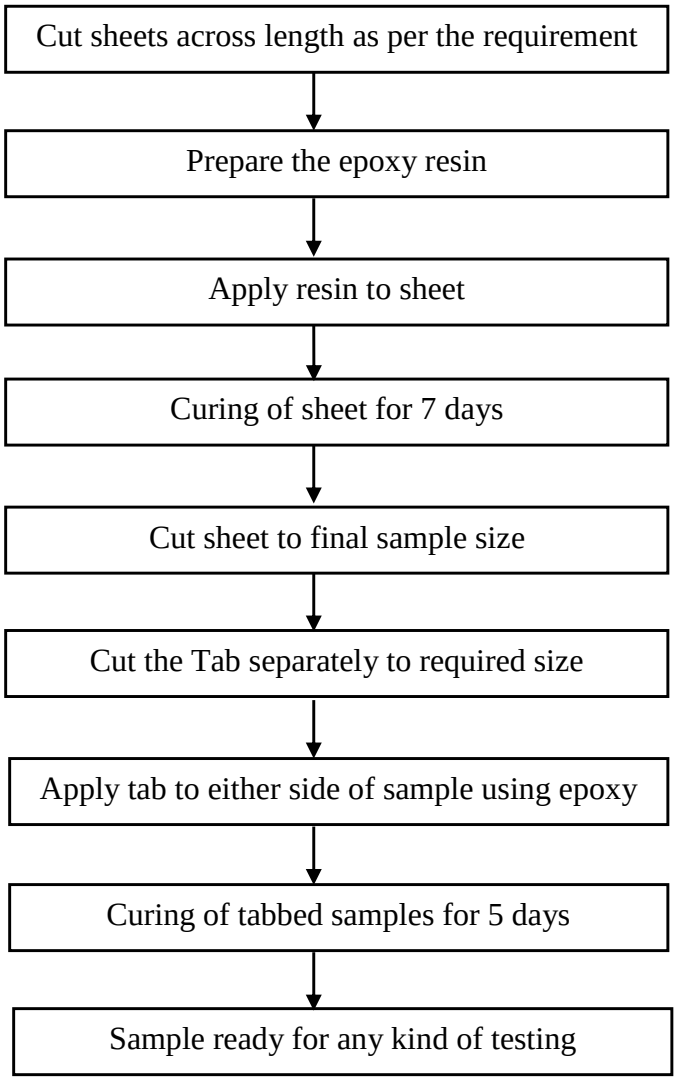

4.4 TEST MATRICES:

Table T6: Test matrix Details (For Accelerated Degradation)

Bath Type	Bath Name	Bath Temperature (°C)	Holding Time (month)	No. of samples which were stretched at				No. of samples for final testing	Total Samples
				20 %	40 %	60 %	80 %	Tension test & Micrograph (Two samples from each loading)	
Water Bath	T1	45	1*	2	2	2	2	8	8
	T4	55		2	2	2	2	8	8
NaOH Bath	T2	45		2	2	2	2	8	8
	T3	55		2	2	2	2	8	8
Water Bath	T1	45	2*	2	2	2	2	8	8
	T4	55		2	2	2	2	8	8
NaOH Bath	T2	45		2	2	2	2	8	8
	T3	55		2	2	2	2	8	8
Total pieces at particular load				16	16	16	16	**Total samples covered under my thesis**	**64****
Water Bath	T1	45	6	2	2	2	2	8	8
	T4	55		2	2	2	2	8	8
NaOH Bath	T2	45		2	2	2	2	8	8
	T3	55		2	2	2	2	8	8
Water Bath	T1	45	12	2	2	2	2	8	8
	T4	55		2	2	2	2	8	8
NaOH Bath	T2	45		2	2	2	2	8	8
	T3	55		2	2	2	2	8	8
Overall Total Samples									128

***** & ****** Holding time and number of samples that would be covered under my thesis work.

Table T7: Test matrix Details (For Natural Degradation)

S. No.	Holding Time (months)	Samples for Testing	Total Samples
		Tensile test & SEM	
1	6	2	2
2	12	2	2
		Total Samples	4

In above experiment according to the planned test matrix (refer Table T6 and Table T7) overall numbers of samples were estimated initially as 132. The work was done mainly on the first two sets of samples i.e. holding time of 1 & 2 months, which amounted to a total of 64 samples.
The tensile test of actual sample was first conducted on a Universal Testing Machine to determine the actual failure load (peak load) the sample can bear. On basis of that failure load the loading weight for samples was calculated. The first set of samples which would be stretched to 20%, 40%, 60% & 80% of failure load and at temperature variation of 45^{o}& 55^{o}C would be taken out of bath after a time of 1 & 2 months and would be checked for its ultimate tensile strength. Two samples out of each varied load and temperature would be tested for their tensile strength. One failed sample under each load would also be tested for micrograph and compositional details.

There would be 4 samples to be studied for the natural weathering & would be kept at ambient conditions for a period of 6 & 12 months. After that they would also be tested in similar manner.

4.5 Graphs for loading values of samples (percentage of Ultimate Tensile Load):

The following table T8 and graphs (Fig.4.21 to Fig.4.28) shows the values at which samples were stretched to different percentage load as mentioned earlier.

Table T8 Loading values (percentage of Ultimate Tensile Load) for samples

* Loading Value (%) of Ultimate Tensile Load	**Actual Values (KN)	*Stress Value (GPa)
20%	0.38	0.047
40%	0.76	0.096
60%	1.24	0.155
80%	1.62	0.203

*Note that area of cross-section considered is $8mm^2$ (refer Fig.4.3) and failure load for calculating percentage loading value was considered as 2KN (minimum failure load).

** Actual values are the loading value shown by tensile testing machine.

1) The graphs of specimen which were subjected to **20% loading of U.T.L.** before putting in bath are shown below:

Fig.4.21 Graph showing loading value of sample subjected to 20% load of U.T.L.

Fig.4.22 Graph showing stress value of sample subjected to 20% load of U.T.L.

2) The graphs of specimen which were subjected to **40% loading of U.T.L.** before putting in bath are shown below:

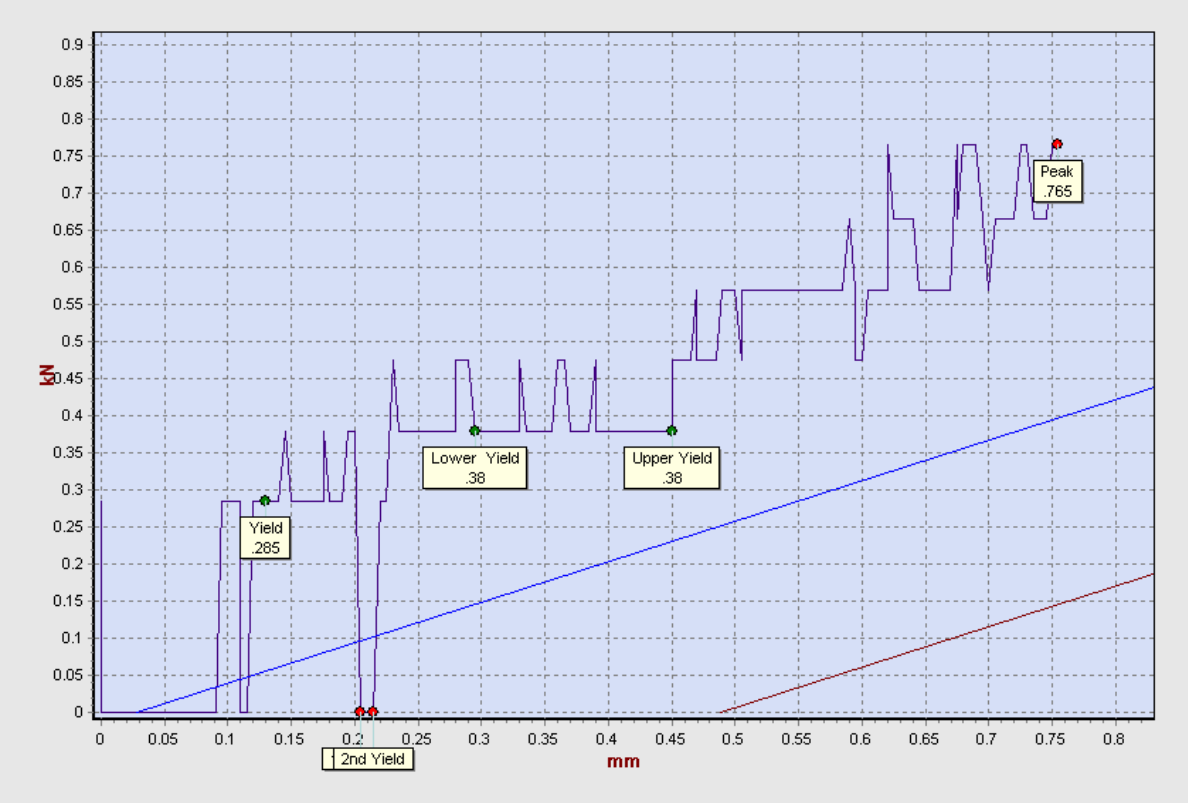

Fig.4.23 Graph showing loading value of sample subjected to 40% load of U.T.L.

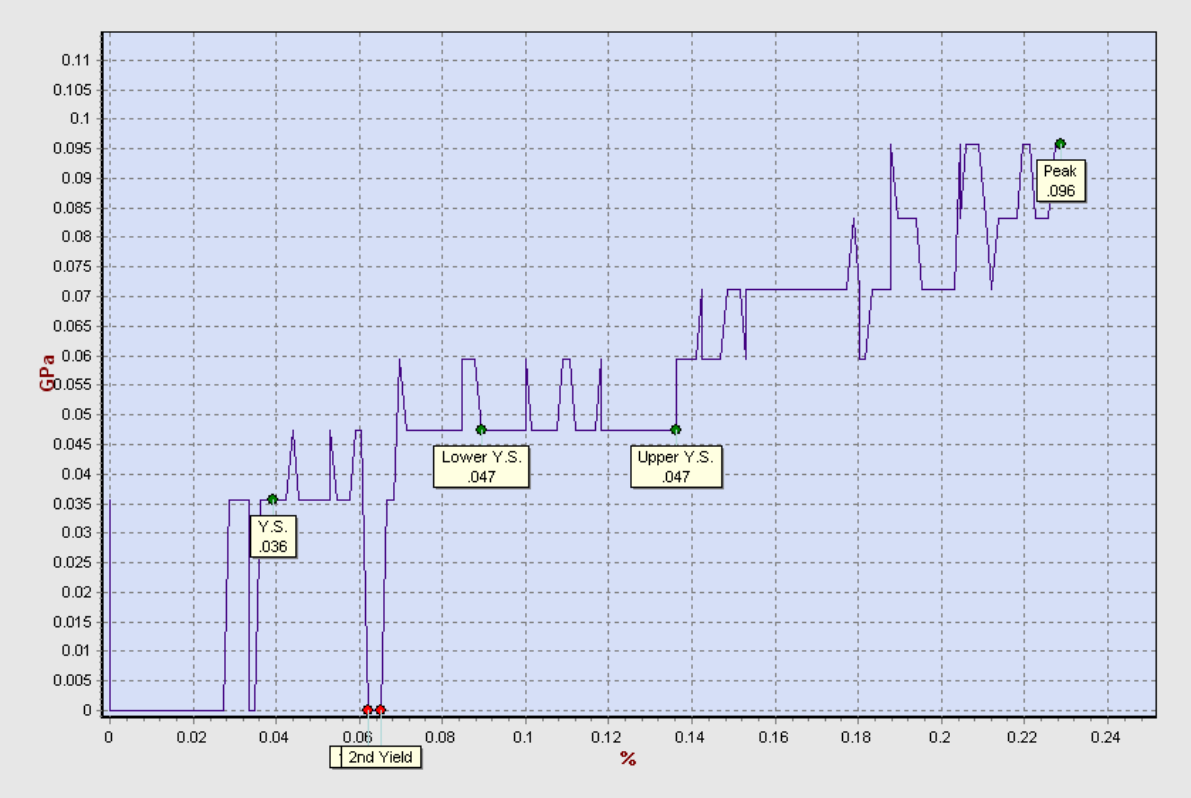

Fig.4.24 Graph showing stress value of sample subjected to 40% load of U.T.L.

3) The graphs of specimen which were subjected to **60% loading of U.T.L.** before dipping in bath are shown below:

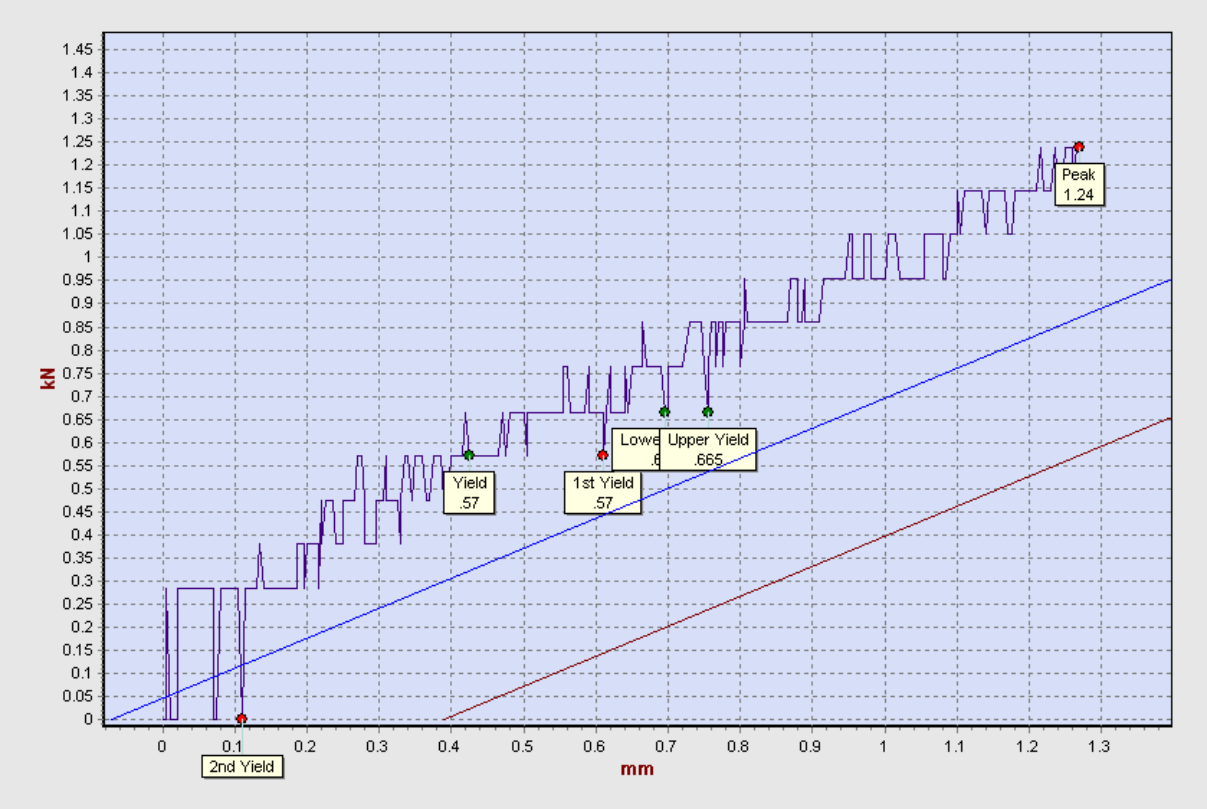

Fig.4.25 Graph showing loading value of sample subjected to 60% load of U.T.L.

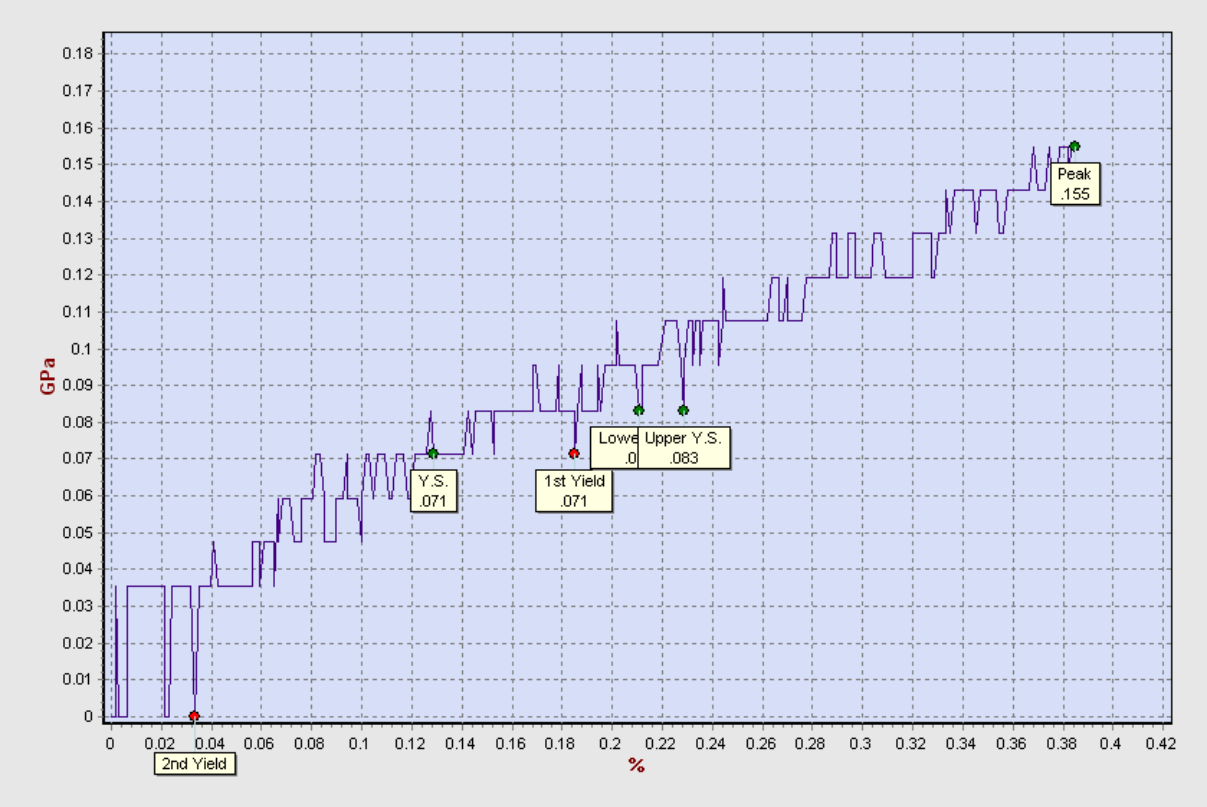

Fig.4.26 Graph showing stress value of sample subjected to 60% load of U.T.L.

4) The graphs of specimen which were subjected to **80% loading of U.T.L.** before dipping in bath are shown below:

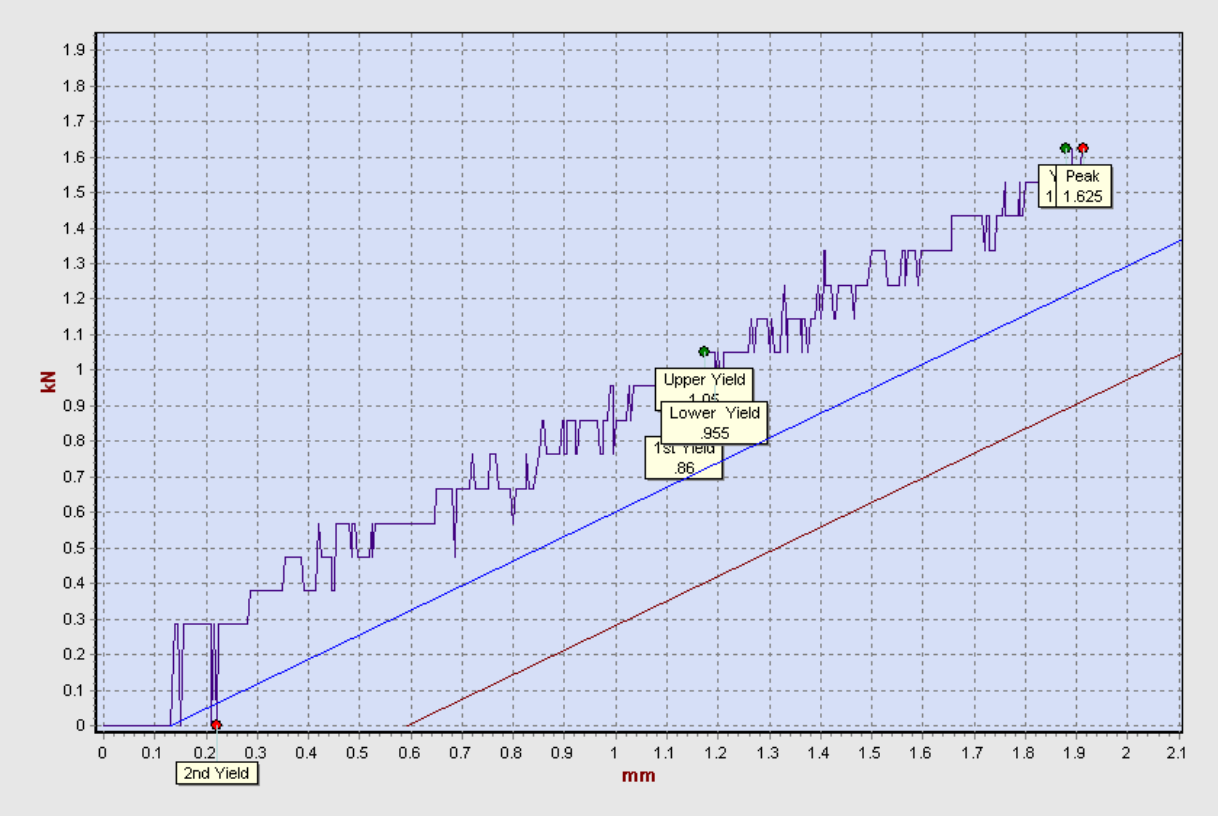

Fig.4.27 Graph showing loading value of sample subjected to 80% load of U.T.L.

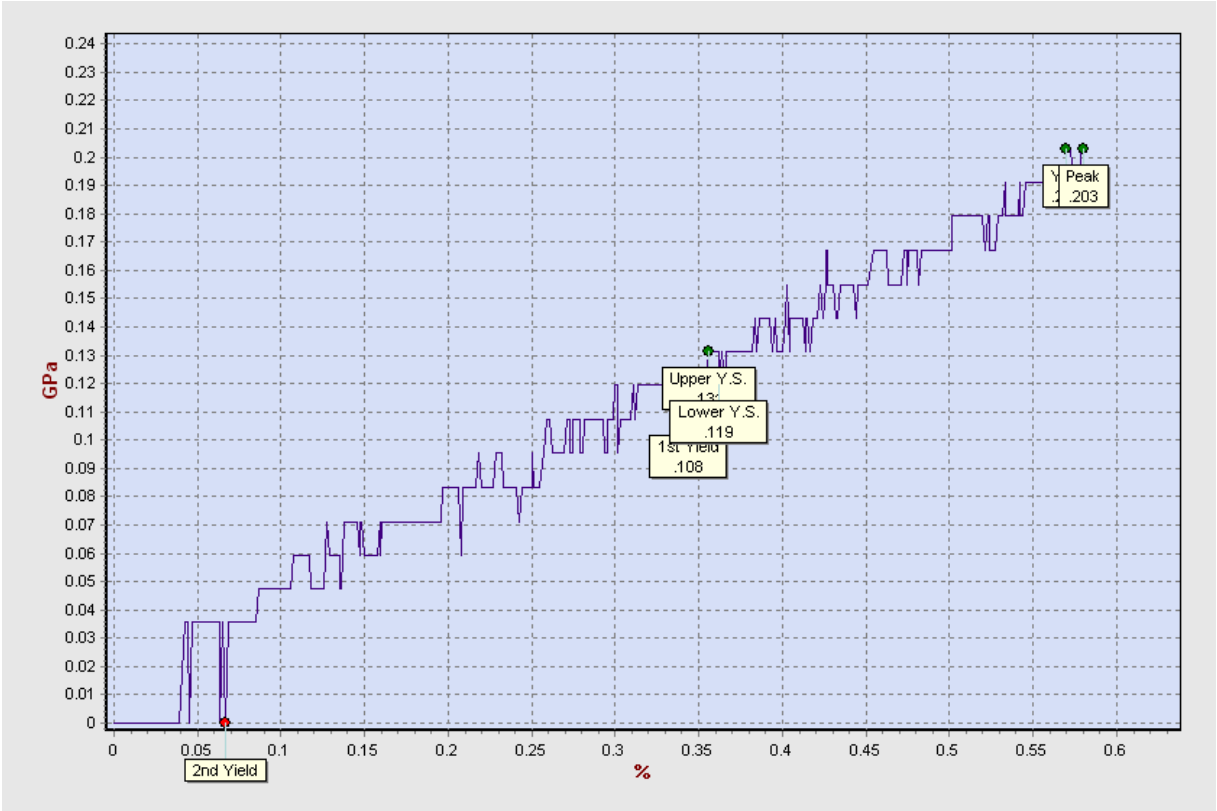

Fig.4.28 Graph showing stress value of sample subjected to 80% load of U.T.L.

4.6 Fibre Volume Fraction and its calculations:

Fibre volume fraction means the amount of fibre present in the composite material. There are several methods available to find but we had chosen the method of the "Ignition Test".

This method determines the mass of the resin by determining the ignition loss of a cured polymer composite. To achieve this a specimen of known mass was heated until the resin matrix was oxidised and converted to volatile materials. The ash was removed and the residual (assumed to be the fully fibre) was weighed. The fibre volume fraction was determined by knowing accurate values for the density of the fibre and the composites. Any part of epoxy that was not oxidised will affect the calculation of fibre volume fraction. Similarly any volatiles such as water or residual solvent would cause errors unless they were small enough to be ignored. The details of sample tested and test results are given in tableT9.

The fibre volume fraction was calculated as per formula shown below: [33]

$$V_f = \frac{\rho_m W_f}{\rho_f W_m + \rho_m W_f}$$

Where
V_f = volume fraction of fibres
W_f = weight of fibres
W_m = weight of matrix
ρ_f = density of fibres
ρ_m = density of matrix

Table T9 Details of samples tested for volume fraction

Sample No.	Length (cm)	Weight of whole sample in gms	Weight of sample after burning (i.e. fibre weight) in gms	Weight fraction
1	8.4	1.4021	0.7527	0.54
2	8.4	1.4077	0.7770	0.55
3	10.7	1.7175	0.9913	0.58
4	10.7	1.7130	0.9989	0.58

Density of fibre* = 2.6 g/cm^3

Density of Epoxy resin* = 1.3 g/cm^3

*As per the manufacturer's specifications [11]

- Using the above data and putting in the equation mentioned above gives:

  Fibre volume fraction = 40%

CHAPTER 5 FINITE ELEMENT MODELLING

5.1 FINITE ELEMENT METHOD:

Finite Element Method is a very versatile method. It can also be seen from the fact that it has been used as an important tool for analyses and design in almost every industry. Finite element method not only give the behavioural insight of the different part of the structure but it also analyze the structure taking the individual behaviour of these parts into consideration and because of this fact it is becoming popular with the engineering field.

Basic idea of the finite element method originated from advances in aircraft structure analysis. Turner et al. derived stiffness matrices for truss, beam and other elements and presented their findings in 1956. In the early 1960s, engineers used the method of approximate solution of problem in stress analysis, fluid flow, heat transfer and other areas. Today the developments in mainframe computers and availability of powerful microcomputer have brought this method within reach of students and engineers working in small industries.

Finite Element Method can be divided into several distinctive steps. Theoretical approach to the method and its different steps are as:

- **Discretization:**

Discretization is the process of dividing domain of problem into small regions or sub domains known as elements. Corner points of elements are called nodes. Figure 5.1 below shows the most used elements:

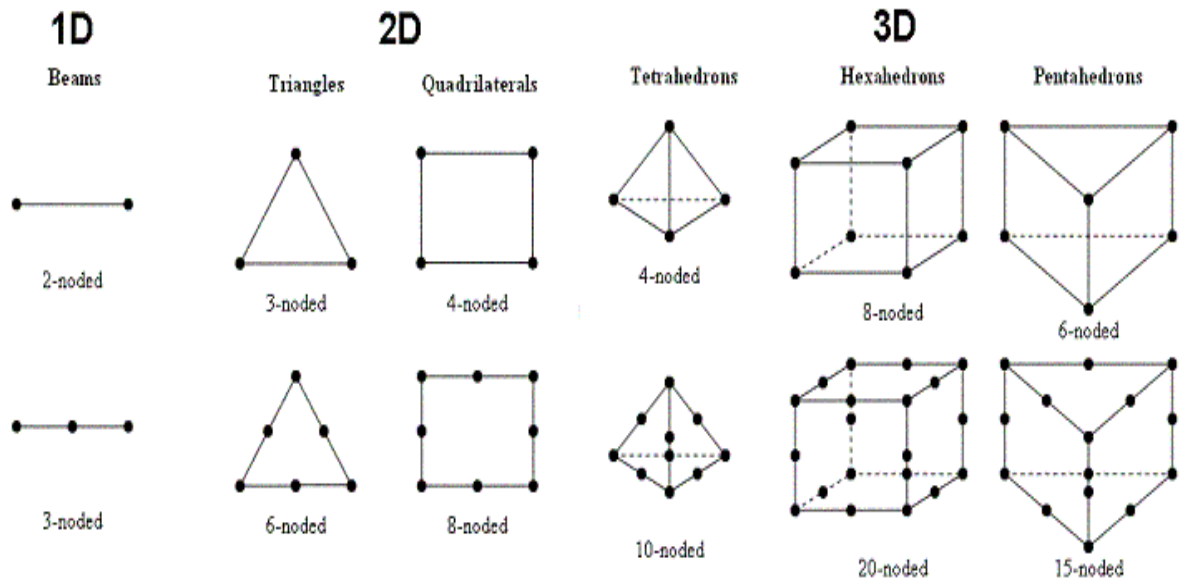

Fig. 5.1 Showing different types of elements [32]

- **Element analysis / Element stiffness matrix:**

The element analysis has two key components, expressing the variable within the elements, and maintaining equilibrium of the elements.

The governing equation is converted to algebraic form which is represented in matrix form and is called element equation or element stiffness matrix. This enables solution by computer. Element stiffness matrix represents the response of elements according to its property in the system for the parameters. Same matrix can be used for all elements of same type.
For conversion of governing equation (differential or integral) into algebraic form we are required to follow following steps:

- **Construction of trial solution**: It is a cyclic process by hit trial. The equation with certain degree of freedom is taken, which is solved by applying boundary condition either at the starting for manual processing or after formulation of system stiffness matrix for solution through computer.
- **Application of optimization criteria**: Optimization criteria are used to find the values of trial function. Two methods for optimization are:
  - Method of weighted residual (differential equation) e.g. Least square Method
  - RITZ variation method (integral equation with some limitation).
- **Estimation of accuracy**: - The accuracy of solution is checked for closeness to exact solution. Also accuracy can be checked by checking the reducing difference of the consecutive solutions obtained by increasing degree of freedom known as property of convergence.

  Sources of error in FEM are:
  - Domain Error - Discretization of domain is approximate.
  - Computational Error - Integration and differentiation induce error.
  - Approximation Error - Assumption of degree of freedom makes the solution approximate.

- **System analysis / system stiffness matrix**

The matrix equations for the individual elements are combined to form the Matrix equations for the entire system called system stiffness matrix. It gives the response of the parameters on the entire system.

- **Incorporation of boundary and loading conditions**

The system stiffness matrix is modified according to the overall boundary conditions. This reduces calculation work and saves time.

- **Solving of the system equations**

The system equations can be solved to give the unknown values at the nodes. If the problem is of an equilibrium nature, then the solution is obtained by solving a set of linear or non-linear equations. System equations can be solved by number of available solvers like gauss elimination or gauss siedel etc.

- **Post processing / Display**

The post processing stage deals with the representation of results. Typically, the deformed configuration, mode shapes, temperature, and stress distribution are displayed at this stage.

5.2 MODELLING APPROACH:

To validate the experimental approach a model with **unit cell approach (UCA)** was developed (refer Fig.5.2). In its simplest initial version, a unit cell model of a material presents a round fibre, surrounded by a matrix layer and is applicable to the simulation of mechanical behaviour of fibre-reinforced composites with equally-sized fibres.

In this model, evidently assumptions about the material structure had been made, neglecting the effect of other inclusions and the matrix on the mechanical behaviour of the chosen cell. Yet, this approach appeared to be very efficient in the analysis of the effect of the arrangement, volume content and shape of inclusions on the overall response of composites. A unit cell model with fibre arrangements helped to study the effect of hygrothermal and mechanical stresses on the deformation in the composite. This software is considered to be good for solving composite problems. The analysis part will be involving the input of mechanical & hygrothermal load and other boundary conditions and the effect of these stresses will be analysed on the degradation of fibre composite material.

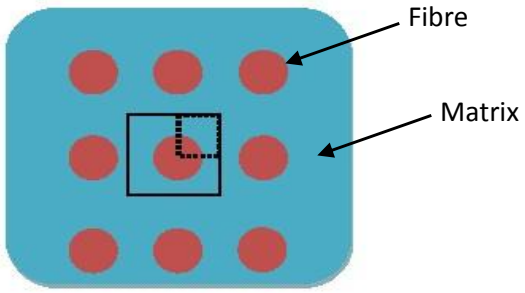

Fig. 5.2 Unit cell approach for modelling a single fibre

Using symmetry, one quarter of the representative volume element (RVE – shown by dotted lines) is modelled as a plane strain unit-cell (infinitely long fibre coming out of the plane of paper). When subjected to moisture boundary condition the moisture typically percolates (diffuses) through the matrix while the fibres are usually impervious to diffusion. Typically when a composite is subjected to combined moisture and mechanical loads, the effect of both tend to get coupled. The differential expansion due to moisture sets up residual stresses in the fibres and the matrix that are time-dependent and governed by the time-scales of diffusion.

5.3 MODELLING PROCEDURE:

The modelling work will be done using Abaqus software (version 6.7) and in Abaqus-CAE module. The step by step procedure of modelling is explained below with all the specifications included in that step. The procedure is explained below as per actual method of preparation of model.

1) CREATING MODEL: Firstly as we discussed that model is based upon the unit cell modelling so we had prepared the two part models, differently representing matrix (i.e. epoxy) Fig.5.4 and other as fibre (Fig. 5.3). Here considering the symmetry of the model we had considered only one quarter and a 2D model as it will save time for analysis.

Just using the sketcher module we have created the geometry as per the sketching tools available in Abaqus.

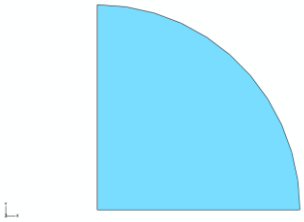

Fig. 5.3 One quarter model of single Fibre

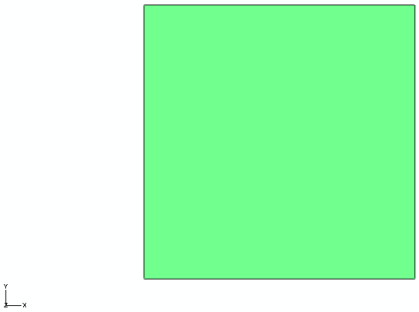

Fig. 5.4 One quarter model of Matrix

The dimensions of above model are 1x1mm for matrix and 0.8mm for fibre. Both the model is made as "planar shell" as base feature.

2) CREATING MATERIAL: The composite considered here is glass fiber-polymer matrix composite made up of E-glass fiber and epoxy matrix. So we had defined two materials, one for fiber and other for matrix. The various properties used are mentioned in the tables T10 and T11 below:

Table T10 Mechanical and Thermal properties of material [33]

Material	**Density (gms/cm^3)**	**Poisson's Ratio**	**Coefficient of thermal expansion (m/m per ^0K)**	**Thermal conductivity (W/m-per ^0K)**	**Young's Modulus of Elasticity (MPa)**
E-glass	2.54	0.2	-	3.23	74000
Epoxy	1.38	0.3	$6.13x10^{-6}$	0.346	3440

Table T11 Properties of mass diffusion of material [33]

Material	Temperature (^oC)	Diffusivity Coefficient (mm^2/sec)	Concentration (%)
Epoxy	37	$41x10^{-8}$	100
	50	$102x10^{-8}$	100

*Note that mass diffusion properties for glass fibres are not defined because its diffusivity values are very low as compared to that of epoxy so we can neglect them.

3) CREATING & ASSIGNING SECTION: In Abaqus section are to be defined in order to assign properties to particular part. Here again two sections each for fibre and matrix were created. We had created a "Generalised Plane Strain" section here. After sections were created, they were assigned along with material properties to the parts mentioned above i.e. fibre and matrix respectively.

4) ASSEMBLY OF MODELS: Once we had created two different models we need to assemble them to form a single composite (Fig.5.5). So using the assembly tools we had merged the model into a single composite material.

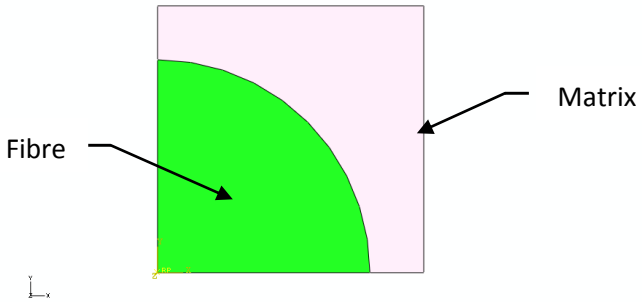

Fig. 5.5 Assembled model of fibre and matrix (one quarter)

5) MESHING: Once the assembly is created we need to mesh the model in order to analyze it. Here seeding is required before meshing in order to decide the size of meshing. Once model is seeded it will mesh the part automatically as shown in Fig.5.6

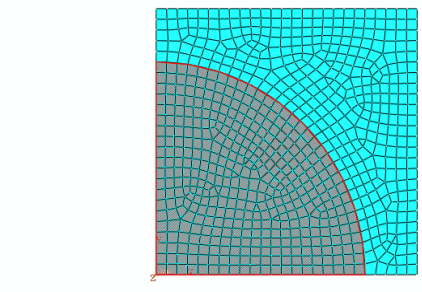

Fig. 5.6 Meshed model

Meshing element used here is **CPEG4T**– 4 noded Generalised Plane Strain, thermally coupled quadrilateral, with bilinear temperature and displacement.

6) CREATING STEPS & BOUNDARY CONDITIONS: Steps are needed to be created in order to apply mechanical and thermal boundary conditions differently.

a) Coupled heat and load model: The modelling steps are as under:

Step 1 – Mechanical Loading: We had created a Static General step here for analysis.

- **Loading conditions**: A Generalised Plane Strain, axial load (20%, 40%, 60%, and 80% of failure load) at the centre of the fibre (Fig.5.7) is applied in order to simulate the stretching of the fibre before immersing in medium.

.

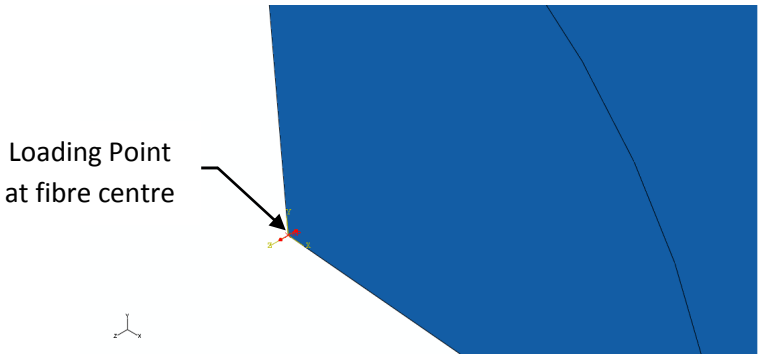

Fig. 5.7 Model showing the axial loading

Step2 – Coupled Temperature-Displacement analysis: In this step we used a Couple temperature-displacement step (in built in Abaqus) to include the effect of both loading and temperature in model. The analysis is done in Transient form.

- **Boundary conditions 1:** Model is fixed here against moving in "y" direction both in linear and rotation form. The figure 5.8 below shows where condition is applied.

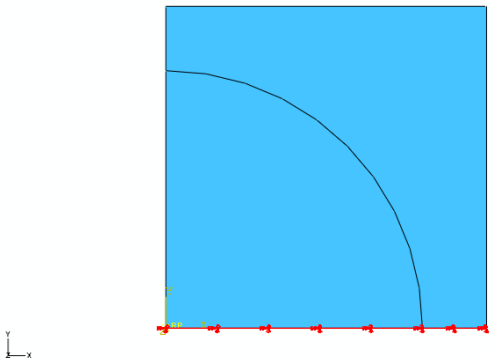

Fig. 5.8 Model showing the boundary condition position

- **Boundary conditions 2:** Model is fixed here against moving in "x" direction both in linear and rotation form. The figure 5.9 below shows where condition is applied.

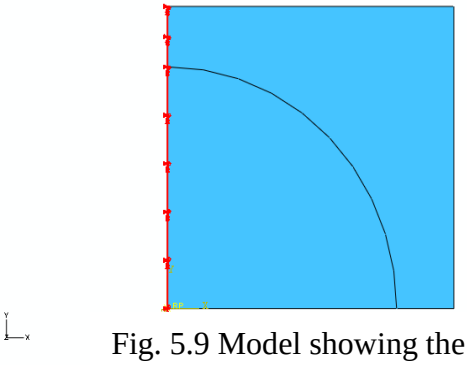

Fig. 5.9 Model showing the boundary condition position

- **Boundary conditions 3:** A temperature boundary condition is applied here in order to simulate the water heating surrounding the composites. The magnitude of temperature was given here as 45^{o}C and 55^{o}C for two tanks with varying temperature. Figure 5.10 below shows where conditions are applied.

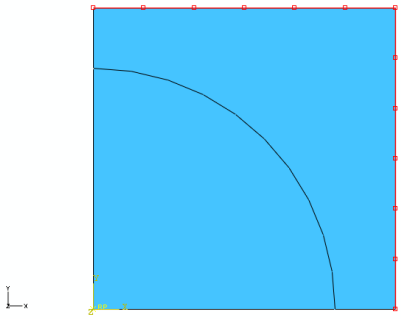

Fig. 5.10 Model showing the temperature boundary condition

- **Boundary conditions 4:** A temperature boundary condition is applied here for ambient condition. The magnitude of temperature is given here taken was 30^{o}C for all tanks. It's applied on the other left edges comparing to above boundary condition 3.

b) Moisture Modeling: The moisture modeling is done separately as it can't be combined within same model.

Step1 - Coupled Temperature-Mass diffusion analysis: The analysis for the moisture is done in this step. As per the experiment details we know that material is surrounded by water which means 100% humidity. This step will include the both effect of temperature and moisture effect on composite material.

- **Boundary conditions:** The moisture intake condition is also applied as boundary condition as shown Figure 5.11 below.

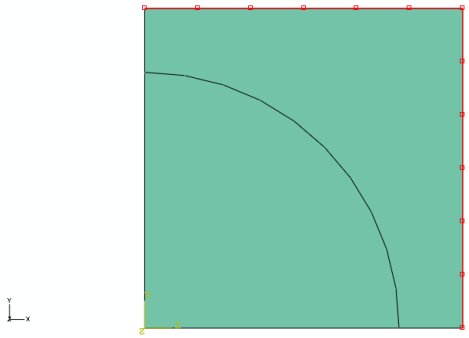

Fig. 5.11 Model showing moisture boundary condition

7) CREATING ANALYSIS JOB: Once all the steps and input parameters are defined the job is submitted for analysis. It will do the analysis stepwise as defined and previous results were carried forward to next step as input solution. The solution was viewed in results section.

5.4 MODELING RESULTS AND DISCUSSIONS:

The results of the modeling are discussed below separately, first for mechanical loaded and temperature model and secondly for moisture ingression.

A) COUPLED TEMPERATURE AND MECHANICAL LOADING MODEL: The following figure (Fig.5.12 to Fig.5.31) shows the results of above said model after period of 1 month and 2 month time.

COMPARISON OF VON MISES STRESSES:

After 1 and 2 months:

- 20% load at 45°C and 55°C

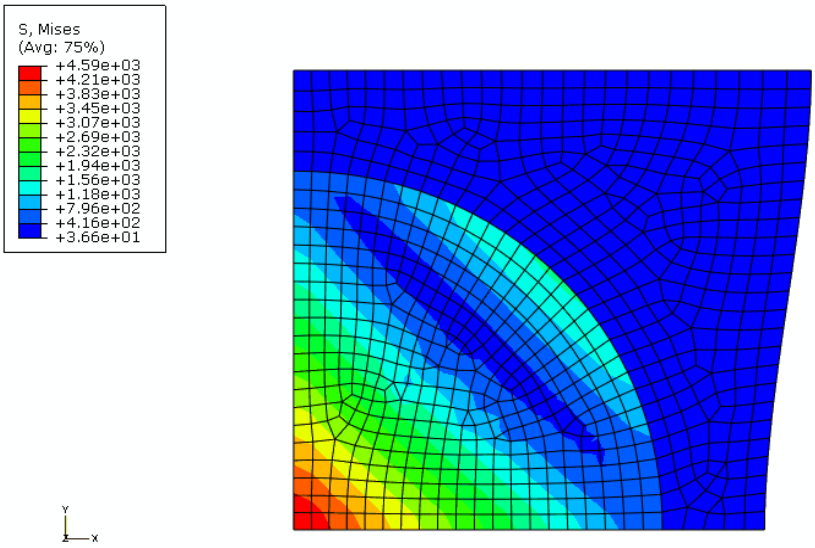

Distance in milli meter (bottom side)	Stress Value MPa
at 0.08	$4.6x10^3$
at 0.4	$2.32\ x10^3$
at 0.8	$4.16\ x10^2$
at 1.00	$3.6\ x10^1$

Fig. 5.12 Von Mises Stress at 20% load at 45°C and 55°C

- 40% load at 45°C and 55°C

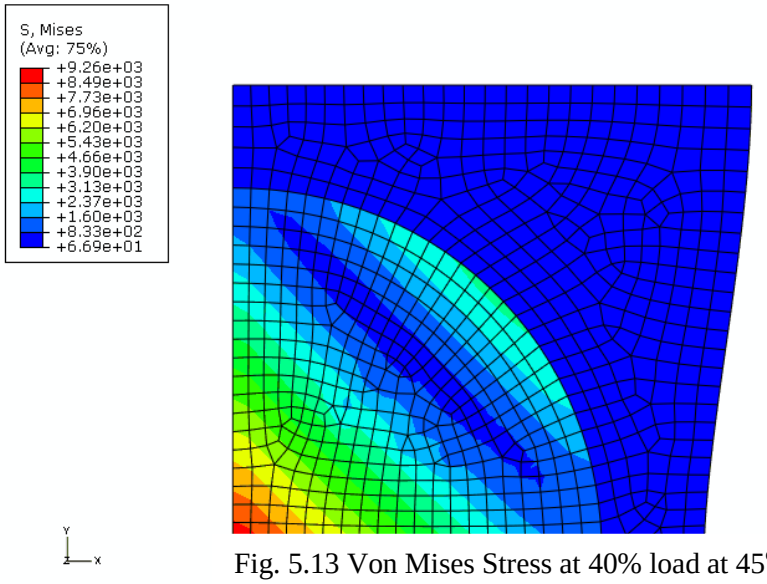

Distance in milli meter (bottom side)	Stress Value MPa
at 0.08	$8.5x10^3$
at 0.4	$4.66\ x10^3$
at 0.8	$8.33\ x10^2$
at 1.00	$6.69\ x10^1$

Fig. 5.13 Von Mises Stress at 40% load at 45°C and 55°C

- 60% load at 45°C and 55°C

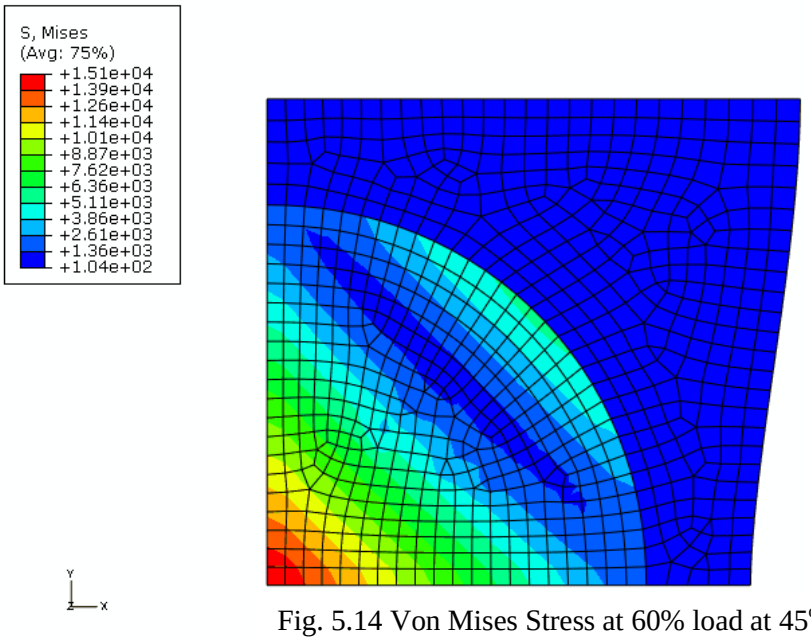

Distance in milli meter (bottom side)	Stress Value MPa
at 0.08	$1.39x10^4$
at 0.4	$7.62\ x10^3$
at 0.8	$1.36\ x10^3$
at 1.00	$1.04\ x10^2$

Fig. 5.14 Von Mises Stress at 60% load at 45°C and 55°C

- 80% load at 45°C and 55°C

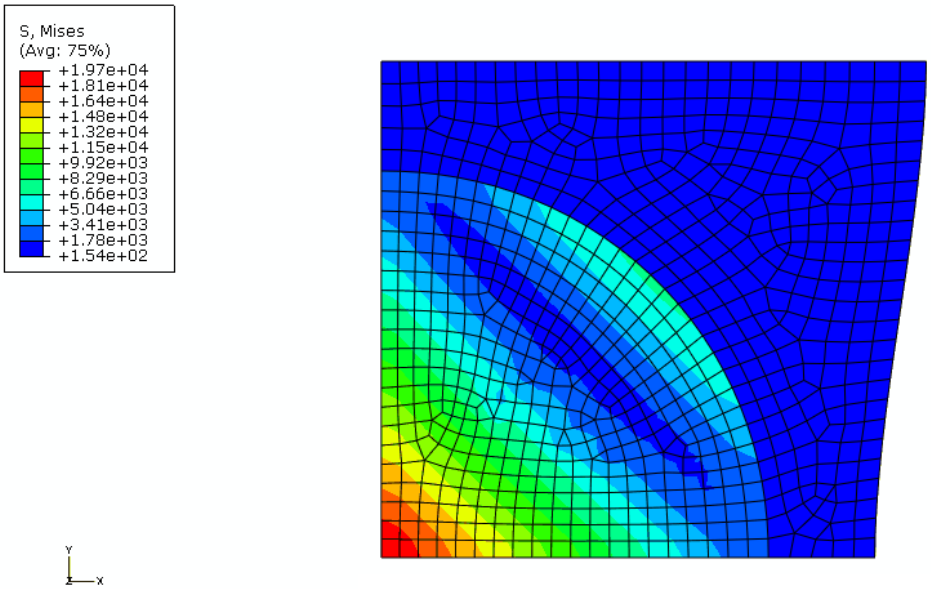

Distance in milli meter (bottom side)	Stress Value MPa
at 0.08	$1.81x10^4$
at 0.4	$9.92\ x10^3$
at 0.8	$1.78\ x10^3$
at 1.00	$1.54\ x10^2$

Fig. 5.15 Von Mises Stress at 80% load at 45°C and 55°C

COMPARISON OF IN PLANE STRAIN:

After 1 and 2 months:

- 20% load at 45°C and 55°C

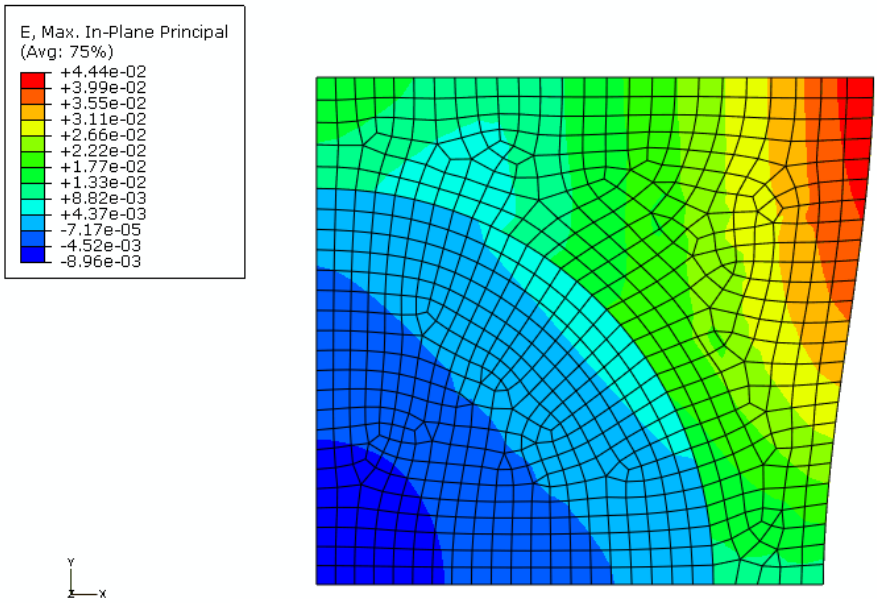

Distance in milli meter (top side)	Strain Value
at 0.08	1.77×10^{-2}
at 0.88	2.66×10^{-2}
at 1.00	4.44×10^{-2}

Fig. 5.16 Plane Strain at 20% load at 45°C and 55°C

- 40% load at 45°C and 55°C

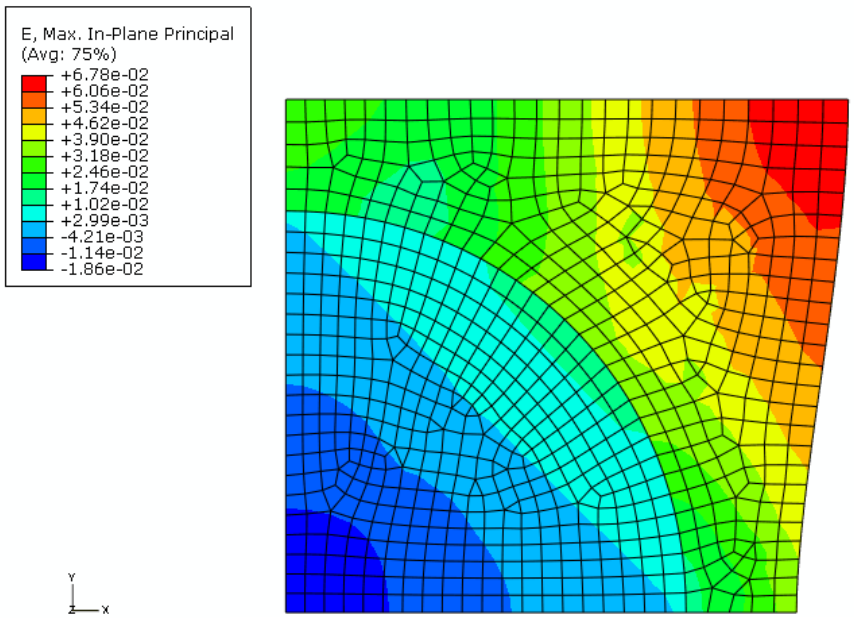

Distance in milli meter (top side)	Strain Value
at 0.08	2.46×10^{-2}
at 0.88	5.34×10^{-2}
at 1.00	6.78×10^{-2}

Fig. 5.17 Plane Strain at 40% load at 45°C and 55°C

➢ 60% load at 45°C and 55°C

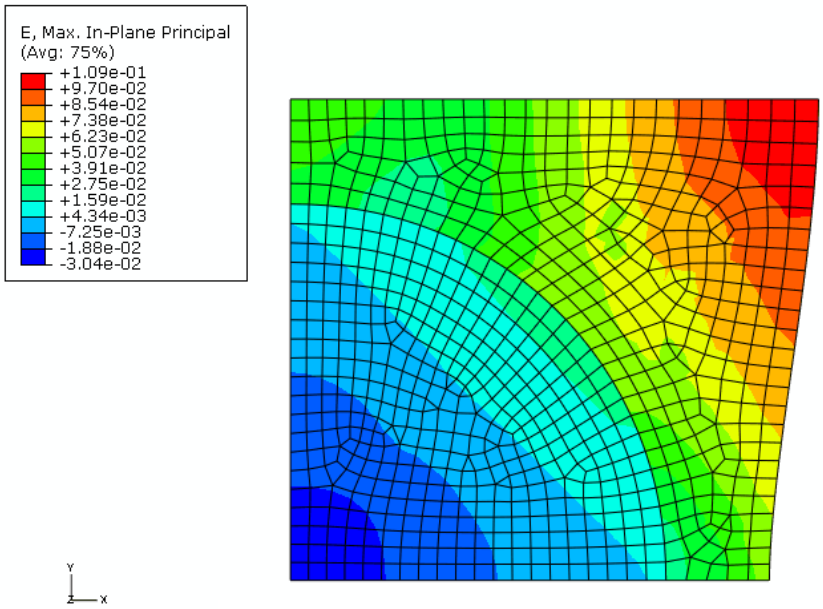

Distance in milli meter (top side)	Strain Value
at 0.08	$3.91x10^{-2}$
at 0.88	$8.54\ x10^{-2}$
at 1.00	$1.09\ x10^{-1}$

Fig. 5.18 Plane Strain at 60% load at 45°C and 55°C

➢ 80% load at 45°C and 55°C

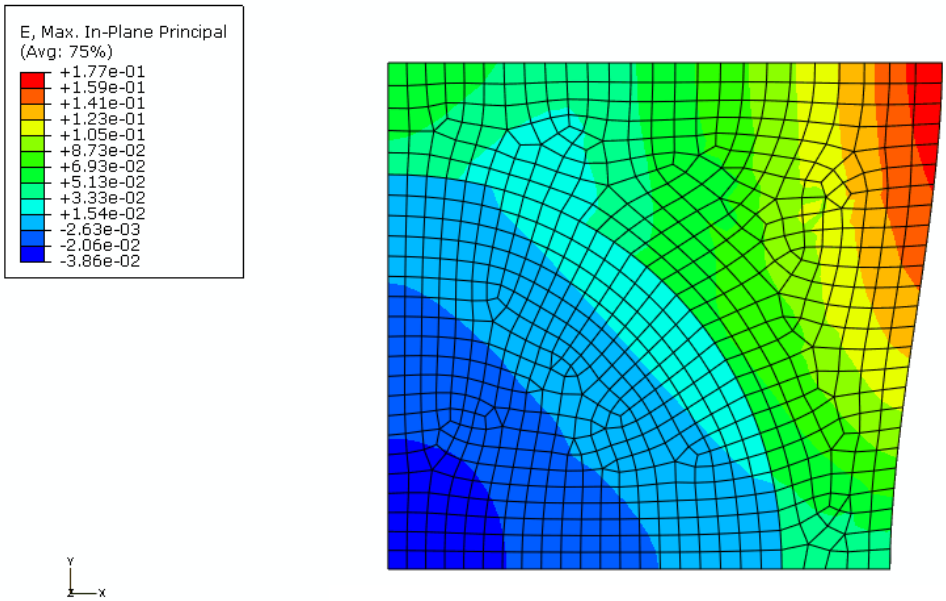

Distance in milli meter (top side)	Strain Value
at 0.08	$6.93x10^{-2}$
at 0.88	$1.05\ x10^{-1}$
at 1.00	$1.77\ x10^{-1}$

Fig. 5.19 Plane Strain at 80% load at 45°C and 55°C

COMPARISON OF IN DISPLACEMENT IN X-DIRECTION:

After 1 and 2 months:

- 20% load at 45°C and 55°C

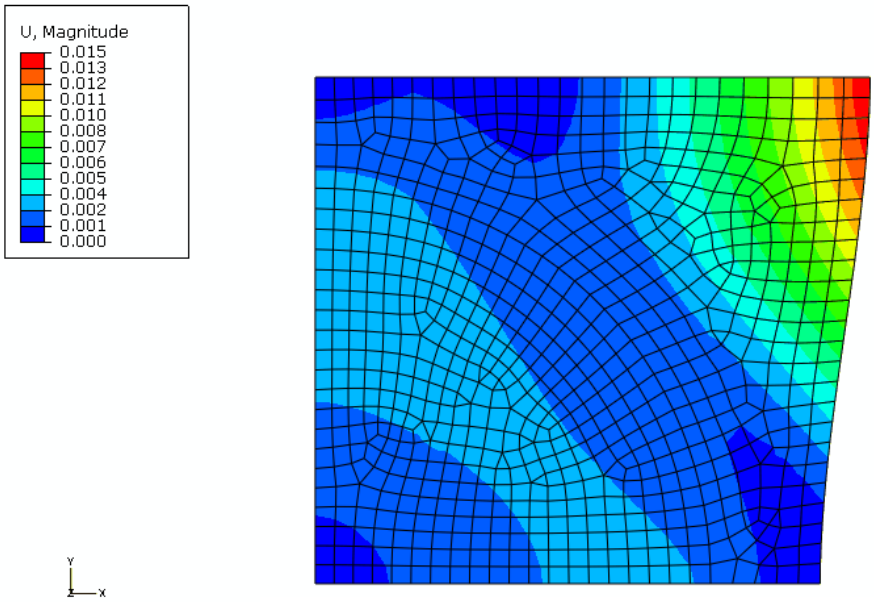

Distance in milli meter (top side)	Displacement milli meter
at 0.08	0
at 0.88	0.008
at 1.00	0.015

Fig. 5.20 Displacement at 20% load at 45°C and 55°C

- 40% load at 45°C and 55°C

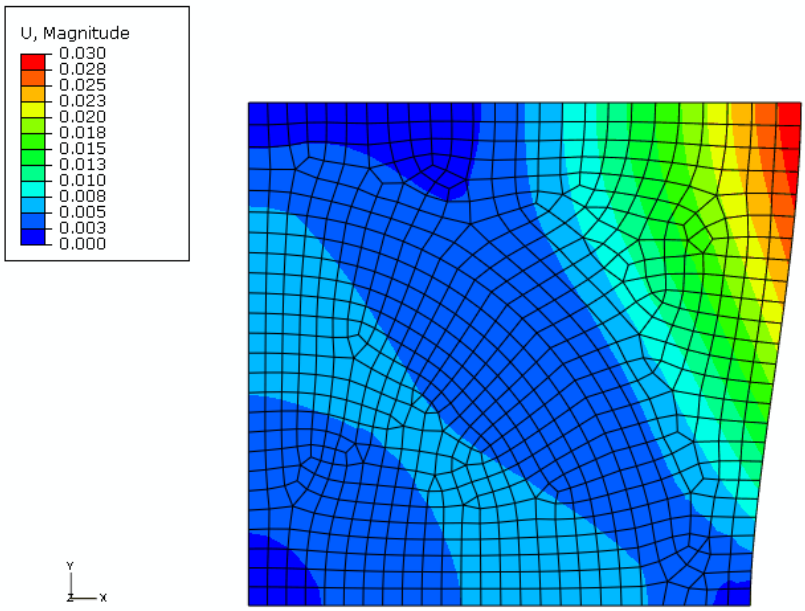

Distance in milli meter (top side)	Displacement milli meter
at 0.08	0
at 0.88	0.018
at 1.00	0.030

Fig. 5.21 Displacement at 40% load at 45°C and 55°C

➢ 60% load at 45°C and 55°C

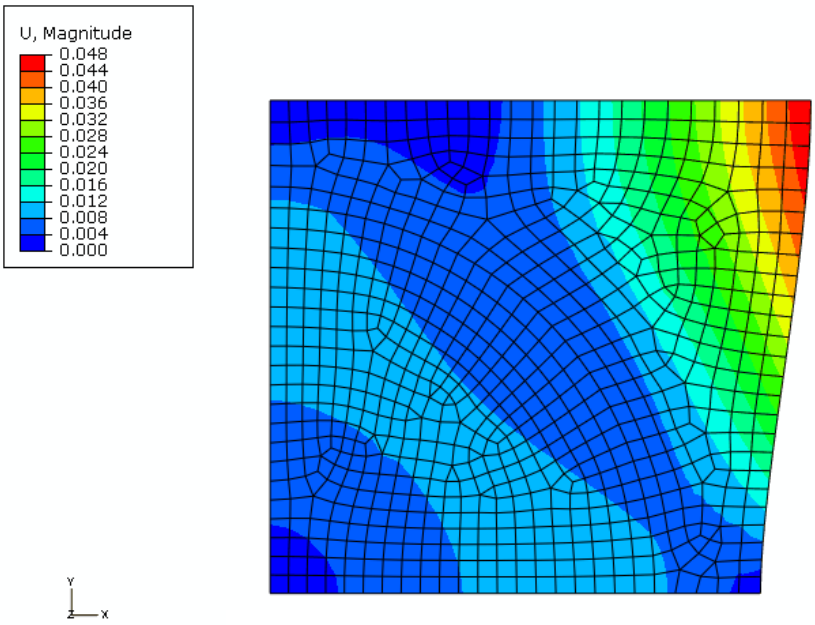

Distance in milli meter (top side)	Displacement milli meter
at 0.08	0
at 0.88	0.032
at 1.00	0.048

Fig. 5.22 Displacement at 60% load at 45°C and 55°C

➢ 80% load at 45°C and 55°C

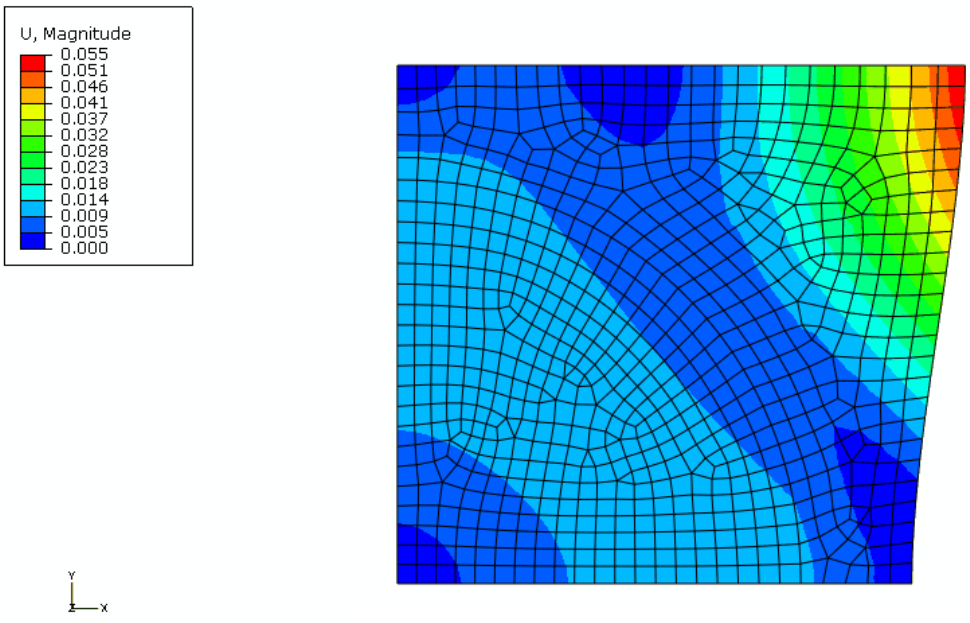

Distance in milli meter (top side)	Displacement milli meter
at 0.08	0
at 0.88	0.037
at 1.00	0.055

Fig. 5.23 Displacement at 80% load at 45°C and 55°C

COMPARISON OF TEMPERATURE AT INTEGRATION POINTS:

After 1 month:

- 20% ,40%,60% and 80% load at 45°C (318K)

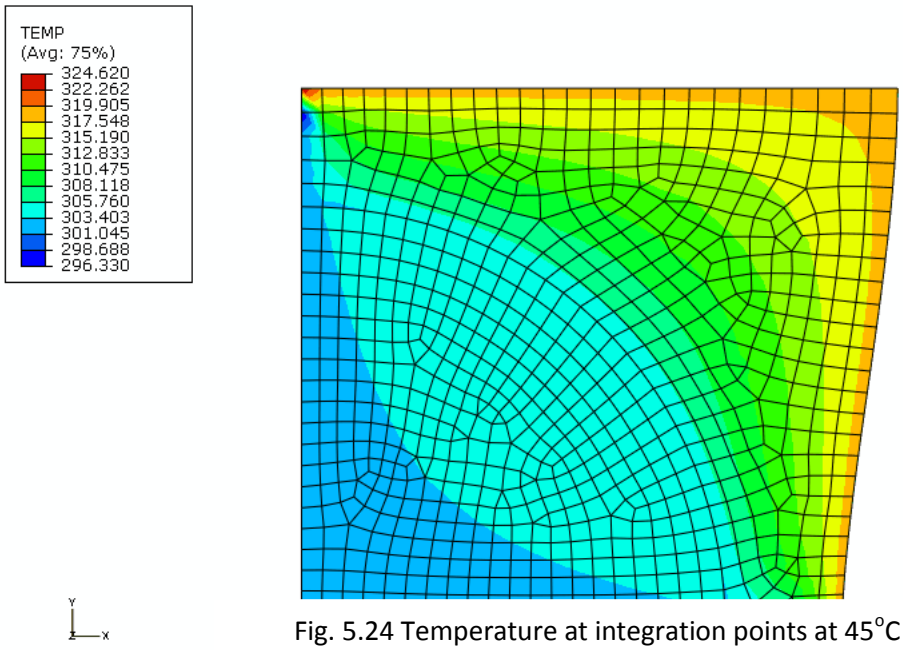

Distance in milli meter (middle side)	Temperature °K
at 0.08	303.4
at 0.88	310.4
at 1.00	317.5

Fig. 5.24 Temperature at integration points at 45°C for all loads

- 20% ,40%,60% and 80% load at 55°C (328K)

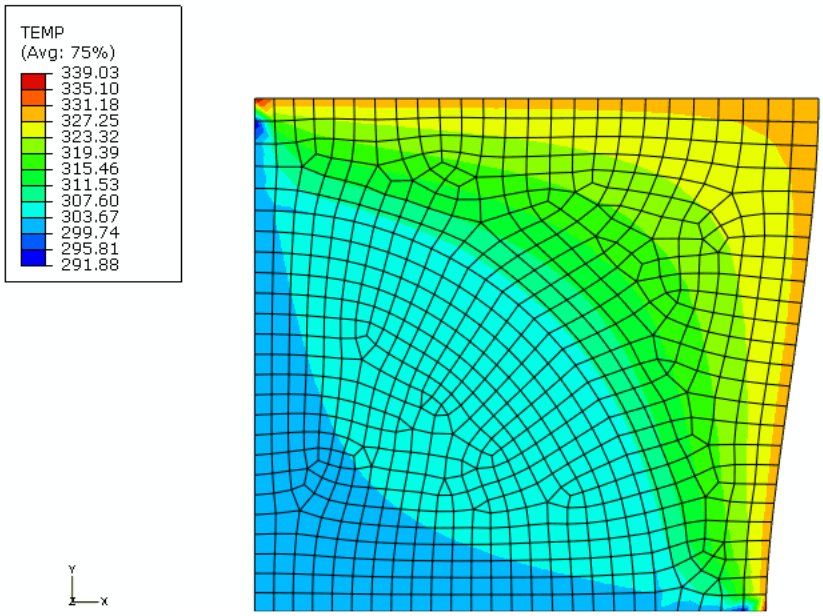

Distance in milli meter (middle side)	Temperature °K
at 0.08	303.6
at 0.88	315.4
at 1.00	327.2

Fig. 5.25 Temperature at integration points at 55°C for all loads

After 2 months:

- 20%,40%,60% and 80% load at 45°C (318K)

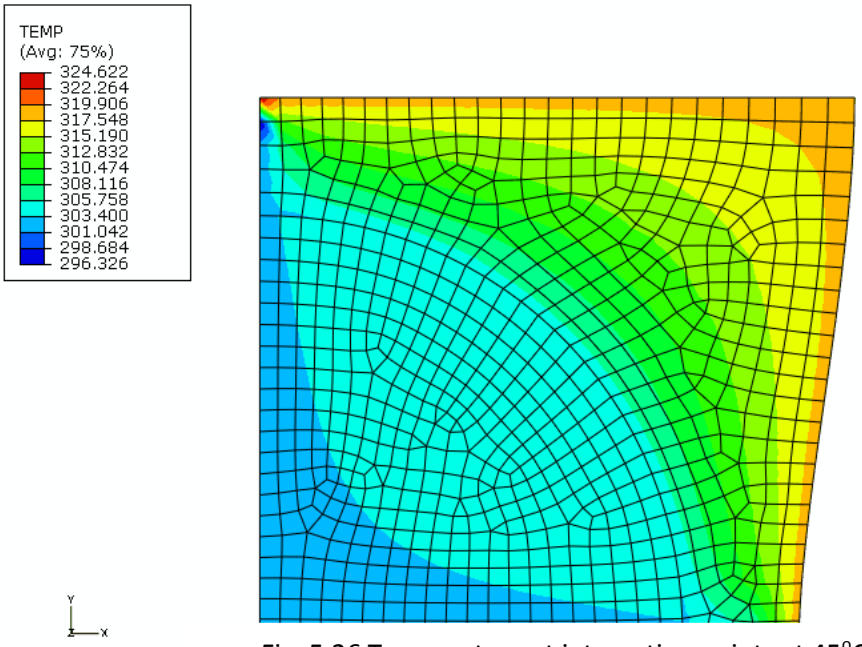

Distance in milli meter (middle side)	Temperature °K
at 0.08	303.4
at 0.88	312.4
at 1.00	317.5

Fig. 5.26 Temperature at integration points at 45°C for all loads

- 20% ,40%,60% and 80% load at 55°C (328K)

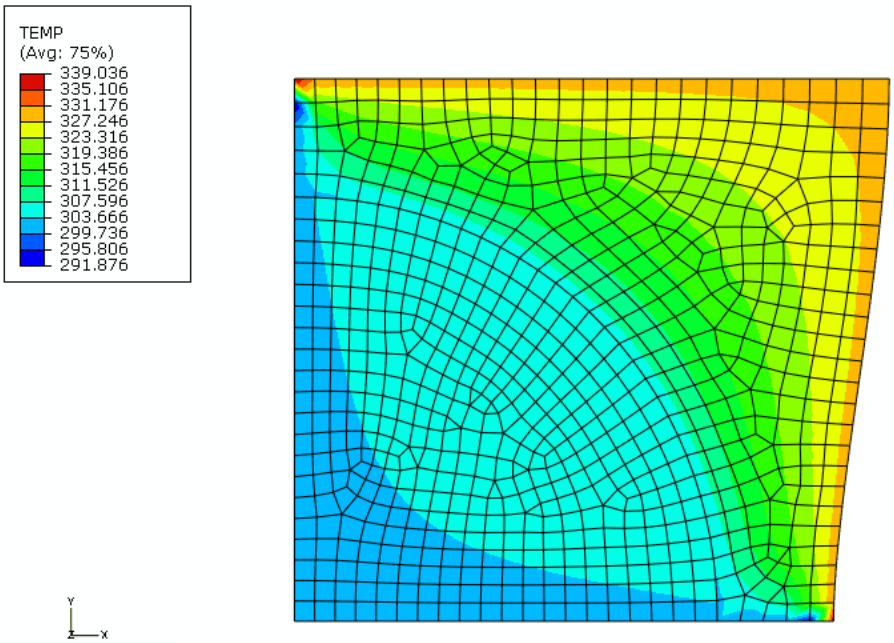

Distance in milli meter (middle side)	Temperature °K
at 0.08	303.6
at 0.88	319.3
at 1.00	327.2

Fig. 5.27 Temperature at integration points at 55°C for all loads

B) MASS DIFFUSION MOISTURE MODEL: Below are the results of the moisture modeling as per the parameters discussed earlier.

(a)

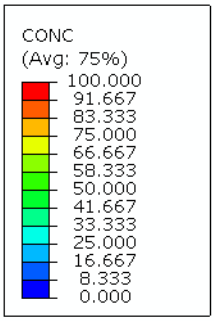

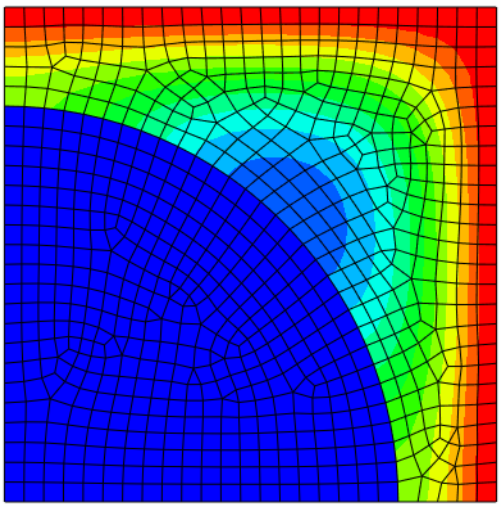

Distance in milli meter (top to bottom)	Concentration (%)
at 0.08	100.0
at 0.16	58.3
at 0.2	33.3

Fig. 5.28 Moisture concentration after 1 month

(b)

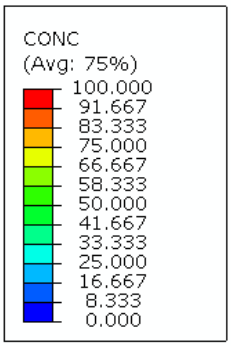

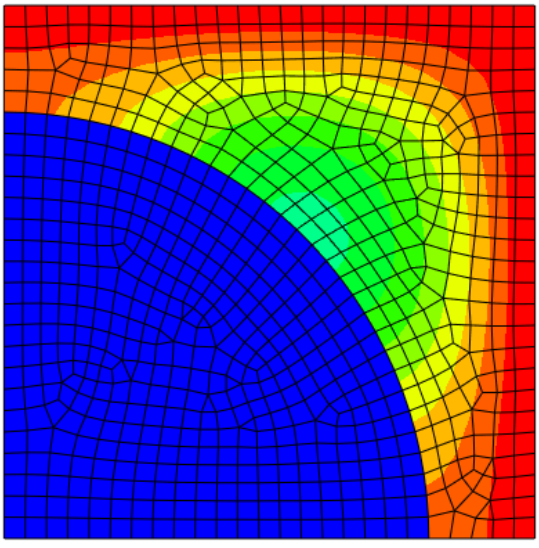

Distance in milli meter (top to bottom)	Concentration (%)
at 0.08	100.0
at 0.16	75.0
at 0.2	66.6

Fig. 5.29 Moisture concentration after 2 months

(c)

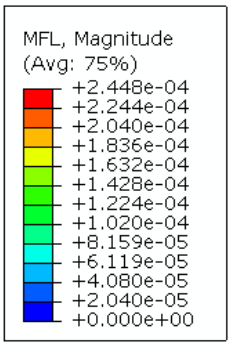

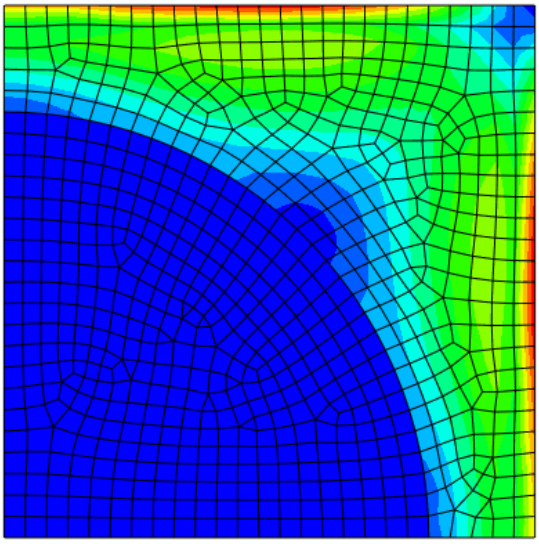

Distance in milli meter (top to bottom)	Mass flow rate (gm/sec)
at 0.04	2.44×10^{-4}
at 0.12	1.42×10^{-4}
at 0.32	4.08×10^{-5}

Fig. 5.30 Mass flow rate after 1 month

(d)

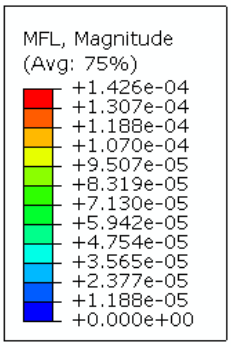

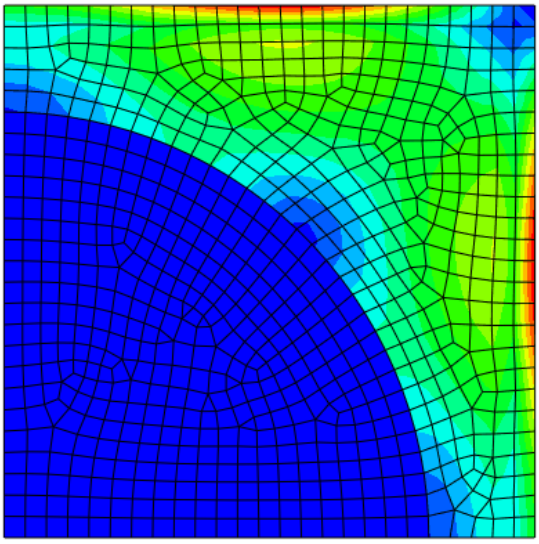

Distance in milli meter (top to bottom)	Mass flow rate (gm/sec)
at 0.04	1.426×10^{-4}
at 0.12	8.31×10^{-5}
at 0.32	2.37×10^{-5}

Fig. 5.31 Mass flow rate after 2 months

Graphical comparison of the results of the various modeling output parameters:

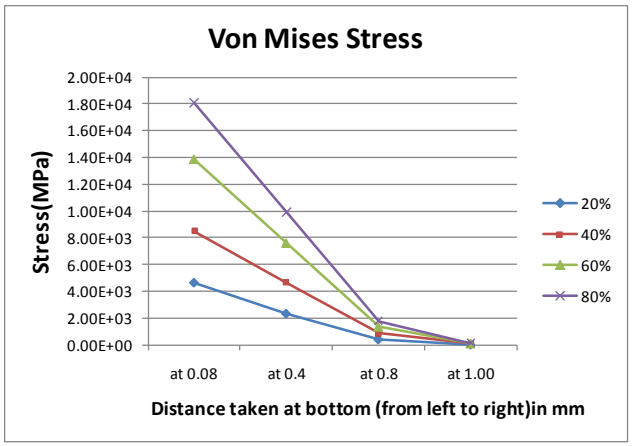

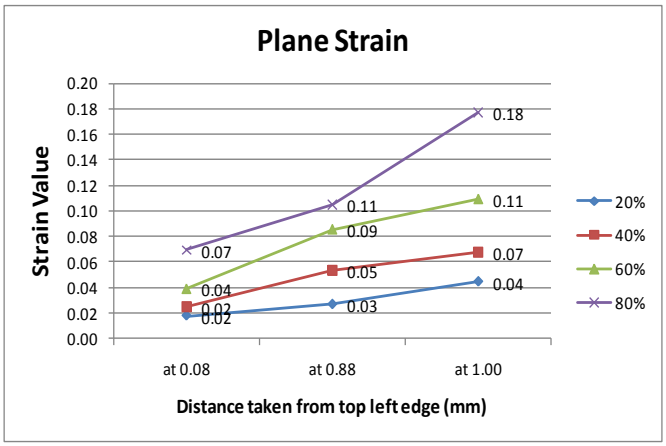

a) b)

Fig. 5.32 Comparison of (a) Von Mises stresses (b) Plane Strain at different load

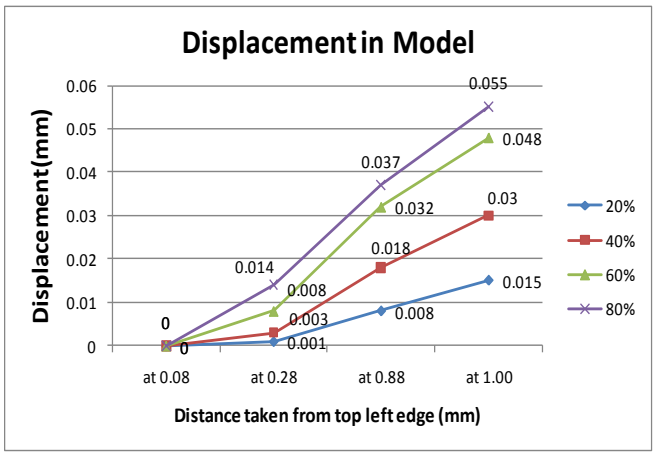

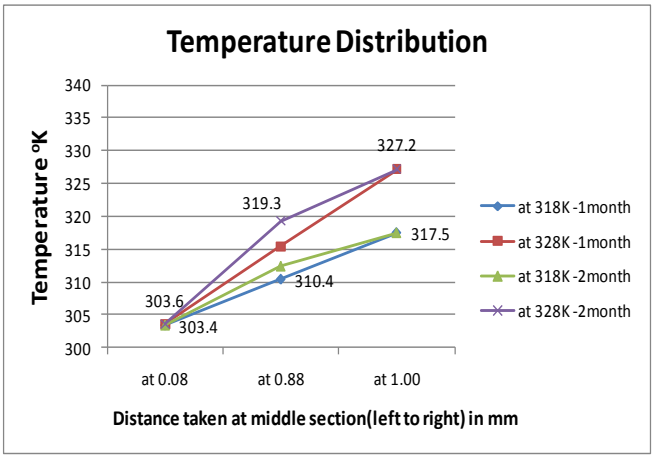

c) d)

Fig. 5.33 Comparison of (c) Displacement at various loads (d) Temperature distribution with respect to time

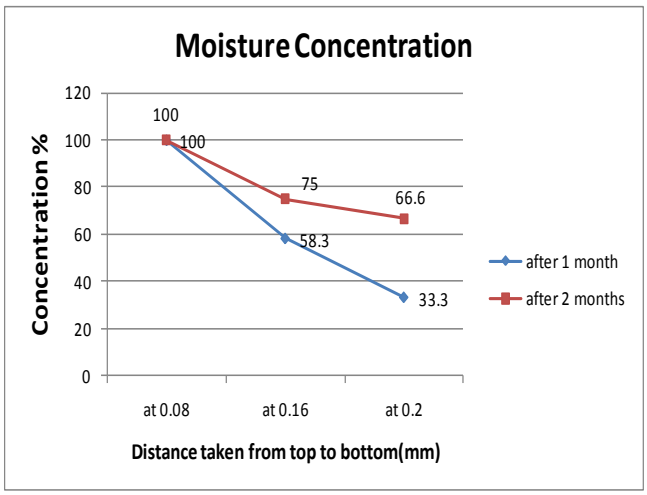

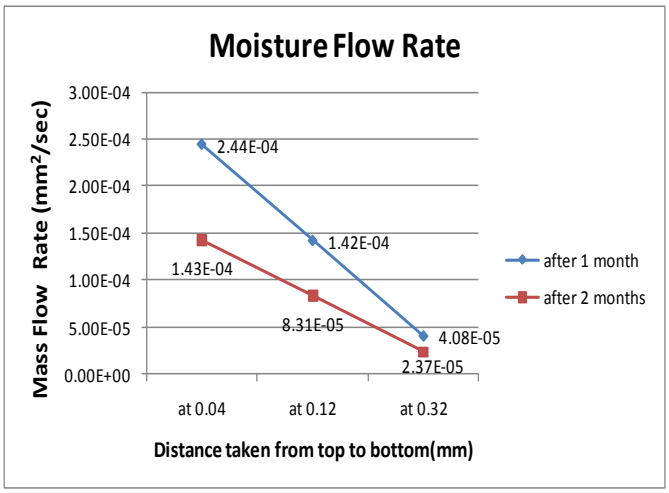

e) f)

Fig. 5.34 Comparison of (e) Moisture Concentration with respect to time (f) Moisture flow rate with respect to time

The summary of the mechanical loading applied on samples is discussed below in table T12 and that of moisture diffusion in table T13.

Table T12 Summary of the mechanical loading (percentage of U.T.L) of samples as per modelling:

Parameter	After 1 month and 2 month			
	20% load (at both 45°C & 55°C)	40% load (at both 45°C & 55°C)	60% load (at both 45°C & 55°C)	80% load (at both 45°C & 55°C)
Von Misses stress (Max) in MPa	4.59×10^{3}	9.26×10^{3}	1.51×10^{4}	1.97×10^{4}
In plane Strain (Max)	4.44×10^{-2}	6.78×10^{-2}	1.09×10^{-1}	1.77×10^{-1}
Displacement at nodes (Max) in mm	0.015	0.030	0.048	0.055

Table T13 Summary of the Moisture diffusion in samples with respect to time

Parameter	After 1 month	After 2 months
Mass flow rate (gms/sec)	2.45×10^{-4}	1.43×10^{-4}
Concentration (%)	100% near edges	100% near edges

CHAPTER 6 TESTING RESULTS AND DISCUSSIONS

6.1 TESTING MACHINES USED IN THE EXPERIMENTATION:

Fig. 6.1 Tensile testing machine used for testing

Fig. 6.2 Gripped specimen on the machine

A Universal Tensile testing machine (Fig.6.1) was used for the testing of the GFRP samples for its tensile strength. All the pre-stretched samples (Fig. 6.2) were tested until they break indicating the peak load and ultimate stress value (Fig.6.3) they can bear after such degradation.

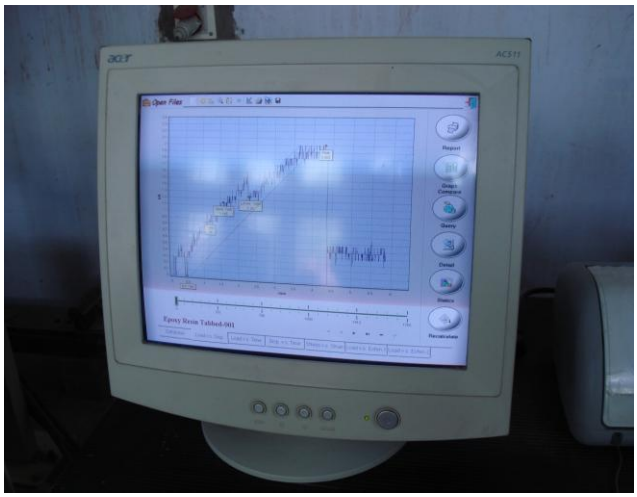

Fig. 6.3 Simultaneous display of output as test was conducted

Fig. 6.4 SEM being conducted on machine

A Scanning Electron Microscope (Fig.6.4) was used to study the condition of fibre and matrix after the specified time period.

6.2 PICTORIAL COMPARISON AND OBSERVATION OF SAMPLES BEFORE AND AFTER THEIR FAILURE WITH RESPECT TO PROGRESSING TIME:

A) Initial sample image before they were immersed in water:

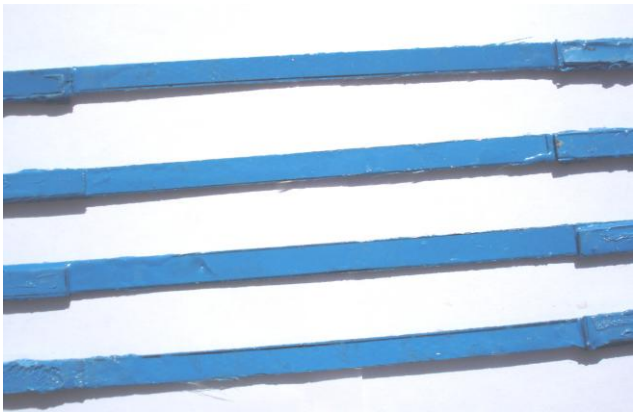

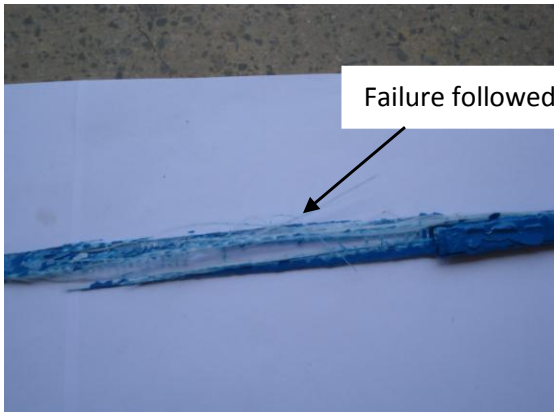

(a) (b)

Fig. 6.5 Shows condition of sample at the start of the experimentation (a) Before test (b) After test

B) Sample after one month of degradation:

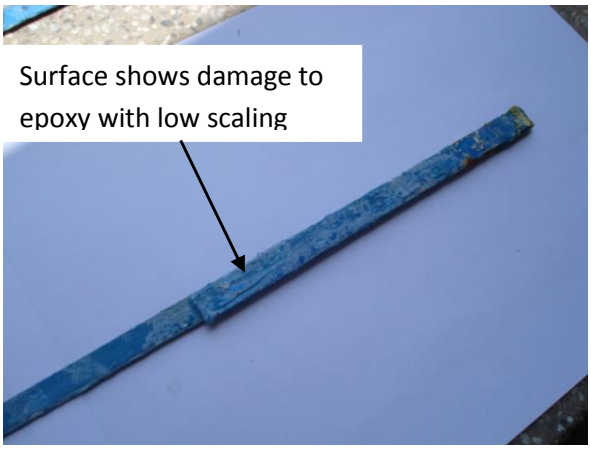

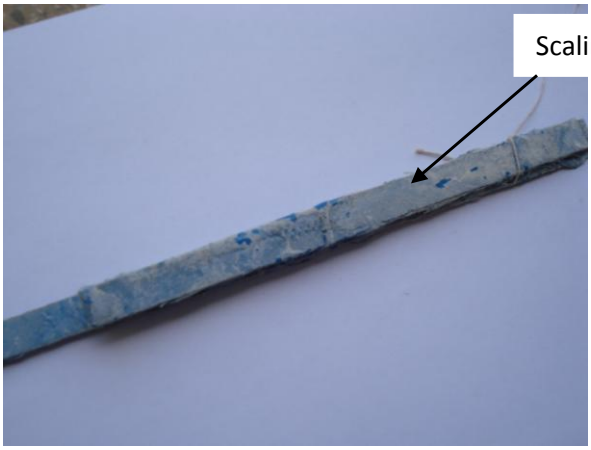

(c) (d)

Fig. 6.6 Shows condition of sample taken out after one month (c) NaOH bath (d) Water bath

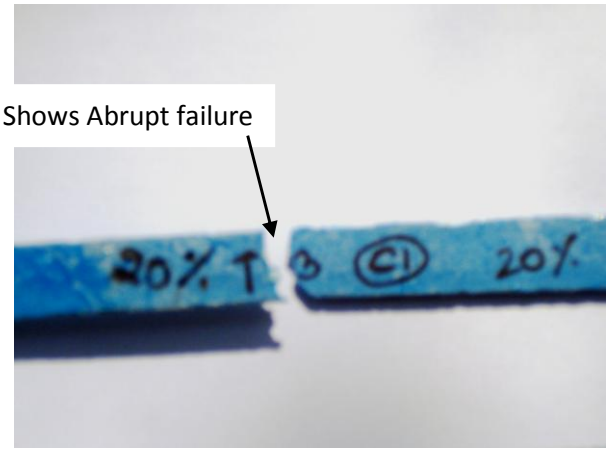

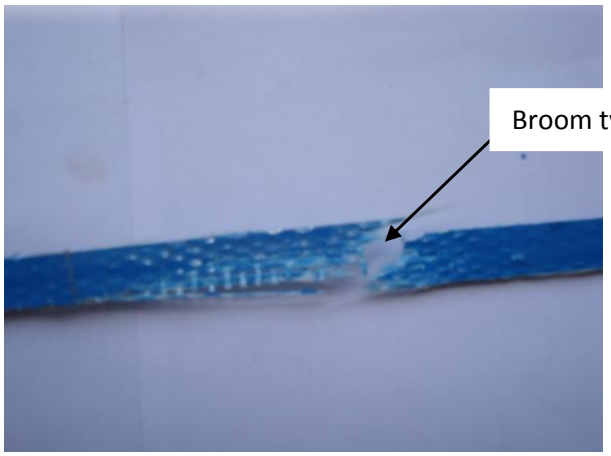

(e) (f)

Fig. 6.7 Shows sample failure after tensile testing held for one month time (e) NaOH bath (f) Water bath

C) Sample after two months of degradation:

(g) (h)

Fig. 6.8 Shows condition of sample taken out after two months (g) NaOH bath (h) Water Bath

(i) (j)

Fig. 6.9 Shows sample failure after tensile testing held for two month time (i) NaOH bath (j) Water Bath

VISUAL OBSERVATIONS:

As per the visual observation the initial sample (Fig.6.5) had fine shiny epoxy coating and the failure of sample also showed broom type failure which is an indicative of good load failure.

After 1 month (Fig.6.6 and 6.7) there was scale formation on the samples, with water immersed samples showing heavy scale formation. Surface observation showed that epoxy had lost its shine and outer edges on either side showed little fanning out. But still after bending (by hands) the epoxy showed considerable strength and flexibility. The condition of aqueous NaOH immersed samples had gone very bad. The samples had lost their flexibility and we can easily break the samples by bending with hands like breaking a chips wafer. The epoxy had gone very brittle and top surface of some samples showed the chipping out of top surface of epoxy coating.

After 2 months (Fig.6.8 and 6.9) same observations were noted with more scale formation on water immersed samples and damage especially on aqueous NaOH immersed samples.

6.3 DETAILS OF S.E.M IMAGES AND E.D.X. RESULTS OF ALL SAMPLES WITH RESPECT TO TIME AT EACH LOAD PERCENTAGE OF U.T.L.

The results of the tensile strength of various samples along with their SEM details are shown as follows:

6.3.1 S.E.M. AND E.D.X. BEFORE THE START OF EXPERIMENTATION:

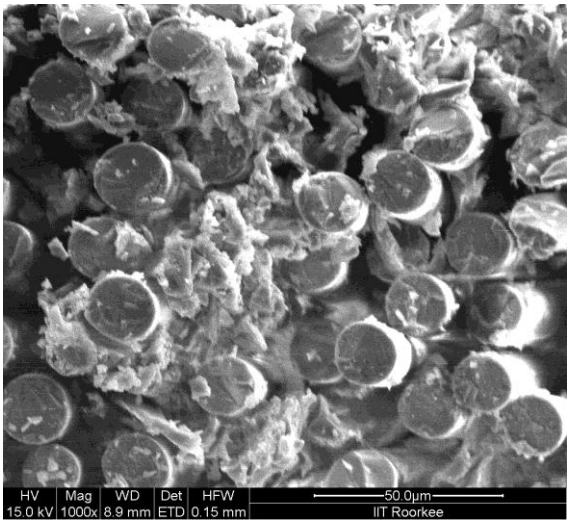

Fig. 6.10 SEM of cross-section

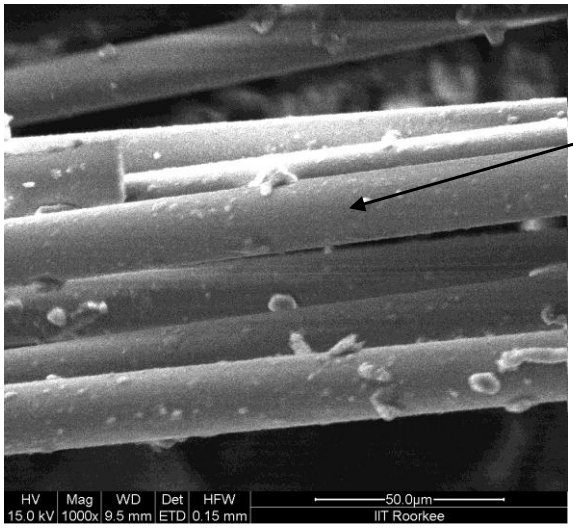

Fig. 6.11 SEM of longitudinal section

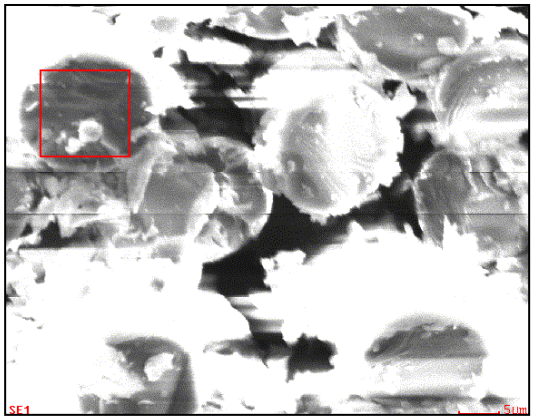

Fig. 6.12 Position of EDX shown in image (in Black Box)

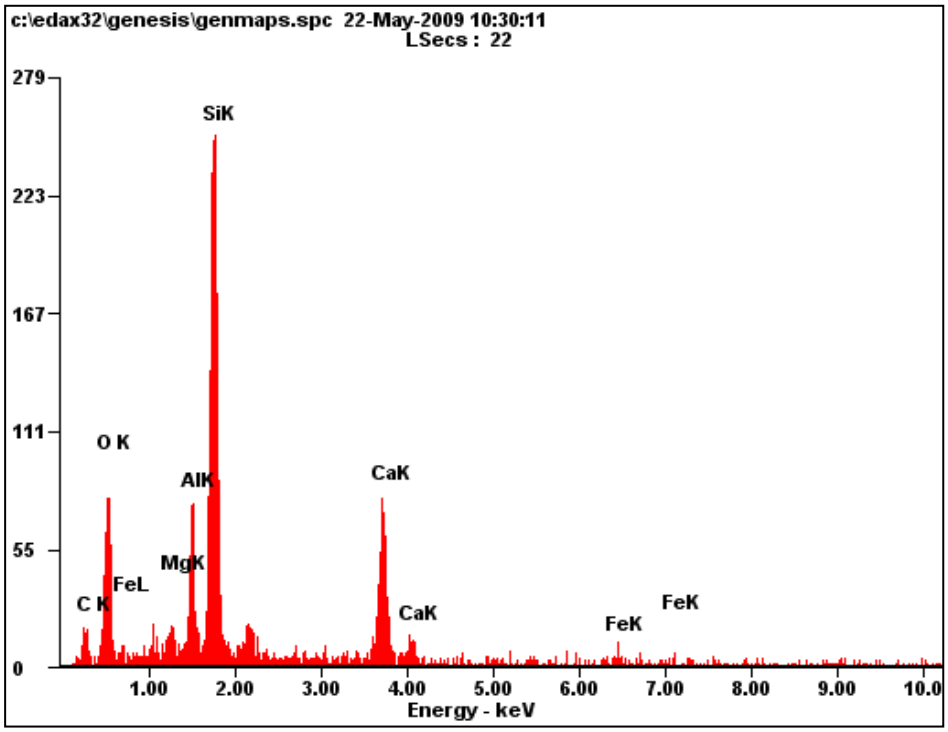

a)

Element	*Wt%*
CK	10.06
OK	28.05
MgK	01.14
AlK	06.95
SiK	31.10
CaK	18.75
FeK	03.93

b)

Fig.6.13 (a) Energy vs Electron volt graph at start, (b) Element percentage taken by EDX

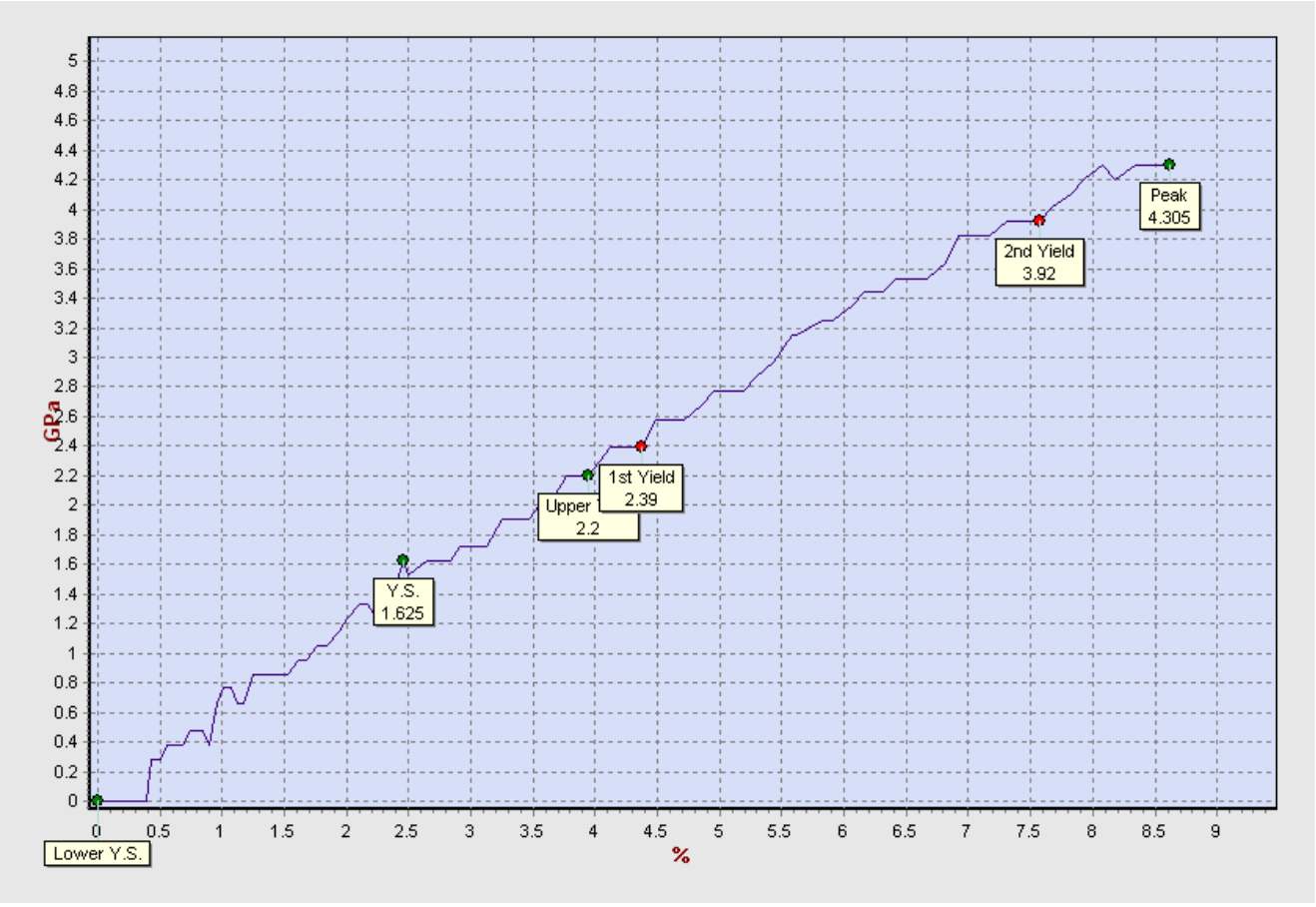

Fig.6.14 Tensile test result of the sample before the start of experimentation

6.3.2 S.E.M. IMAGES AFTER ONE MONTH:

A) S.E.M. AND E.D.X. RESULTS OF WATER TANK T1 (after 1 month)

Holding Parameters:
Plain water bath
Time: 1 month
Temperature: 45^{o}C

1) The results of specimen which were subjected to **20% loading** (T1, 1month) are shown below:

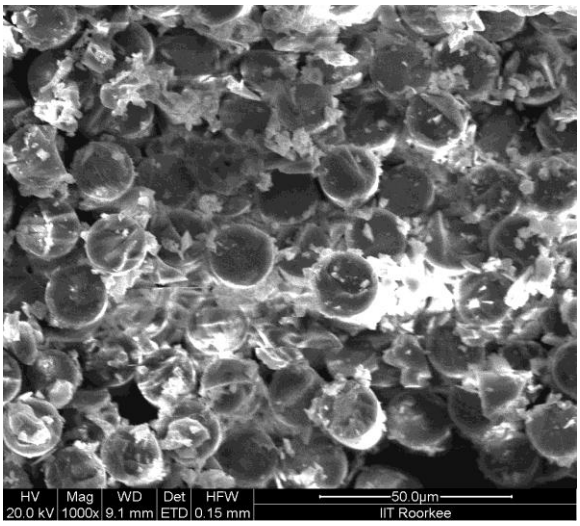

Fig.6.15 SEM image of specimen at 20% load

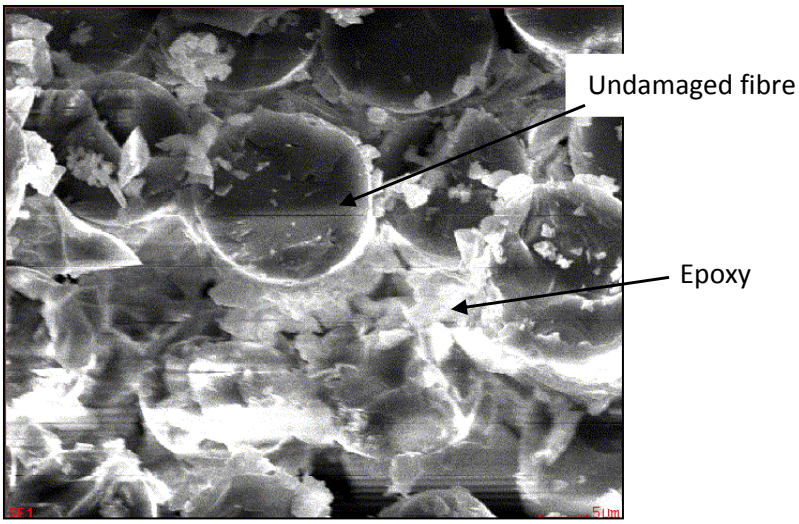

Fig.6.16 SEM image of specimen for EDX

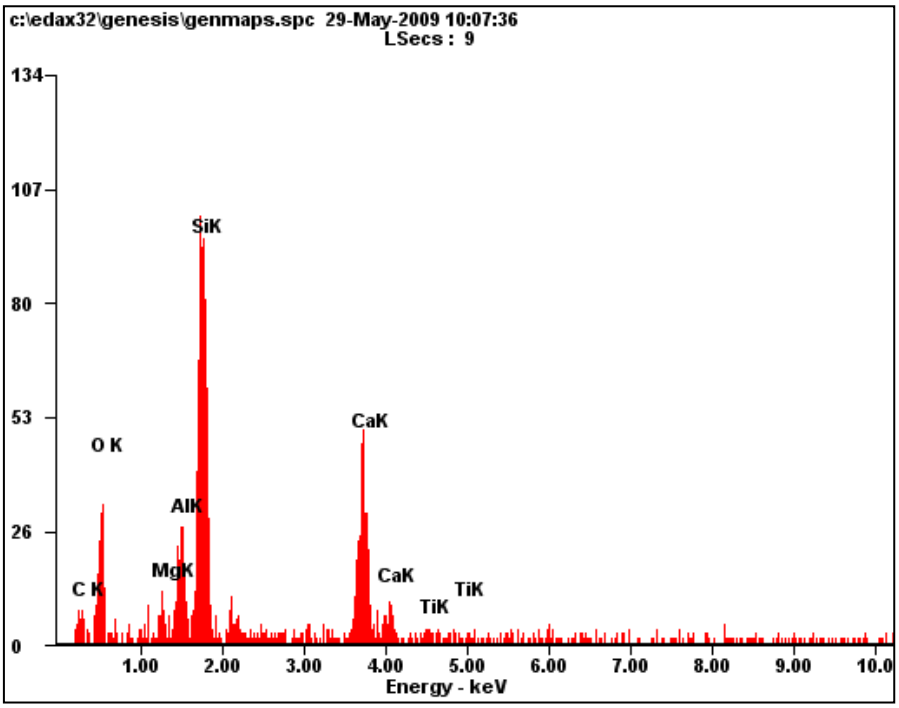

a)

Element	*Wt%*
CK	15.49
OK	31.31
MgK	02.21
AlK	05.96
SiK	26.55
CaK	16.64
TiK	00.84

b)

Fig.6.17 (a) Energy vs Electron volt graph for 20% load, (b) Element percentage taken by EDX

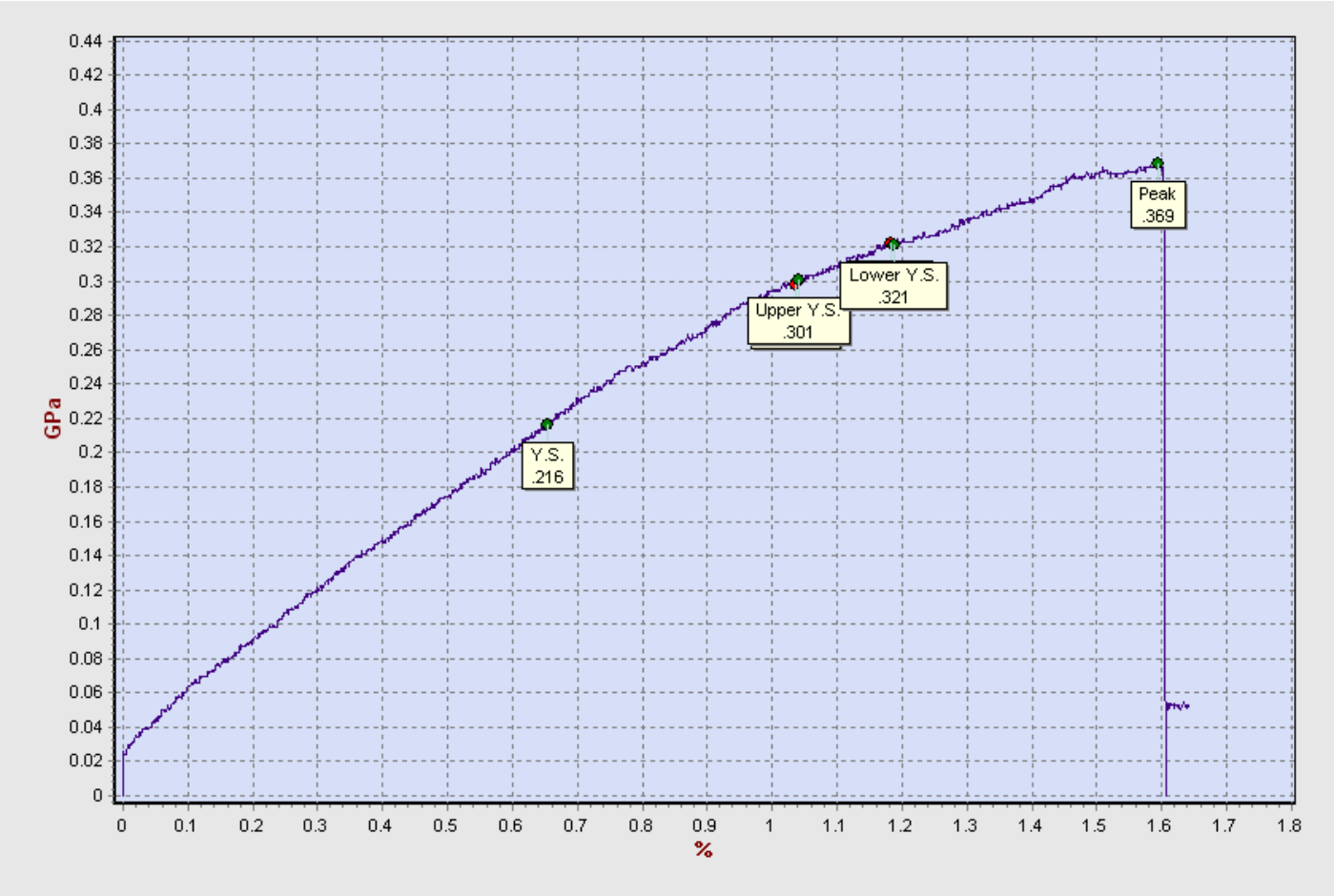

Fig.6.18 Stress vs Strain graph of sample loaded at 20% of U.T.L (Water Tank T1)

2) The results of specimen which were subjected to **40% loading** (T1, 1month) are shown below:

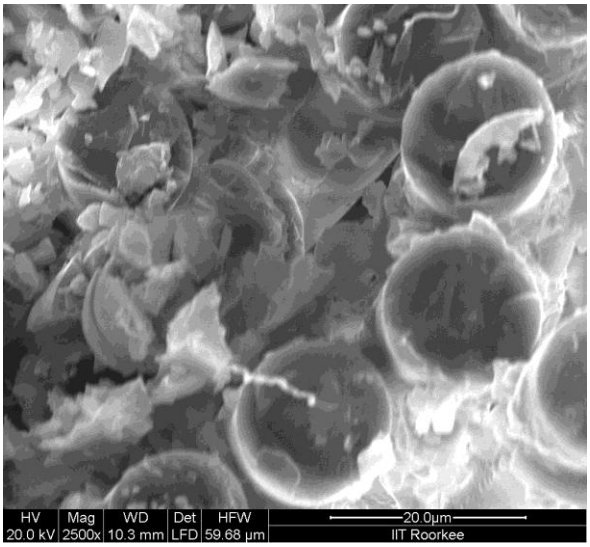

Fig.6.19 SEM image of specimen at 40% load

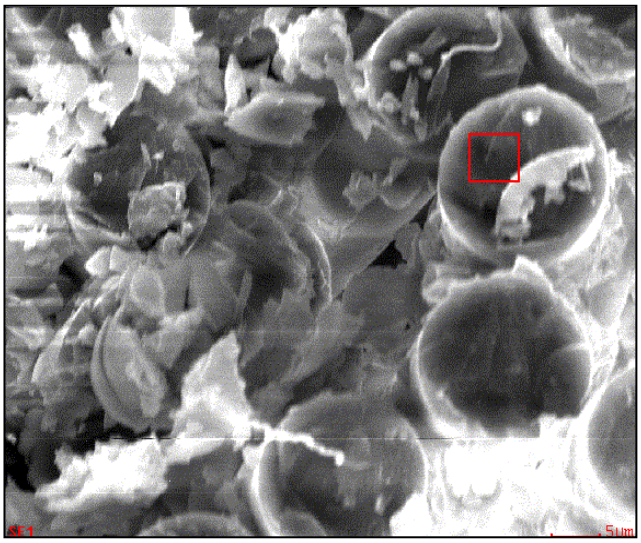

Fig.6.20 SEM image of specimen for EDX

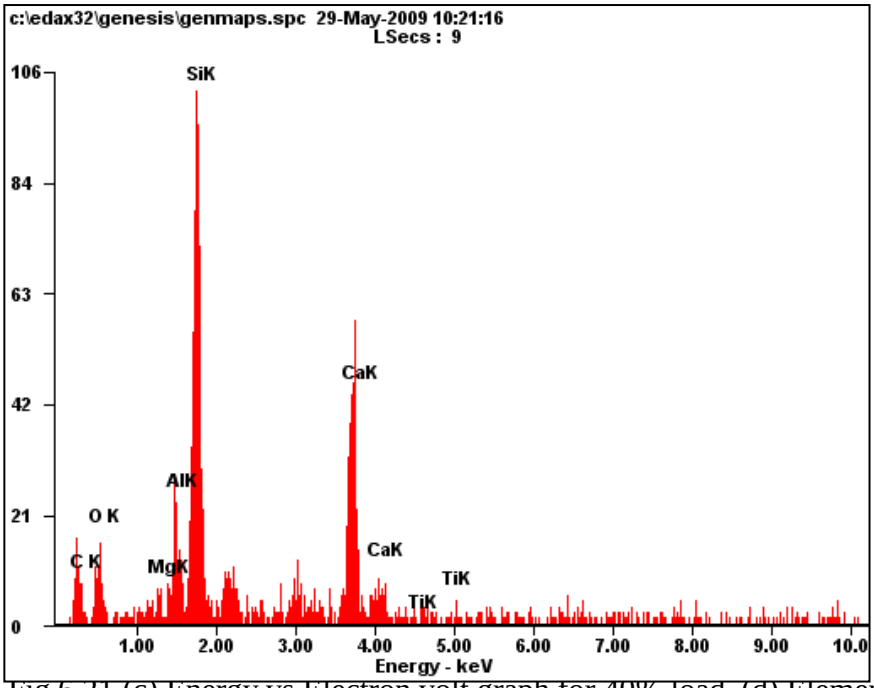

Element	*Wt%*
CK	35.28
OK	16.85
MgK	01.61
AlK	04.80
SiK	21.84
CaK	16.14
TiK	01.49

d)

Fig.6.21 (c) Energy vs Electron volt graph for 40% load, (d) Element percentage taken by EDX

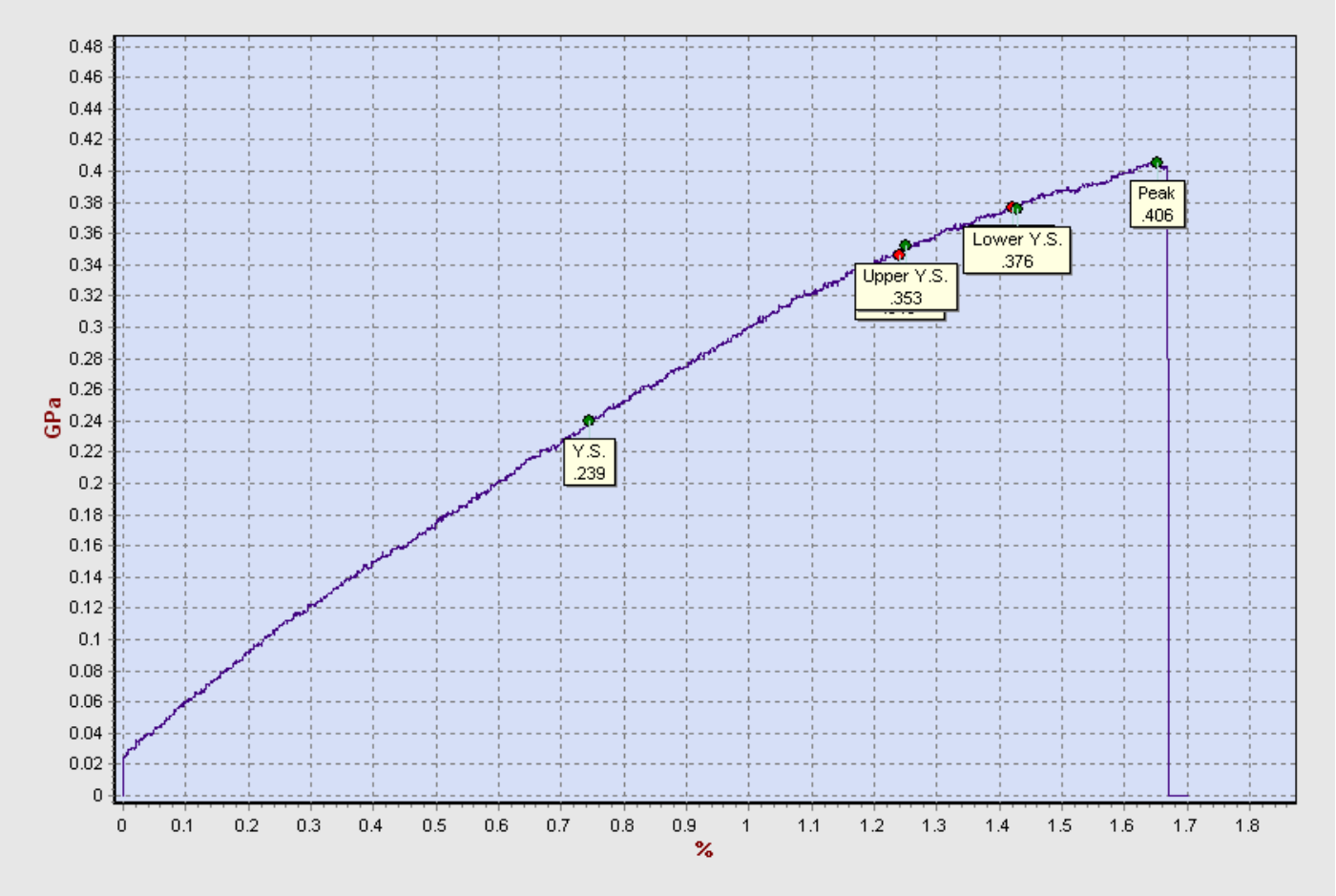

Fig.6.22 Stress vs Strain graph of sample loaded at 40% of U.T.L (Water Tank T1)

3) The results of specimen which were subjected to **60% loading** (T1, 1month) are shown below:

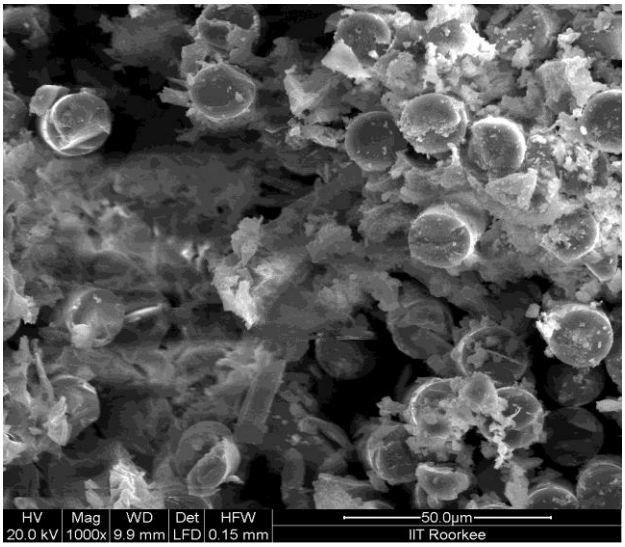

Fig.6.23 SEM image of specimen at 60% load

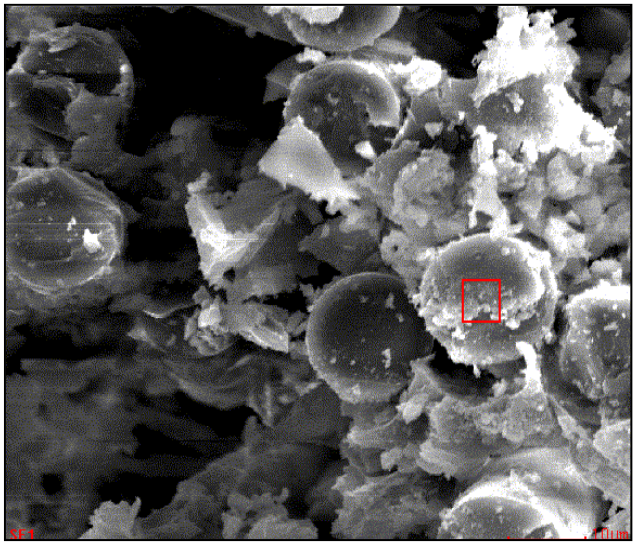

Fig. 6.24 SEM image of specimen for EDX

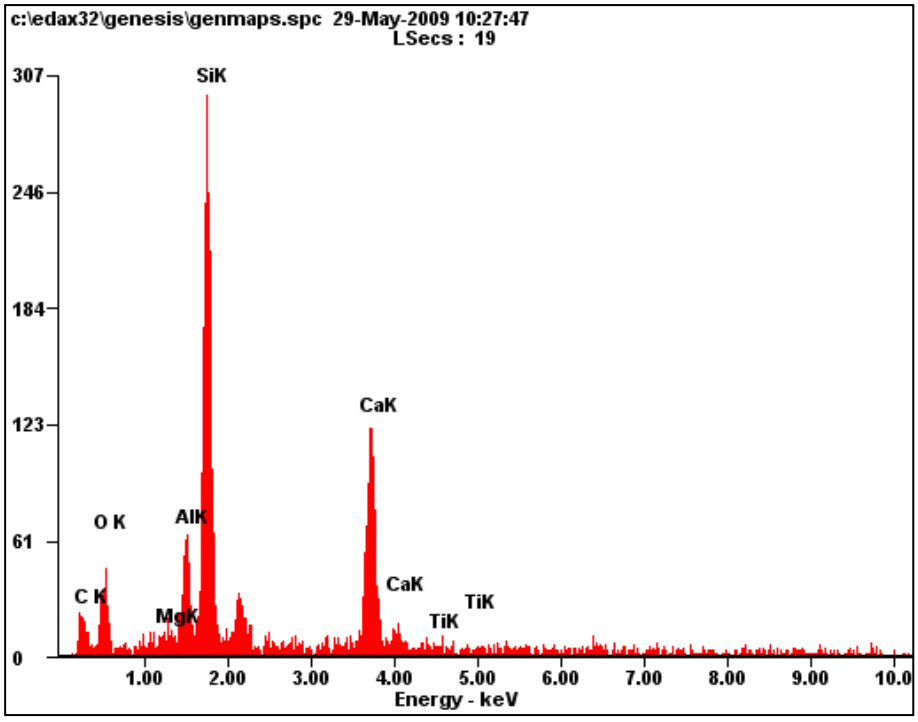

Element	*Wt%*
CK	26.01
OK	22.24
MgK	01.01
AlK	05.57
SiK	25.16
CaK	16.96
TiK	01.05

e) f)

Fig. 6.25 (e) Energy vs Electron volt graph for 60% load, (f) Element percentage taken by EDX

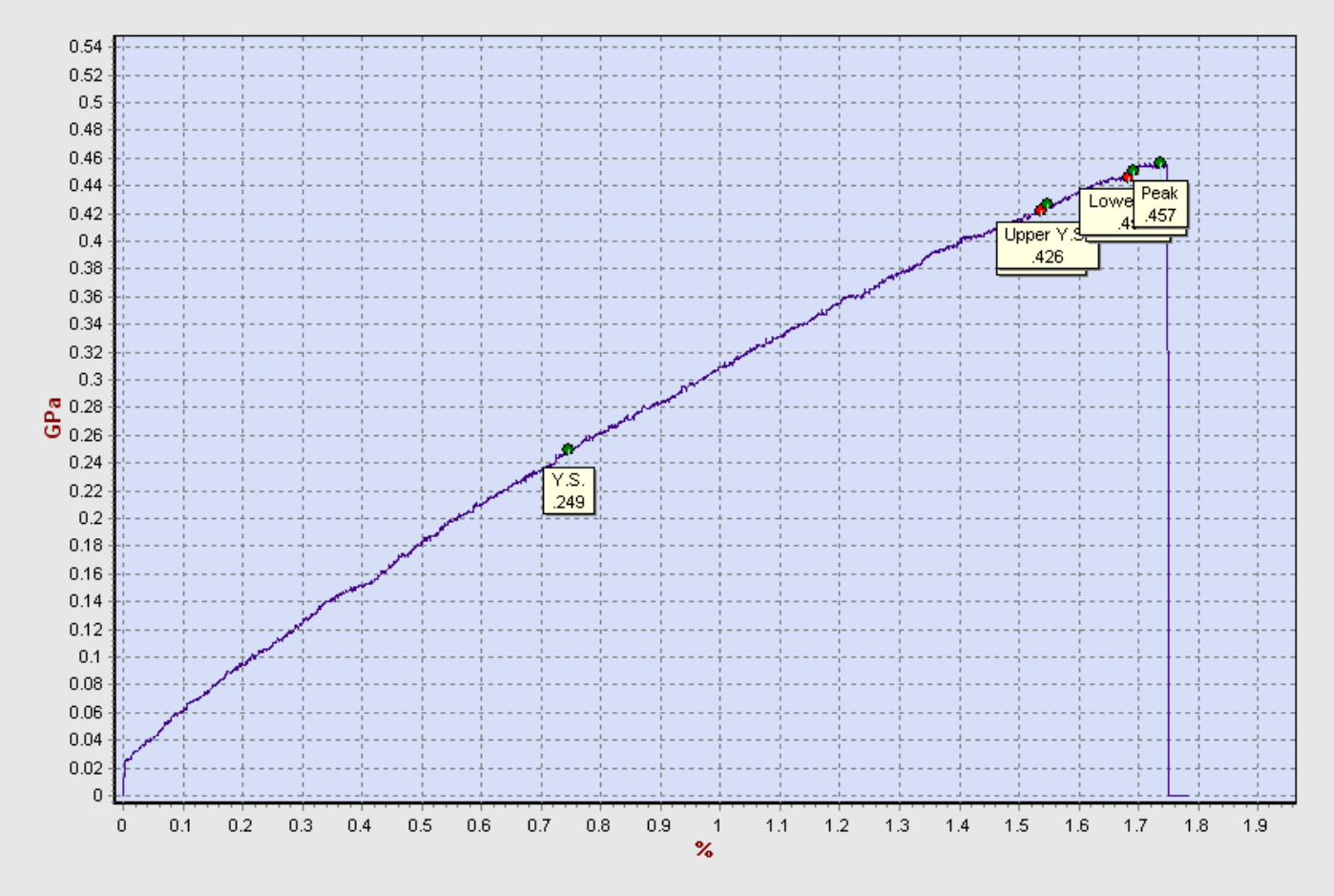

Fig.6.26 Stress vs Strain graph of sample loaded at 60% of U.T.L (Water Tank T1)

4) The results of specimen which were subjected to **80% loading** (T1, 1month) are shown below

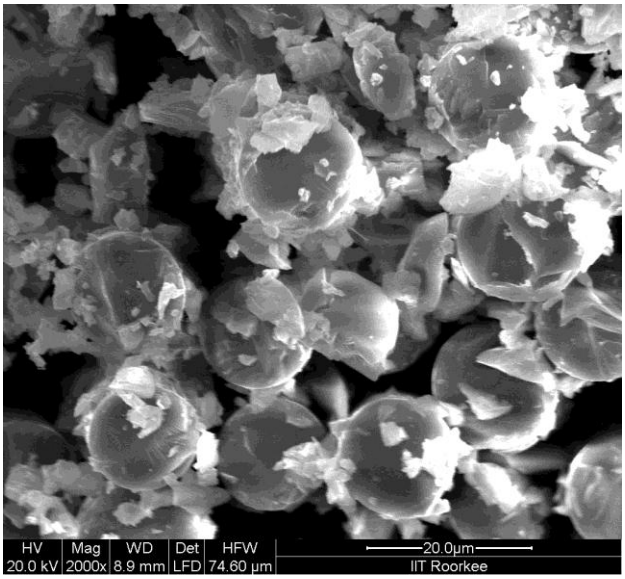

Fig.6.27 SEM image of specimen at 80% load

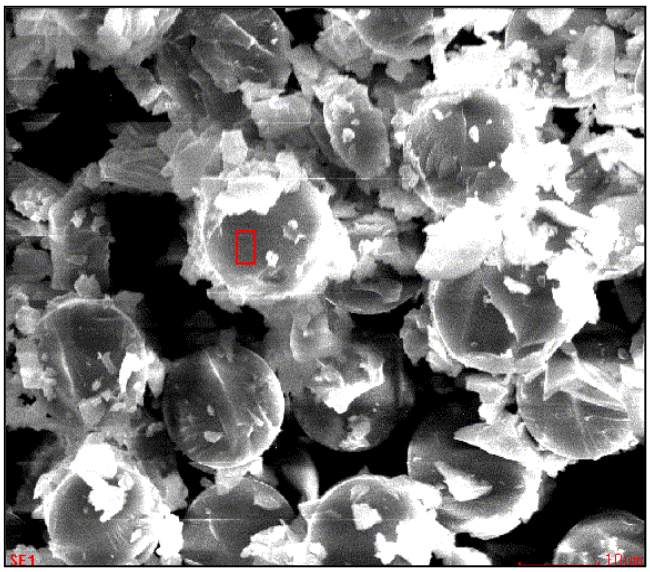

Fig.6.28 SEM image of specimen for EDX

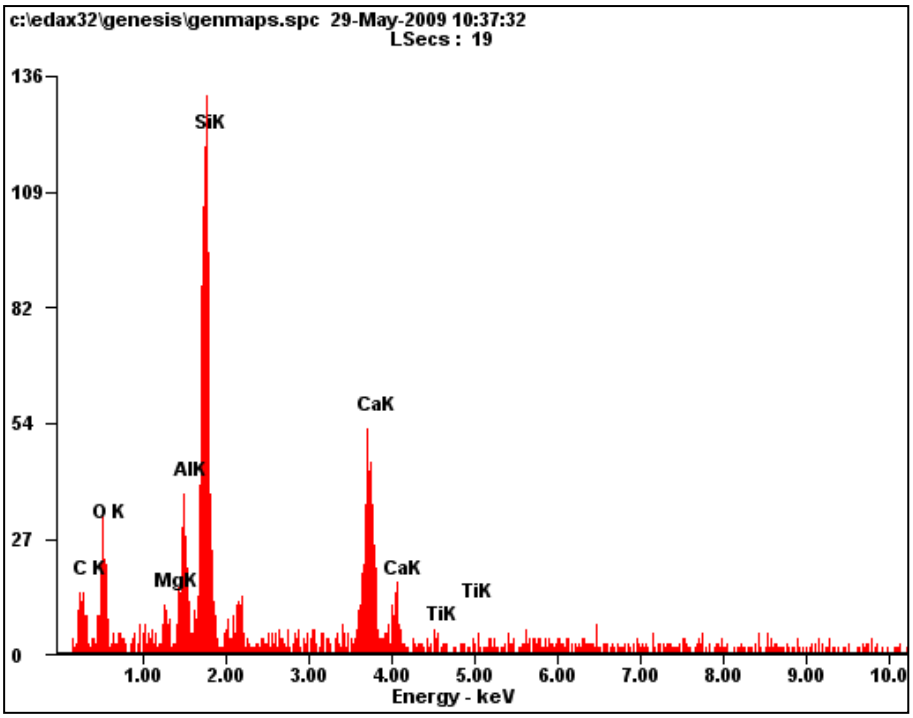

Element	*Wt%*
CK	26.82
OK	25.31
MgK	01.80
AlK	05.71
SiK	23.54
CaK	15.06
TiK	00.75

g) h)

Fig.6.29 (g) Energy vs Electron volt graph for 80% load, (h) Element percentage taken by EDX

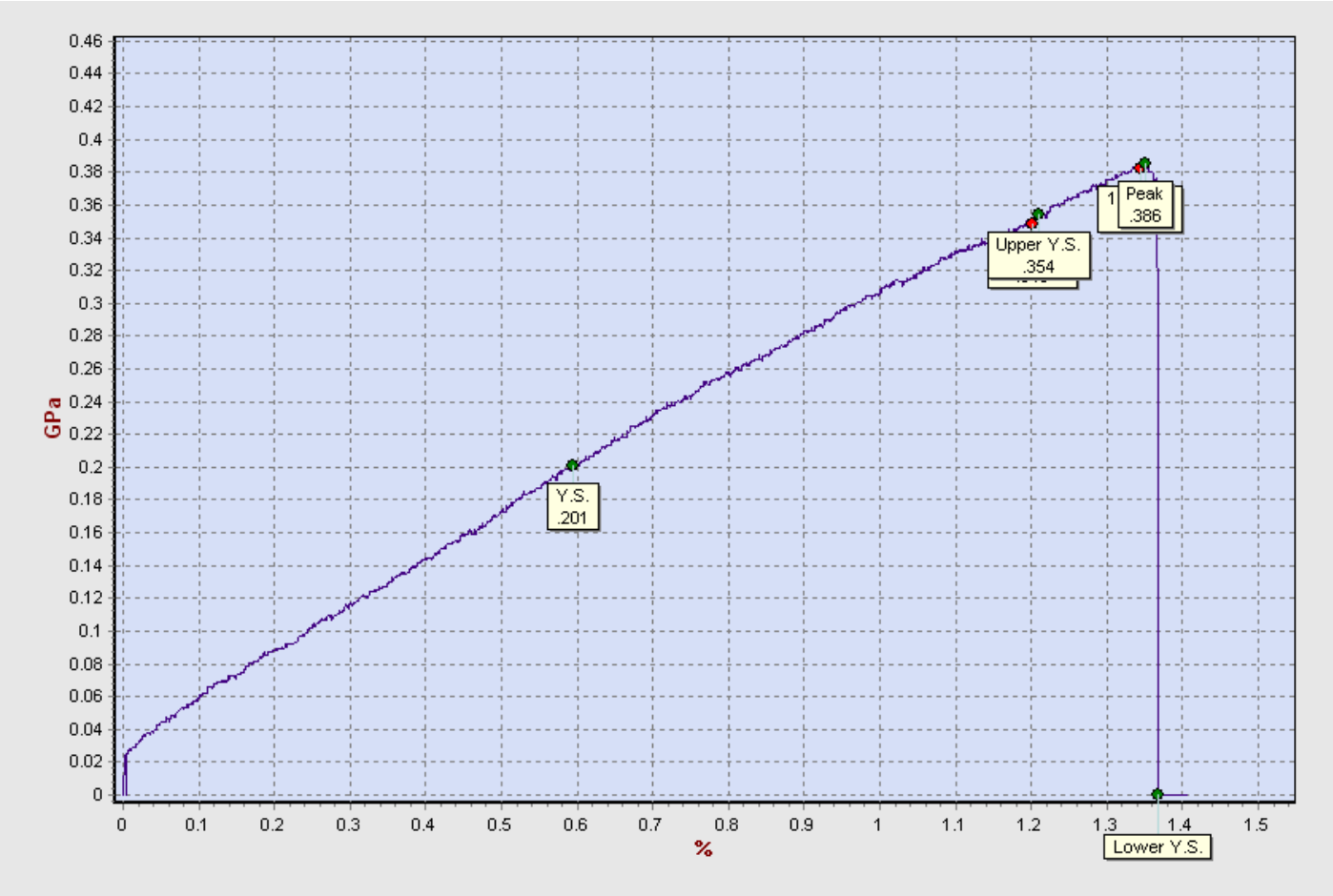

Fig.6.30 Stress vs Strain graph of sample loaded at 80% of U.T.L (Water Tank T1)

B) S.E.M. AND E.D.X. RESULTS OF NaOH TANK T2 (after 1 month)

Holding Parameters:
NaOH bath
Time: 1 month
Temperature: 45^{o}C

1) The results of specimen which were subjected to **20% loading** (T2, 1month) are shown below:

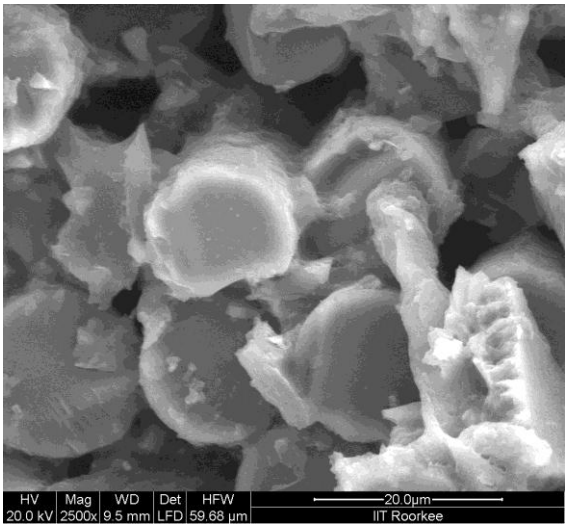

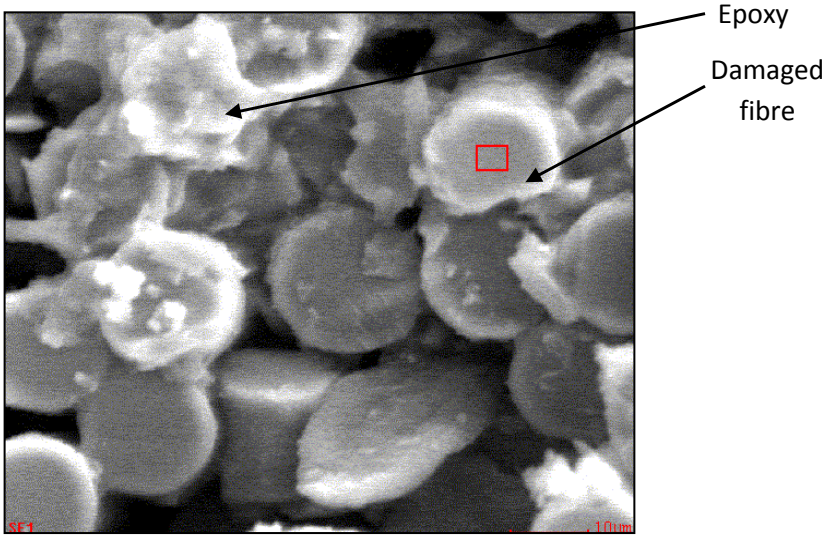

Fig.6.31 SEM image of specimen at 20% load Fig.6.32 SEM image of specimen for EDX

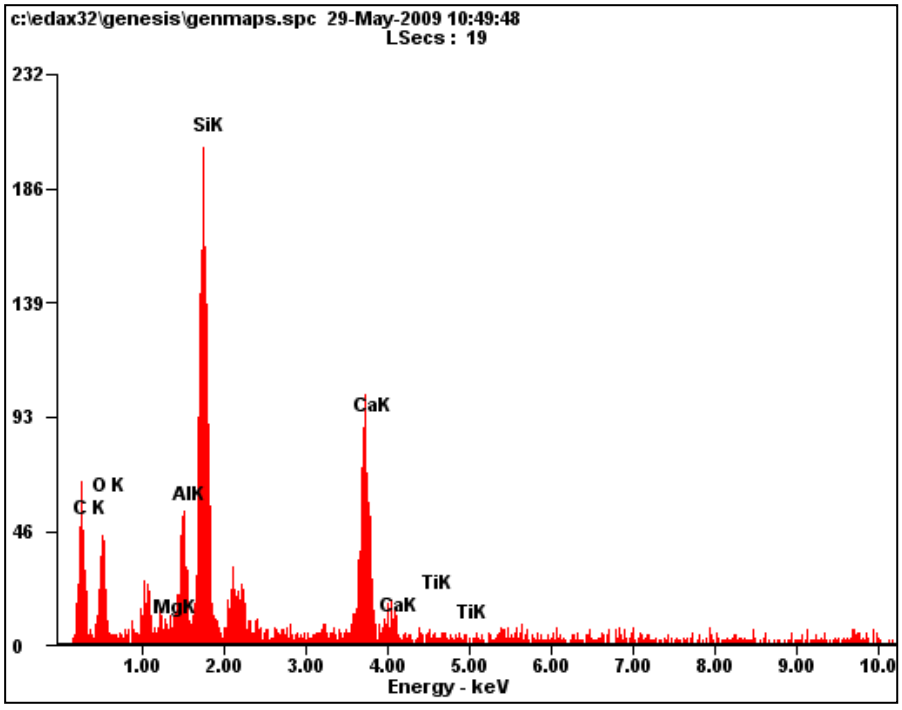

a)

Element	*Wt%*
CK	44.45
OK	19.84
MgK	00.75
AlK	03.84
SiK	16.72
CaK	12.77
TiK	00.63

b)

Fig.6.33 (a) Energy vs Electron volt graph for 20% load, (b) Element percentage taken by EDX

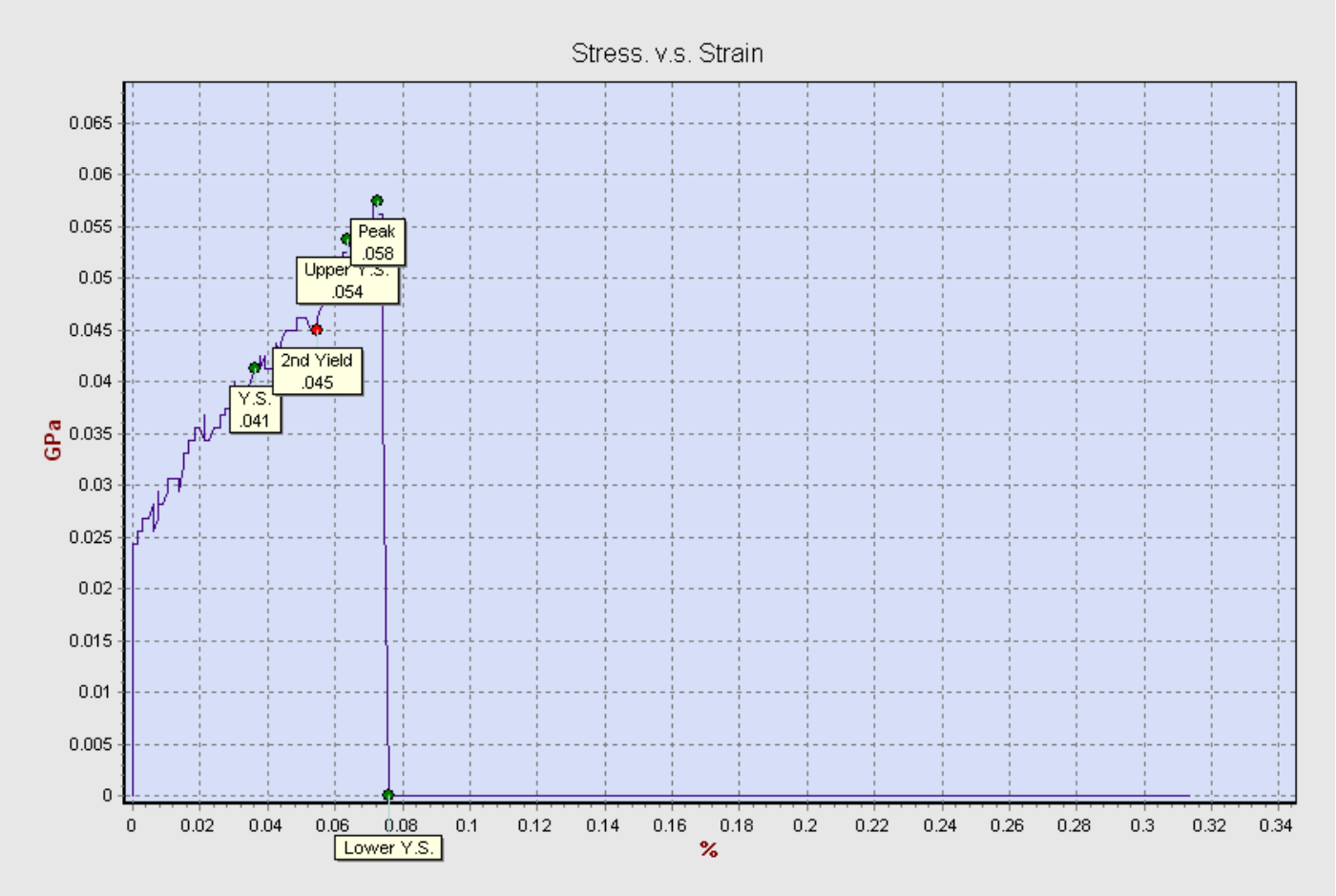

Fig.6.34 Stress vs Strain graph of sample loaded at 20% of U.T.L (NaOH Tank T2)

2) The results of specimen which were subjected to **40% loading** (T2, 1month) are shown below:

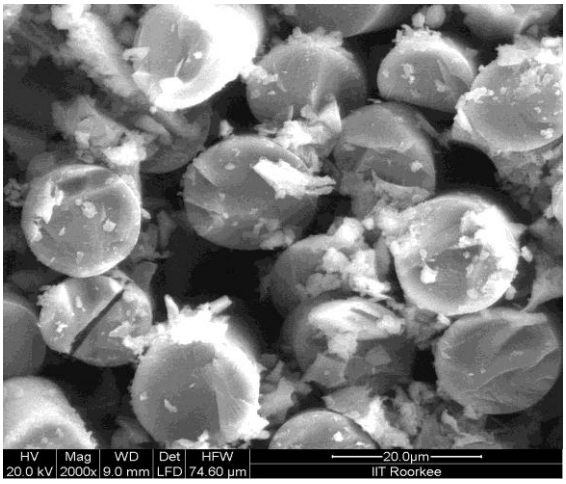

Fig.6.35 SEM image of specimen at 40% load

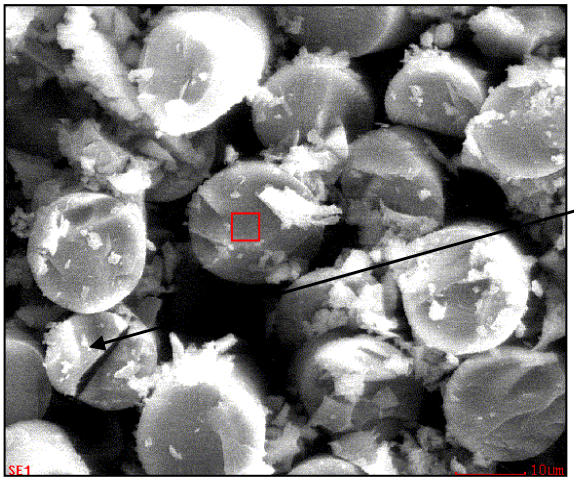

Fig.6.36 SEM image of specimen for EDX

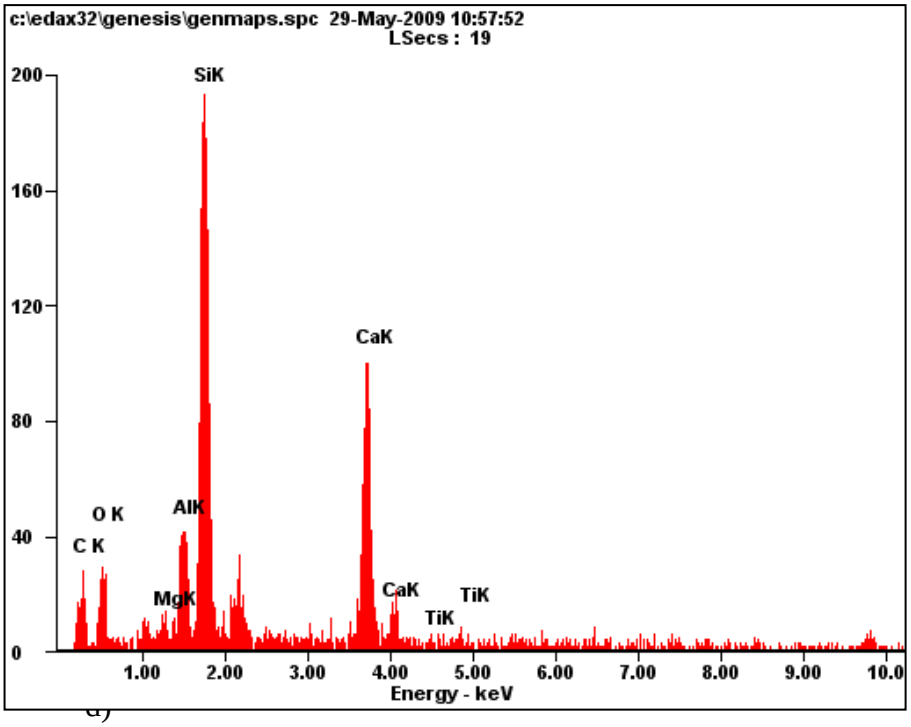

d)

Element	*Wt%*
CK	30.92
OK	20.37
MgK	01.27
AlK	05.36
SiK	23.55
CaK	16.82
TiK	00.71

Fig.6.37 (c) Energy vs Electron volt graph for 40% load, (d) Element percentage taken by EDX

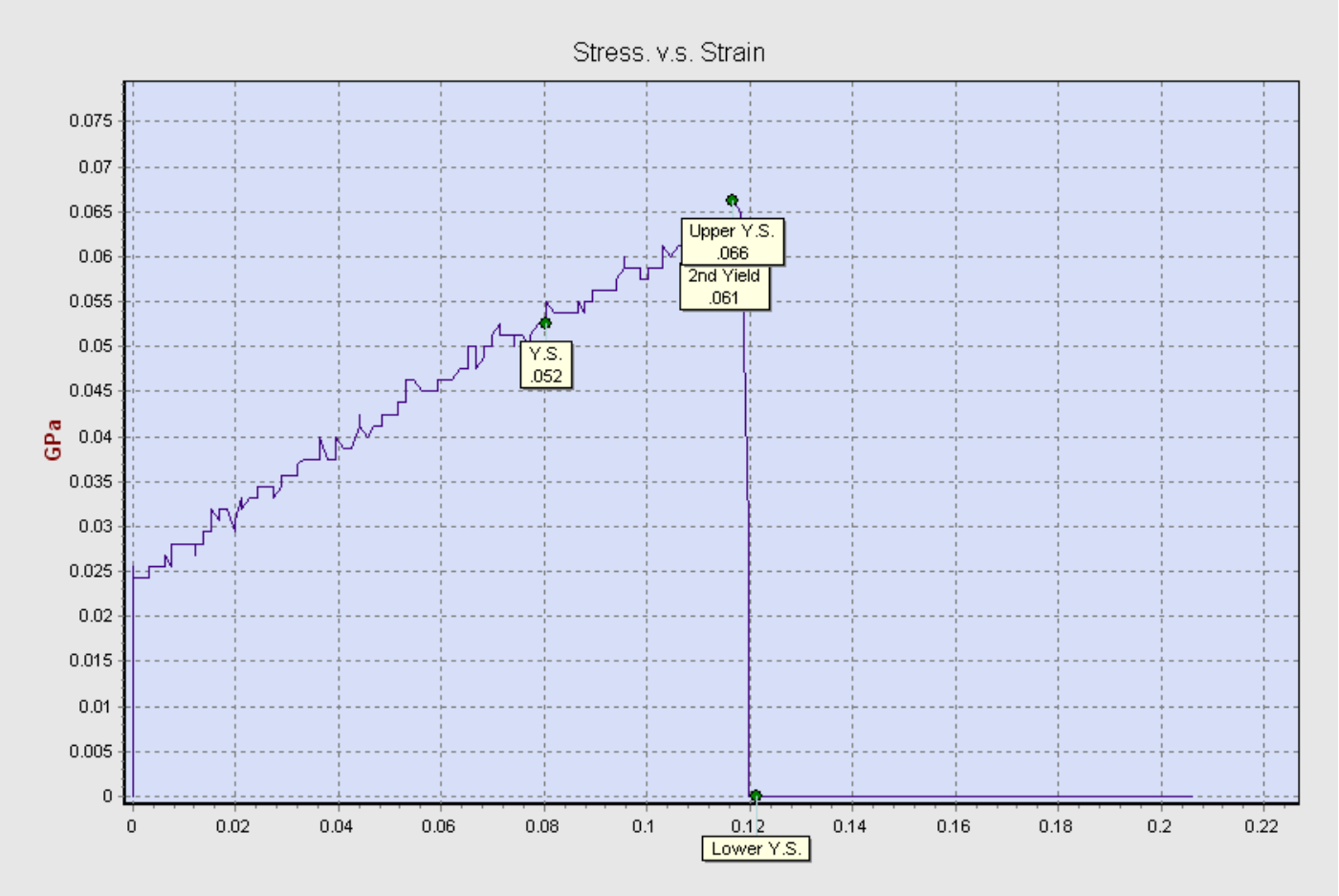

Fig.6.38 Stress vs Strain graph of sample loaded at 40% of U.T.L (NaOH Tank T2)

3) The results of specimen which were subjected to **60% loading** (T2, 1month) are shown below:

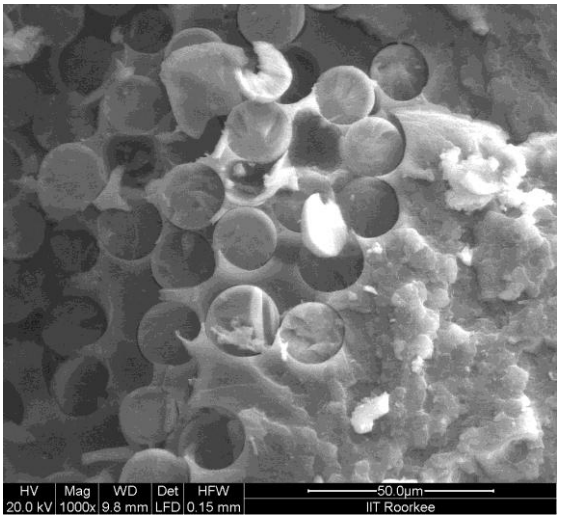

Fig.6.39 SEM image of specimen at 60% load

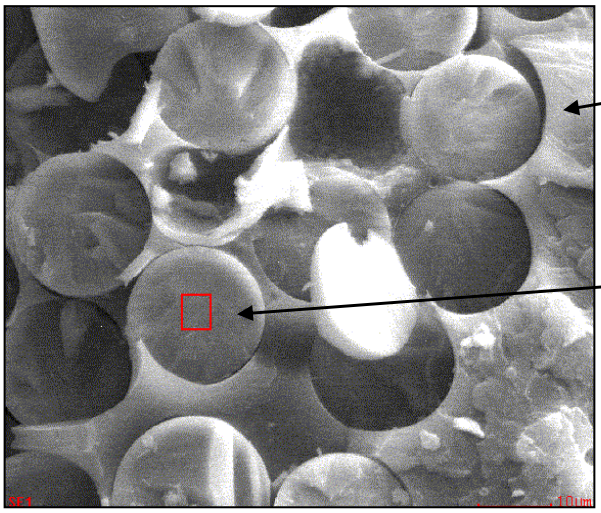

Fig.6.40 SEM image of specimen for EDX

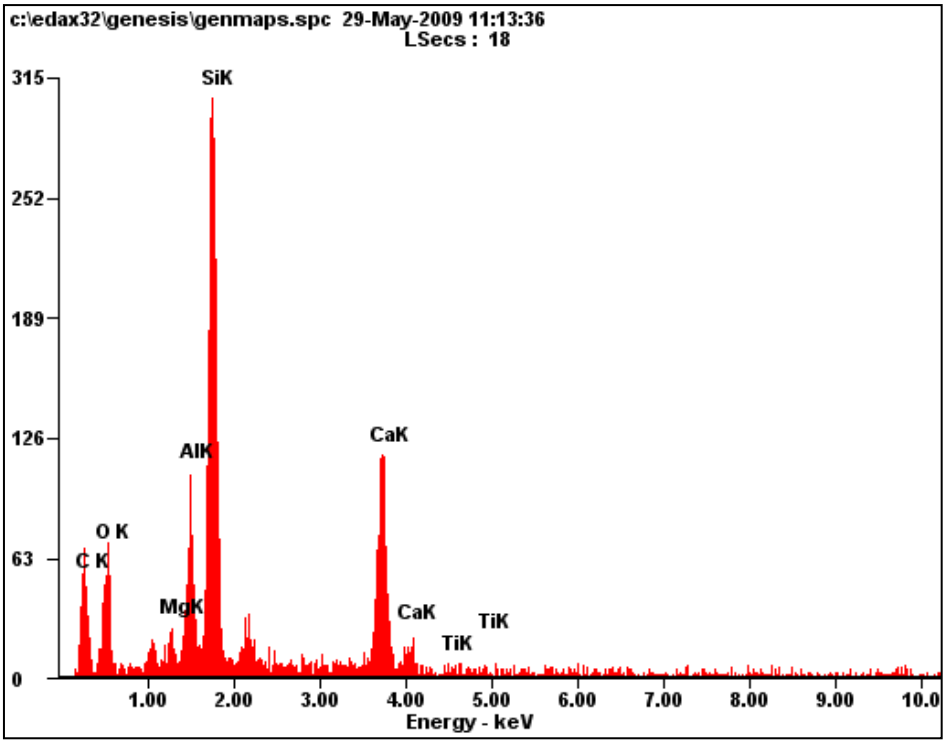

e)

Element	*Wt%*
CK	39.38
OK	22.76
MgK	00.90
AlK	04.95
SiK	19.90
CaK	11.66
TiK	00.45

f)

Fig.6.41 (e) Energy vs Electron volt graph for 60% load, (f) Element percentage taken by EDX

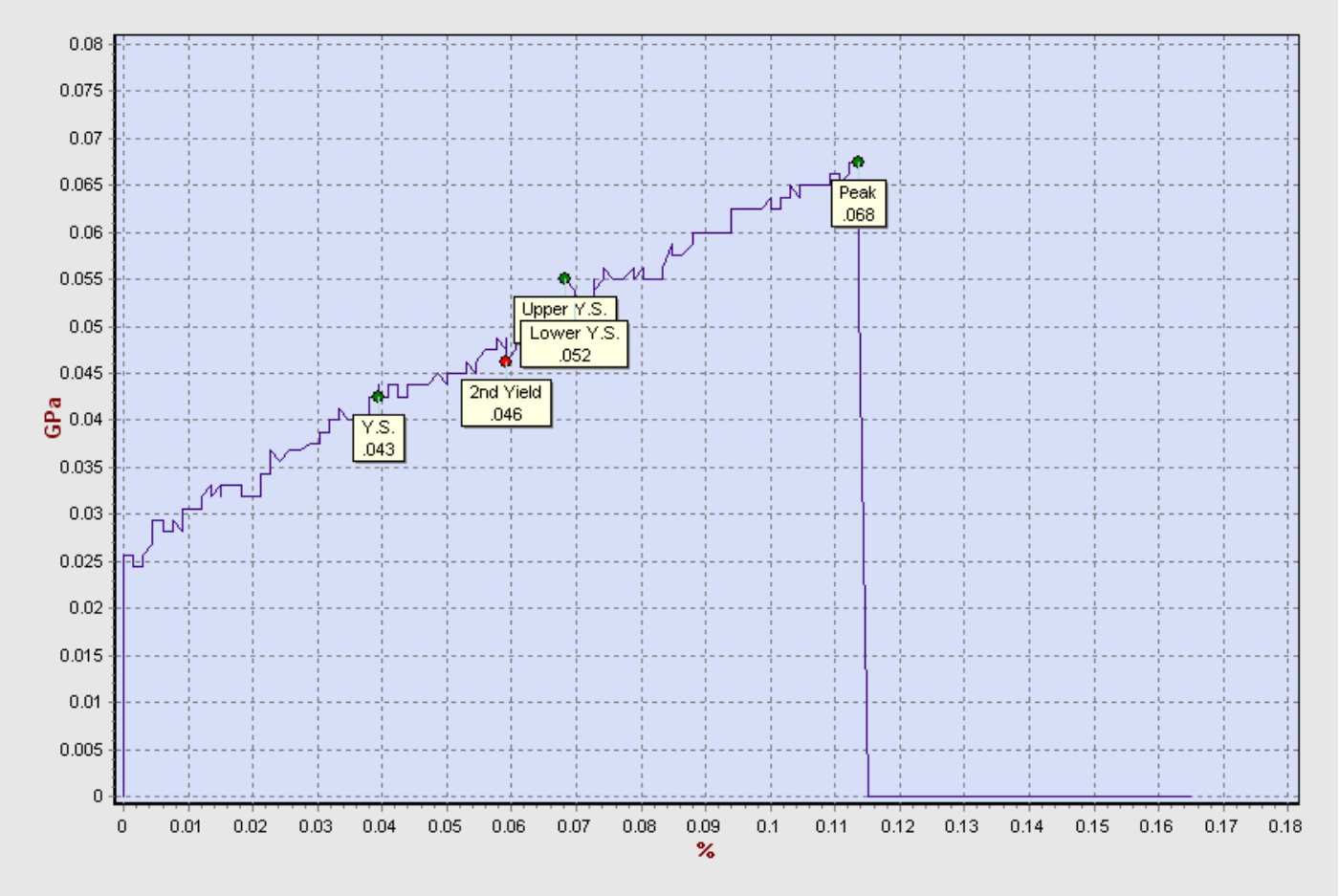

Fig.6.42 Stress vs Strain graph of sample loaded at 60% of U.T.L (NaOH Tank T2)

4) The results of specimen which were subjected to **80% loading** (T2, 1month) are shown below:

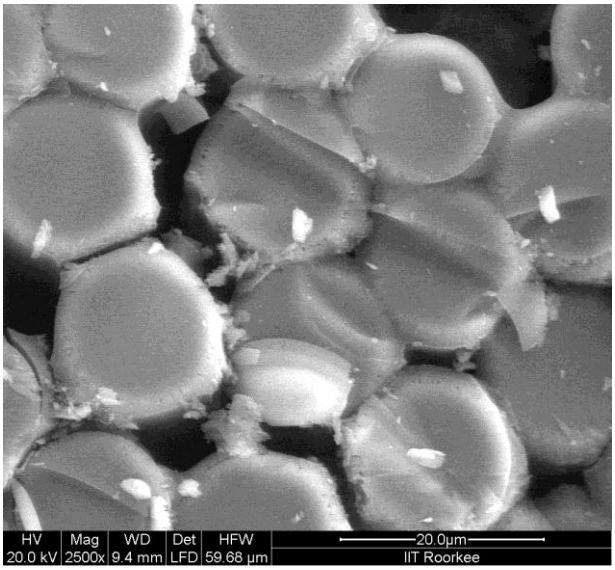

Fig.6.43 SEM image of specimen at 80% load

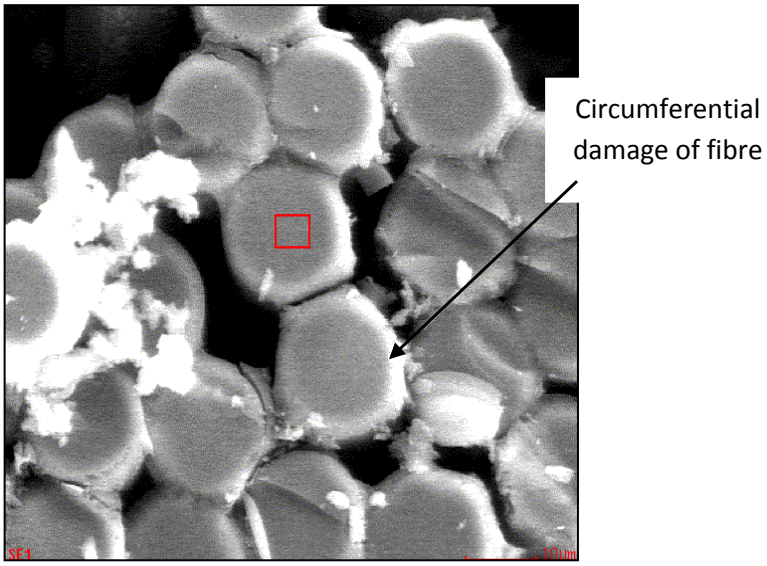

Fig.6.44 SEM image of specimen for EDX

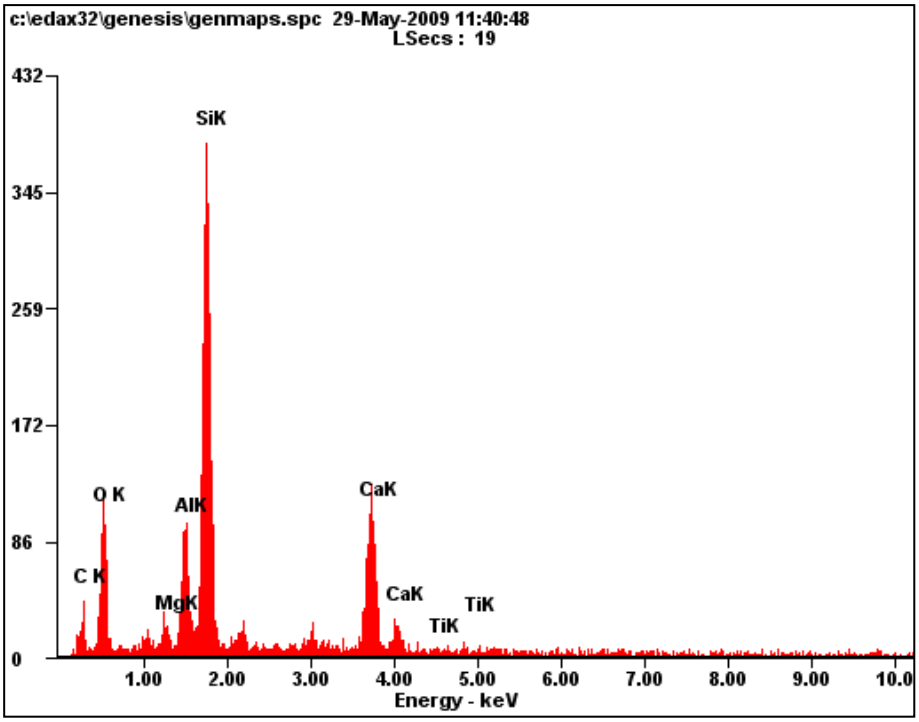

g)

Element	*Wt%*
CK	22.00
OK	31.76
MgK	01.36
AlK	06.15
SiK	25.16
CaK	13.18
TiK	00.40

h)

Fig.6.45 (g) Energy vs Electron volt graph for 80% load, (h) Element percentage taken by EDX

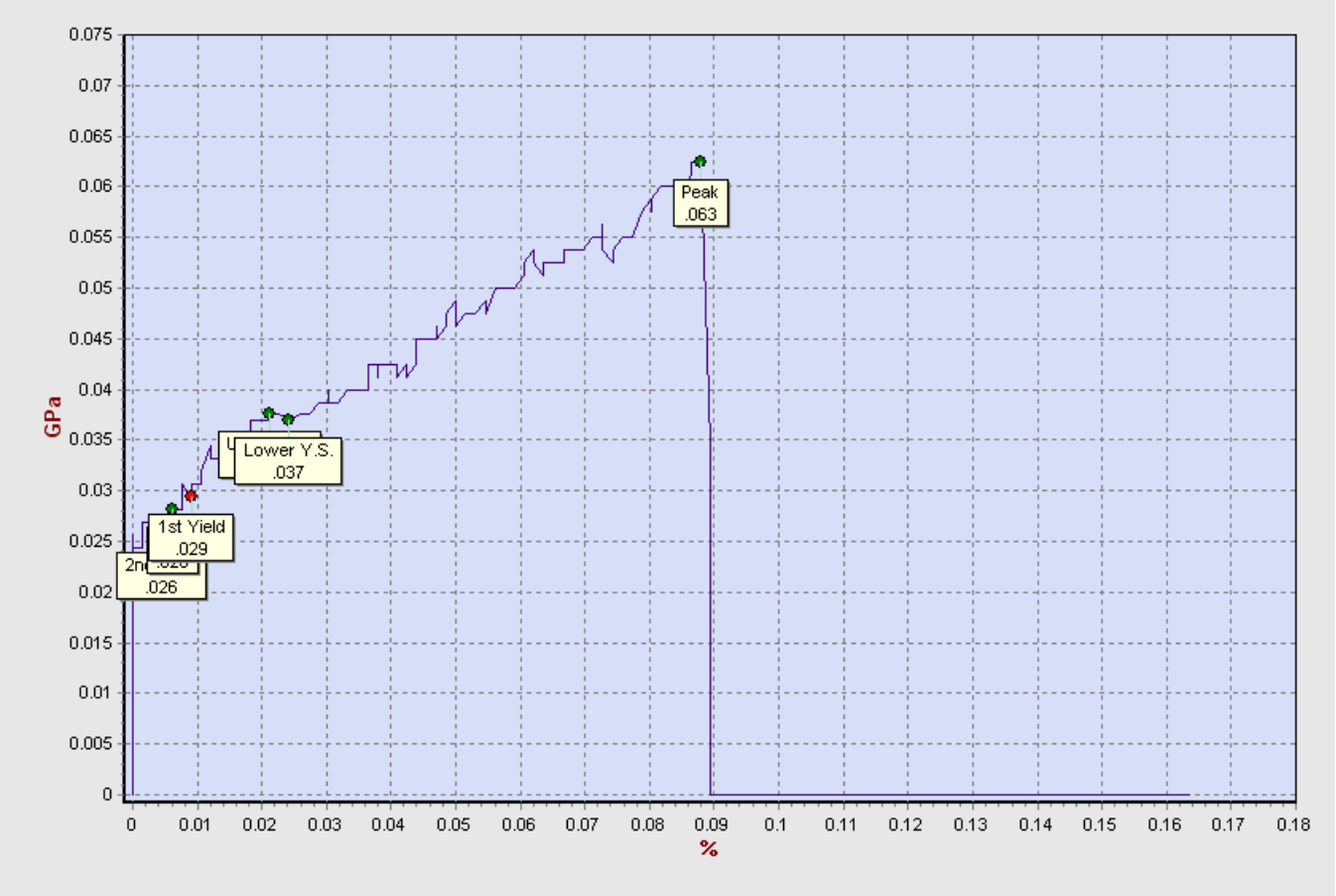

Fig.6.46 Stress vs Strain graph of sample loaded at 80% of U.T.L (NaOH Tank T2)

C) S.E.M. AND E.D.X. RESULTS OF NaOH TANK T3 (after 1 month)

Holding Parameters:
NaOH bath
Time: 1 month
Temperature: 55^{o}C

1) The results of specimen which were subjected to **20% loading** (T3, 1month) are shown below:

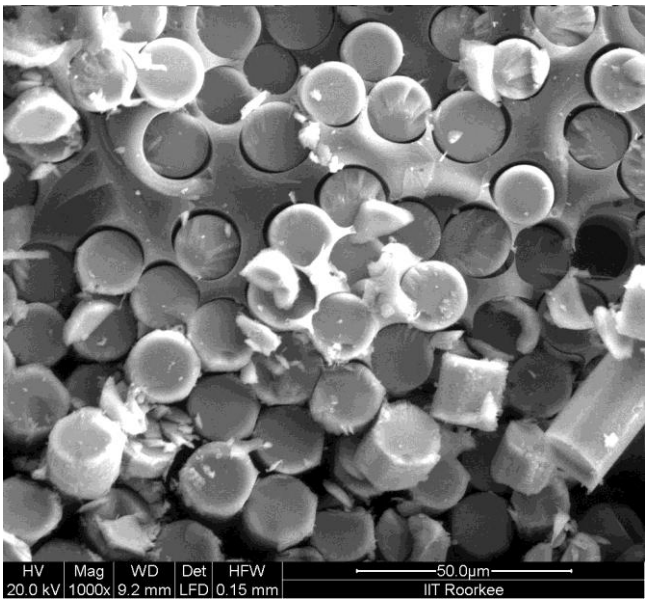

Fig.6.47 SEM image of specimen at 20% load

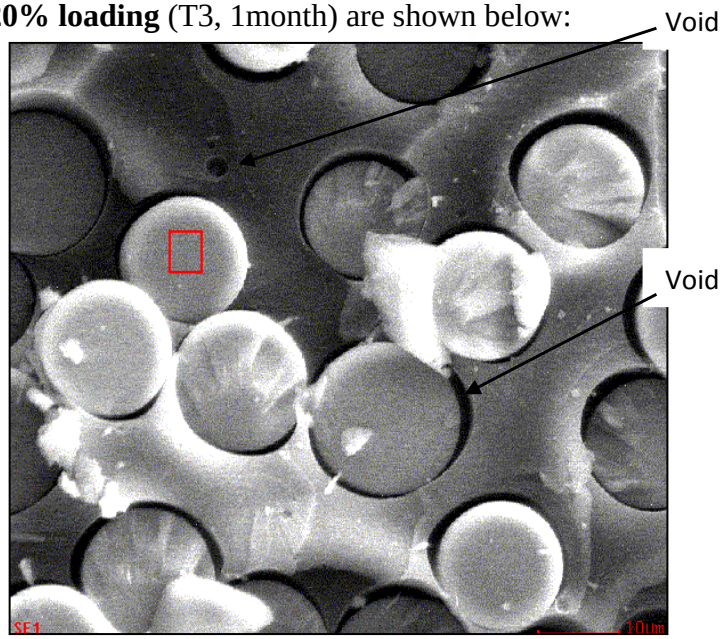

Fig.6.48 SEM image of specimen for EDX

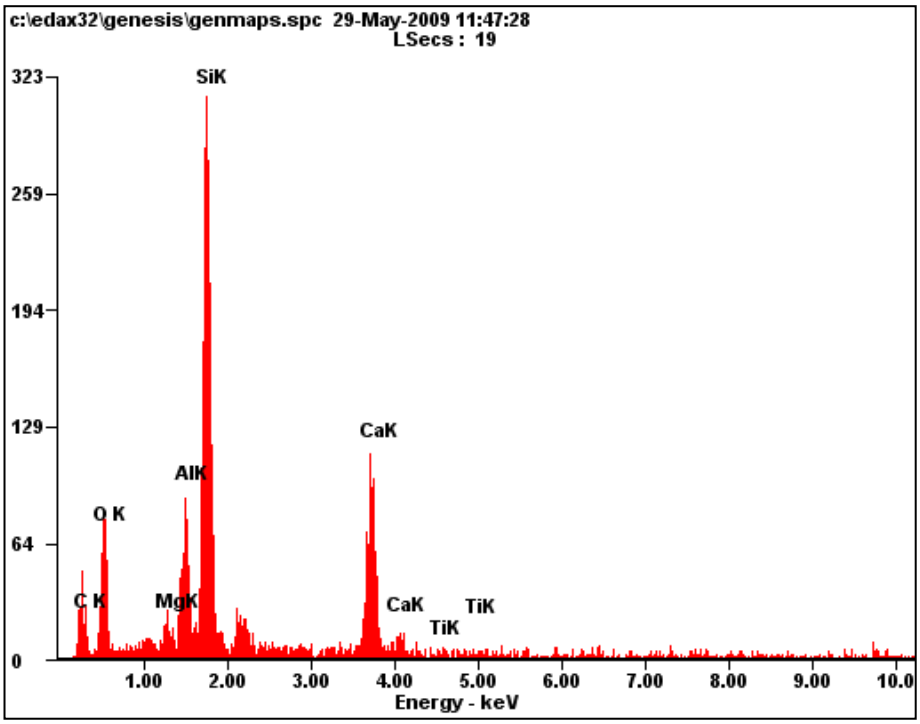

a)

Element	*Wt%*
CK	30.38
OK	26.62
MgK	01.15
AlK	05.64
SiK	23.18
CaK	12.55
TiK	00.49

b)

Fig.6.49 (a) Energy vs Electron volt graph for 20% load, (b) Element percentage taken by EDX

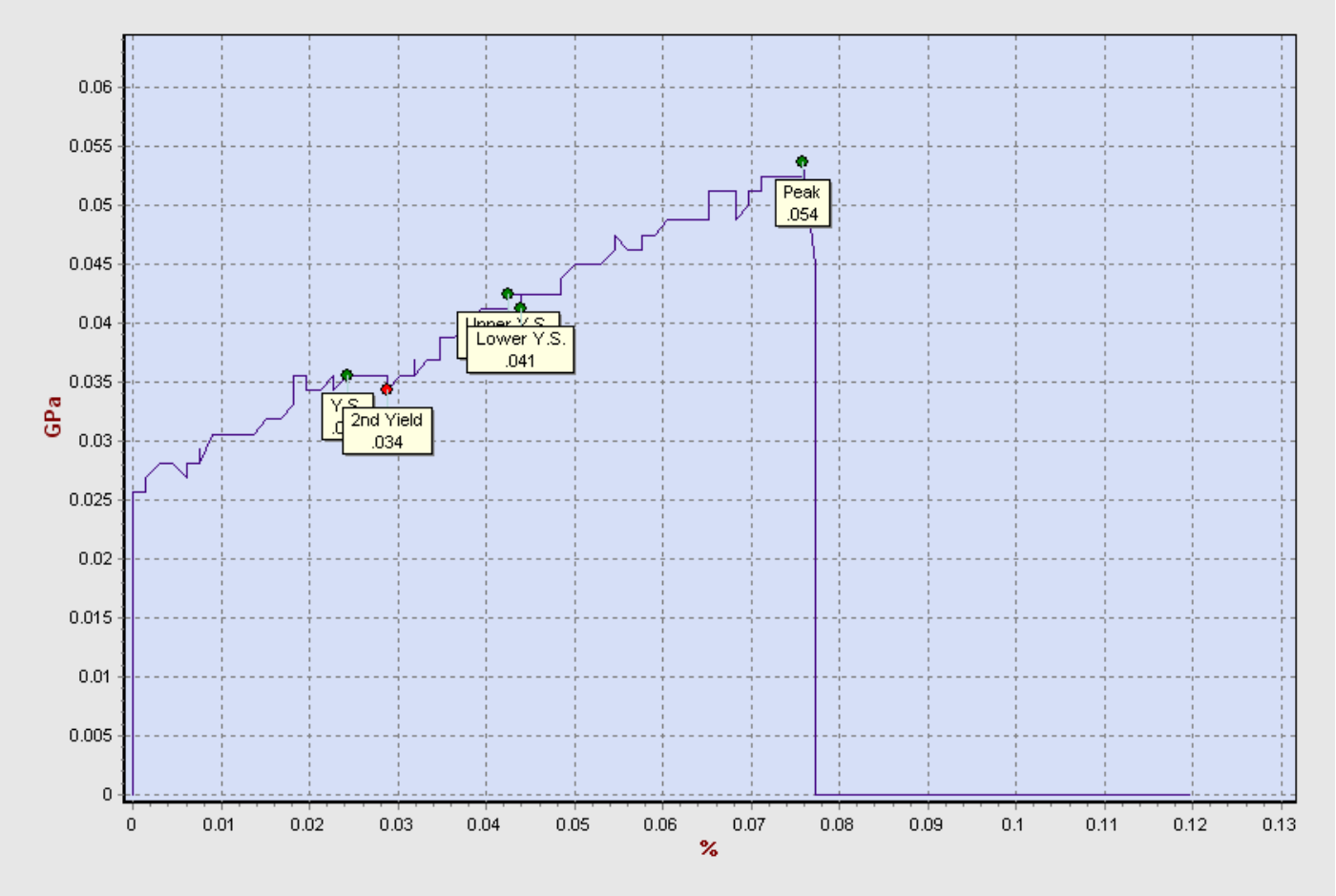

Fig.6.50 Stress vs Strain graph of sample loaded at 20% of U.T.L (NaOH Tank T3)

2) The results of specimen which were subjected to **40% loading** (T3, 1month) are shown below:

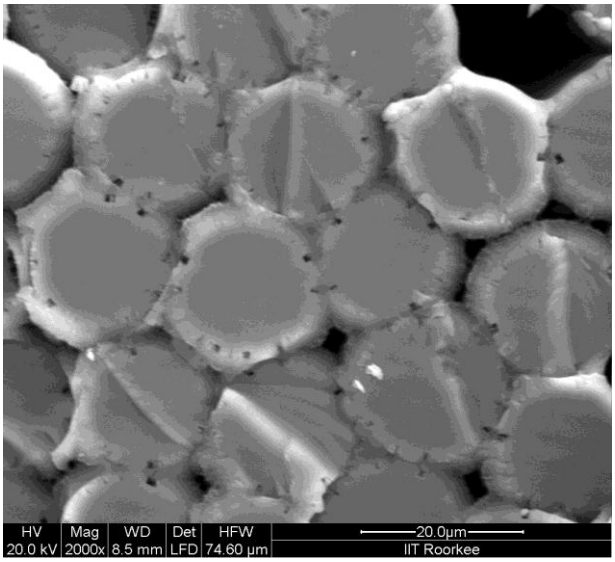

Fig.6.51 SEM image of specimen at 40% load

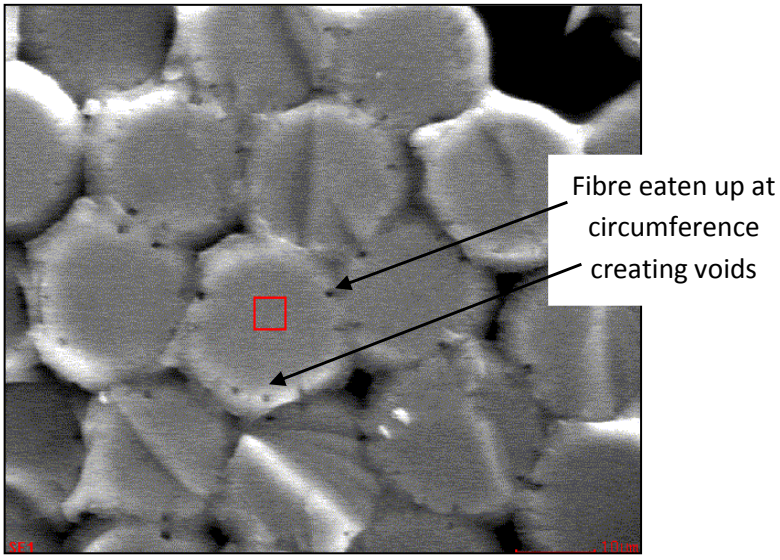

Fig.6.52 SEM image of specimen for EDX

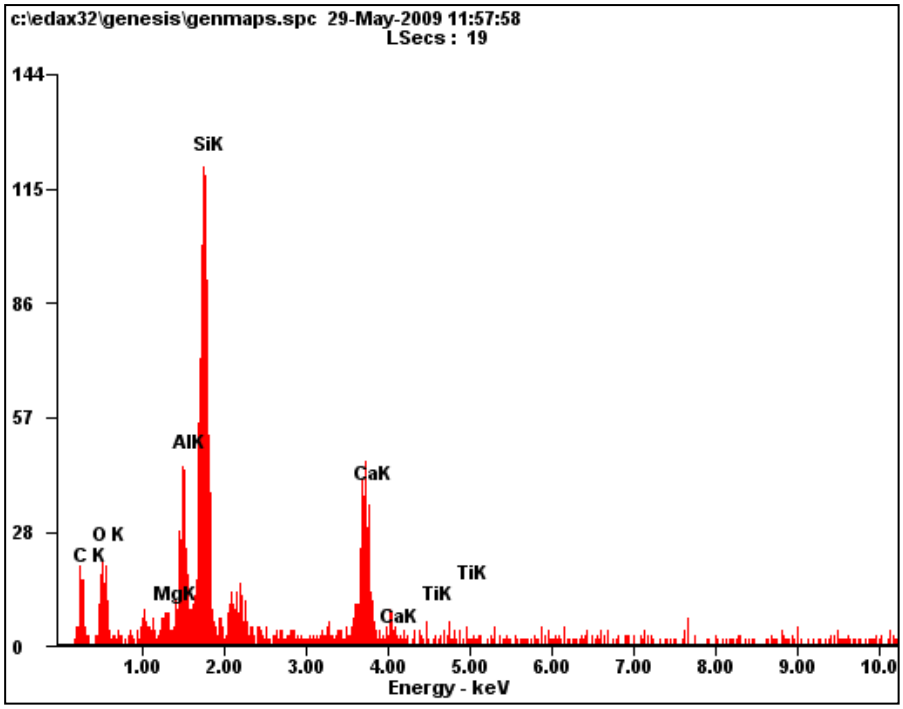

c)

Element	*Wt%*
CK	33.10
OK	18.06
MgK	01.71
AlK	06.32
SiK	24.07
CaK	15.51
TiK	00.23

d)

Fig.6.53 (c) Energy vs Electron volt graph for 40% load, (d) Element percentage taken by EDX

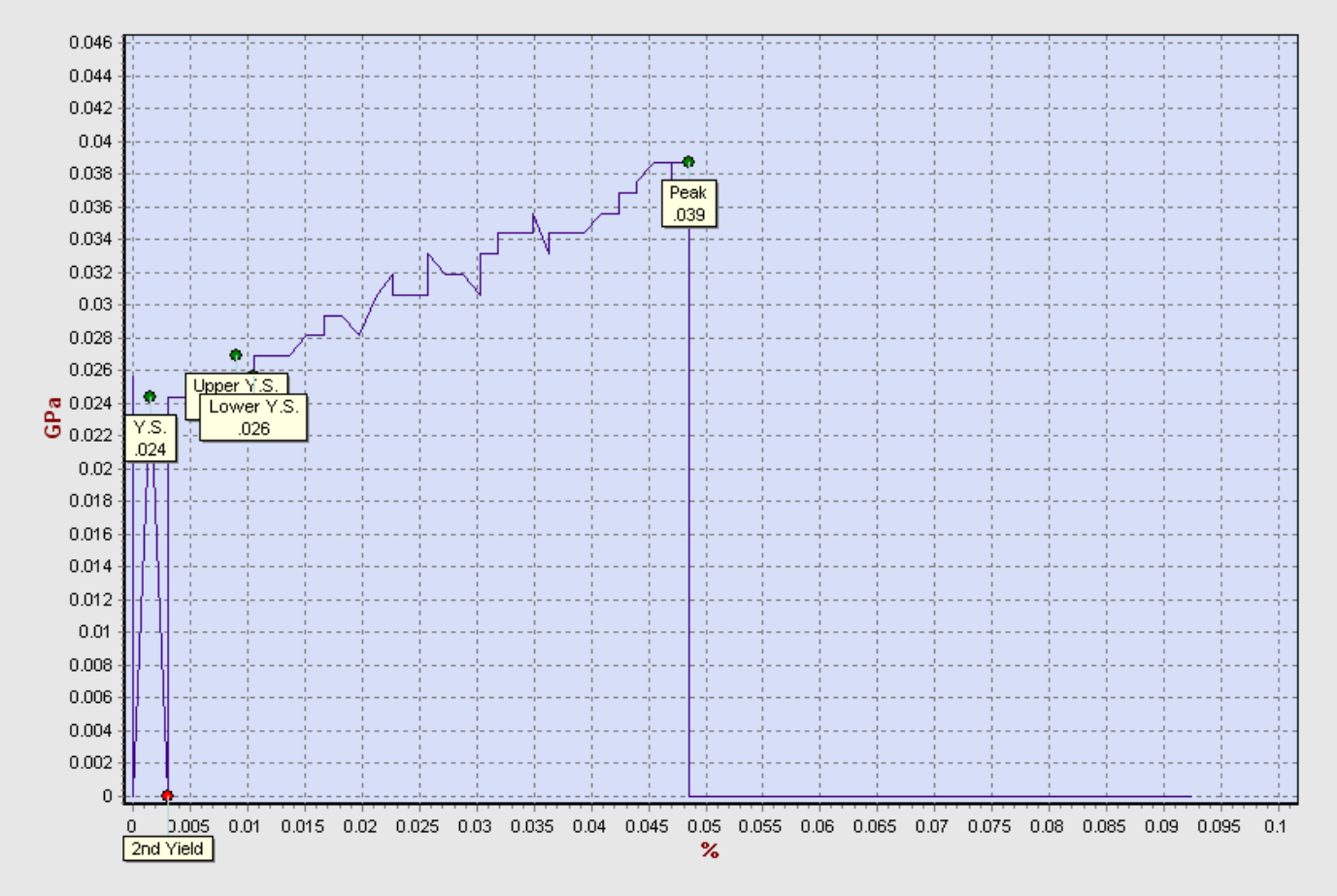

Fig.6.54 Stress vs Strain graph of sample loaded at 40% of U.T.L (NaOH Tank T3)

3) The results of specimen which were subjected to **60% loading** (T3, 1month) are shown below:

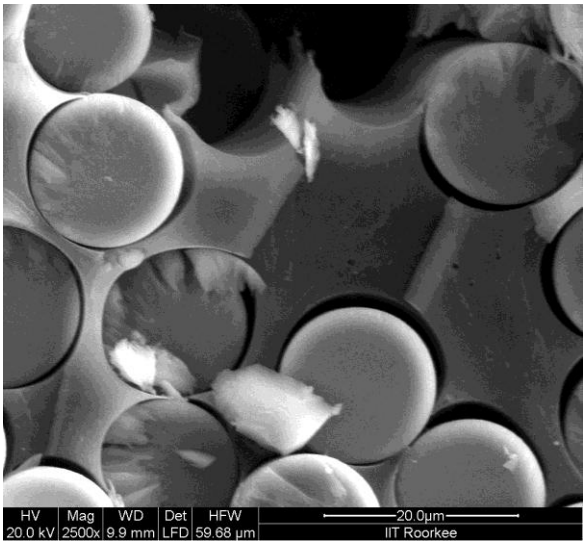

Fig.6.55 SEM image of specimen at 60% load

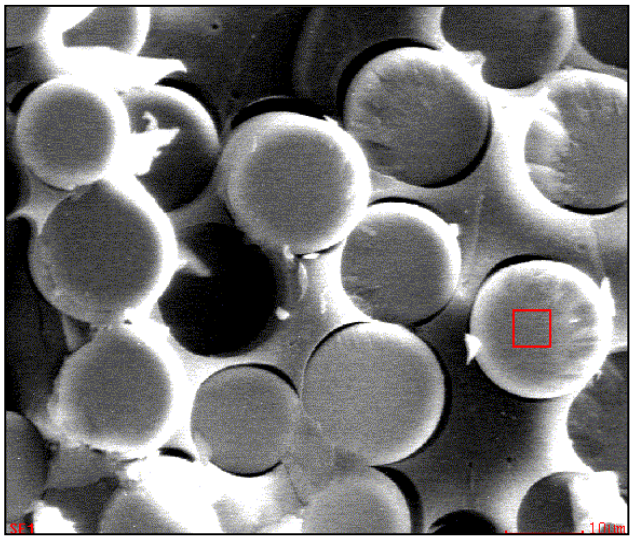

Fig.6.56 SEM image of specimen for EDX

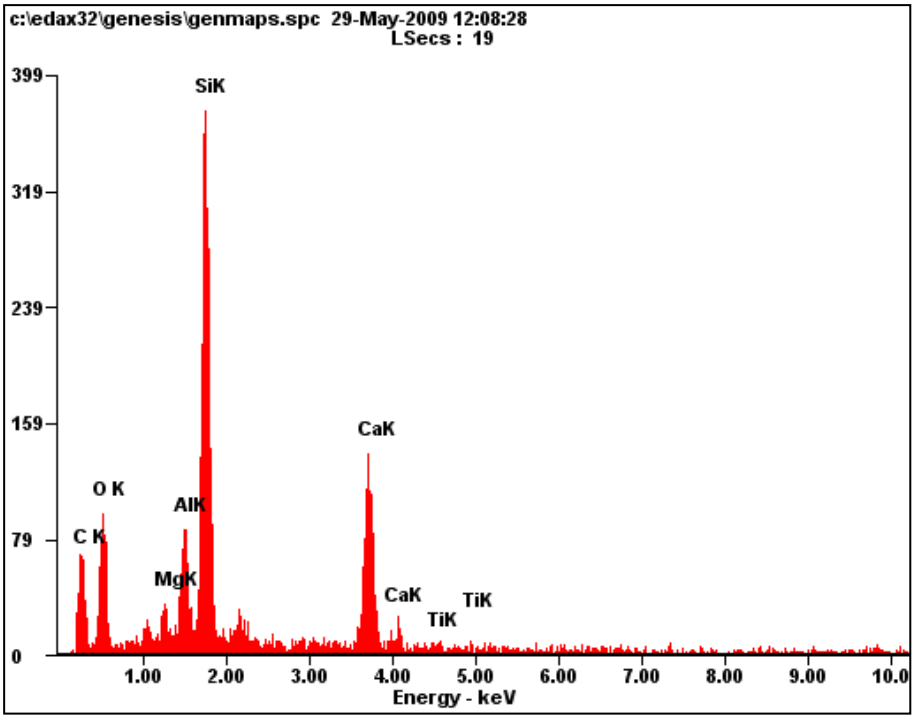

Element	*Wt%*
CK	36.25
OK	26.08
MgK	00.96
AlK	04.35
SiK	19.58
CaK	11.10
TiK	00.68

e) f)

Fig.6.57 (e) Energy vs Electron volt graph for 60% load, (f) Element percentage taken by EDX

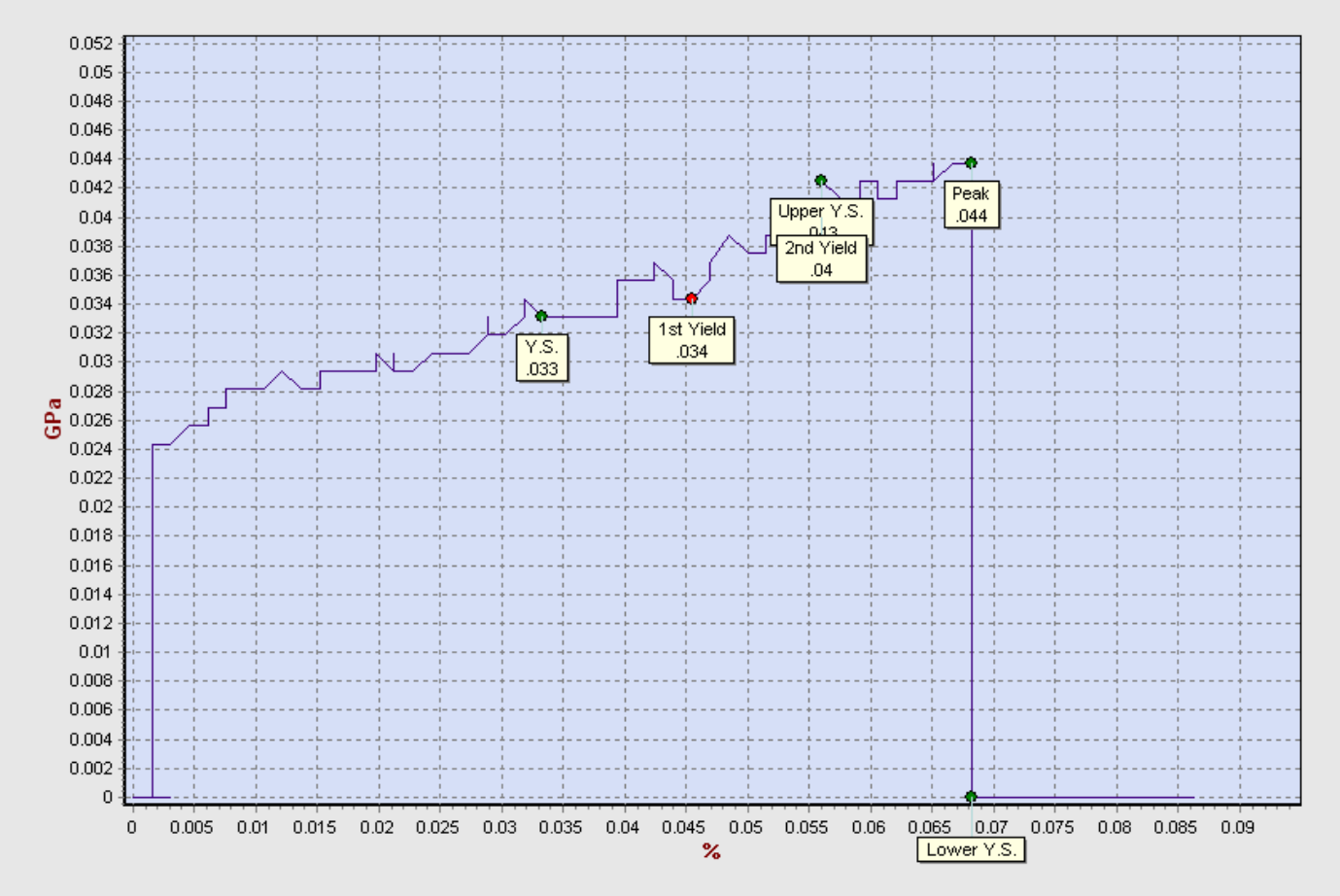

Fig.6.58 Stress vs Strain graph of sample loaded at 60% of U.T.L (NaOH Tank T3)

4) The results of specimen which were subjected to **80% loading** (T3, 1month) are shown below:

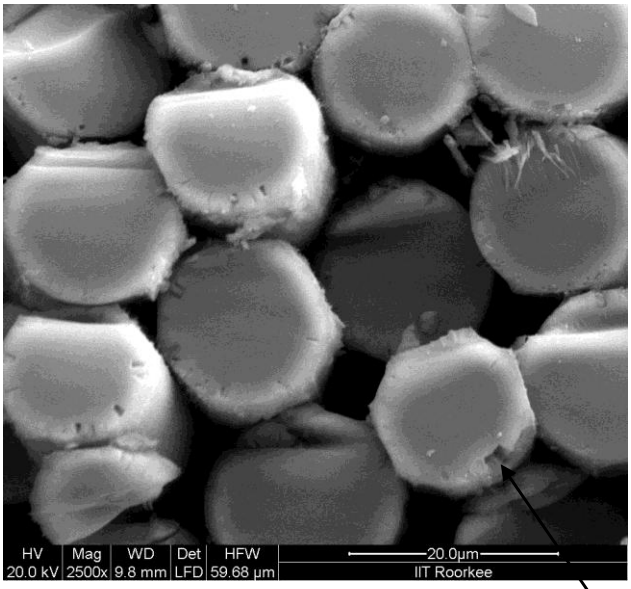

Fig.6.59 SEM image of specimen at 80% load

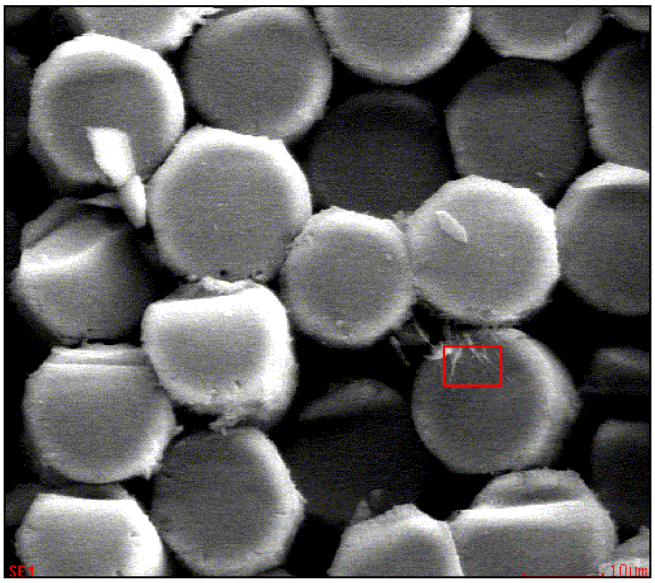

Fig.6.60 SEM image of specimen for EDX

Major damage to fibre

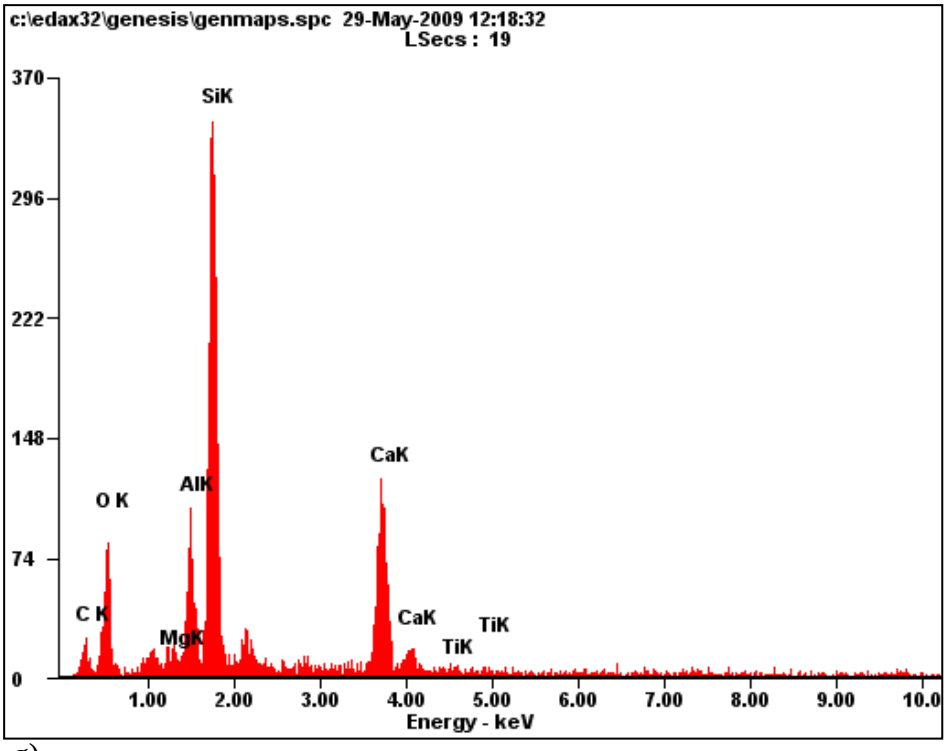

g)

Element	*Wt%*
CK	18.62
OK	30.69
MgK	01.28
AlK	06.07
SiK	26.61
CaK	15.99
TiK	00.74

h)

Fig.6.61 (g) Energy vs Electron volt graph for 80% load, (h) Element percentage taken by EDX

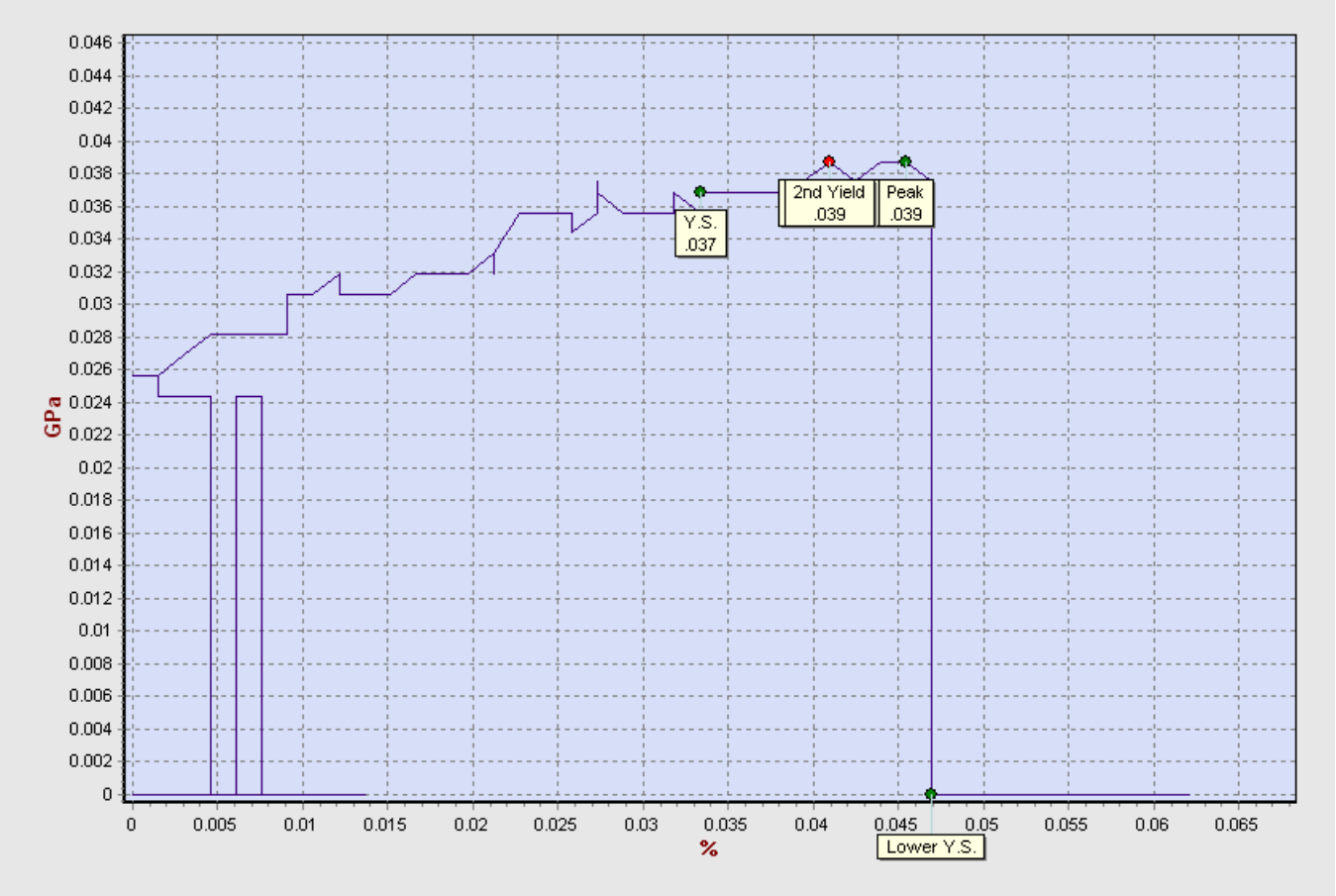

Fig.6.62 Stress vs Strain graph of sample loaded at 80% of U.T.L (NaOH Tank T3)

D) S.E.M. AND E.D.X. RESULTS OF WATER TANK T4 (after 1 month)

Holding Parameters:
Water bath
Time: 1 month
Temperature: 55^{o}C

1) The results of specimen which were subjected to **20% loading** (T4, 1month) are shown below:

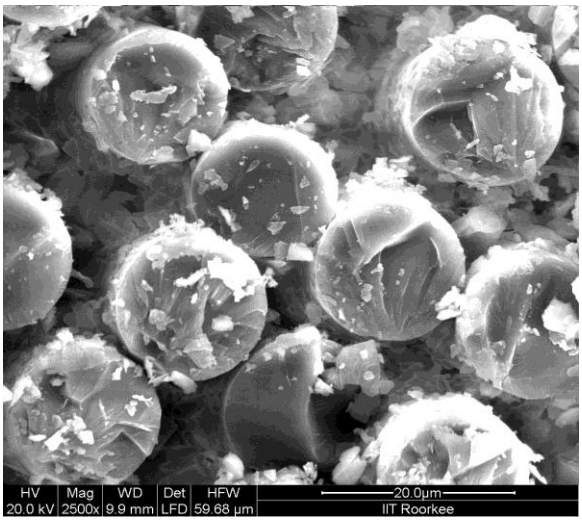

Fig.6.63 SEM image of specimen at 20% load

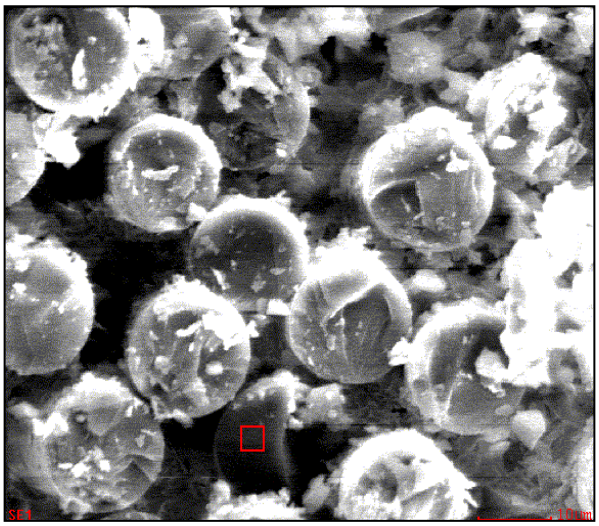

Fig.6.64 SEM image of specimen for EDX

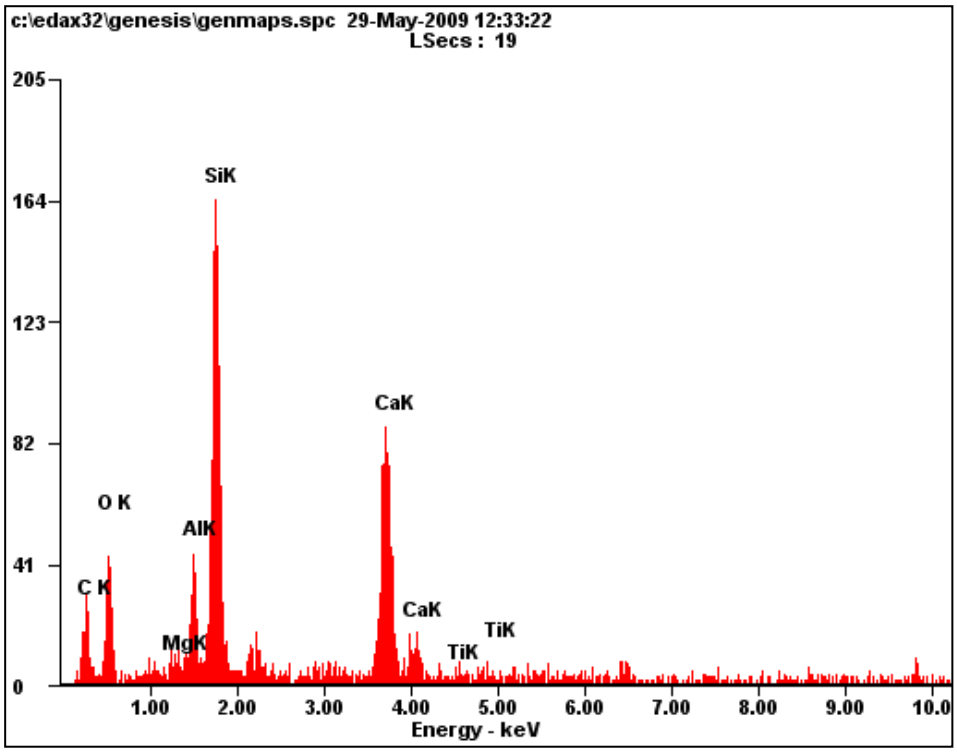

a)

Element	*Wt%*
CK	29.49
OK	26.43
MgK	00.98
AlK	04.40
SiK	19.91
CaK	18.26
TiK	00.52

b)

Fig.6.65 (a) Energy vs Electron volt graph for 20% load, (b) Element percentage taken by EDX

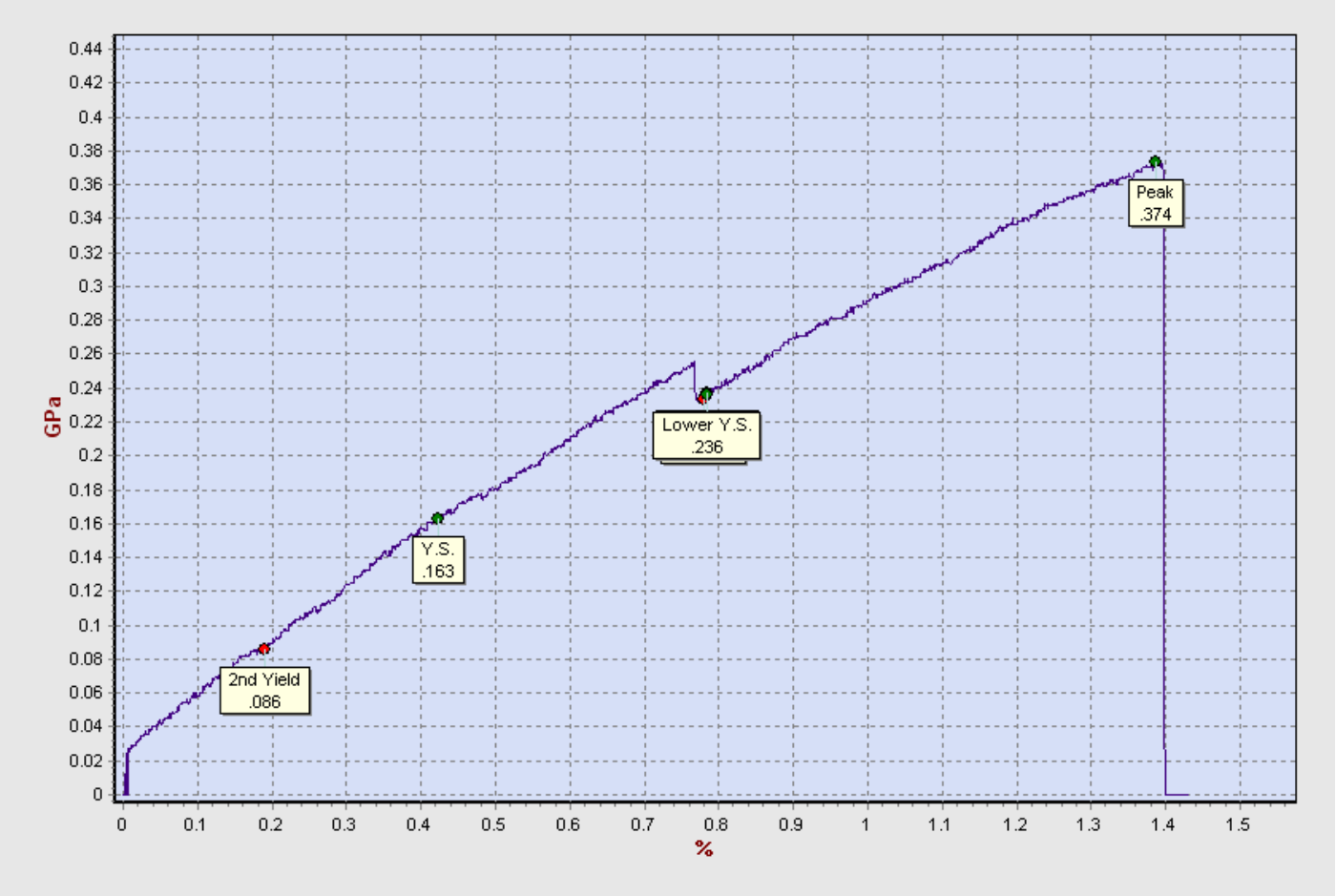

Fig.6.66 Stress vs Strain graph of sample loaded at 20% of U.T.L (Water Tank T4)

2) The results of specimen which were subjected to **40% loading** (T4, 1month) are shown below:

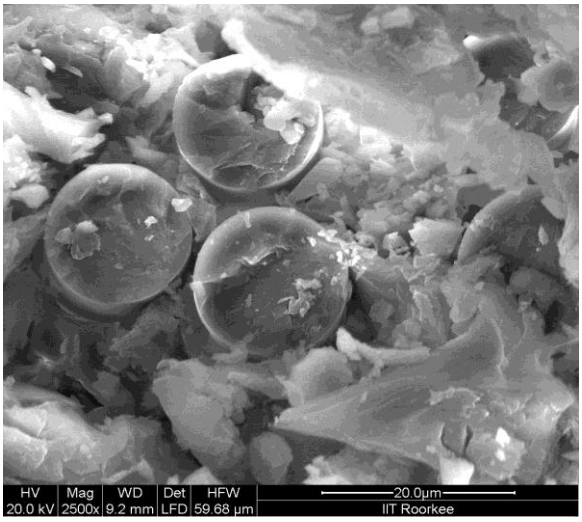

Fig.6.67 SEM image of specimen at 40% load

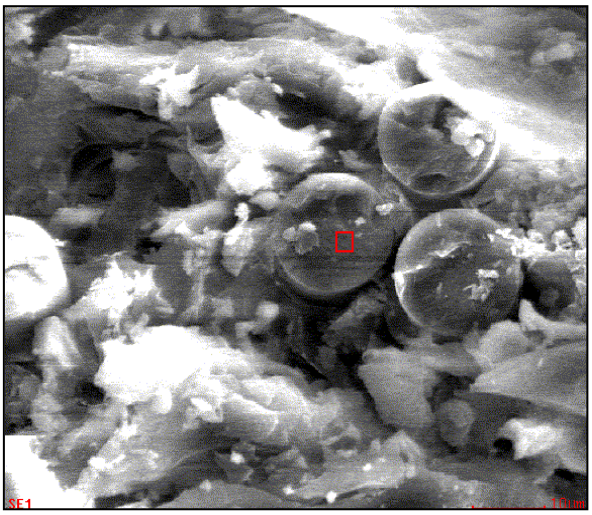

Fig.6.68 SEM image of specimen for EDX

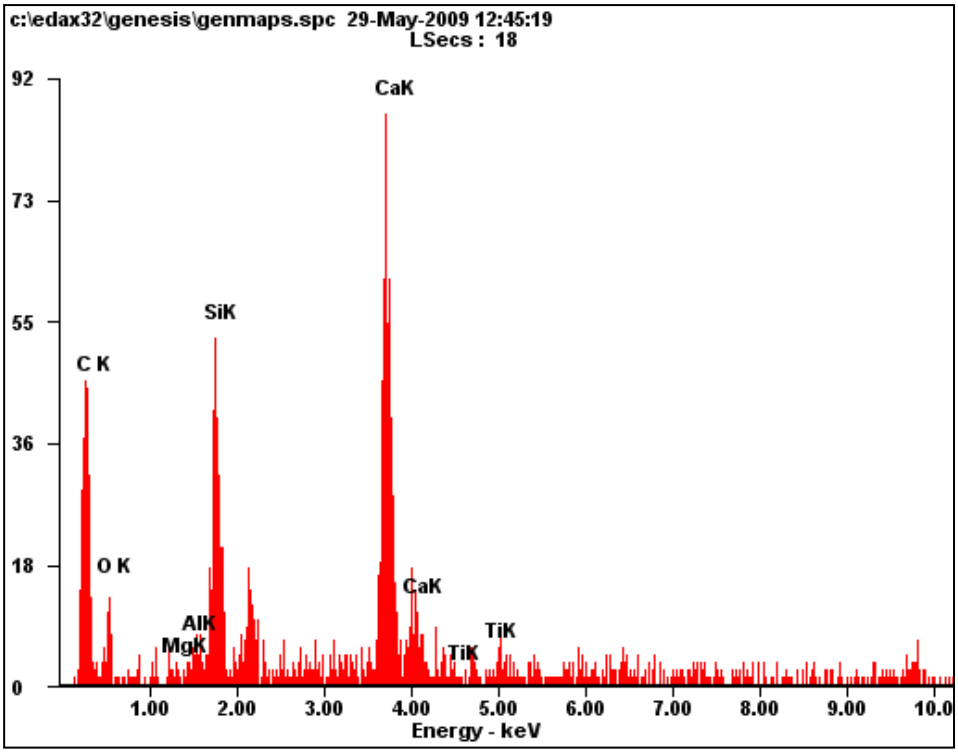

c)

Element	*Wt%*
CK	55.41
OK	12.97
MgK	00.62
AlK	01.53
SiK	08.13
CaK	20.02
TiK	01.32

d)

Fig.6.69 (c) Energy vs Electron volt graph for 40% load, (d) Element percentage taken by EDX

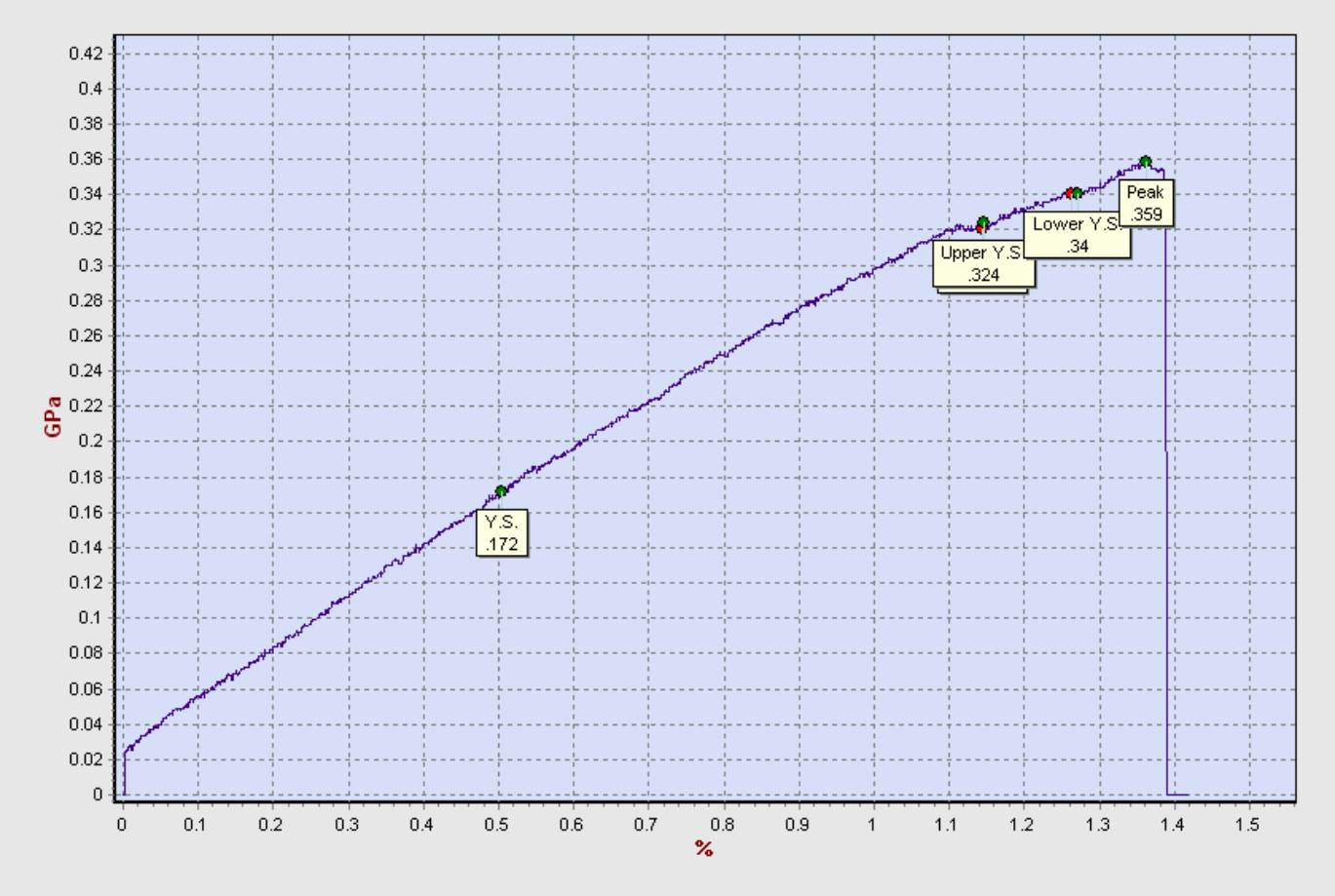

Fig.6.70 Stress vs Strain graph of sample loaded at 40% of U.T.L (Water Tank T4)

3) The results of specimen which were subjected to **60% loading** (T4, 1month) are shown below:

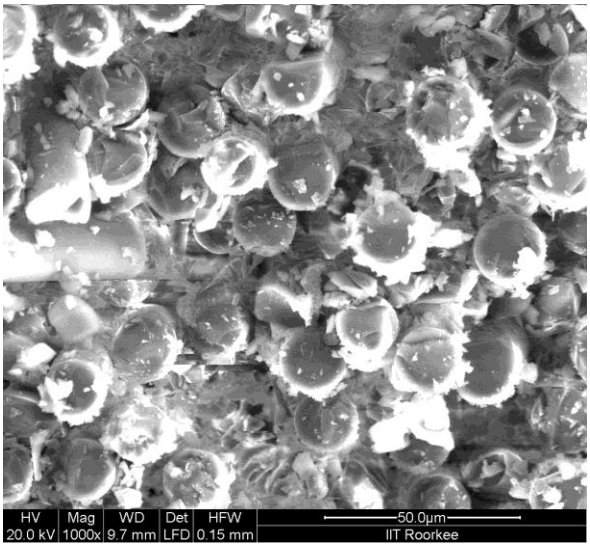

Fig.6.71 SEM image of specimen at 60% load

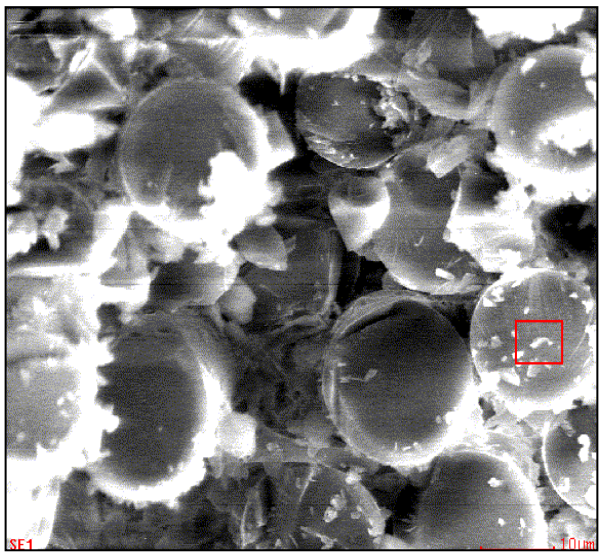

Fig.6.72 SEM image of specimen for EDX

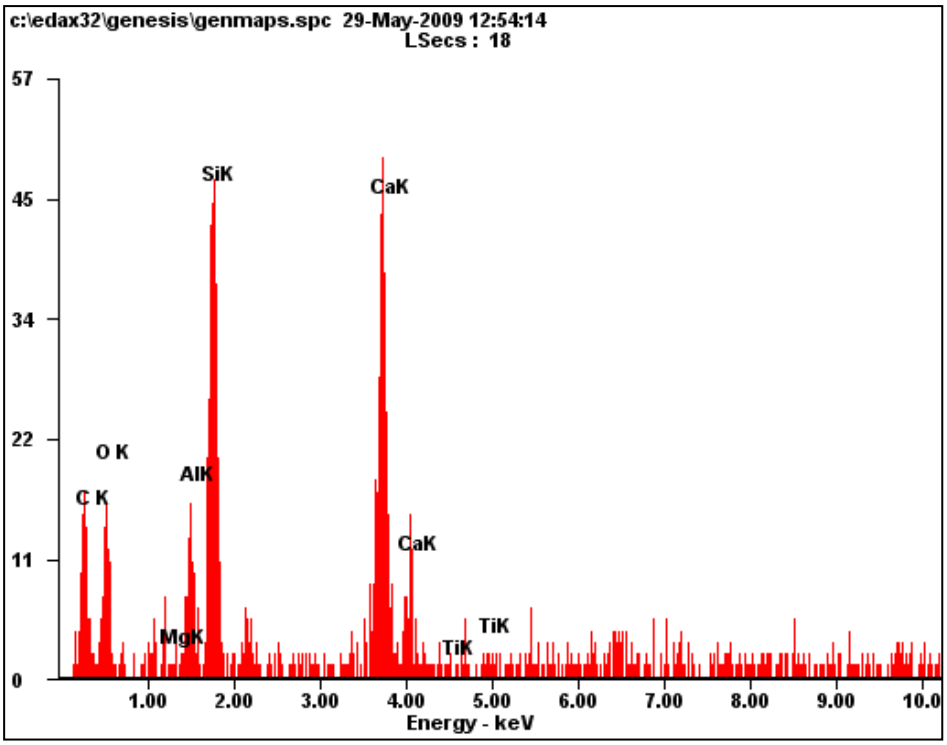

e)

Element	*Wt%*
CK	36.05
OK	26.24
MgK	00.80
AlK	03.54
SiK	13.32
CaK	18.96
TiK	01.09

f)

Fig.6.73 (e) Energy vs Electron volt graph for 60% load, (f) Element percentage taken by EDX

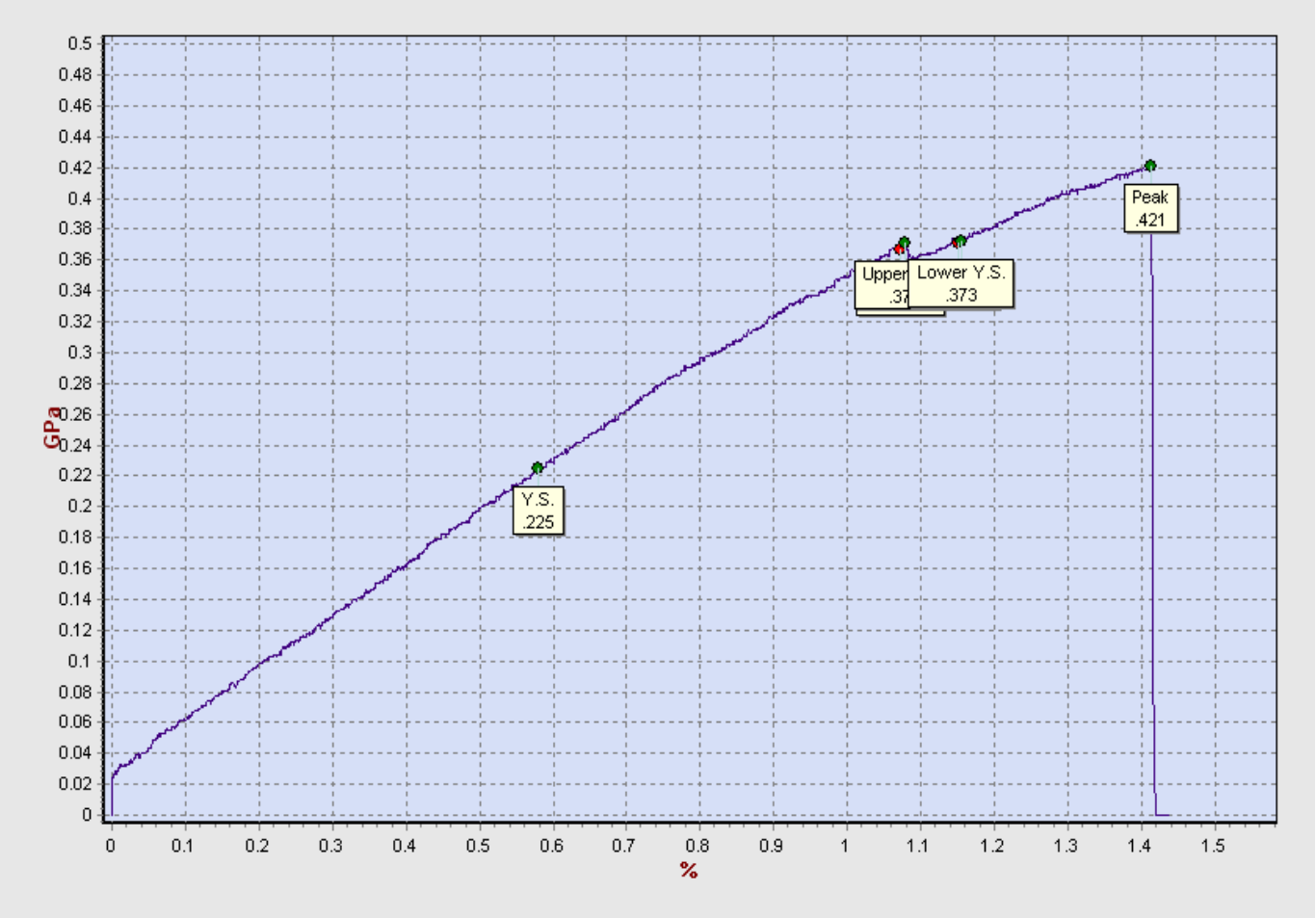

Fig.6.74 Stress vs Strain graph of sample loaded at 60% of U.T.L (Water Tank T4)

4) The results of specimen which were subjected to **80% loading** (T4, 1month) are shown below:

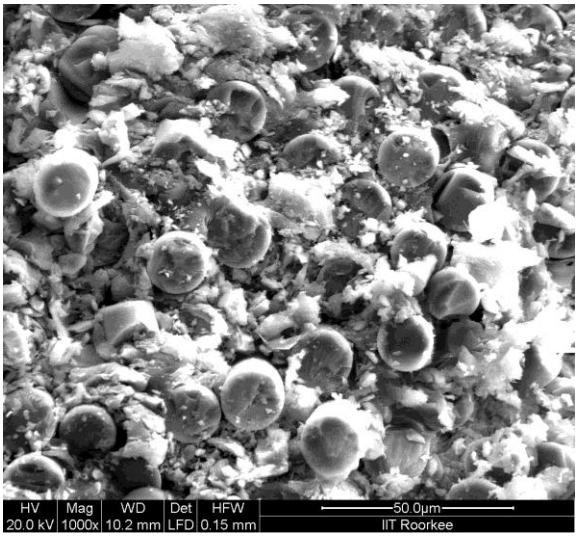

Fig.6.75 SEM image of specimen at 80% load

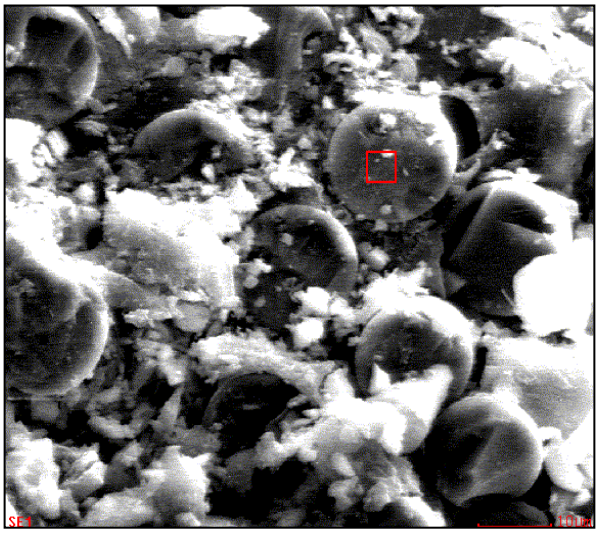

Fig.6.76 SEM image of specimen for EDX

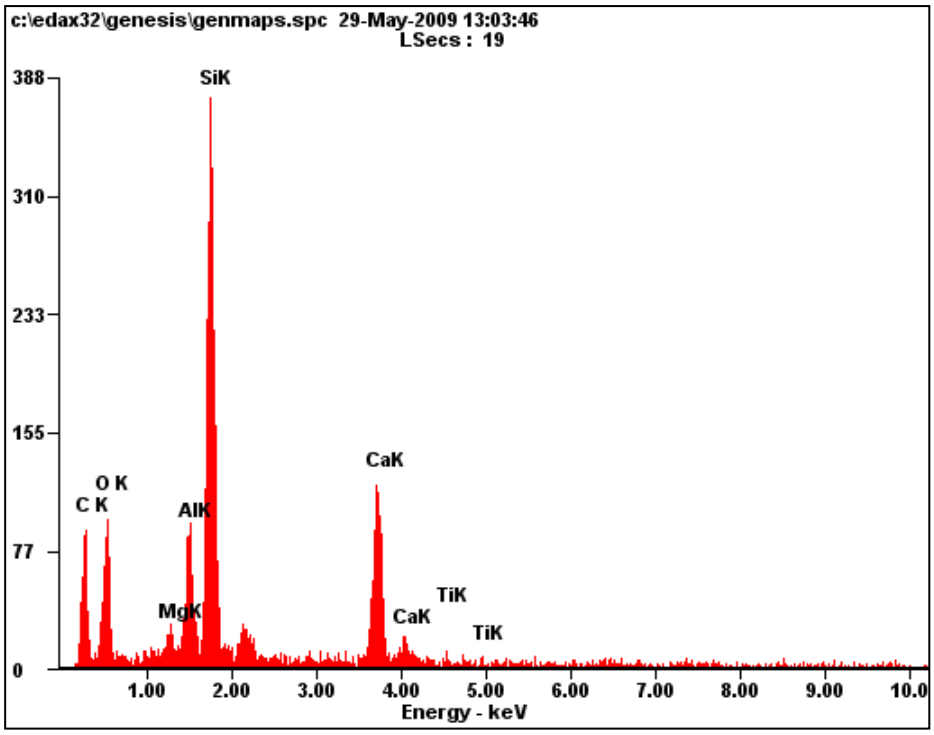

g)

Element	*Wt%*
CK	39.68
OK	25.45
MgK	01.06
AlK	04.44
SiK	18.52
CaK	10.34
TiK	00.51

h)

Fig.6.77 (g) Energy vs Electron volt graph for 80% load, (h) Element percentage taken by EDX

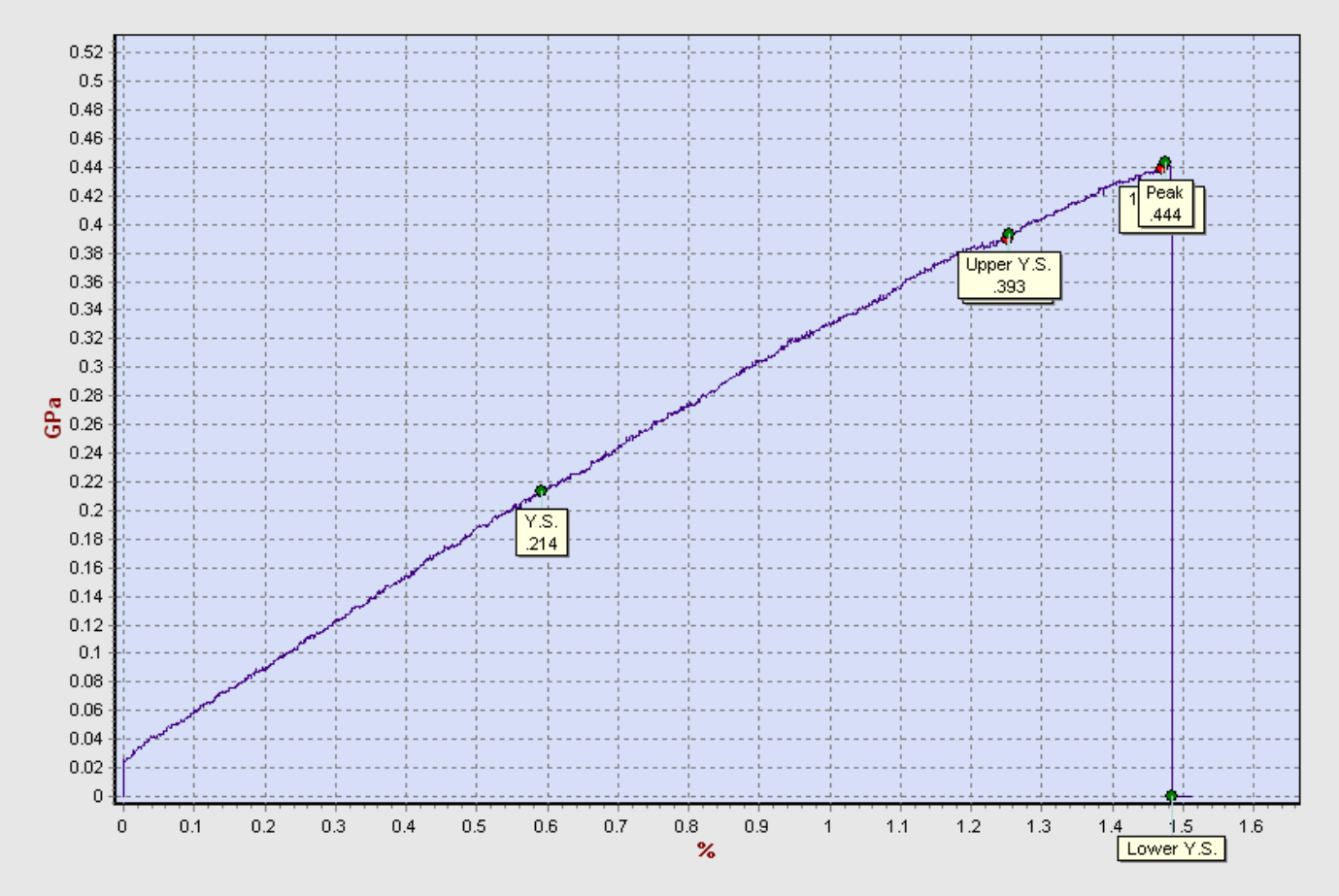

Fig.6.78 Stress vs Strain graph of sample loaded at 80% of U.T.L (Water Tank T4)

6.3.3 S.E.M. IMAGES AFTER TWO MONTHS

A) S.E.M. AND E.D.X. RESULTS OF WATER TANK T1 (after 2 months):

Holding Parameters:
Water bath
Time: 2 month
Temperature: 45^{o}C

1) The results of specimen which were subjected to **20% loading** (T1, 2months) are shown below:

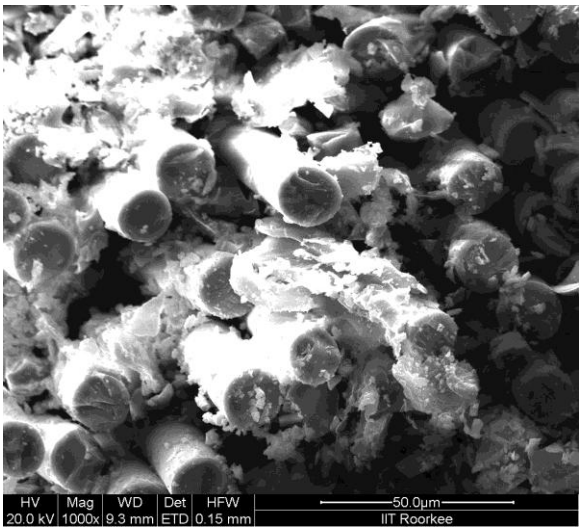

Fig.6.79 SEM image of specimen at 20% load

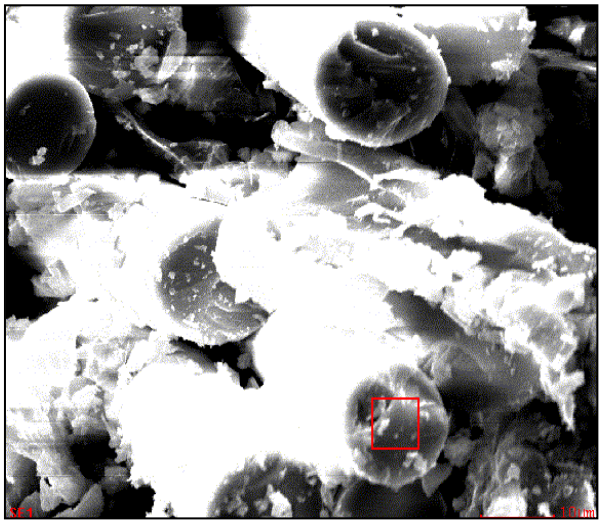

Fig.6.80 SEM image of specimen for EDX

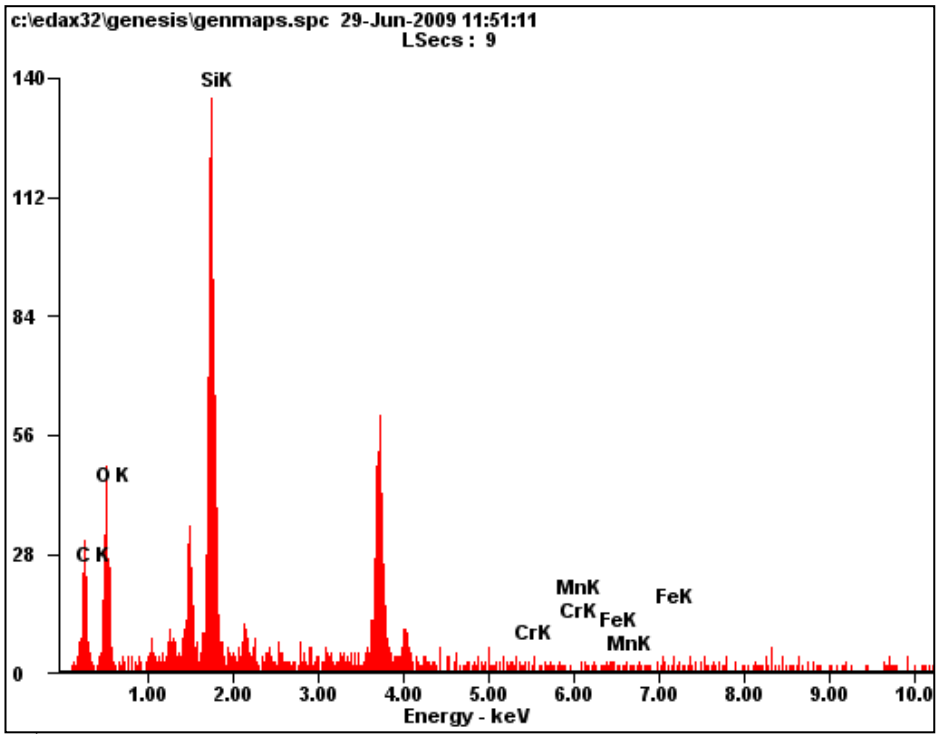

a)

Element	*Wt%*
CK	40.00
OK	34.22
SiK	25.01
CrK	00.33
MnK	00.00
FeK	00.44

b)

Fig.6.81 (a) Energy vs Electron volt graph for 20% load, (b) Element percentage taken by EDX

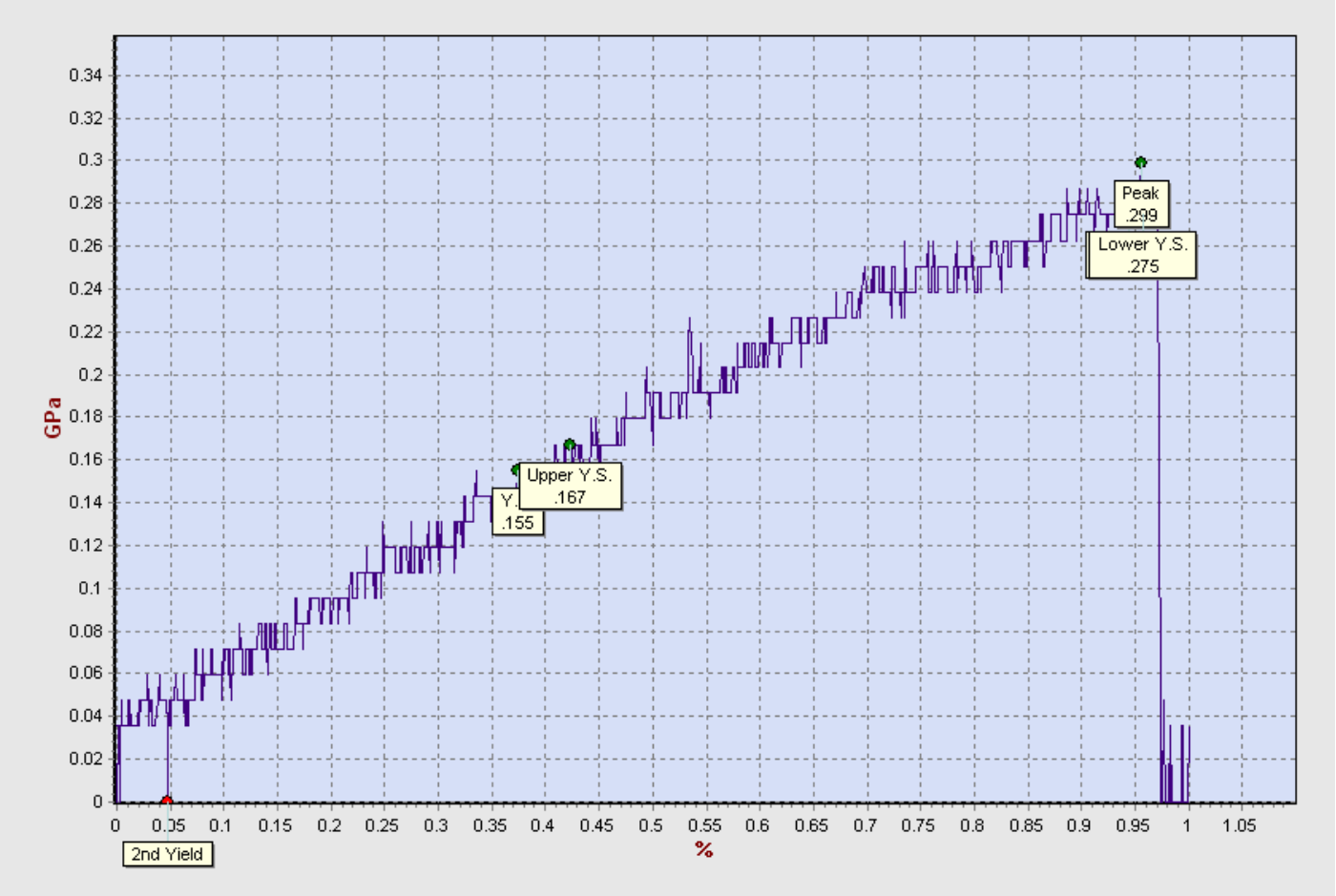

Fig.6.82 Stress vs Strain graph of sample loaded at 20% of U.T.L (Water Tank T1)

2) The results of specimen which were subjected to **40% loading** (T1, 2months) are shown below:

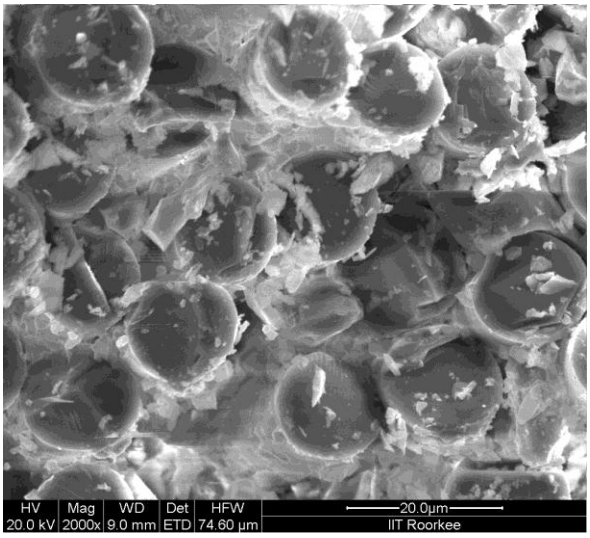

Fig.6.83 SEM image of specimen at 40% load

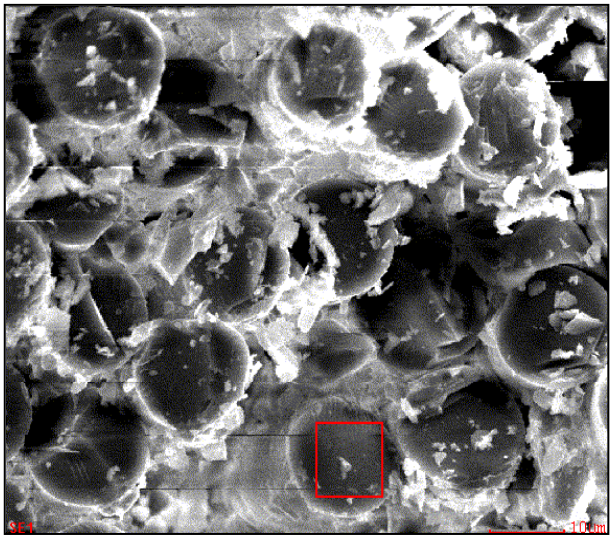

Fig.6.84 SEM image of specimen for EDX

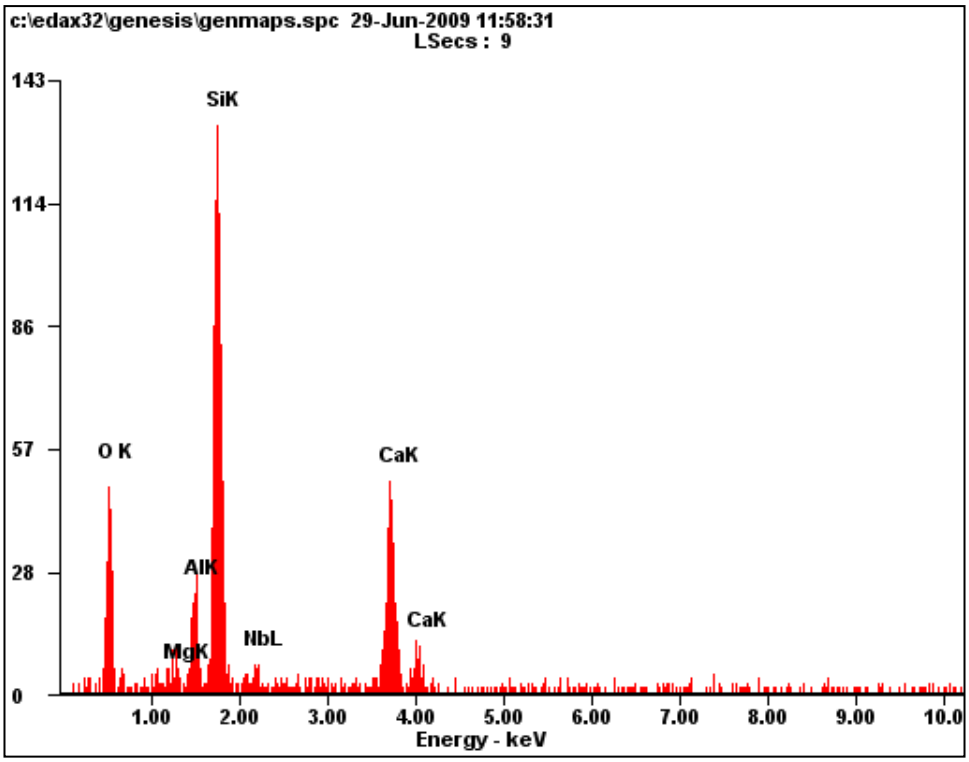

c)

Element	*Wt%*
OK	40.96
MgK	01.77
AlK	05.85
SiK	30.61
NbL	02.90
CaK	16.92

d)

Fig.6.85 (c) Energy vs Electron volt graph for 40% load, (d) Element percentage taken by EDX

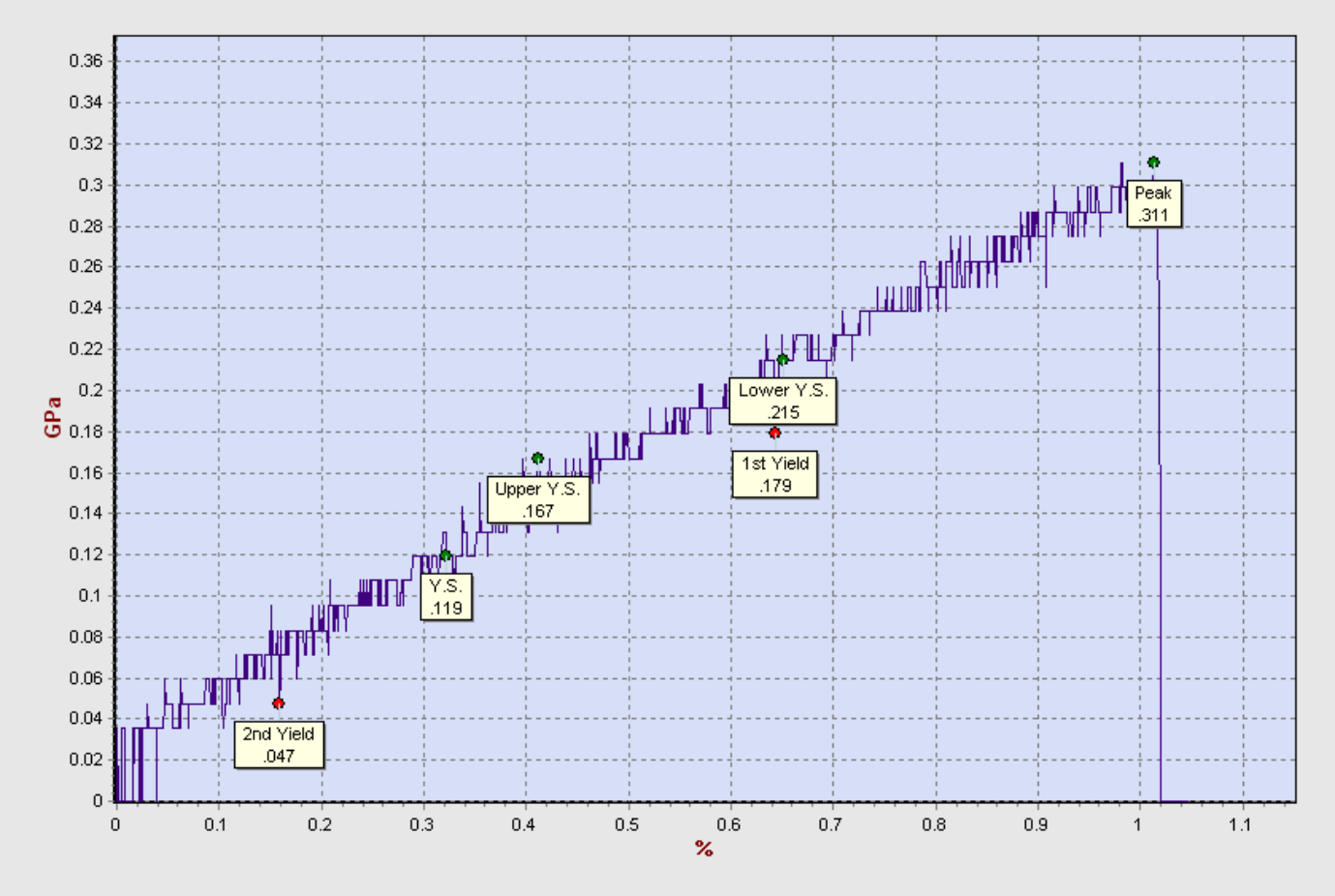

Fig.6.86 Stress vs Strain graph of sample loaded at 40% of U.T.L (Water Tank T1)

3) The results of specimen which were subjected to **60% loading** (T1, 2months) are shown below:

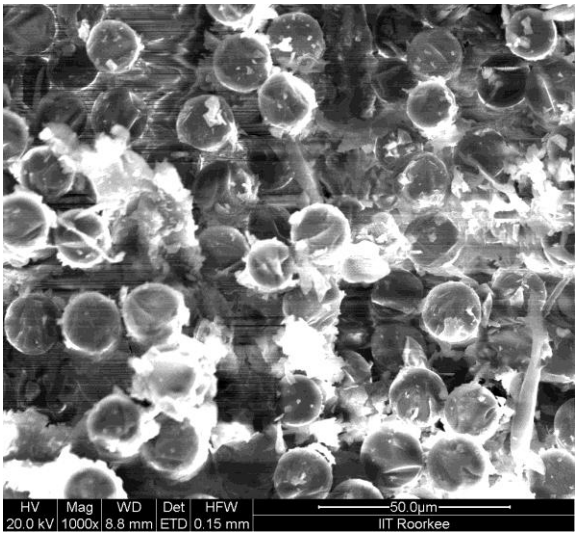

Fig.6.87 SEM image of specimen at 60% load

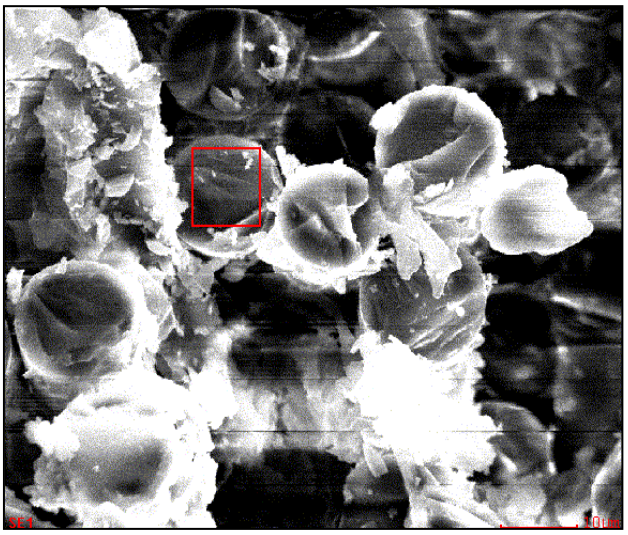

Fig.6.88 SEM image of specimen for EDX

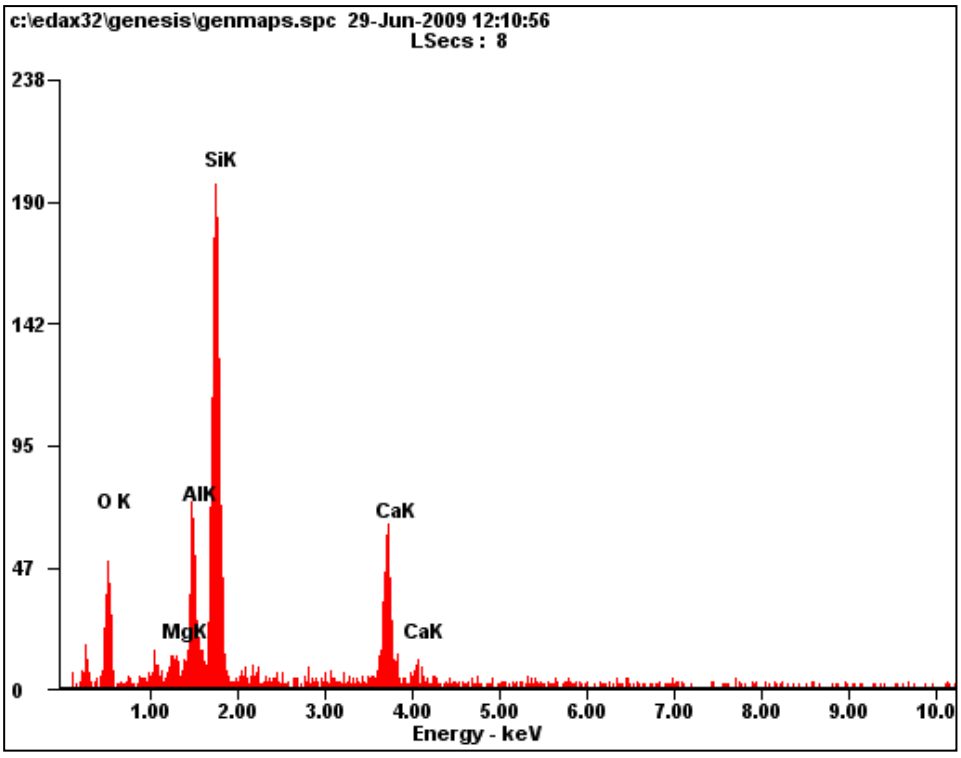

Element	*Wt%*
OK	34.83
MgK	02.00
AlK	10.74
SiK	35.83
CaK	16.60

e) f)

Fig.6.89 (e) Energy vs Electron volt graph for 60% load, (f) Element percentage taken by EDX

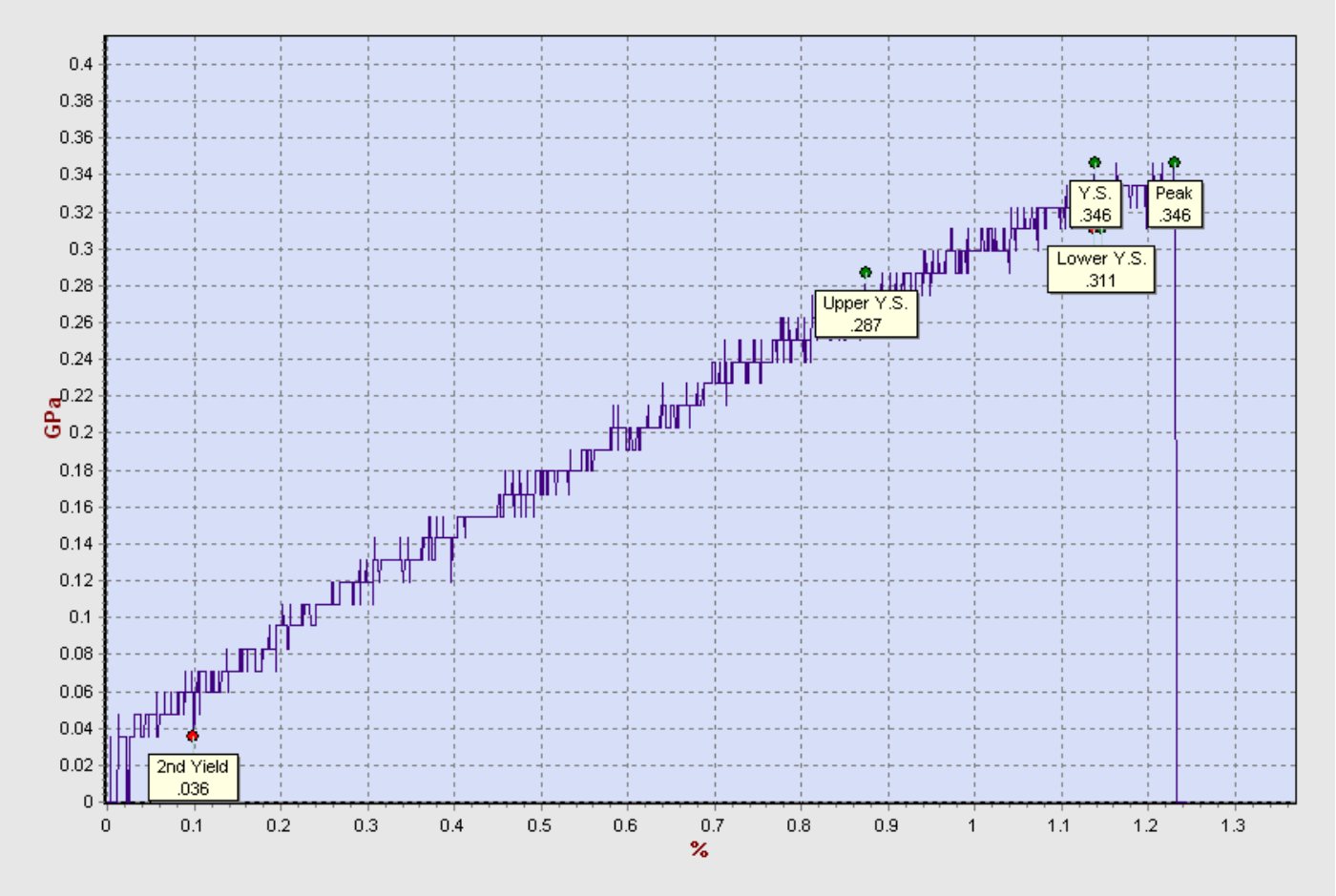

Fig.6.90 Stress vs Strain graph of sample loaded at 60% of U.T.L (Water Tank T1)

4) The results of specimen which were subjected to **80% loading** (T1, 2months) are shown below:

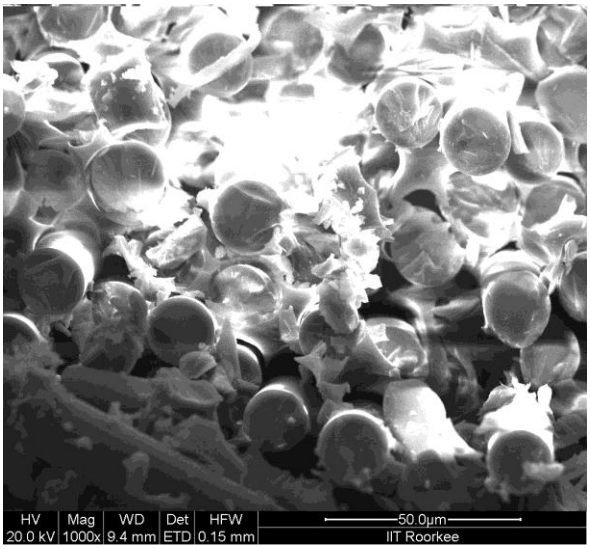

Fig.6.91 SEM image of specimen at 80% load

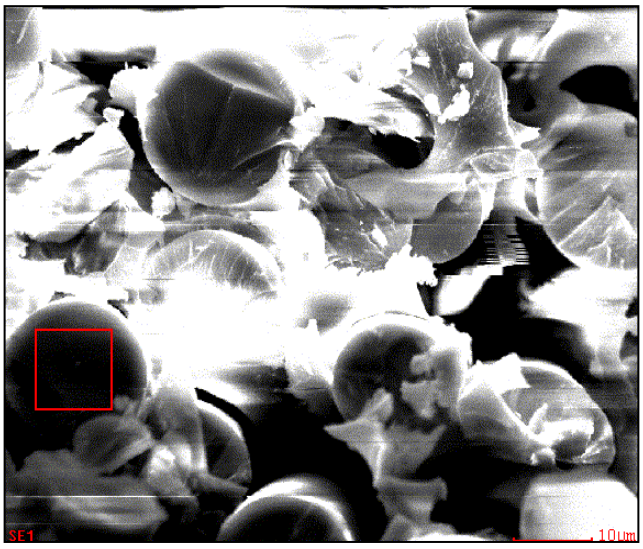

Fig.6.92 SEM image of specimen for EDX

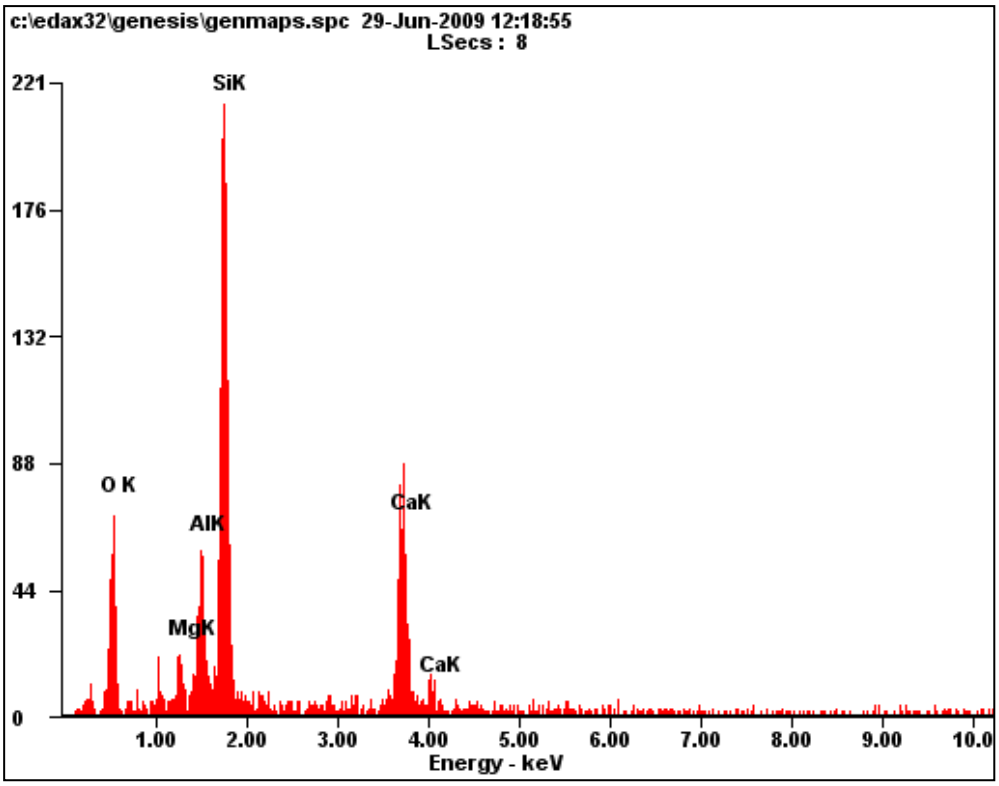

g)

Element	*Wt%*
OK	36.57
MgK	01.85
AlK	06.97
SiK	31.61
CaK	20.99

h)

Fig.6.93 (g) Energy vs Electron volt graph for 60% load, (h) Element percentage taken by EDX

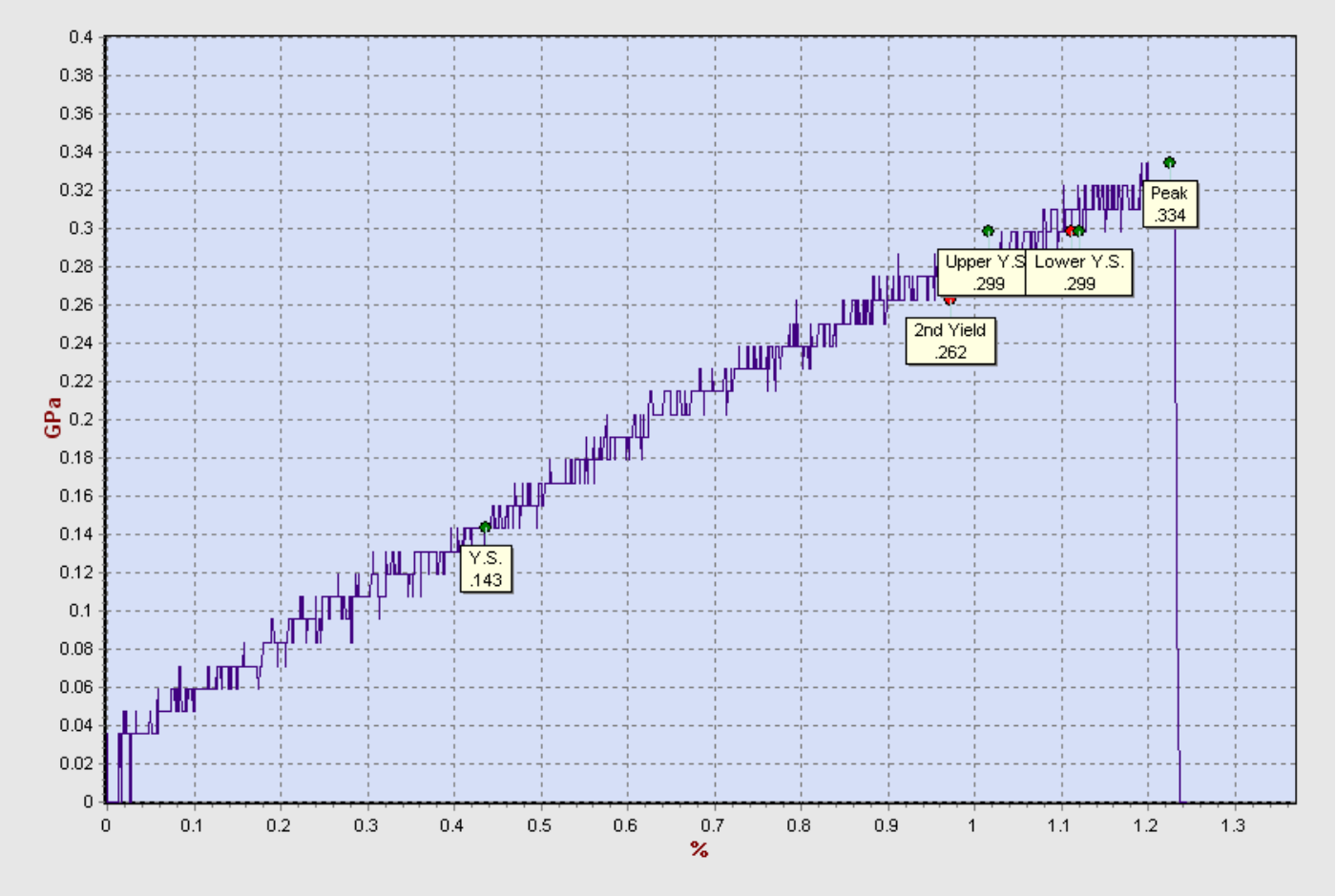

Fig.6.94 Stress vs Strain graph of sample loaded at 80% of U.T.L (Water Tank T1)

B) S.E.M. AND E.D.X. RESULTS OF NaOH TANK T2 (after 2 months)

Holding Parameters:
NaOH bath
Time: 2 month
Temperature: 45^{o}C

1) The results of specimen which were subjected to **20% loading** (T2, 2months) are shown below:

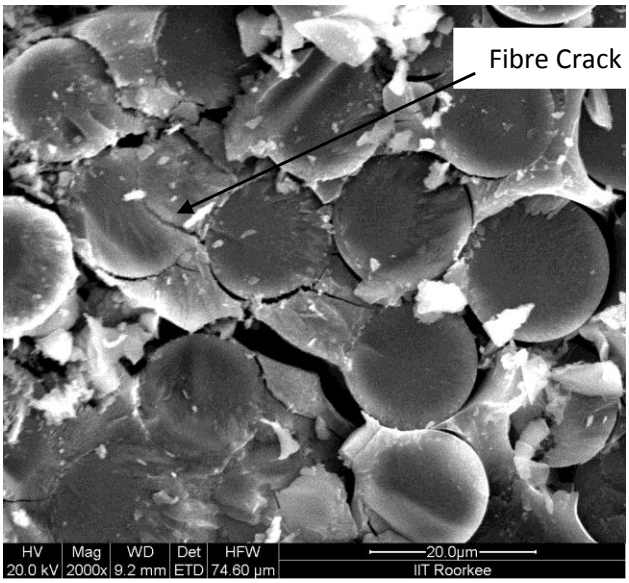

Fig.6.95 SEM image of specimen at 20% load

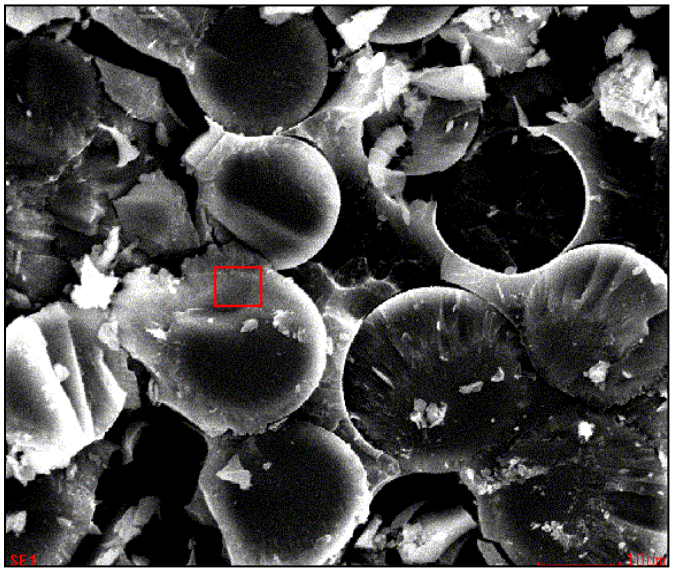

Fig.6.96 SEM image of specimen for EDX

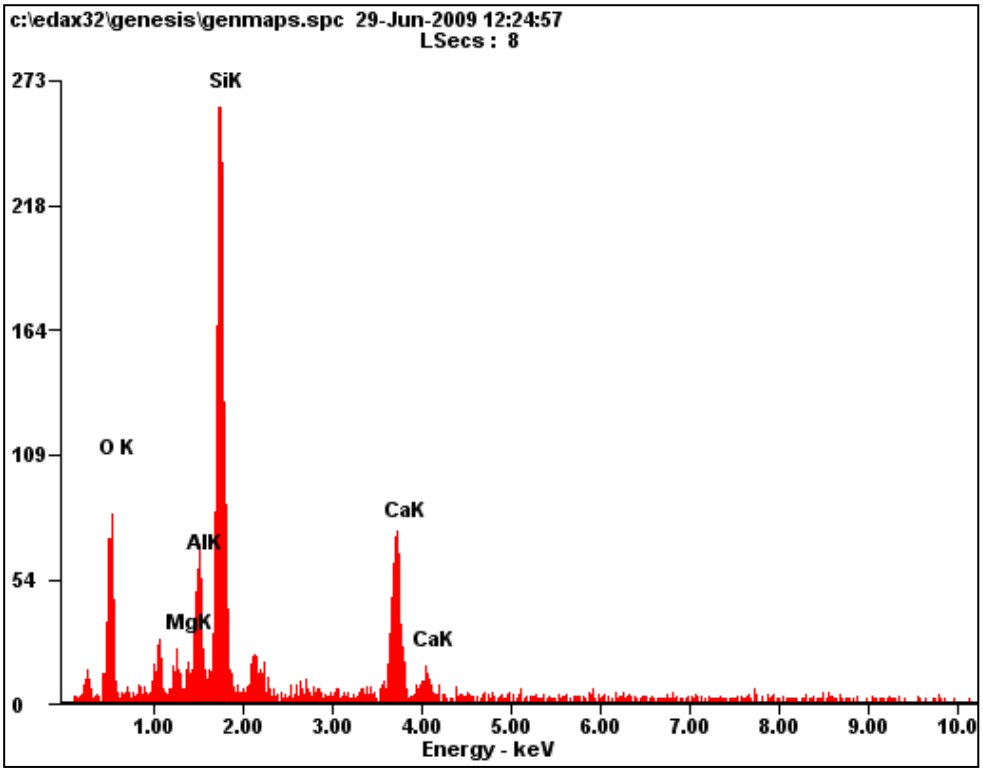

a)

Element	*Wt%*
OK	39.61
MgK	02.28
AlK	06.78
SiK	33.66
CaK	16.67

b)

Fig.6.97 (a) Energy vs Electron volt graph for 20% load, (b) Element percentage taken by EDX

Fig.6.98 Stress vs Strain graph of sample loaded at 20% of U.T.L (NaOH Tank T2)

2) The results of specimen which were subjected to **40% loading** (T2, 2months) are shown below:

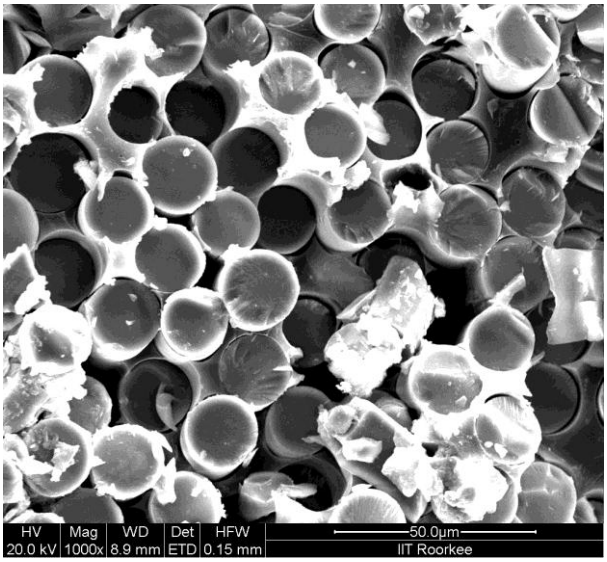

Fig.6.99 SEM image of specimen at 40% load

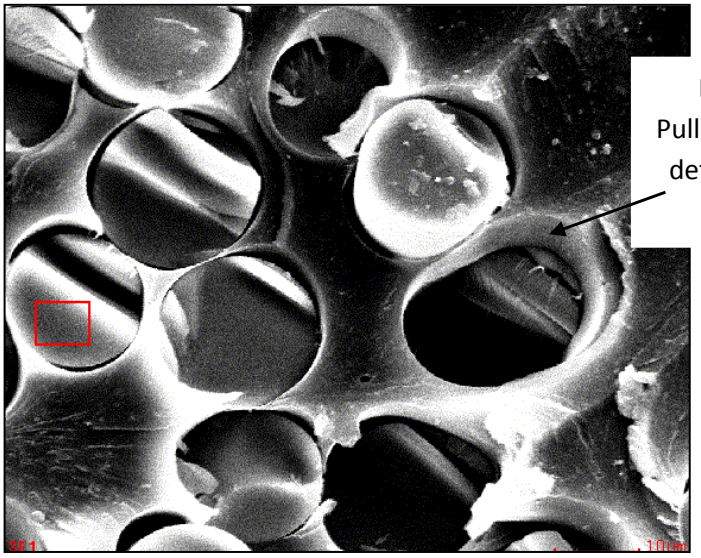

Fig.6.100 SEM image of specimen for EDX

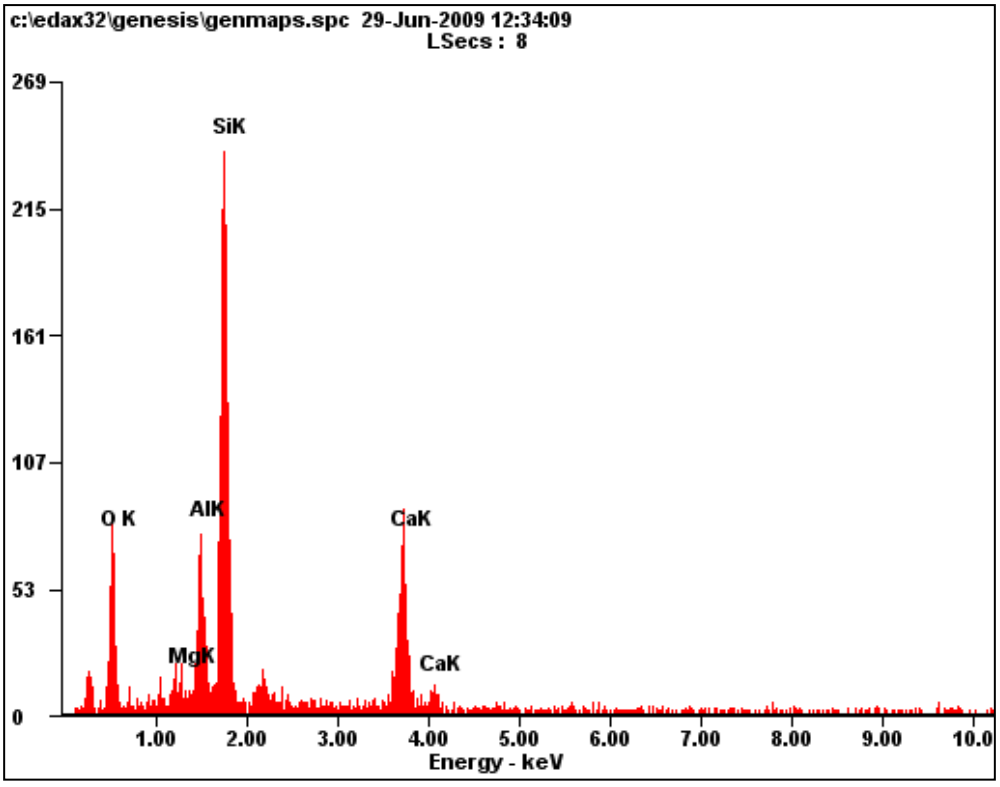

c)

Element	*Wt%*
OK	36.73
MgK	01.80
AlK	08.67
SiK	34.04
CaK	16.76

d)

Fig.6.101 (c) Energy vs Electron volt graph for 40% load, (d) Element percentage taken by EDX

Fig.6.102 Stress vs Strain graph of sample loaded at 40% of U.T.L (NaOH Tank T2)

3) The results of specimen which were subjected to **60% loading** (T2, 2months) are shown below:

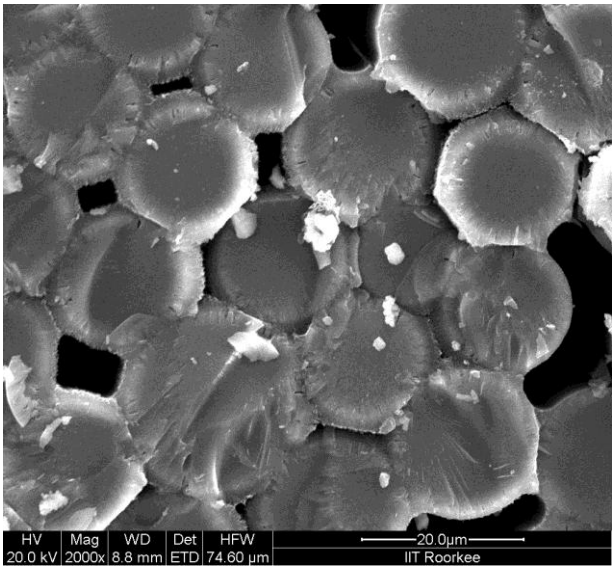

Fig.6.103 SEM image of specimen at 60% load

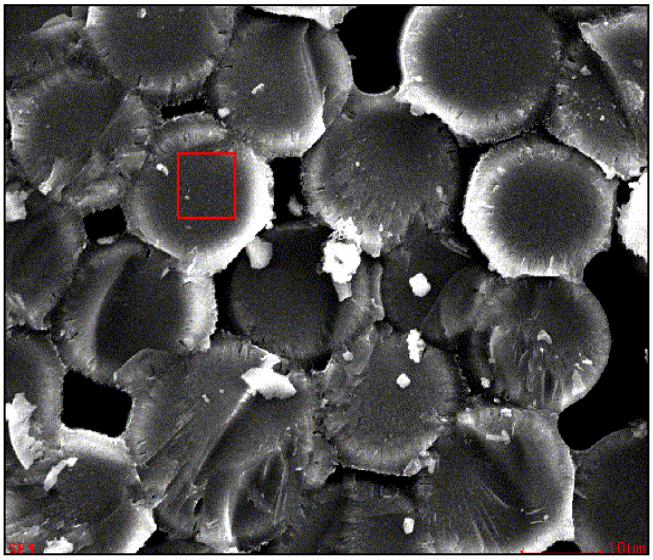

Fig.6.104 SEM image of specimen for EDX

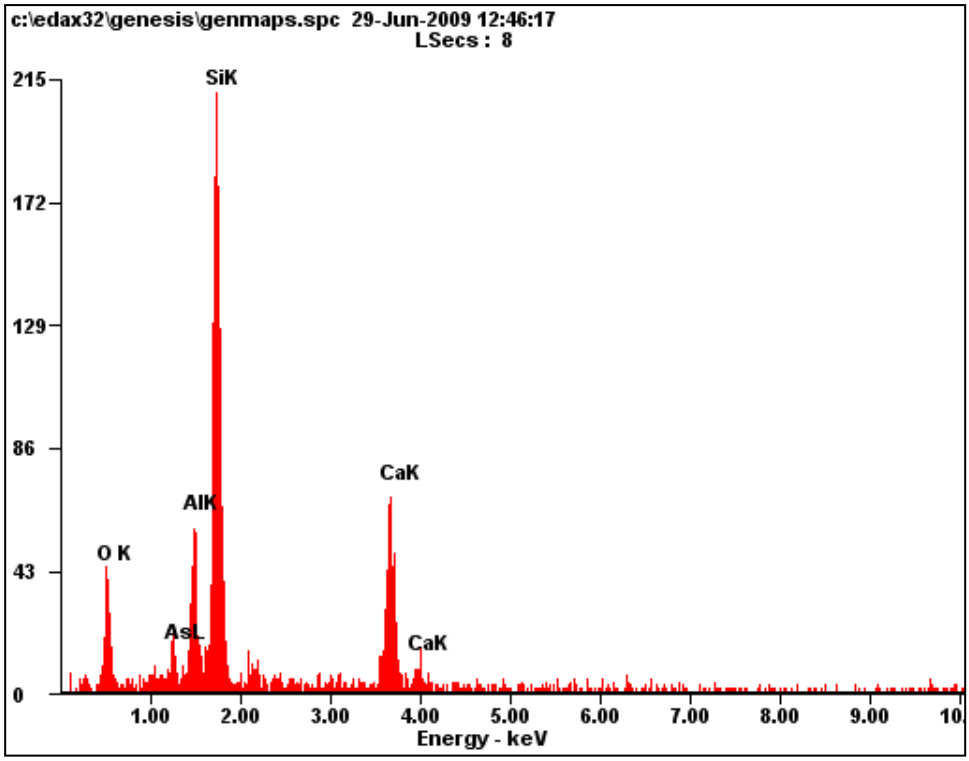

e)

Element	Wt%
OK	30.88
AsL	02.52
AlK	08.13
SiK	36.33
CaK	21.14

f)

Fig.6.105 (e) Energy vs Electron volt graph for 60% load, (f) Element percentage taken by EDX

Fig.6.106 Stress vs Strain graph of sample loaded at 60% of U.T.L (NaOH Tank T2)

4) The results of specimen which were subjected to **80% loading** (T2, 2months) are shown below:

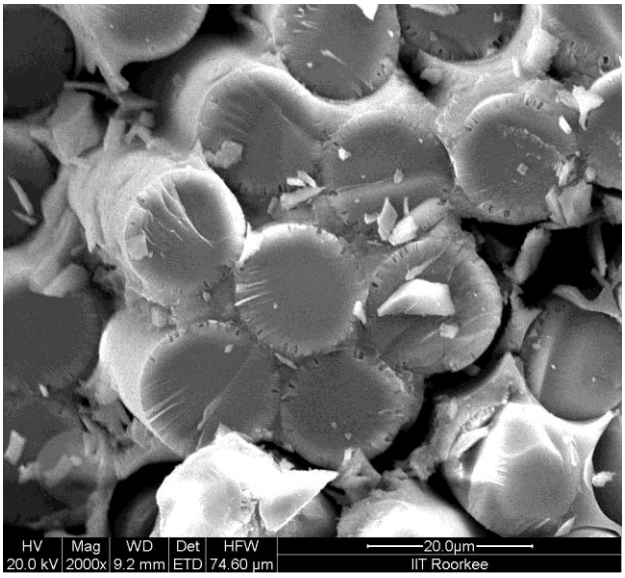

Fig.6.107 SEM image of specimen at 80% load

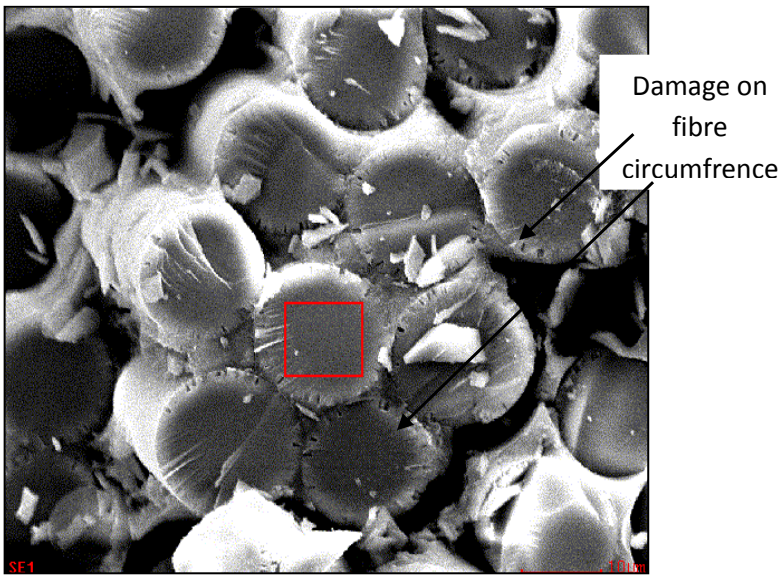

Fig.6.108 SEM image of specimen for EDX

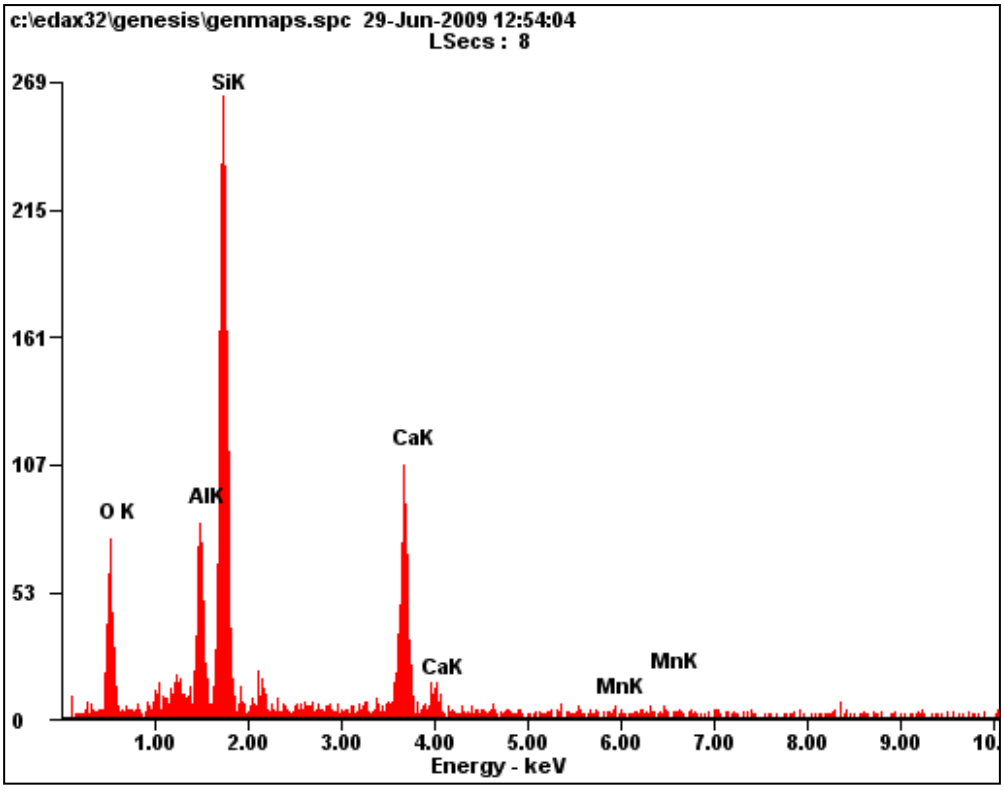

g)

Element	*Wt%*
OK	36.02
AlK	08.60
SiK	34.75
CaK	19.99
MnK	00.65

h)

Fig.6.109 (g) Energy vs Electron volt graph for 80% load, (h) Element percentage taken by EDX

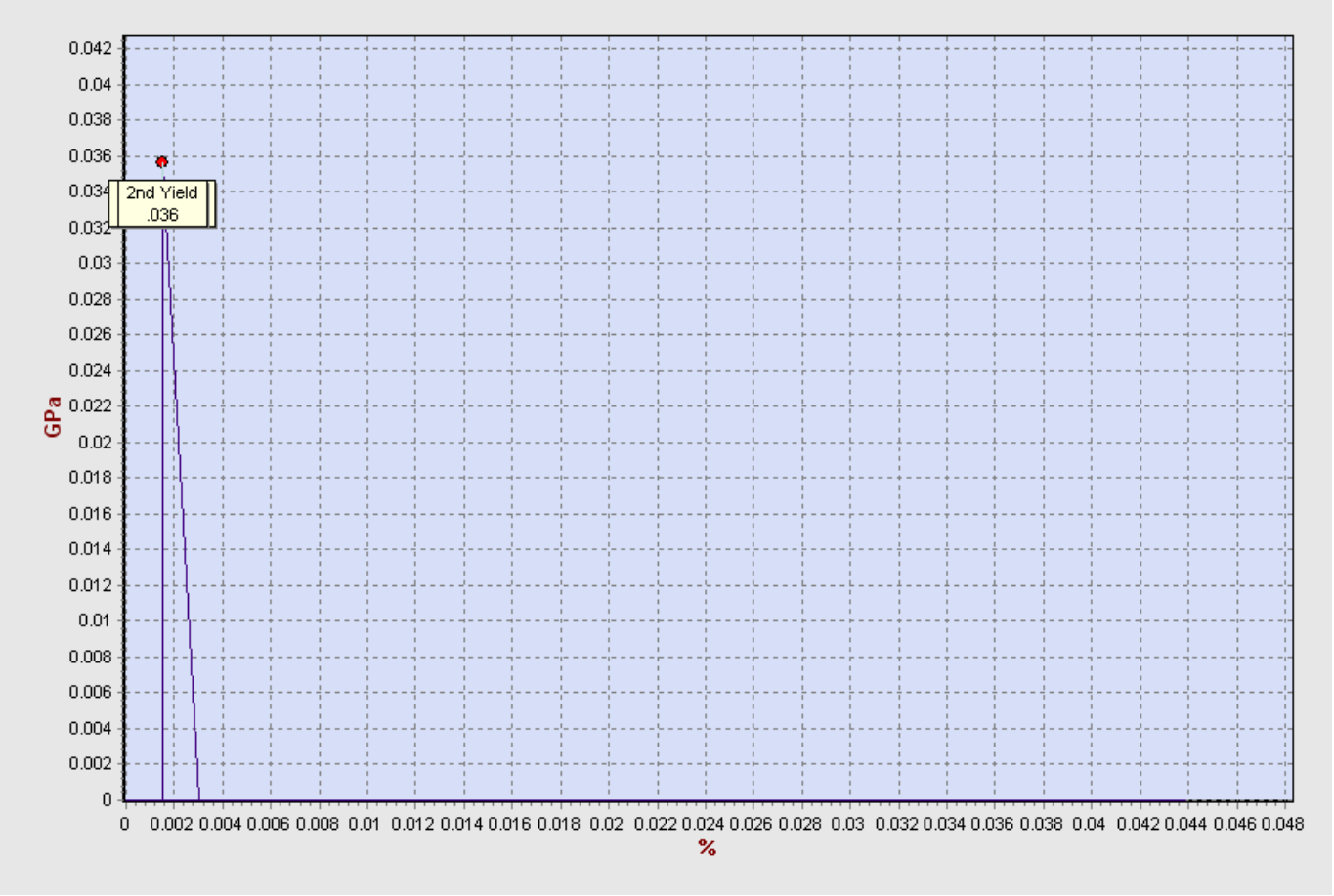

Fig.6.110 Stress vs Strain graph of sample loaded at 80% of U.T.L (NaOH Tank T2)

C) S.E.M. AND E.D.X. RESULTS OF NaOH TANK T3 (after 2 months)

Holding Parameters:
NaOH bath
Time: 2 month
Temperature: 55^{o}C

1) The results of specimen which were subjected to **20% loading** (T3, 2months) are shown below:

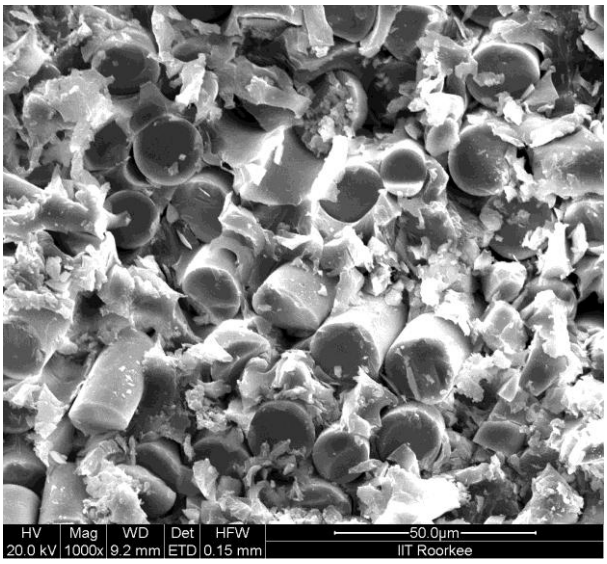

Fig.6.111 SEM image of specimen at 20% load

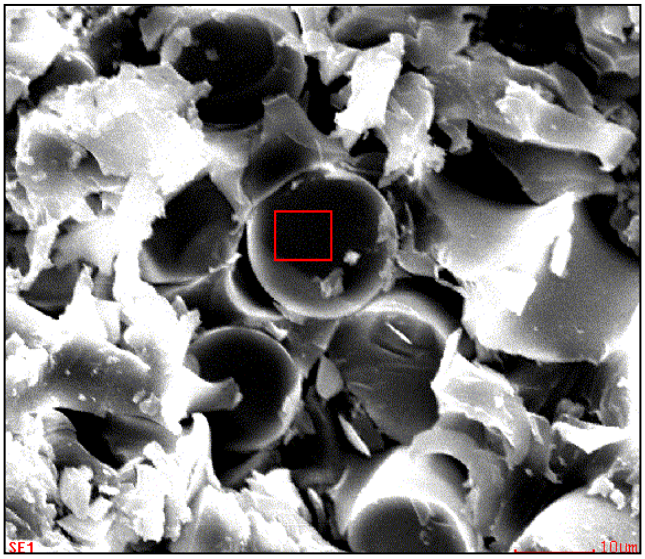

Fig.6.112 SEM image of specimen for EDX

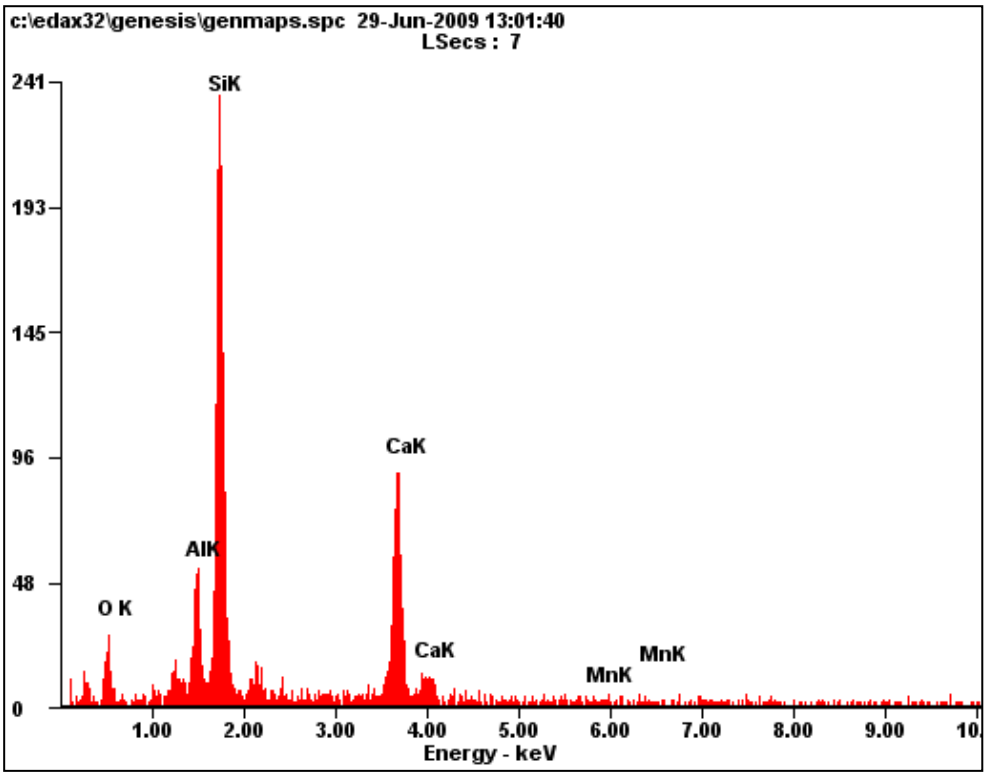

a)

Element	*Wt%*
OK	23.25
AlK	08.20
SiK	40.56
CaK	26.47
MnK	00.51

b)

Fig.6.113 (a) Energy vs Electron volt graph for 20% load, (b) Element percentage taken by EDX

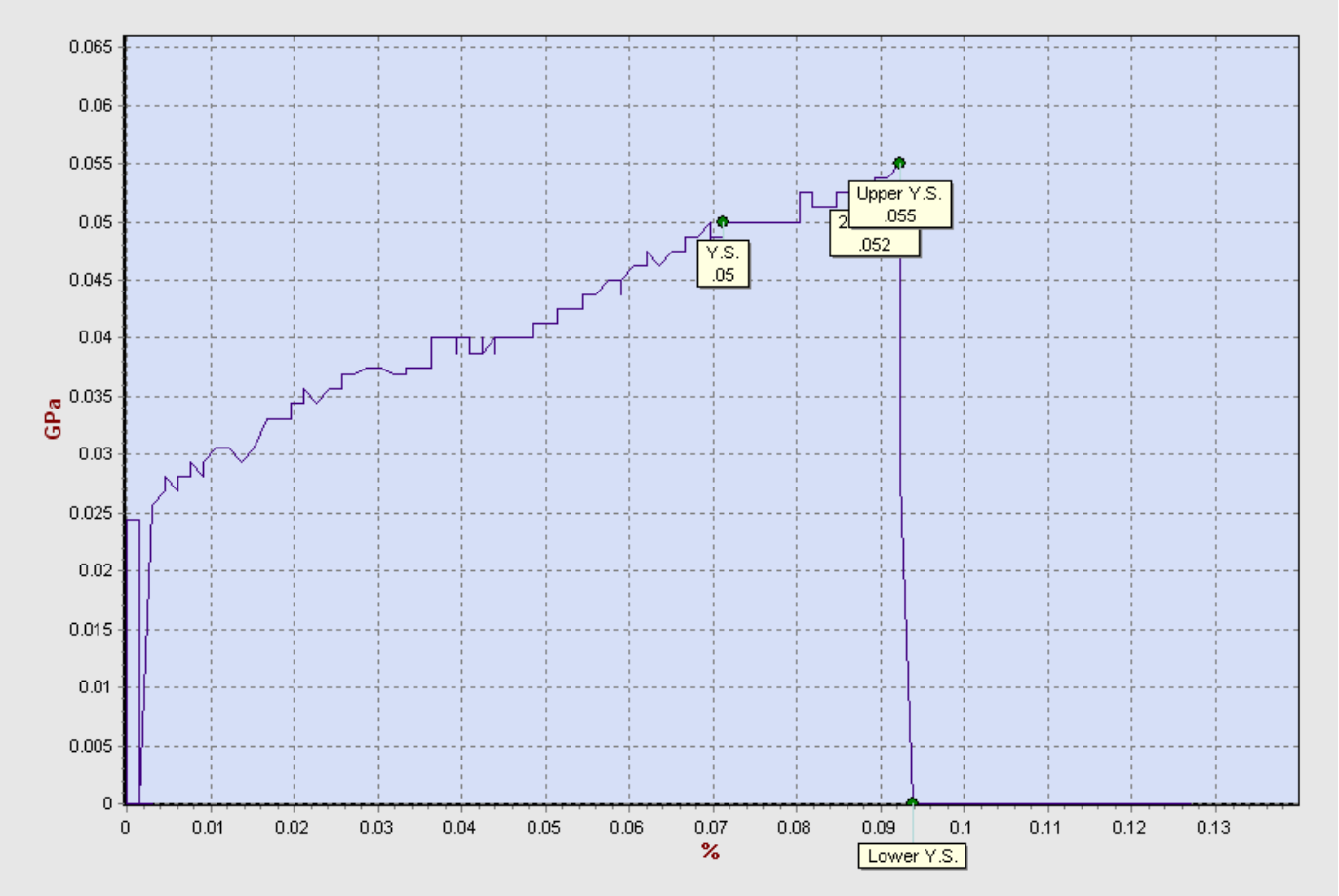

Fig.6.114 Stress vs Strain graph of sample loaded at 20% of U.T.L (NaOH Tank T3)

2) The results of specimen which were subjected to **40% loading** (T3, 2months) are shown below:

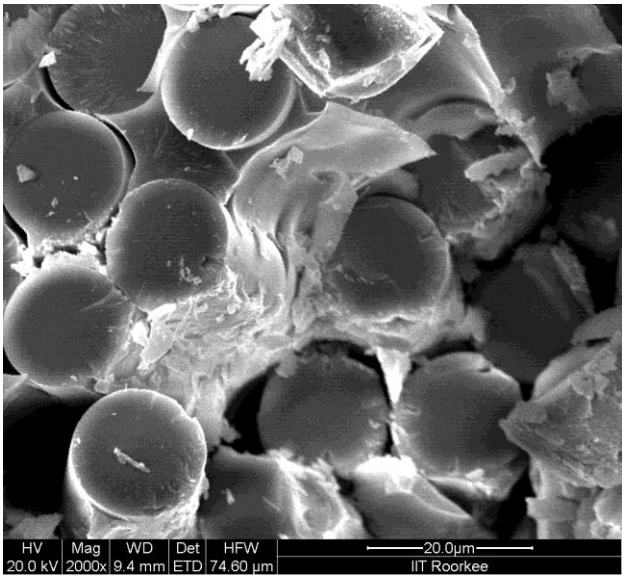

Fig.6.115 SEM image of specimen at 40% load

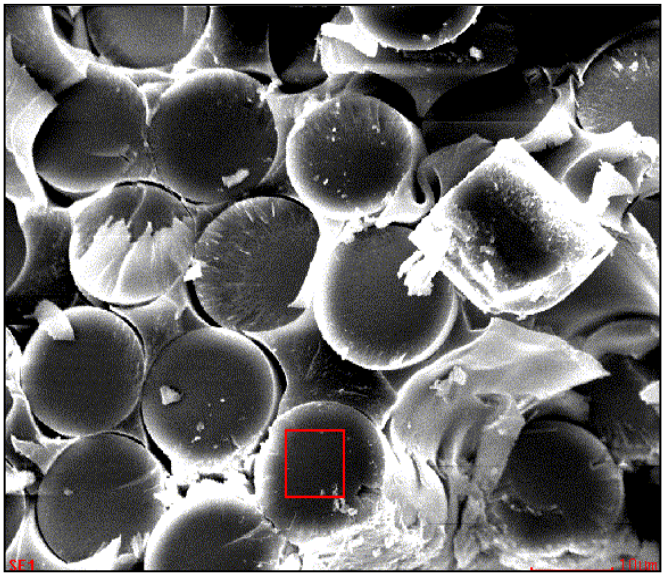

Fig.6.116 SEM image of specimen for EDX

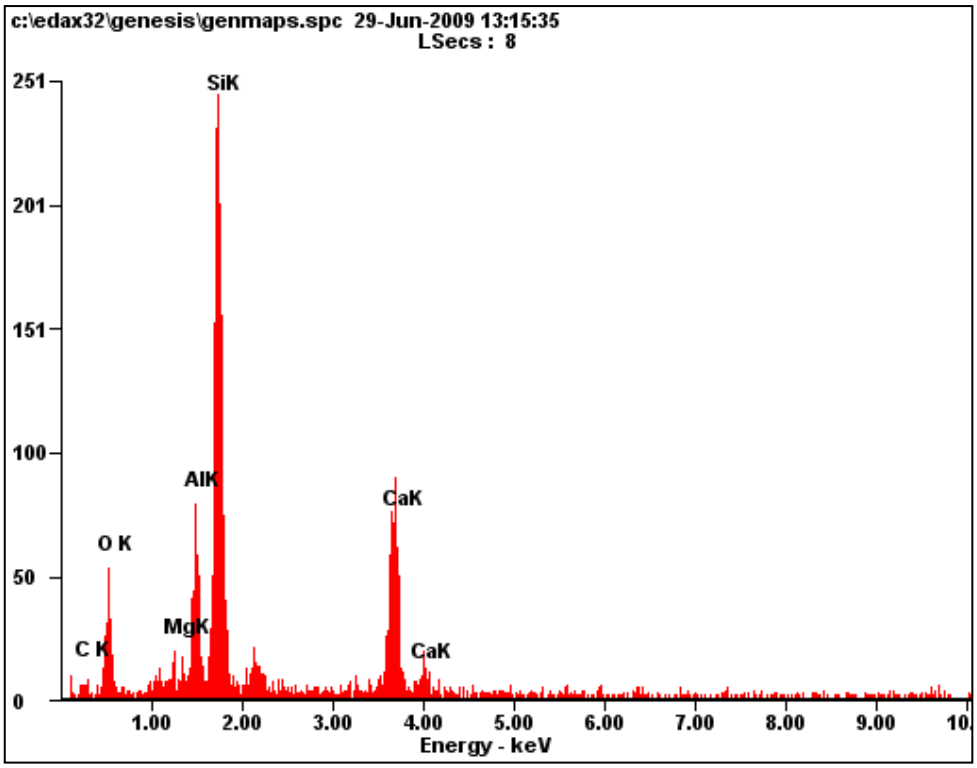

c)

Element	*Wt%*
CK	08.28
OK	28.63
MgK	00.57
AlK	06.43
SiK	33.92
CaK	21.18

d)

Fig.6.117 (c) Energy vs Electron volt graph for 40% load, (d) Element percentage taken by EDX

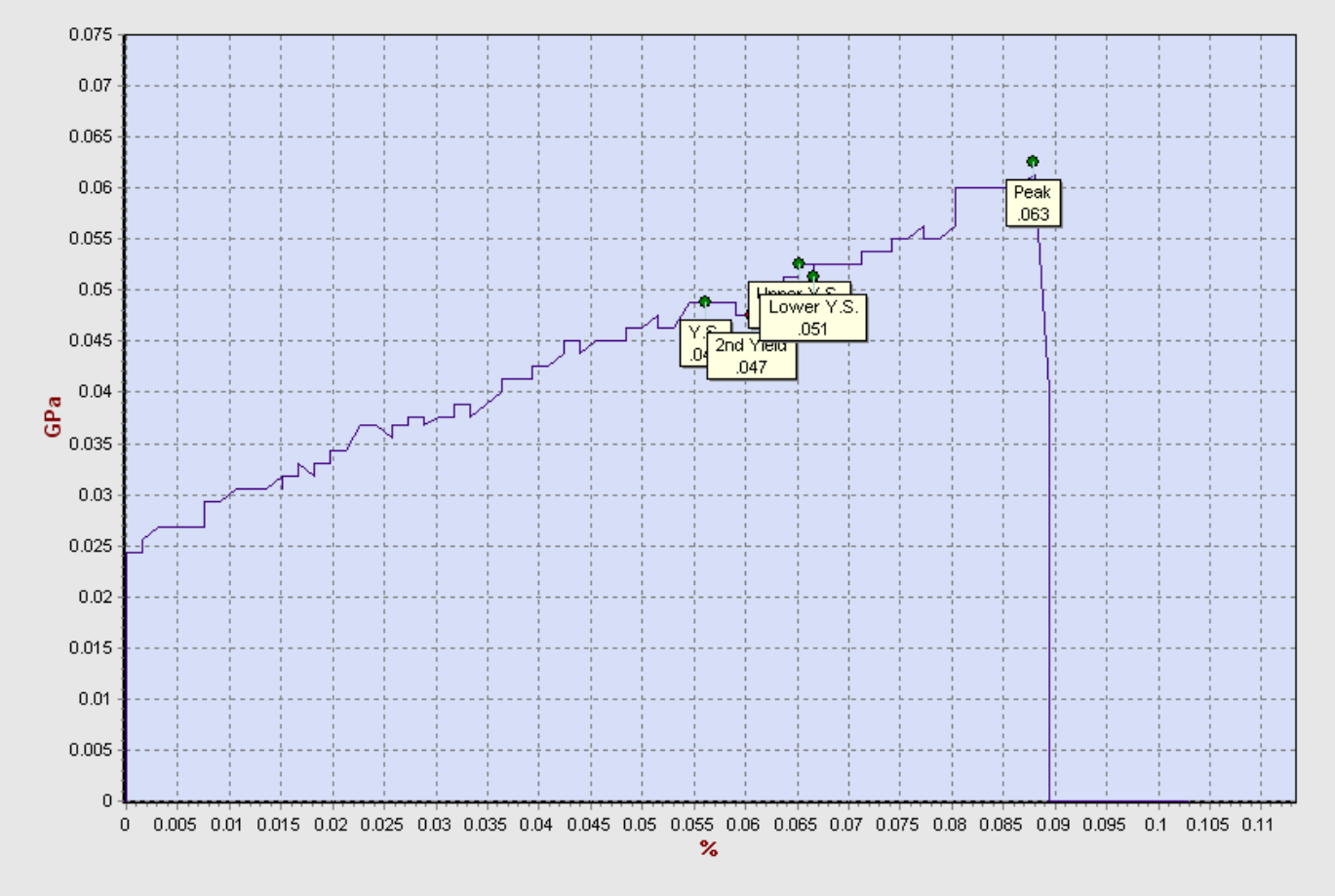

Fig.6.118 Stress vs Strain graph of sample loaded at 40% of U.T.L (NaOH Tank T3)

3) The results of specimen which were subjected to **60% loading** (T3, 2months) are shown below:

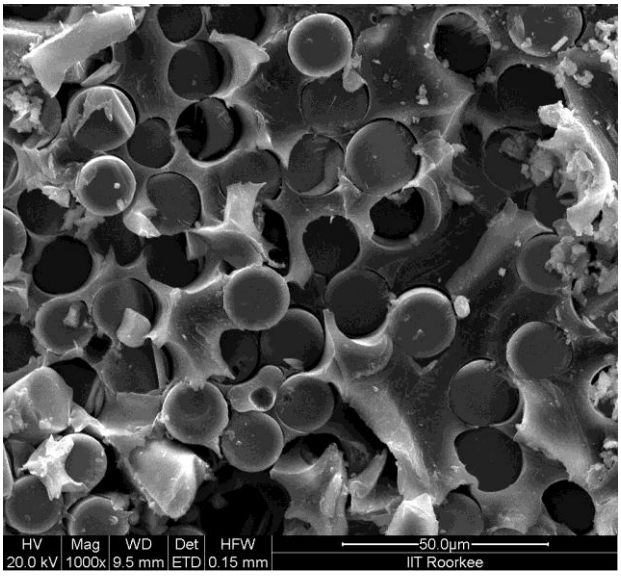

Fig.6.119 SEM image of specimen at 60% load

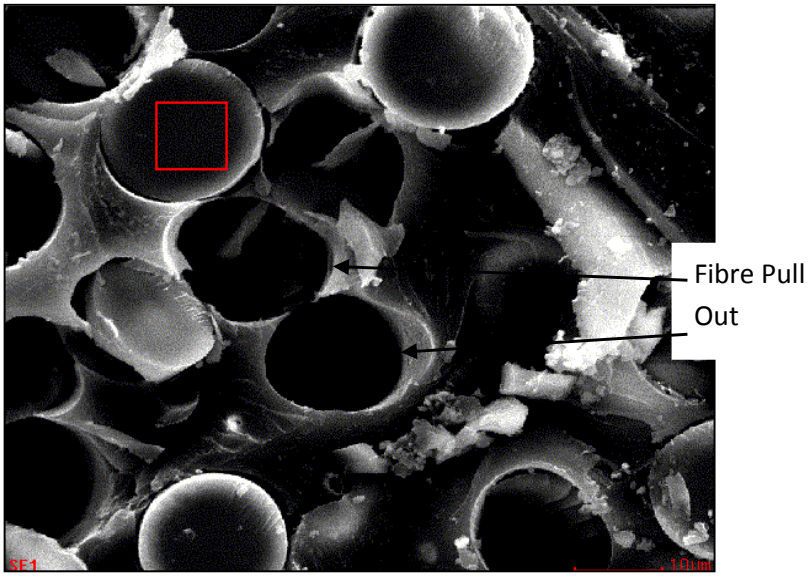

Fig.6.120 SEM image of specimen for EDX

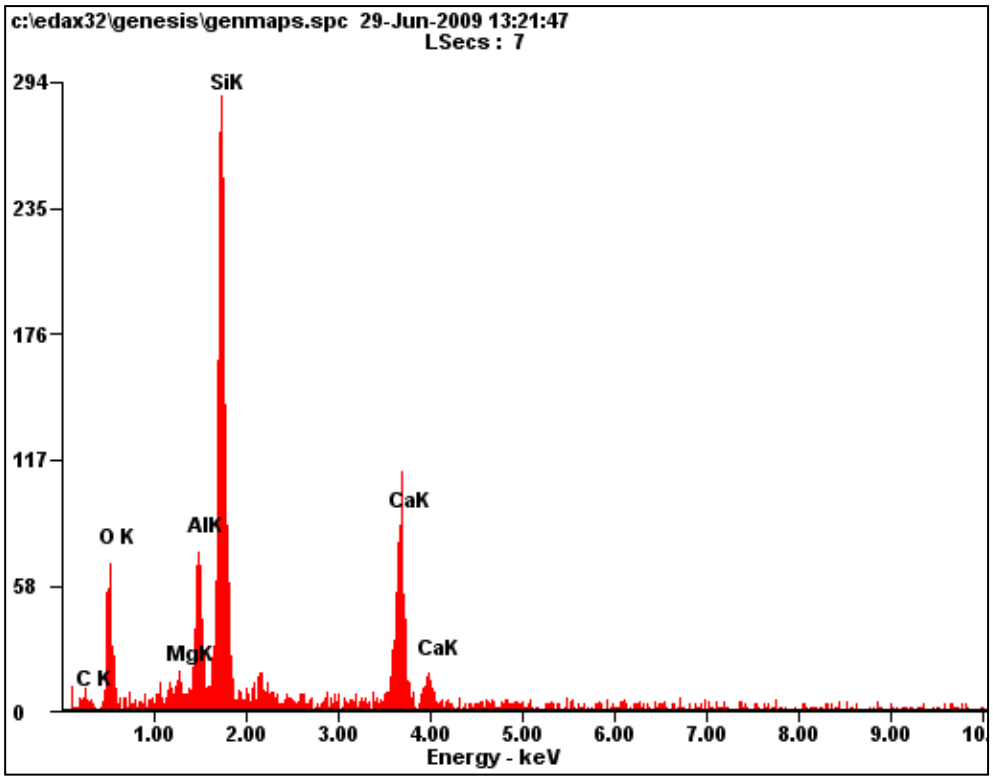

e)

Element	*Wt%*
CK	08.67
OK	32.53
MgK	01.59
AlK	06.63
SiK	31.78
CaK	16.81

f)

Fig.6.121 (e) Energy vs Electron volt graph for 60% load, (f) Element percentage taken by EDX

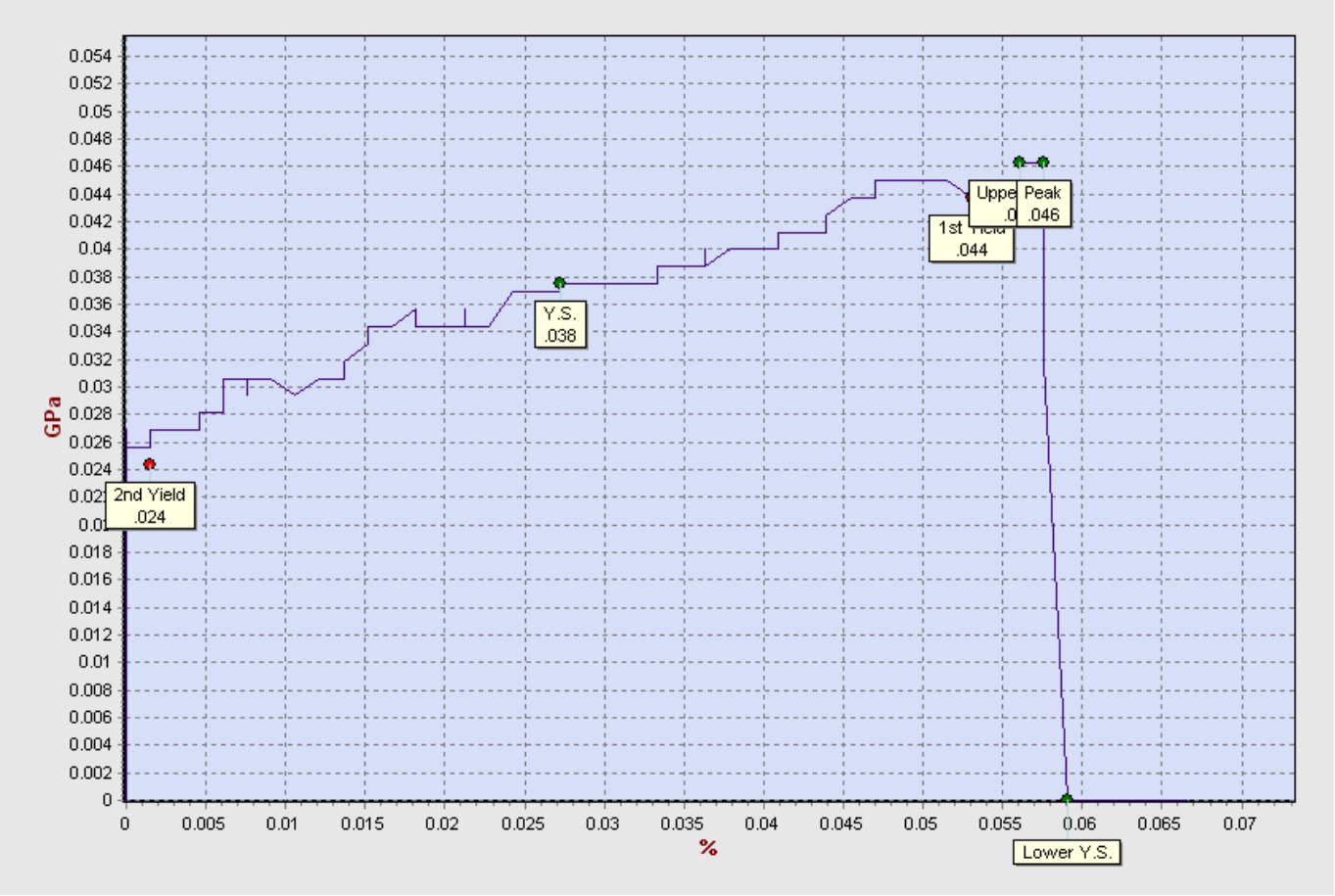

Fig.6.122 Stress vs Strain graph of sample loaded at 60% of U.T.L (NaOH Tank T3)

4) The results of specimen which were subjected to **80% loading** (T3, 2months) are shown below:

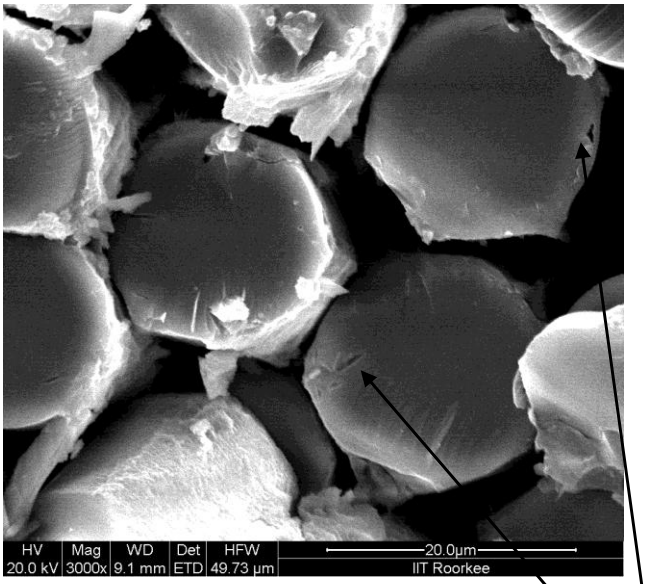

Fig.6.123 SEM image of specimen at 80% load

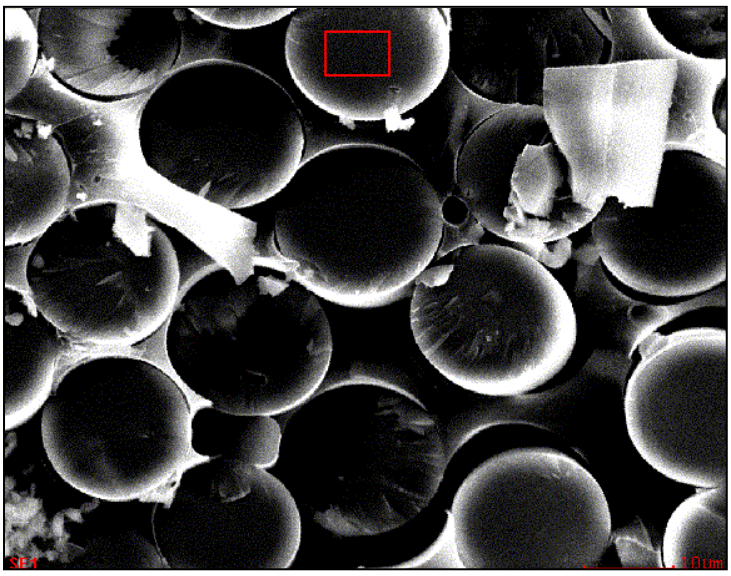

Fig.6.124 SEM image of specimen for EDX

Fibre crack

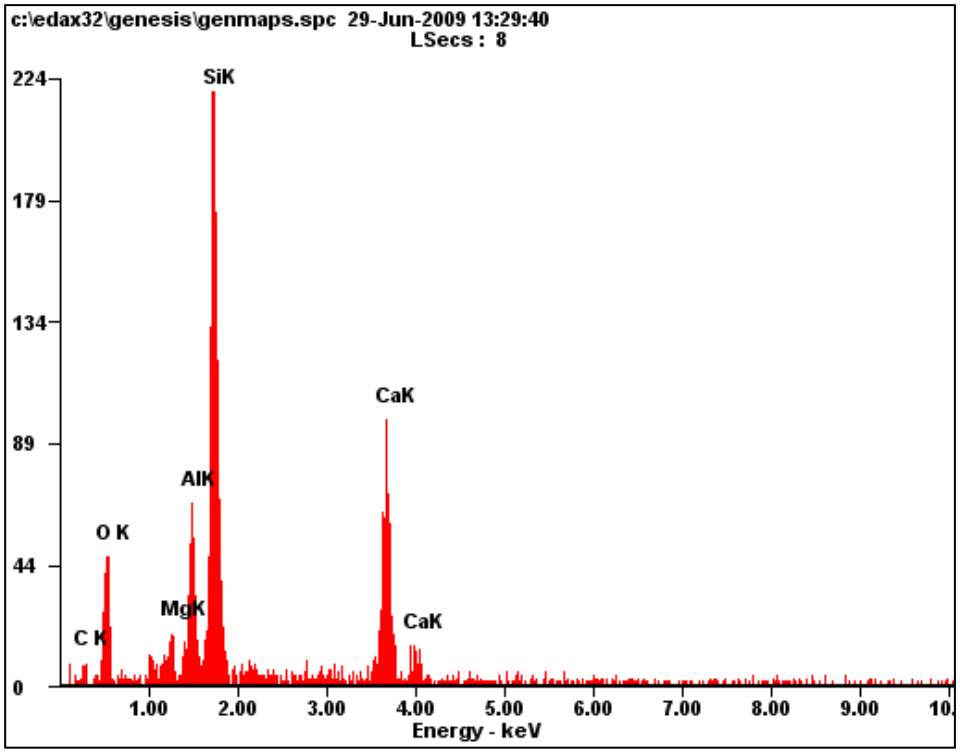

g)

Element	*Wt%*
CK	04.92
OK	30.58
MgK	02.58
AlK	08.62
SiK	33.45
CaK	19.85

h)

Fig.6.125 (g) Energy vs Electron volt graph for 80% load, (h) Element percentage taken by EDX

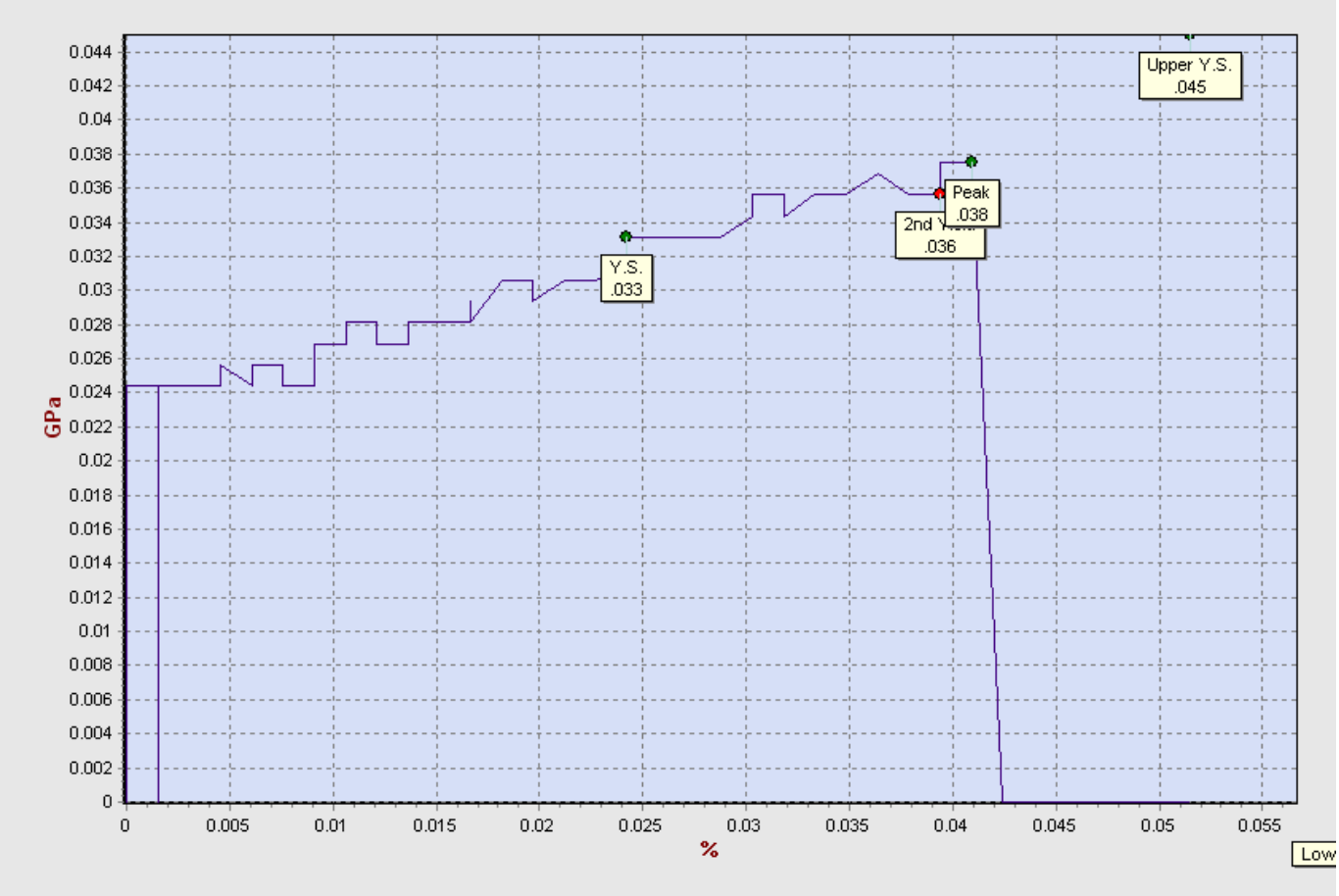

Fig.6.126 Stress vs Strain graph of sample loaded at 80% of U.T.L (NaOH Tank T3)

D) S.E.M. AND E.D.X. RESULTS OF WATER TANK T4 (after 2 months)

Holding Parameters:
Water bath
Time: 2 month
Temperature: 55^{o}C

1) The results of specimen which were subjected to **20% loading** (T4, 2months) are shown below:

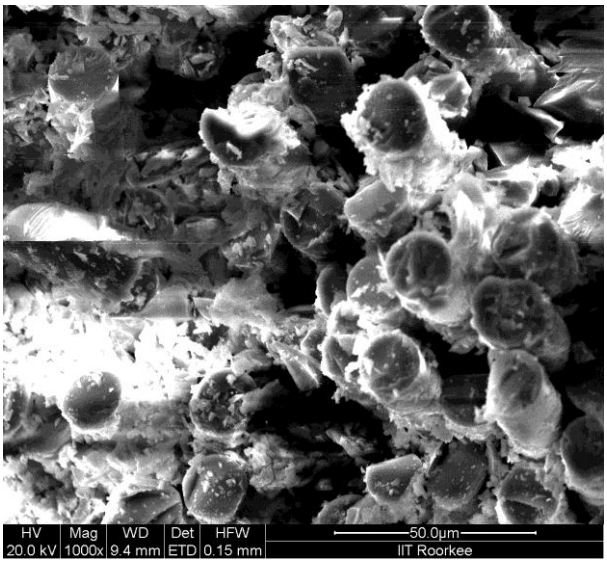

Fig.6.127 SEM image of specimen at 20% load

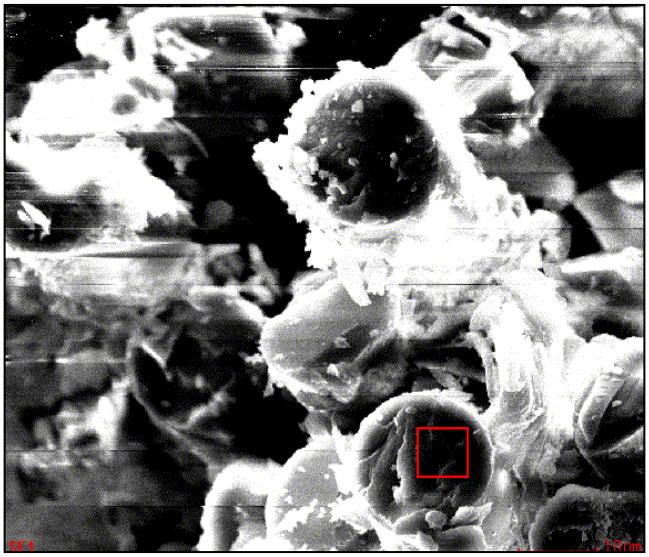

Fig.6.128 SEM image of specimen for EDX

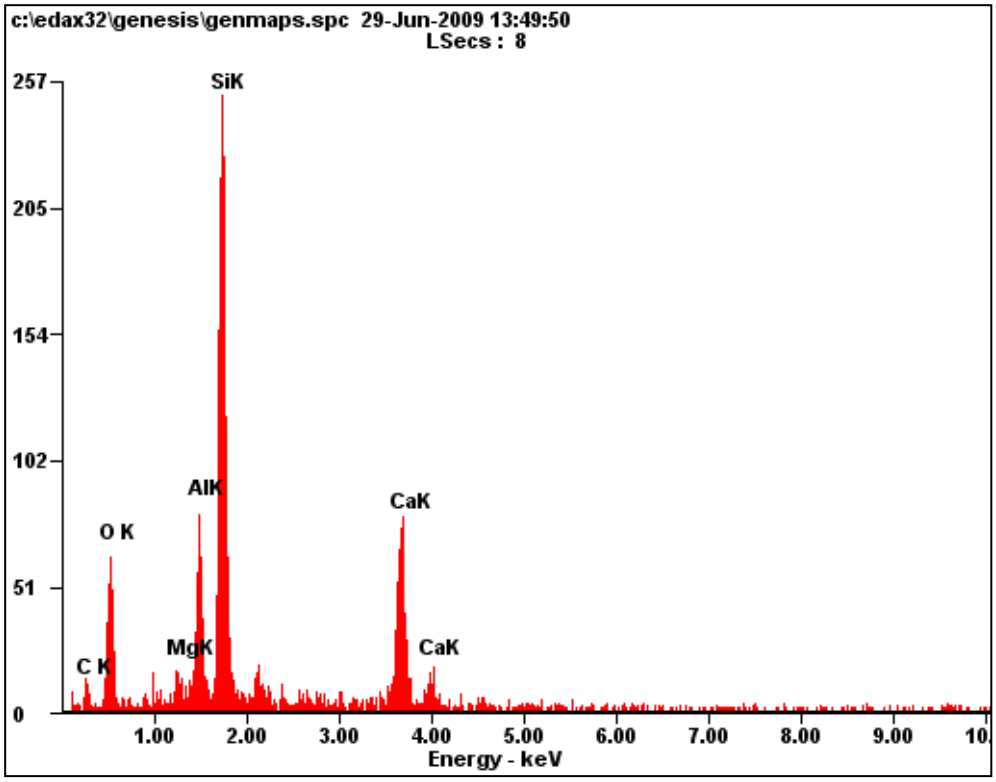

a)

Element	*Wt%*
CK	11.74
OK	32.11
MgK	01.75
AlK	06.40
SiK	30.93
CaK	16.07

b)

Fig.6.129 (a) Energy vs Electron volt graph for 20% load, (b) Element percentage taken by EDX

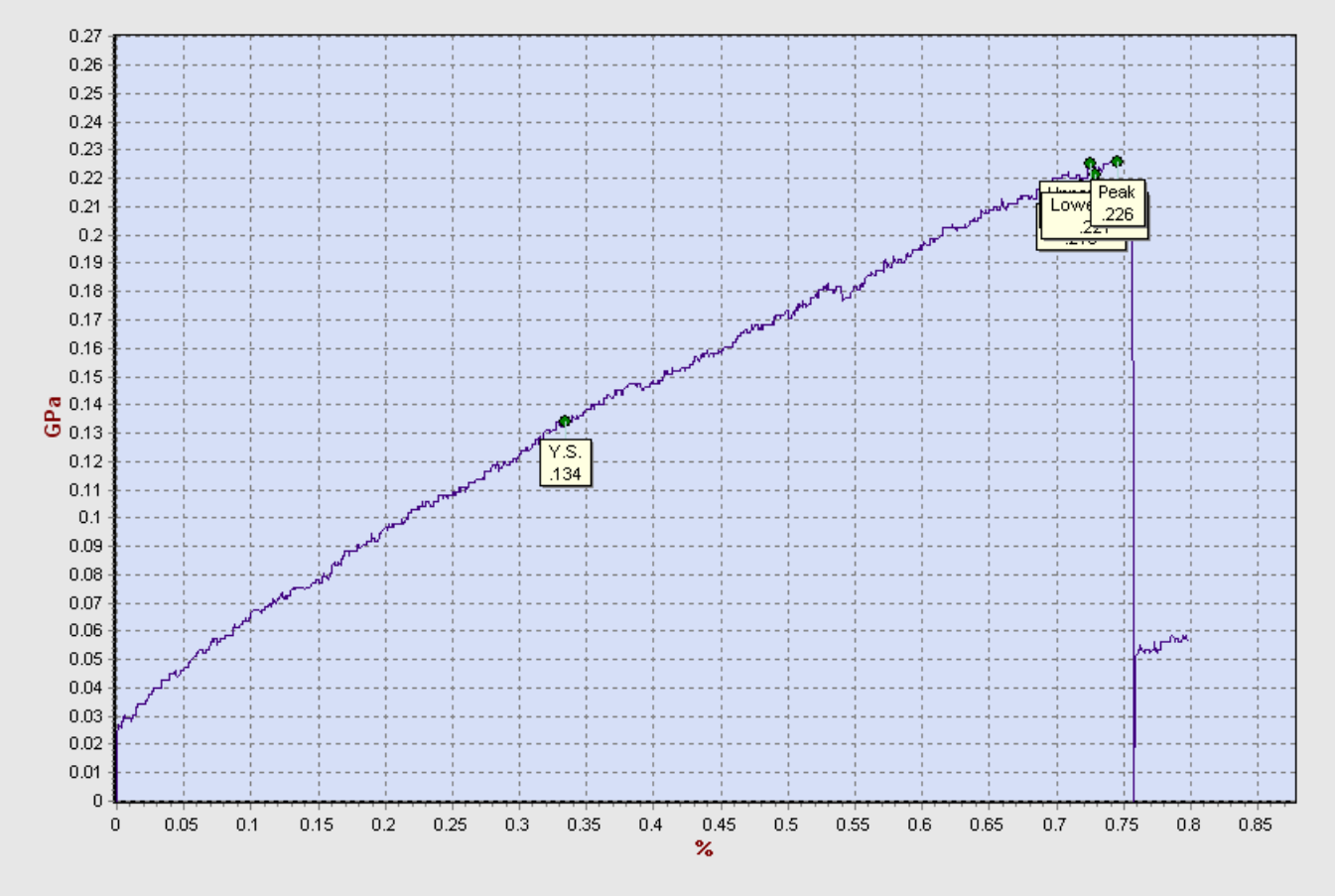

Fig.6.130 Stress vs Strain graph of sample loaded at 20% of U.T.L (Water Tank T4)

2) The results of specimen which were subjected to **40% loading** (T4, 2months) are shown below:

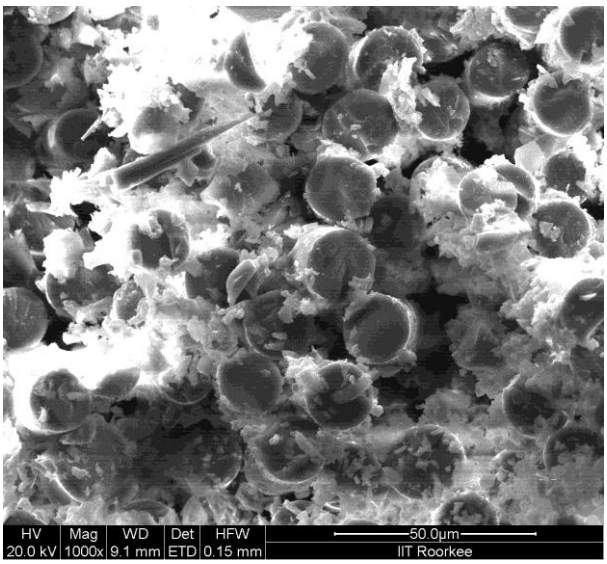

Fig.6.131 SEM image of specimen at 40% load

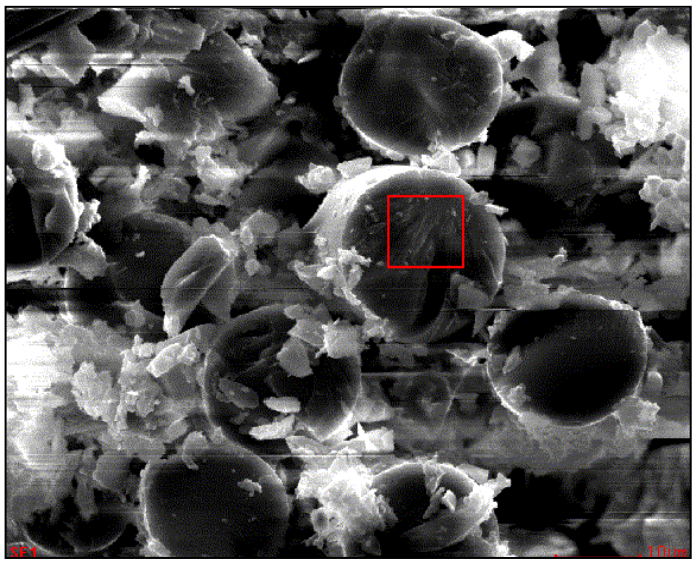

Fig.6.132 SEM image of specimen for EDX

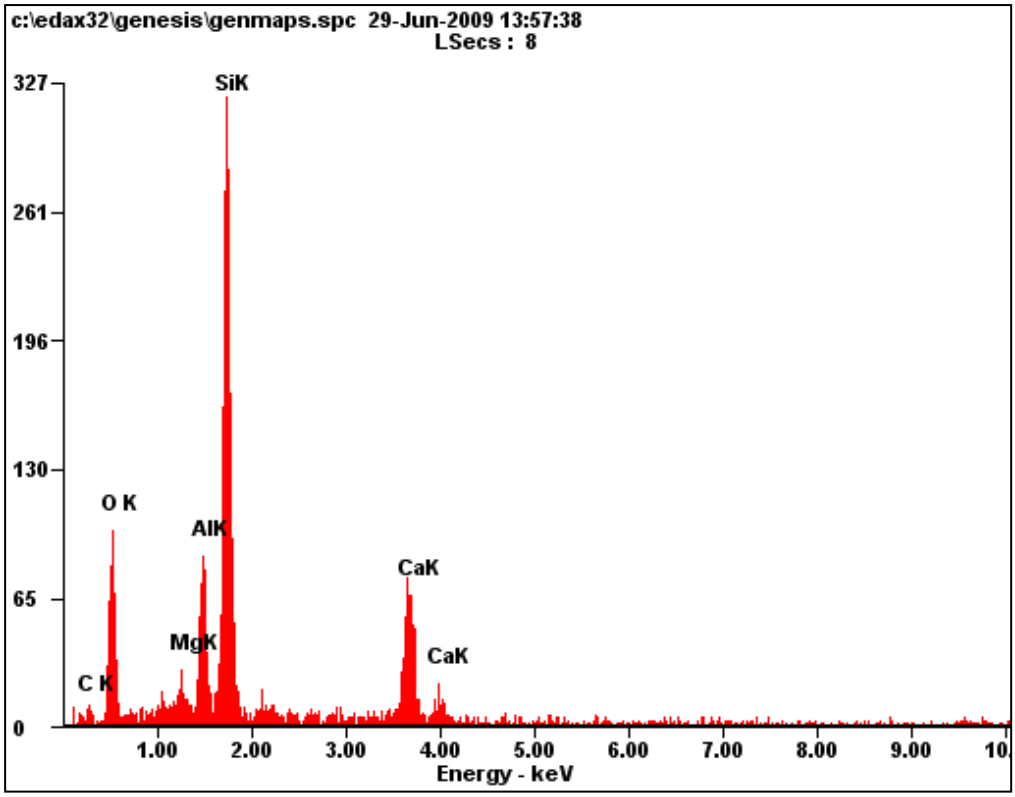

c)

Element	*Wt%*
CK	04.95
OK	38.40
MgK	02.13
AlK	06.99
SiK	32.39
CaK	14.14

d)

Fig.6.133 (c) Energy vs Electron volt graph for 40% load, (d) Element percentage taken by EDX

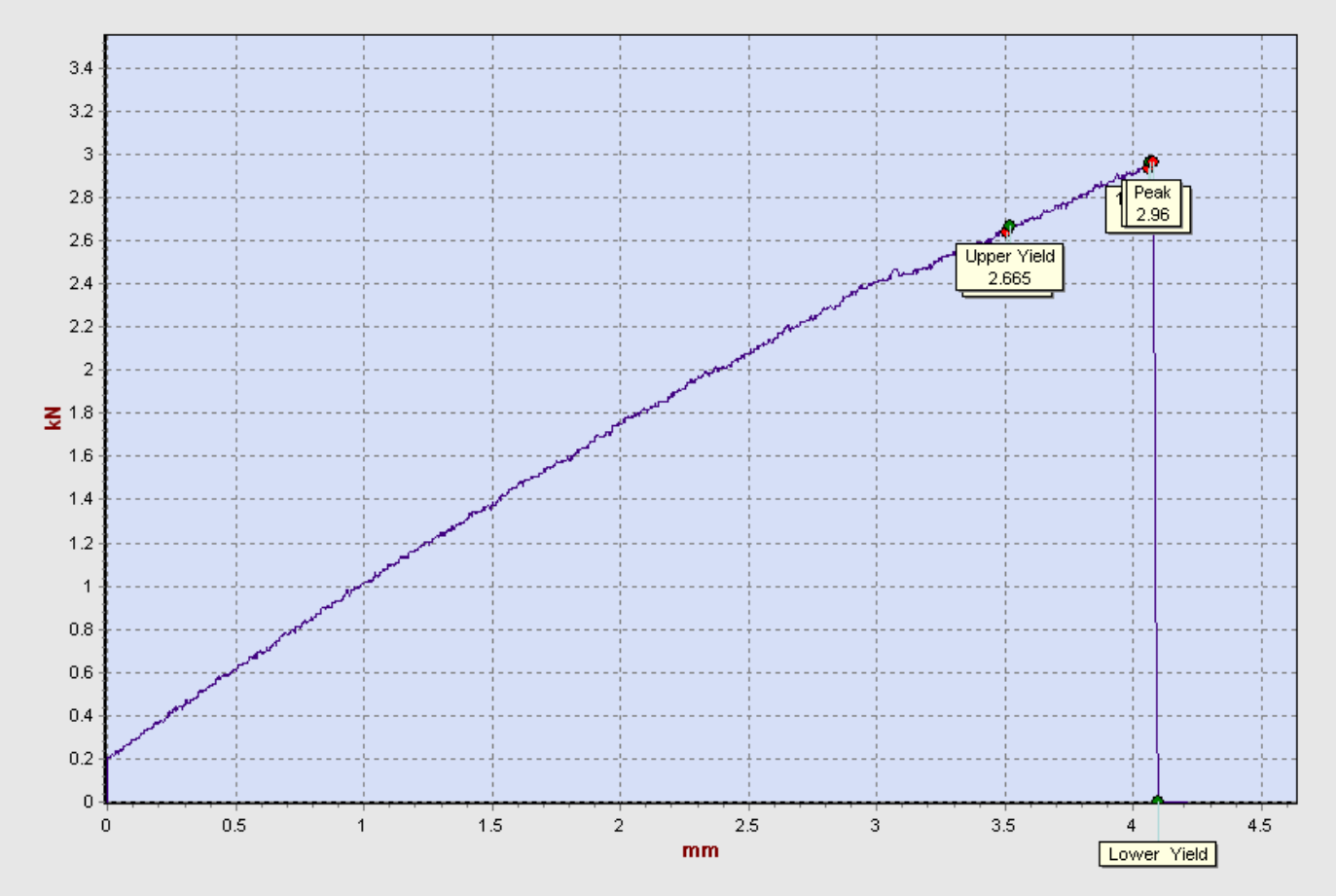

Fig.6.134 Stress vs Strain graph of sample loaded at 40% of U.T.L (Water Tank T4)

3) The results of specimen which were subjected to **60% loading** (T4, 2months) are shown below:

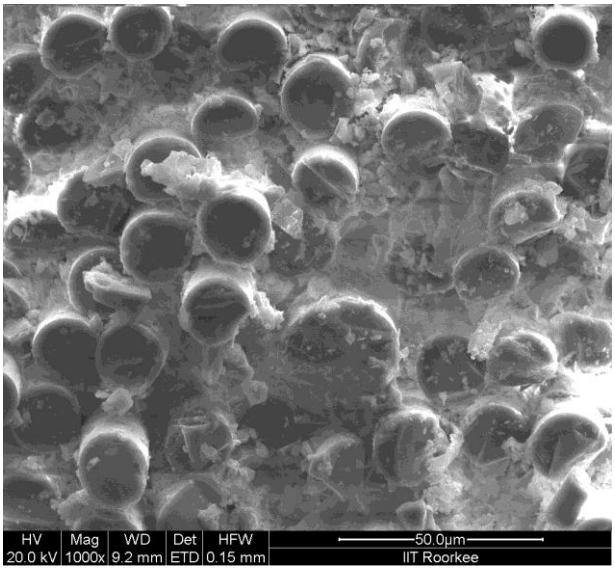

Fig.6.135 SEM image of specimen at 60% load

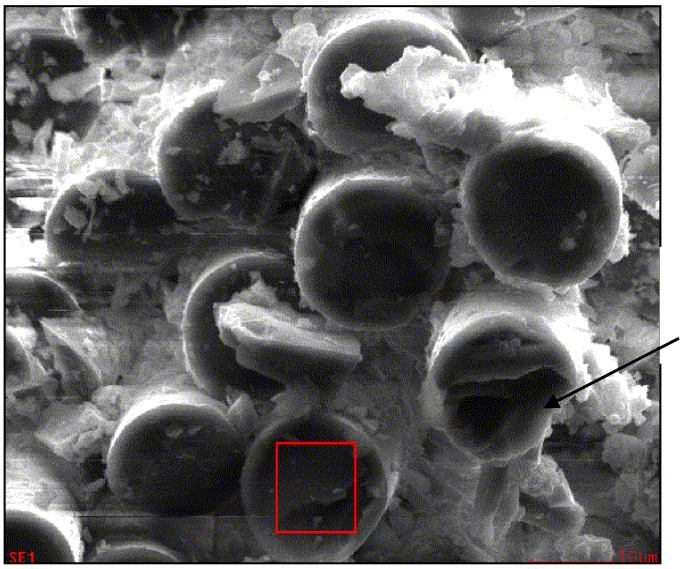

Fig.6.136 SEM image of specimen for EDX

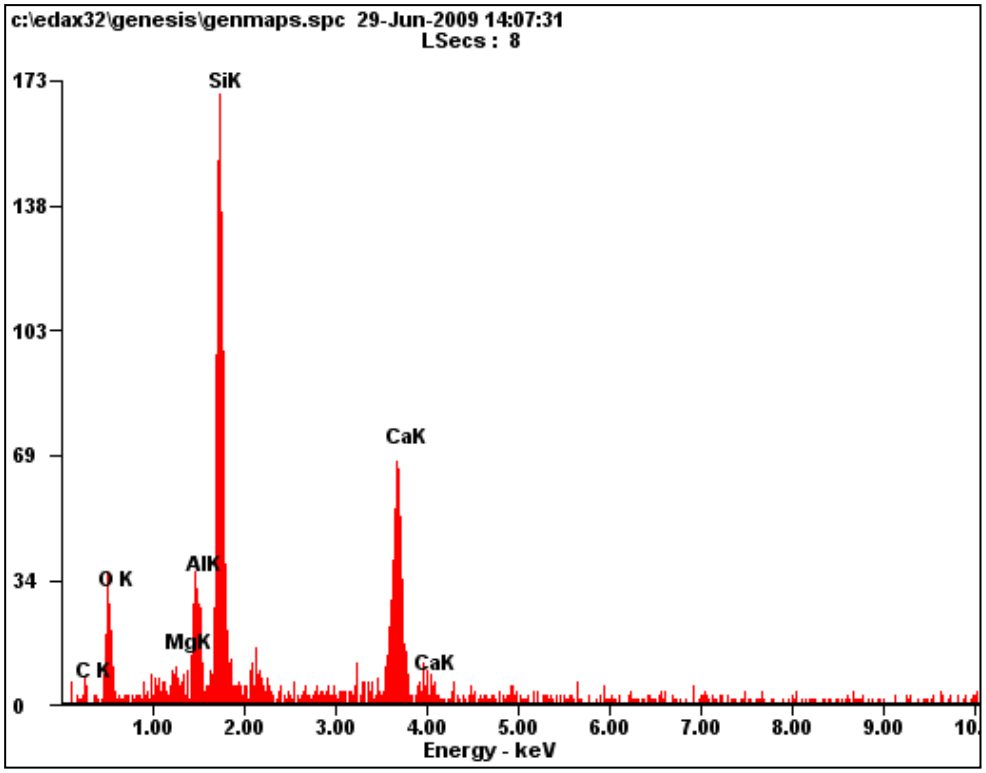

e)

Element	*Wt%*
CK	06.88
OK	26.42
MgK	01.70
AlK	06.11
SiK	34.34
CaK	22.55

f)

Fig.6.137 (e) Energy vs Electron volt graph for 60% load, (f) Element percentage taken by EDX

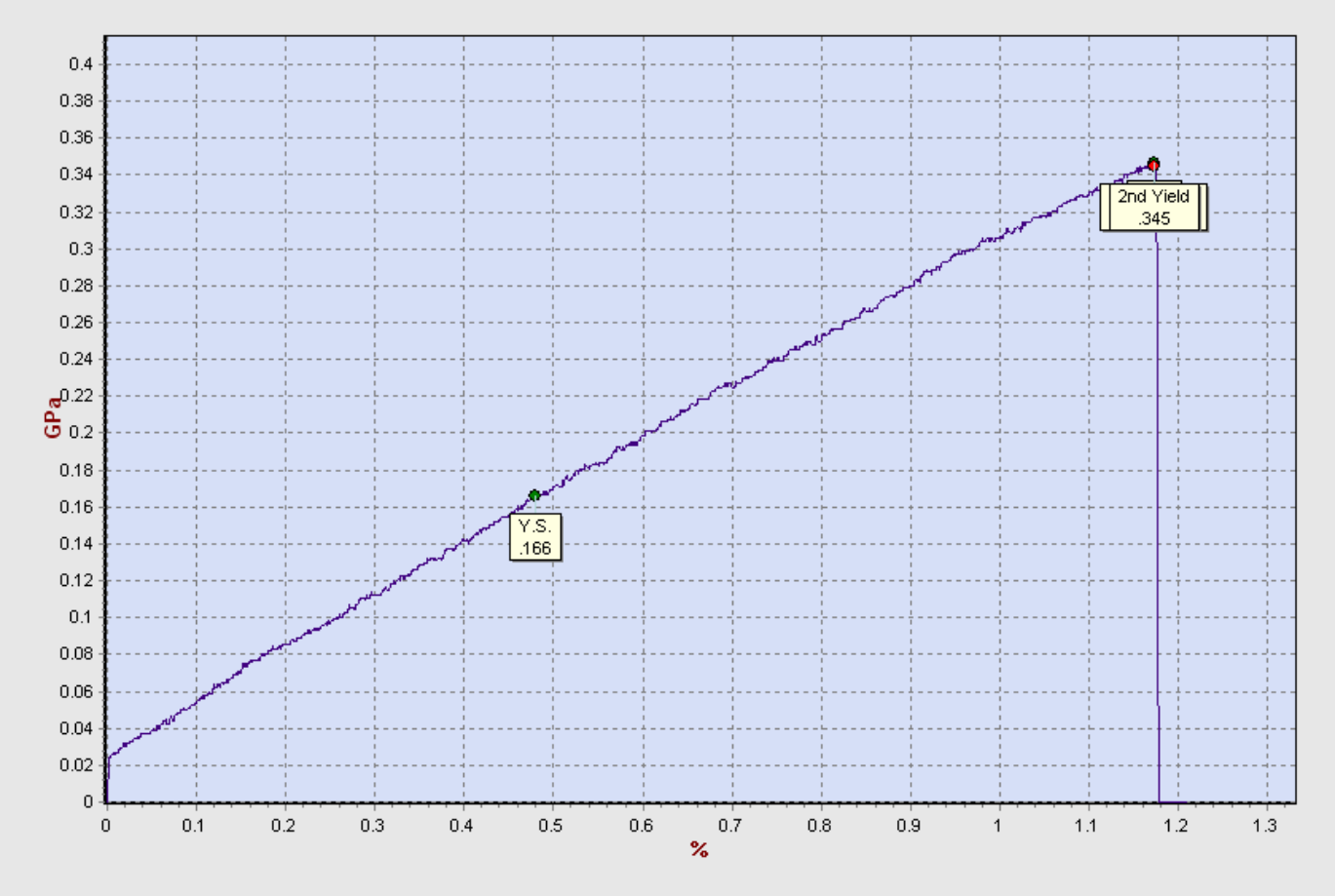

Fig.6.138 Stress vs Strain graph of sample loaded at 60% of U.T.L (Water Tank T4)

4) The results of specimen which were subjected to **80% loading** (T4, 2months) are shown below:

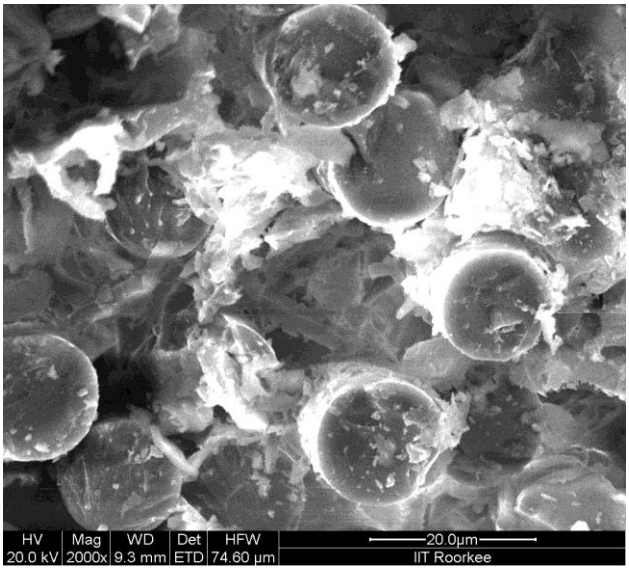

Fig.6.139 SEM image of specimen at 80% load

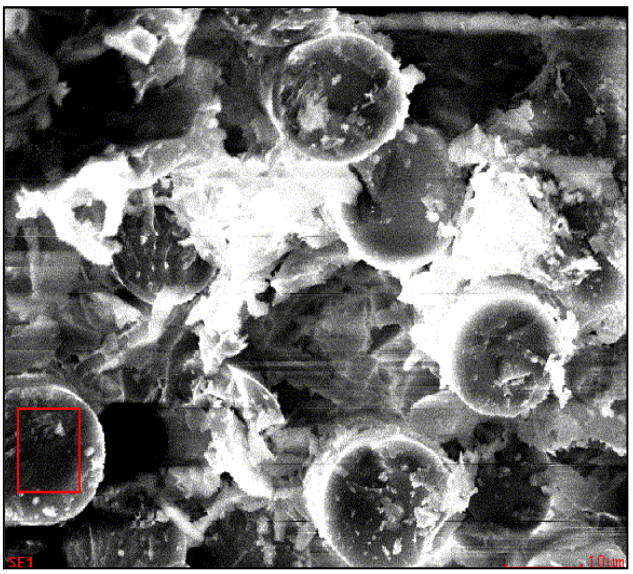

Fig.6.140 SEM image of specimen for EDX

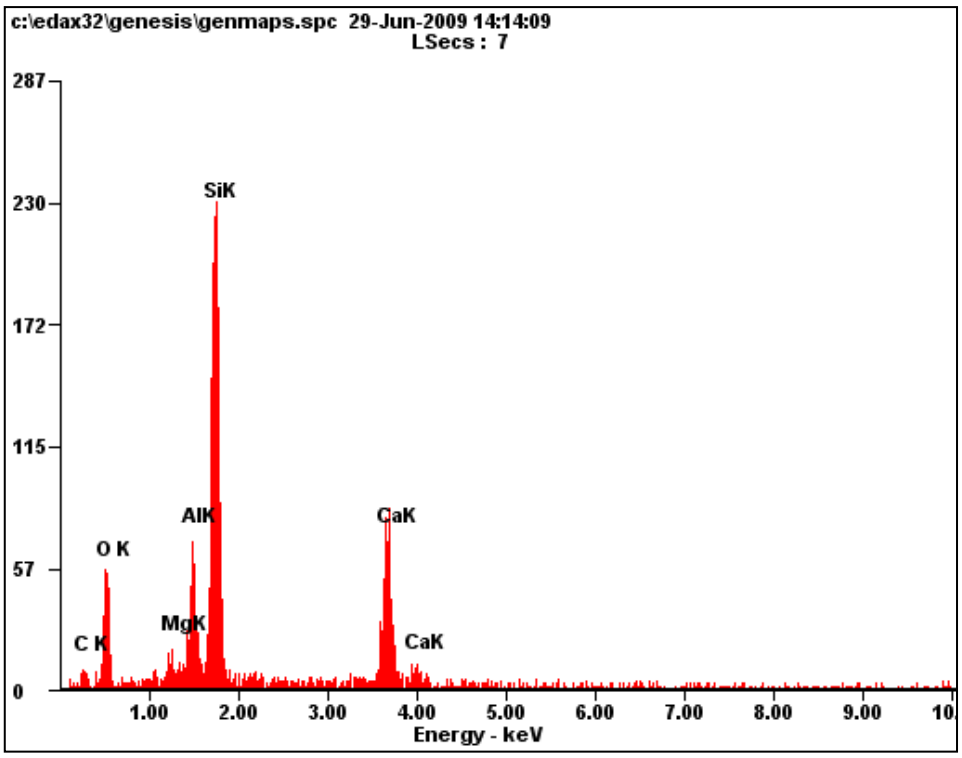

g)

Element	*Wt%*
CK	08.70
OK	30.85
MgK	01.65
AlK	06.29
SiK	33.53
CaK	16.99

h)

Fig.6.141 (g) Energy vs Electron volt graph for 80% load, (h) Element percentage taken by EDX

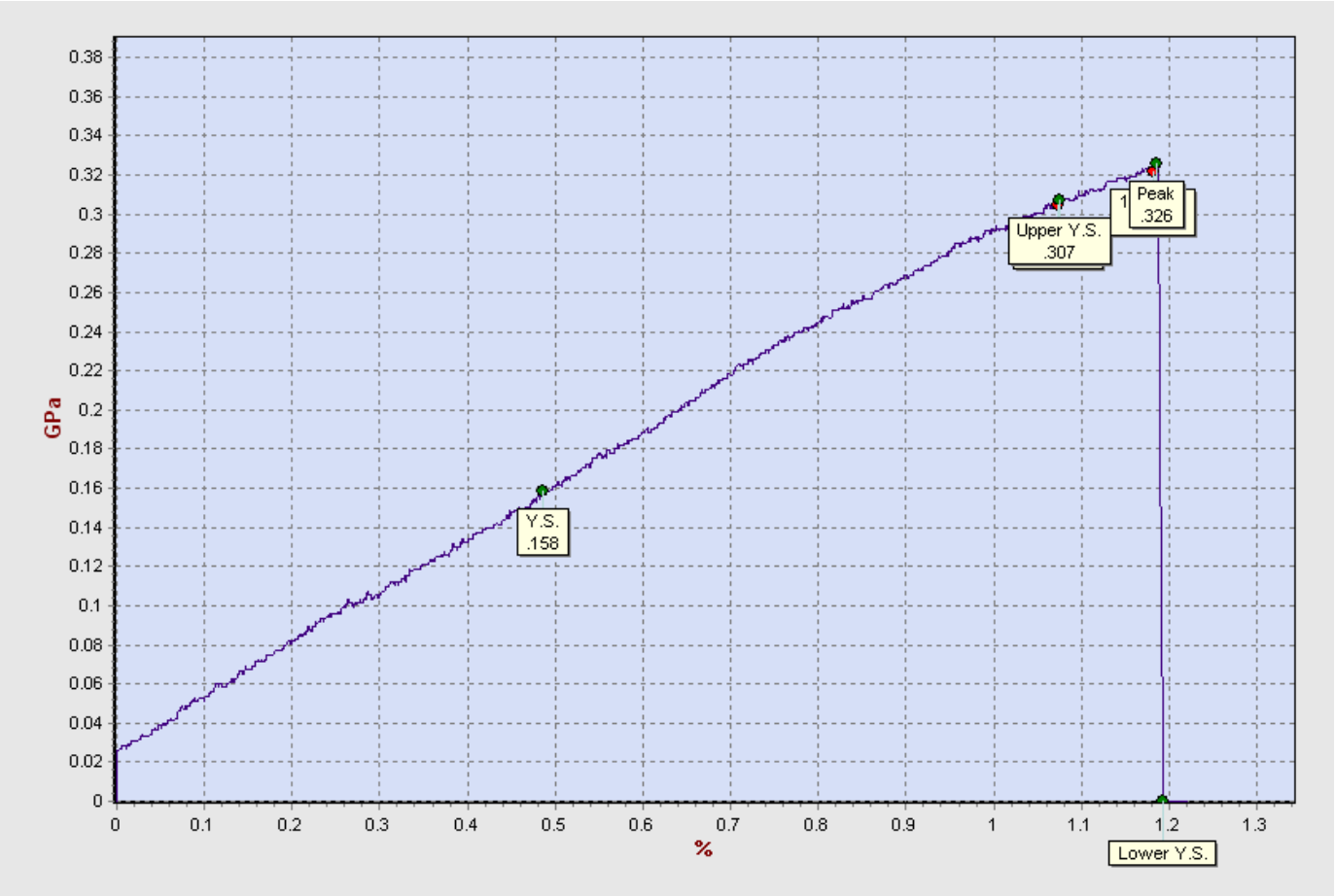

Fig.6.142 Stress vs Strain graph of sample loaded at 80% of U.T.L (Water Tank T4)

The following SEM image (Fig. 6.143 to Fig.6.145) compares the condition of fibres (**on longitudinal side**) at different time stages:

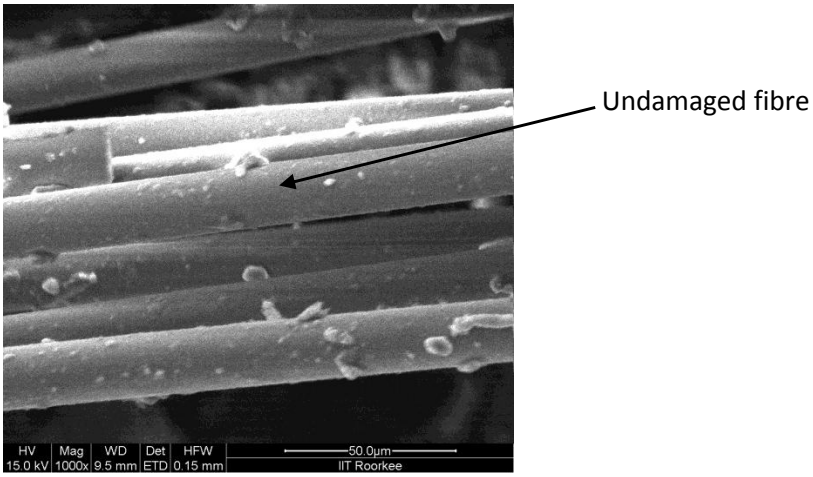

Fig.6.143 SEM at start of experiment

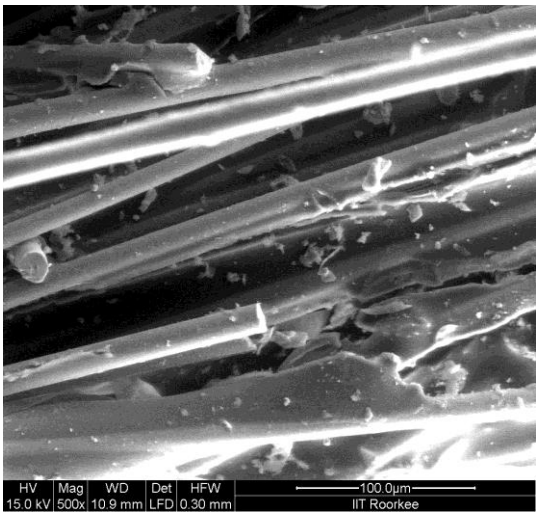

Fig.6.144 SEM after 2 month (Water Bath)

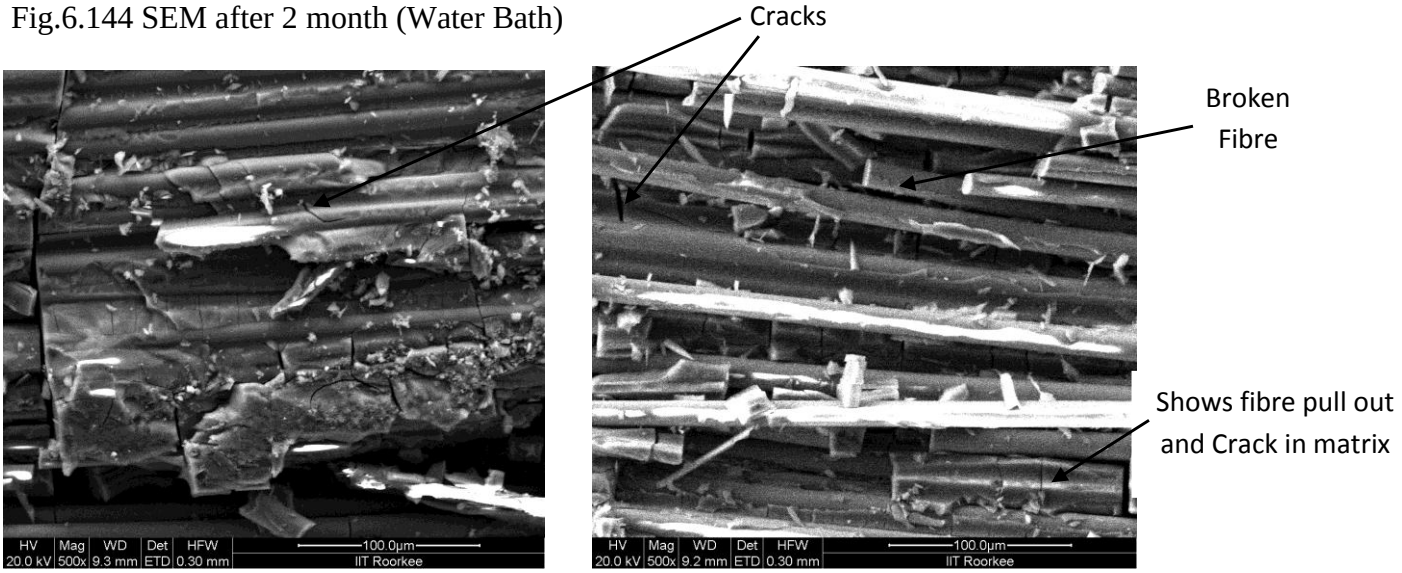

a) b)

Fig.6.145 (a), (b) shows SEM after 2 month (NaOH Bath)

The following SEM images (Fig.6.146 & Fig.6.147) will show the results of the epoxy surface after time period of 1 month:

Image shows irregular patterns and micro holes on surface

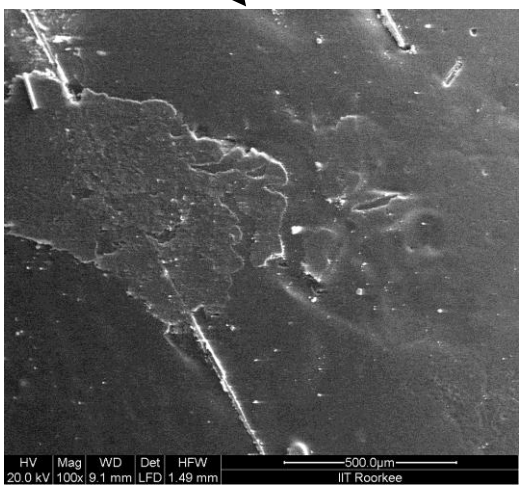

Element	*Wt%*
CK	83.83
OK	12.45
MgK	00.42
AlK	00.47
SiK	01.63
CaK	00.80

Fig.6.146 Shows the SEM image of the epoxy surface in NaOH tank along with its composition (of full image)

Image shows very clear and even surface compared to that of NaOH tank

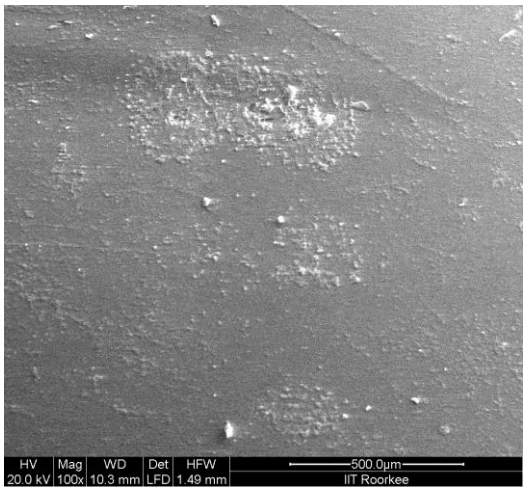

Element	*Wt%*
CK	86.36
OK	11.17
MgK	00.23
AlK	00.88
SiK	00.89
CaK	00.15

Fig.6.147 Shows the SEM image of the epoxy surface in Water tank along with its composition (of full image)

6.4 IMAGE ANALYSIS BY "IMAGE-J" ANALYSER SOFTWARE:

The analysis of all the SEM images was done in order to compare the area fraction of both epoxy as well as of the fibre. The commercially available software Image J was used for analysis of images. Image J is open source software developed by National Institute of Health and considered as powerful for image analysis. Few representative images after analysis by software are shown from Fig.6.148 to Fig.6.154.

Procedure followed for analysis of the SEM images is explained below:

1) The image to be analysed was opened in the software.

2) A line was drawn parallel to the 20µm line (shown on SEM images) using the Set Scale option. That distance was set equivalent to number of pixel (automatically counted by software).

3) Now as the scale was set we had draw a line across fibre edges to measure the length of fibre.

4) To calculate the area fraction, first we had converted the image to RGB colour (we could choose from various colour options, here we had used Red/Green colour to fill the areas of SEM image)

5) After applying above option the colour of image would change (from the grey scale to chosen Red/Green), in which red colour indicated the fibre area, green indicated epoxy and black was for voids. These areas were selected automatically by software according to the image contrast.

6) Using the Split Channel option the software would split the three colours to three different windows representing the fibre area, epoxy area and void area.

7) To calculate the area fraction first we had to tick the option of measure area fraction in Set Measurement menu. To measure the area fraction, the option Analyze →Measure was used. Area to be measured was selected by making a window around it and above mentioned Analyze option showed the results in a tabular form.

At initial Stage:

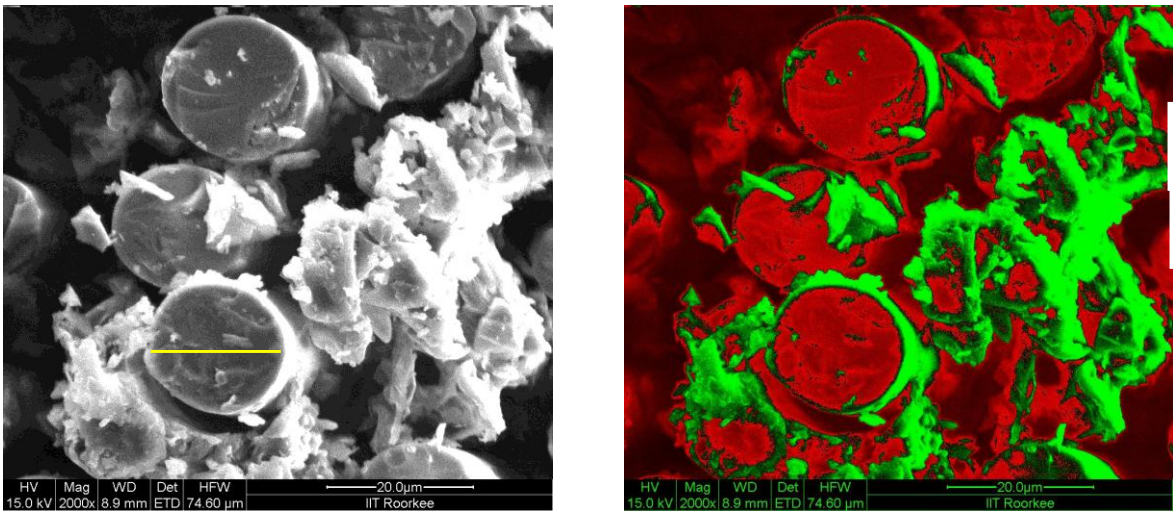

Fig.6.148 (Left) SEM image at Inital Stage, (Right) same SEM image by Image Analyser

* Note the Yellow line on the (Left) SEM image indicates the place of fibre length measurement

After 1 month:

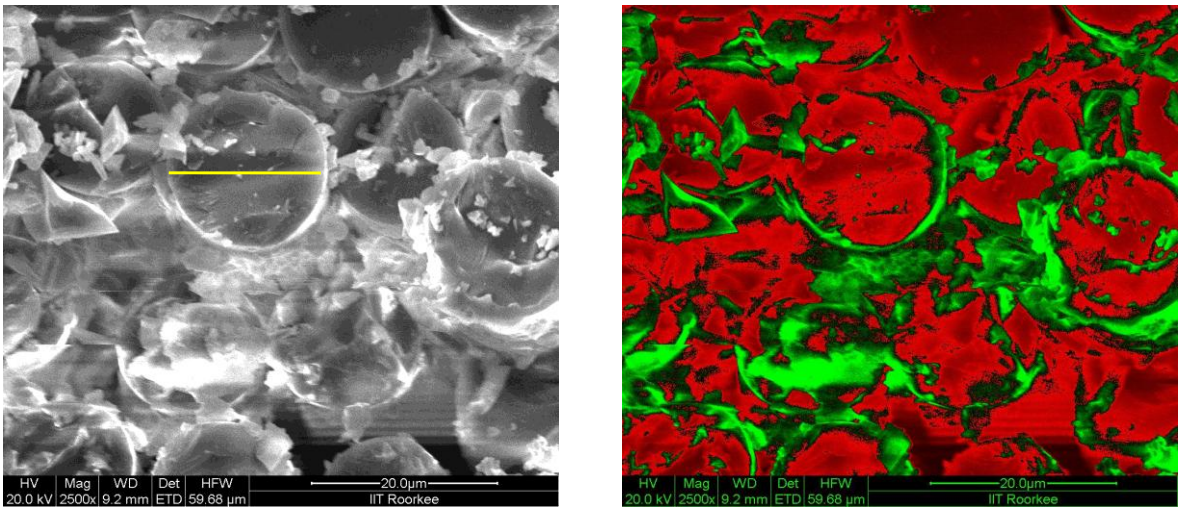

Fig.6.149 (Left) SEM image of Tank T1 at 20% load, (Right) same SEM image by Image Analyser

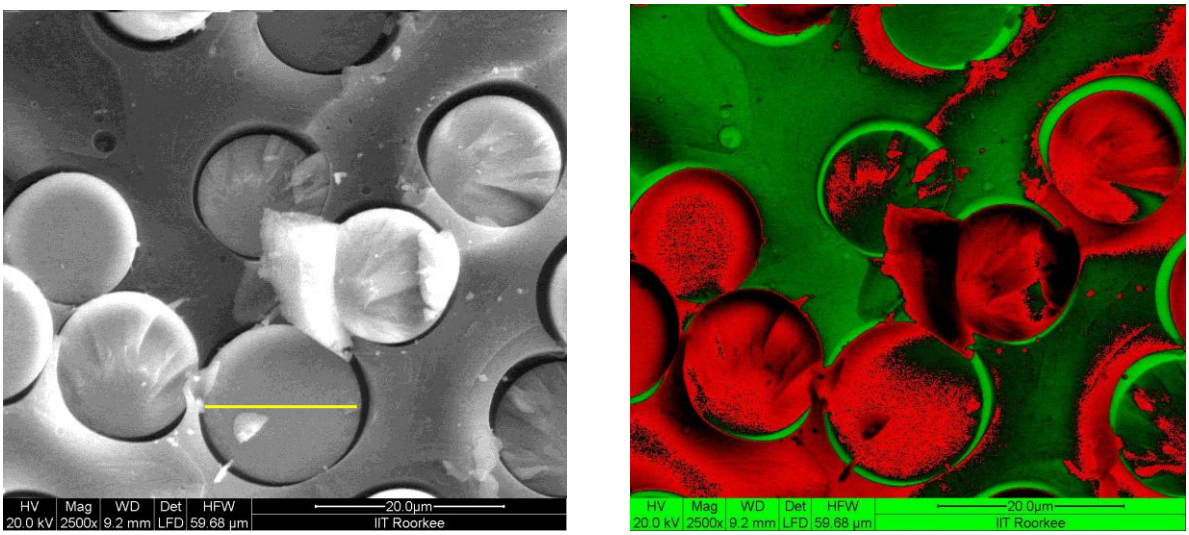

Fig.6.150 (Left) SEM image of Tank T3 at 20% load, (Right) same SEM image by Image Analyser

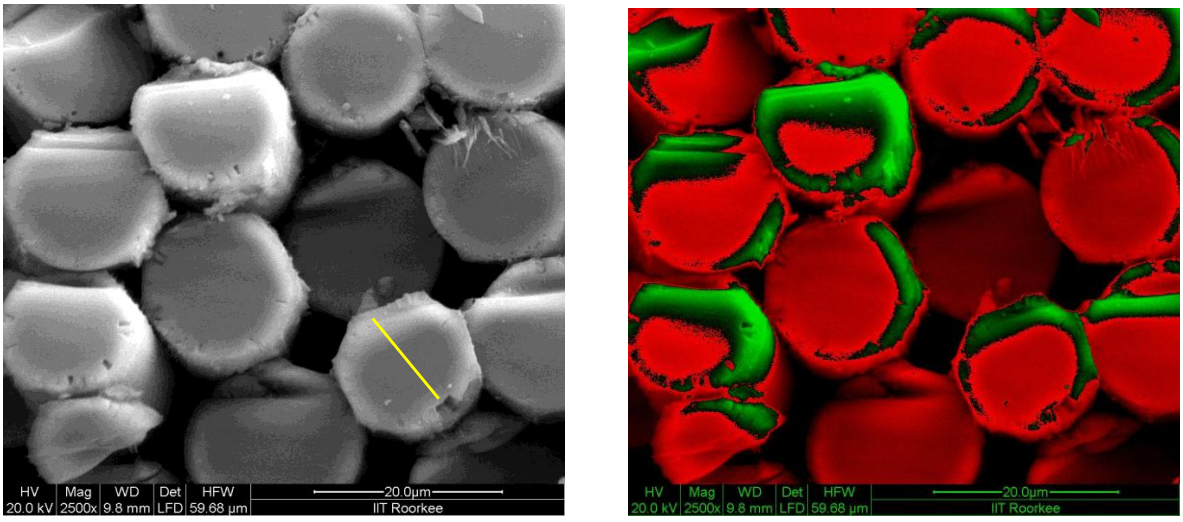

Fig.6.151 (Left) SEM image of Tank T3 at 80% load, (Right) same SEM image by Image Analyser

After 2 months:

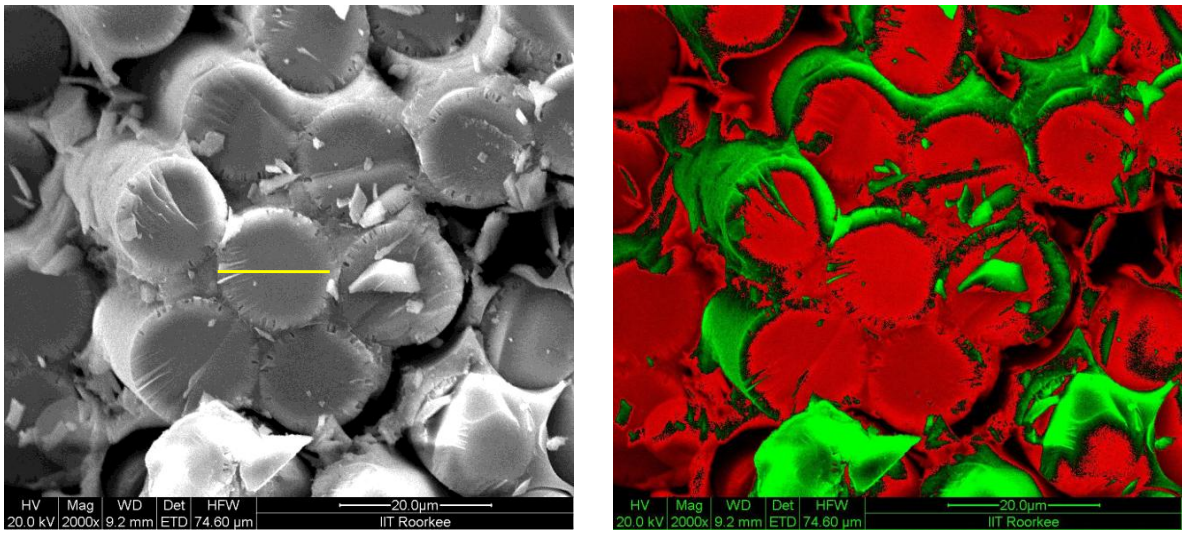

Fig.6.152 (Left) SEM image of Tank T2 at 80% load, (Right) same SEM image by Image Analyser

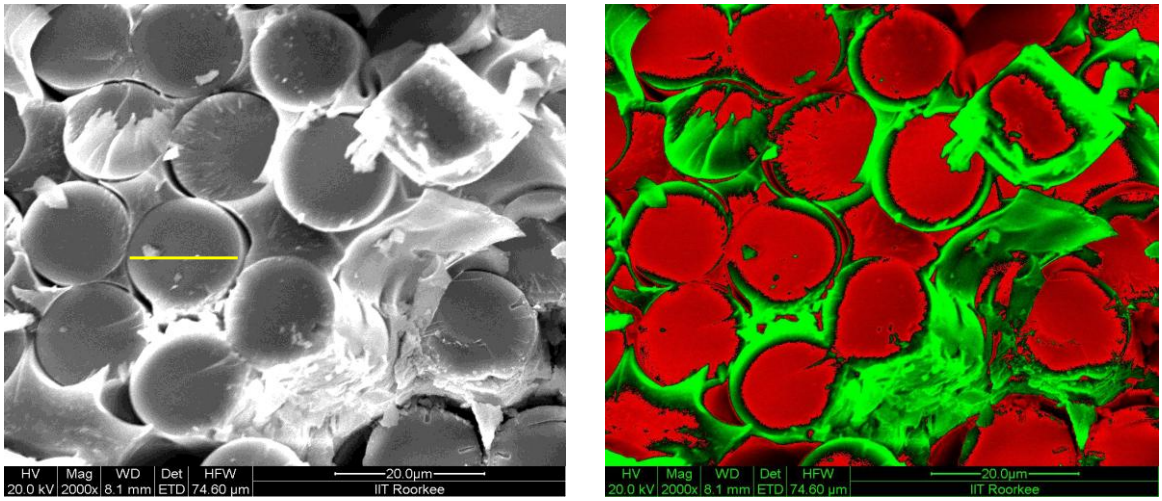

Fig.6.153 (Left) SEM image of Tank T3 at 40% load, (Right) same SEM image by Image Analyser

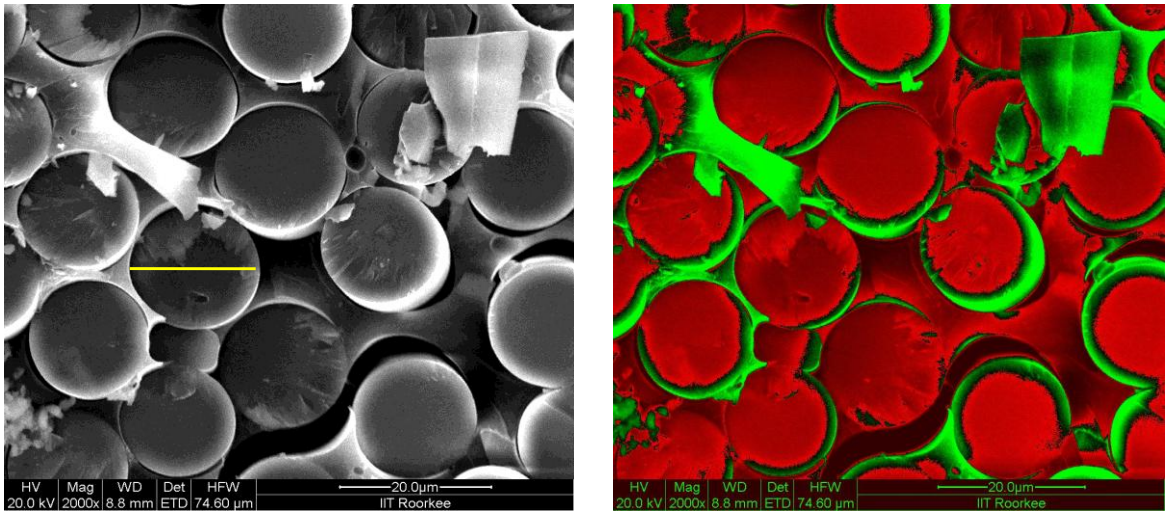

Fig.6.154 (Left) SEM image of Tank T3 at 80% load, (Right) same SEM image by Image Analyser

6.5 Manual Calculation of Fibre Area Fraction:

The SEM images analysed (shown in Fig.148 to Fig.154) by the Image-J software showed discrepancies in some images when software coloured the fibres (in red) and epoxy (in green). It analysed the SEM images based upon the contrast of the image and automatically gave them chosen colour. In order to have more accurate results we had again analysed the SEM by manually selecting each fibre in figure and then calculated its area by the same software and further manual calculation were done to find the area fraction.

The actual procedure followed was as under:

1) The SEM image to be analysed was opened in Image-J software.

2) A line parallel to scale of image was drawn and using the Set Scale option the length of drawn image was set to known value on the image.

3) After the scale was set, we had selected each fibre separately (see Fig.6.155) using a circular selection tool.

4) The area of selected fibre (degraded portion of fibre was not considered in selection) was obtained using Analyse→Measure option.

5) The output of above option gave the area of single selected fibre so we had repeated step 3 and 4 in order to get area of all the fibres (one by one).

6) The area of whole image was also calculated by measuring the length and width of whole image area, which represented the total area.

7) The area of all the fibres was summed up amounting to total fibre area. This area was divided by total area of image to obtain the fibre area fraction.

The Fig.6.155 below shows an example of how the area was selected to calculate the fibre fraction area.

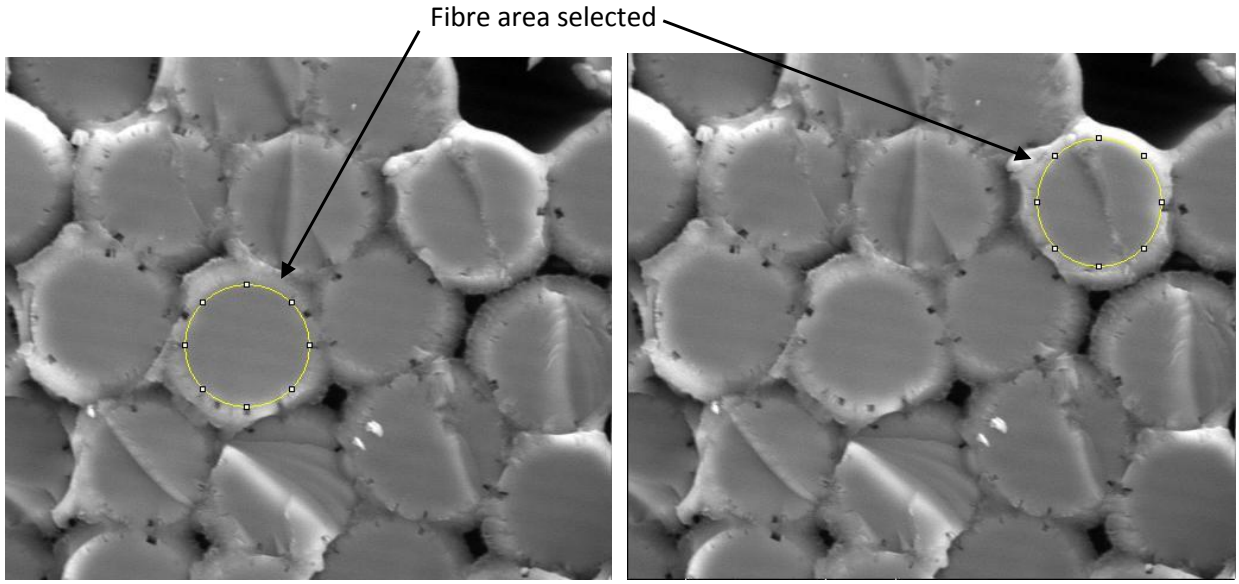

Fig 6.155 SEM images showing the selected fibre area considered for area fraction calculation

After the results were obtained from both colour analysis and manual calculation method, they were compared to analyse the difference between the results of both methods. Table T14 shows the percentage difference in fibre area fraction calculated by the two methods for a few representative samples.

Table T14 Difference of Fibre Area Fraction percentage by Colour Analysis and Manual Method

Sample Name	**A***	**B****	**Percentage Difference**
T2-60% load-2 (1 month)	50.34%	64.33%	**13.99%**
T3-20% load-3 (1 month)	36.94%	54.35%	**17.41%**
T3-80% load-3 (1 month)	54.48%	71.10%	**16.62%**
T3-40% load-3 (1 month)	62.89%	70.93%	**8.04%**
T1-60% load-2 (2 months)	20.32%	44.27%	**23.95%**
T2-20% load-2 (2 months)	30.10%	40.36%	**10.26%**
T2-80% load-2 (2 months)	32.65%	36.82%	**4.17%**
T3-60% load-2 (2 months)	12.73%	54.52%	**41.79%**

* A = Fibre area fraction percentage by manual calculations

**B = Fibre area fraction percentage by colour image analysis

6.6 EVALUATION AND DISCUSSION OF ALL RESULTS:

6.6.1 DISCUSSION OF ULTIMATE TENSILE STRENGTH (U.T.S.) AND PERCENTAGE CHANGE IN U.T.S.

The comparison of the ultimate tensile strength load wise with respect to time is as follows:

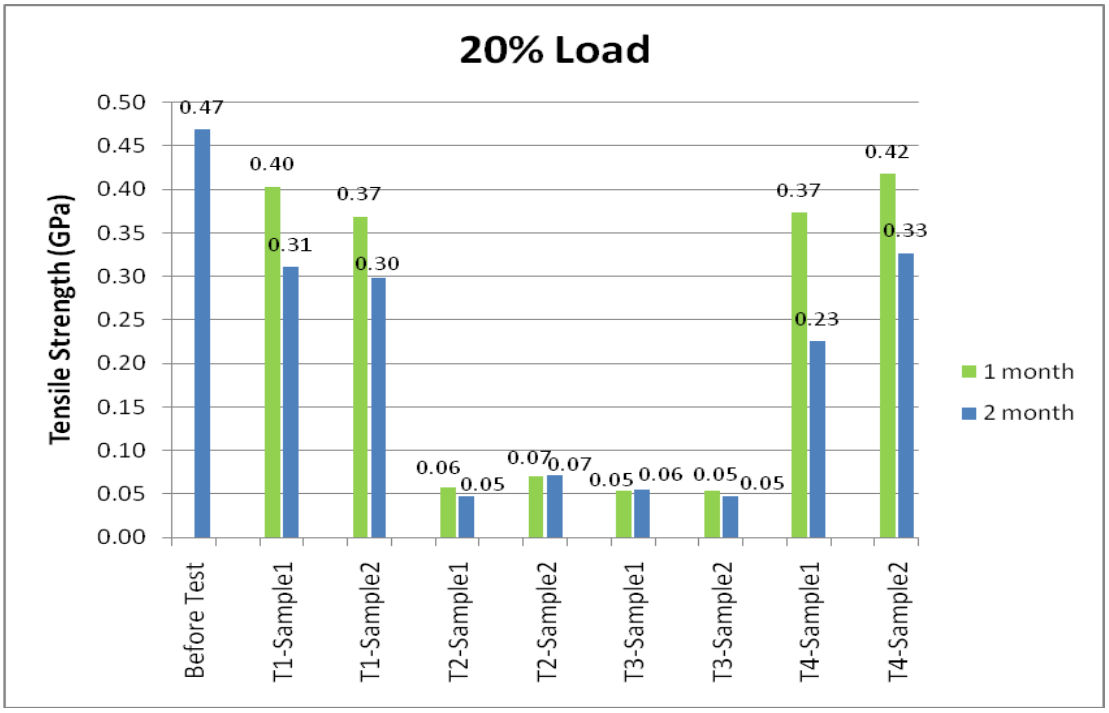

Fig.6.156 Comparison of ultimate tensile strength at 20% load for all tanks

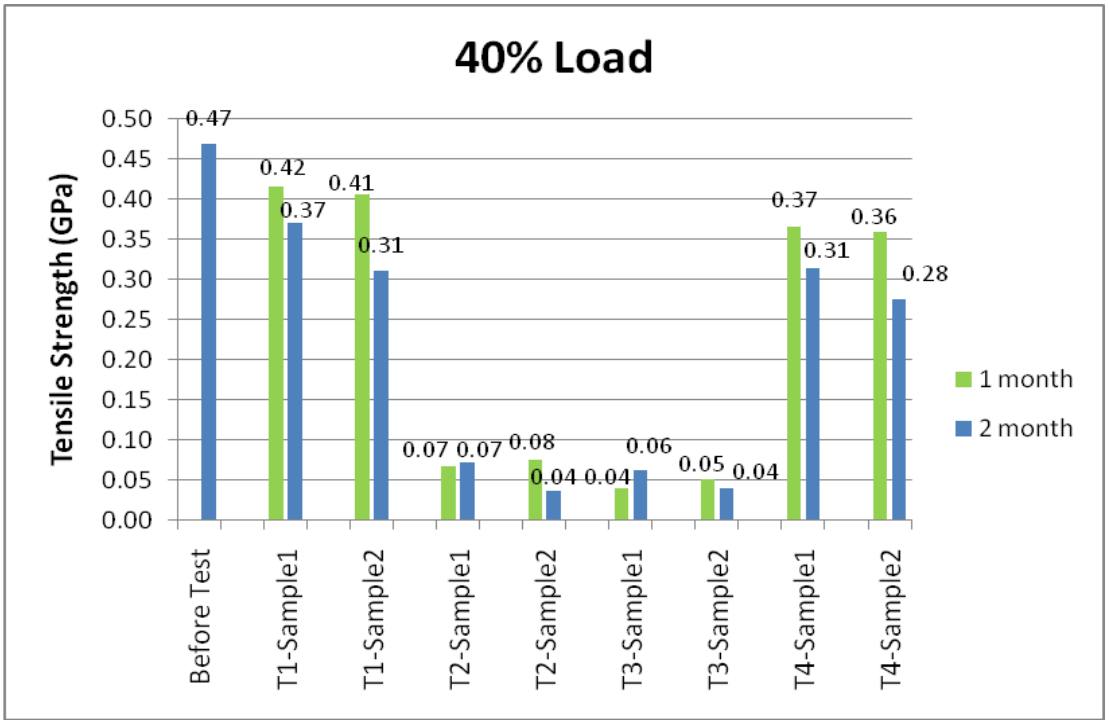

Fig.6.157 Comparison of ultimate tensile strength at 40% load for all tanks

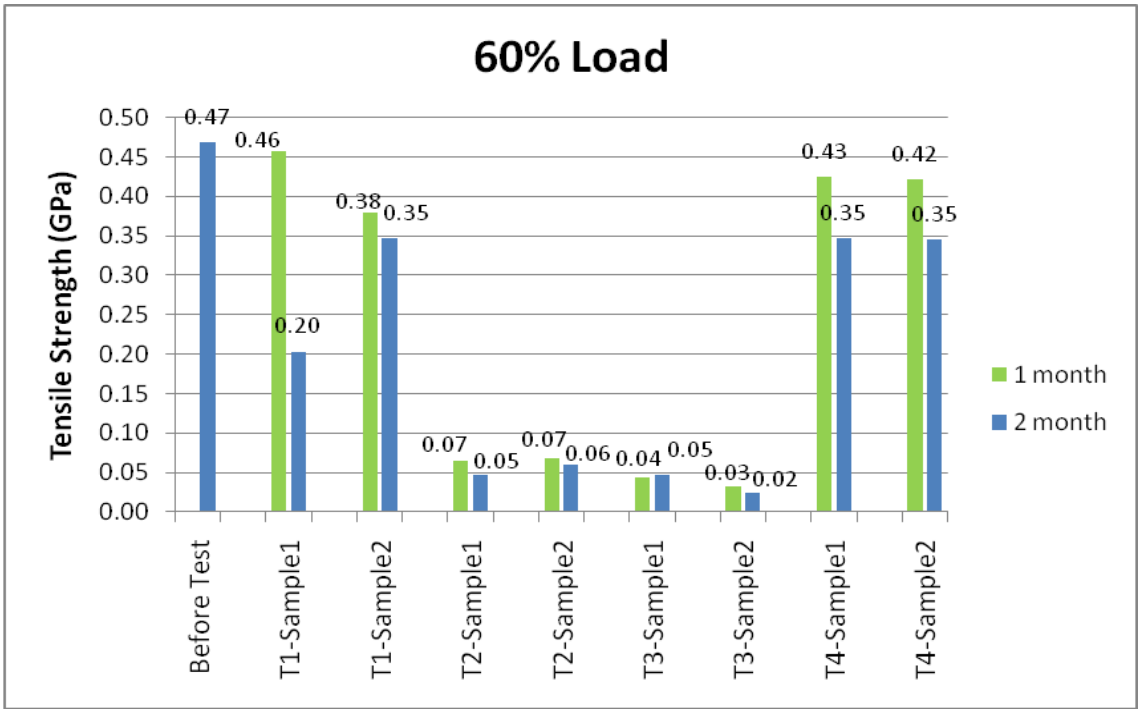

Fig.6.158 Comparison of ultimate tensile strength at 60% load for all tanks

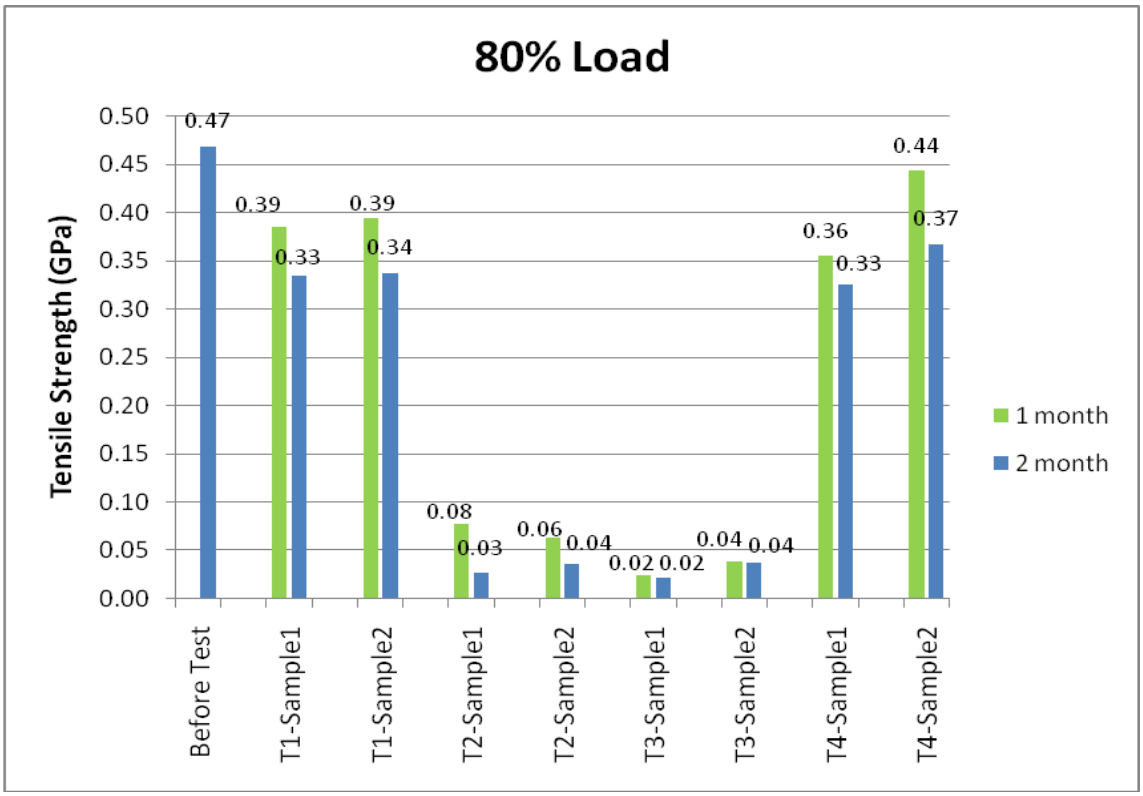

Fig.6.159 Comparison of ultimate tensile strength at 80% load for all tanks

The comparison of the ultimate tensile strength tank wise with respect to time is as follows:

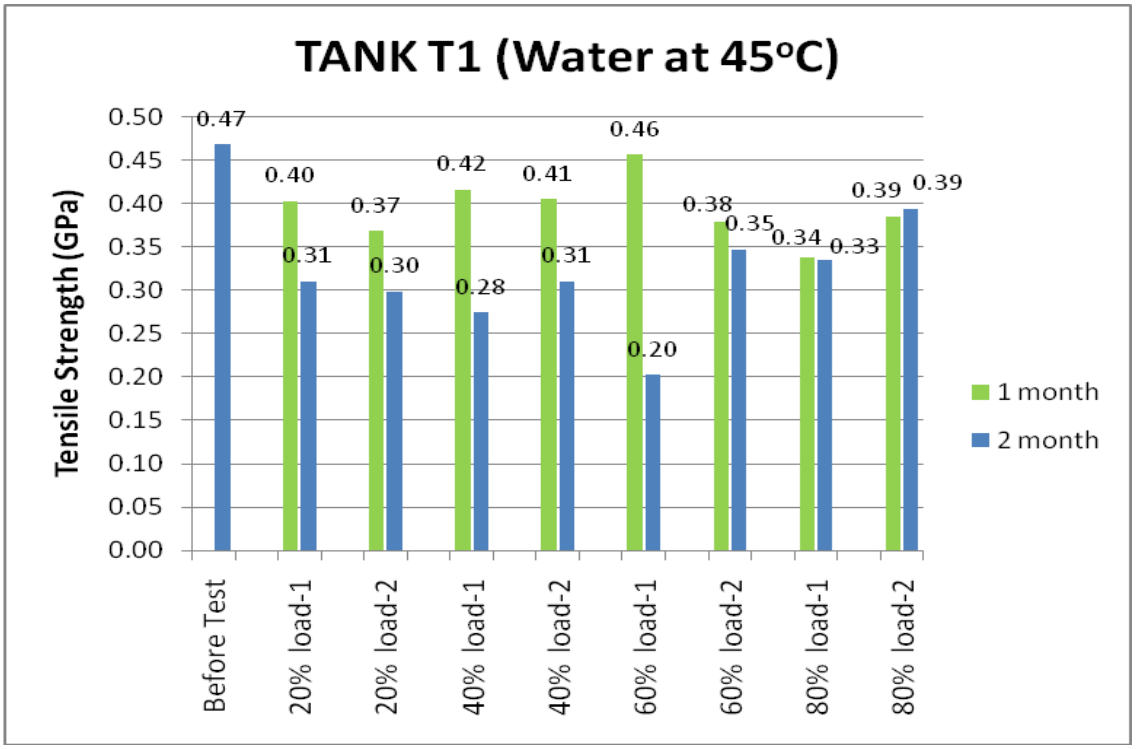

Fig.6.160 Comparison of ultimate tensile strength at T1 tank

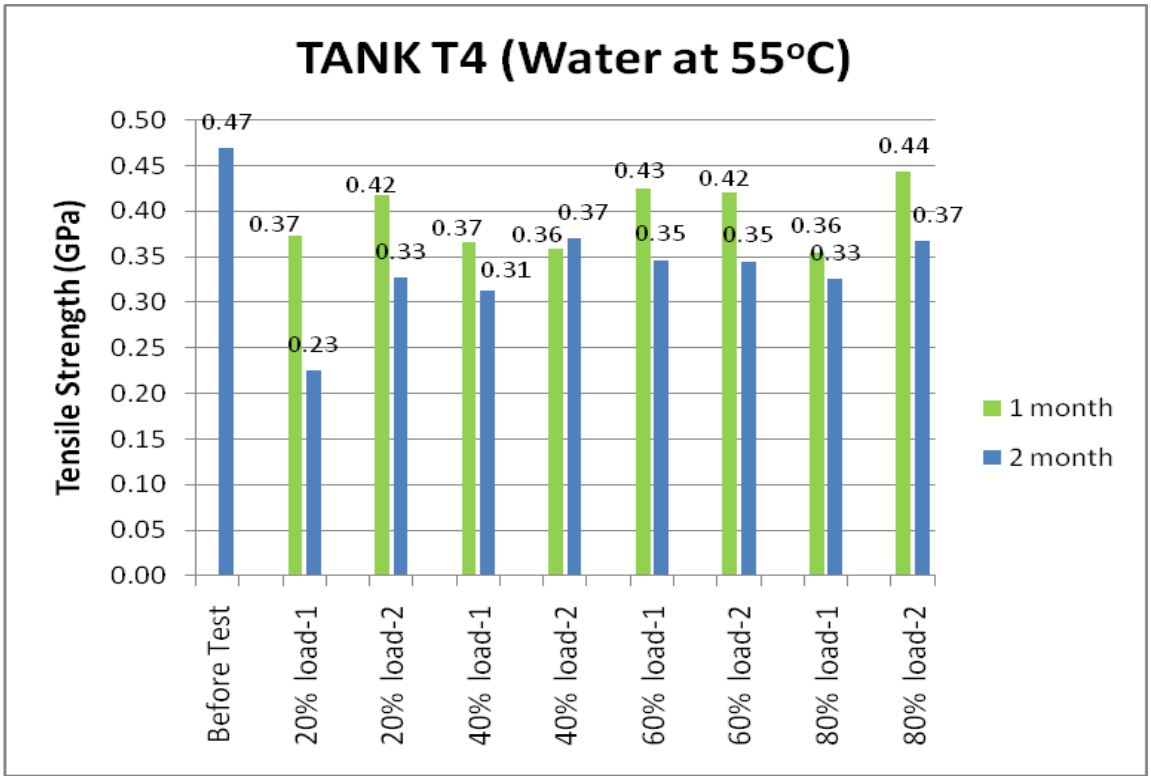

Fig. 6.161 Comparison of ultimate tensile strength at T4 tank

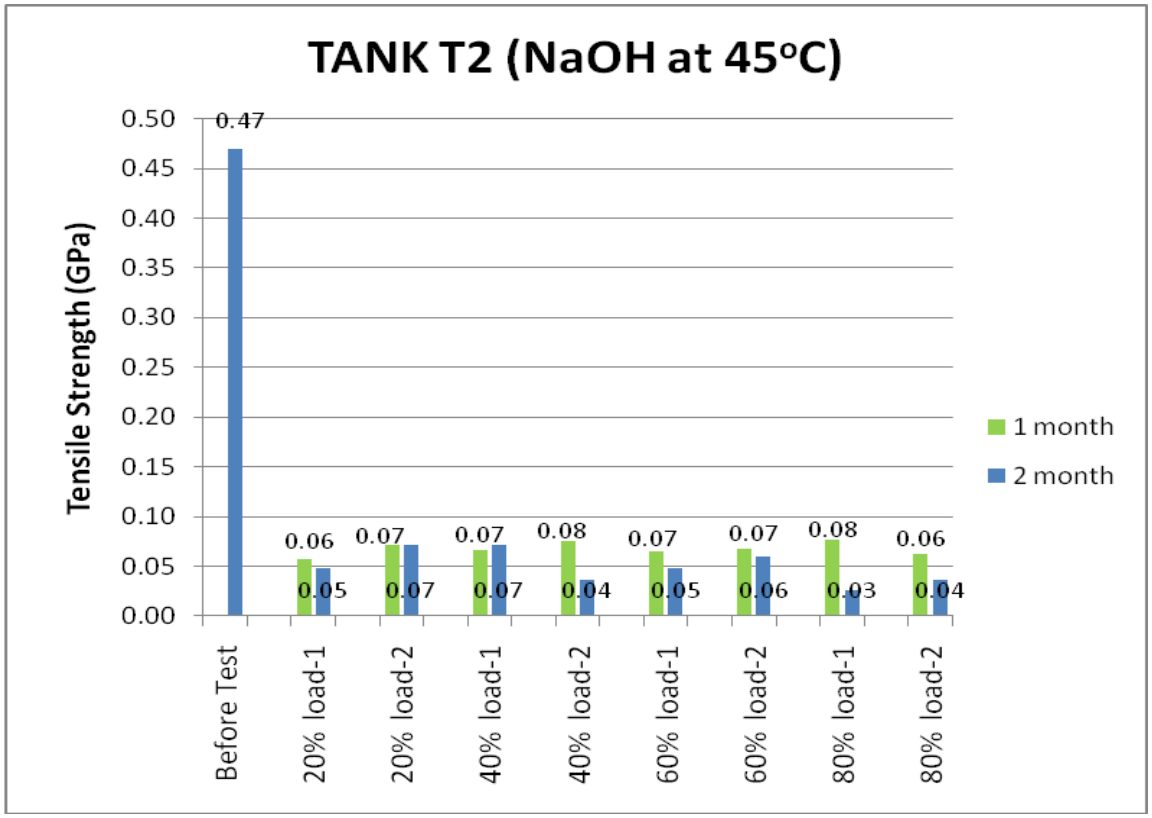

Fig. 6.162 Comparison of ultimate tensile strength at T2 tank

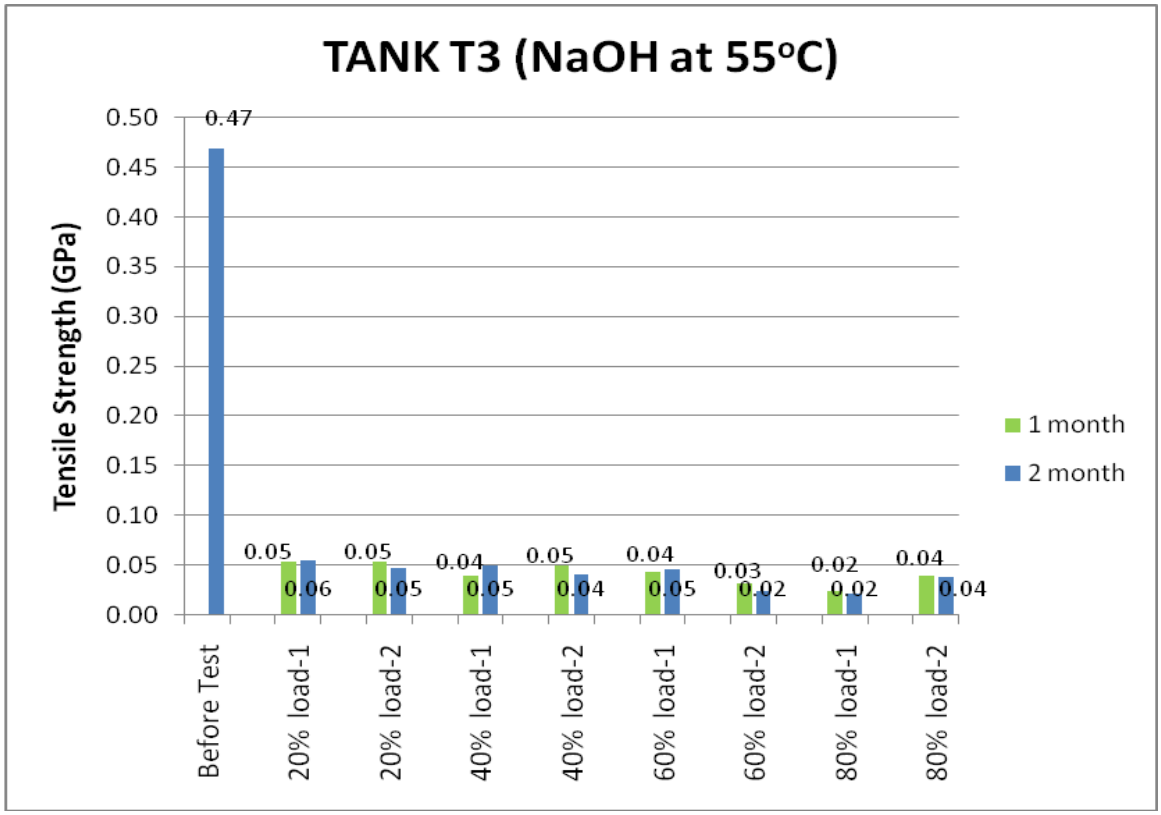

Fig. 6.163 Comparison of ultimate tensile strength at T3 tank

The above graphs (Fig.6.160, Fig.6.161) shows that there is marginal decrease in the ultimate tensile strength of the samples immersed in water for one month compared to that of Initial value. Further after two months considerable decrease in tensile strength can be seen easily. But considering the case of samples in NaOH aqueous solution (Fig.6.162, Fig.6.163) there is very large reduction in the tensile strength with respect to initial value of the tensile strength. This trend is seen in both the NaOH tanks which exhibit little change when compared to each other. The decrease in tensile strength in 55^{o}C tank T3 is more than tank T2 which is at lower temperature of 45^{o}C especially in the first month.

PERCENTAGE DECREASE IN TENSILE STRENGTH

Table T15 Percentage decrease in tensile strength in T1 and T4 tanks samples with respect to time:

Test Name (1month)	**Peak Load (KN)**	**Tensile Strength (1 month) (GPa)**	**% decrease in strength (1month)**	**Test Name (2 months)**	**Peak Load (KN)**	**Tensile Strength (2 month) (GPa)**	**% decrease in strength (2 month)**
Before Test (Avg. value)	3.750	0.469					
T1 = Water at 45^{o}C							
T1-20%load-1	3.225	0.403	**14.05%**	T1-20%load-1	2.485	0.311	**33.77%**
T1-20%load-2	2.950	0.369	**21.38%**	T1-20%load-2	2.390	0.299	**36.30%**
T1-40%load-1	3.330	0.416	**11.25%**	T1-40%load-1	2.200	0.275	**41.36%**
T1-40%load-2	3.245	0.406	**13.51%**	T1-40%load-2	2.485	0.311	**33.77%**
T1-60%load-1	3.655	0.457	**2.59%**	T1-60%load-1	1.625	0.203	**56.69%**
T1-60%load-2	3.035	0.379	**19.11%**	T1-60%load-2	2.770	0.346	**26.17%**
T1-80%load-1	3.085	0.386	**16.78%**	T1-80%load-1	2.675	0.334	**28.70%**
T1-80%load-2	2.700	0.338	**28.04%**	T1-80%load-2	3.155	0.394	**15.91%**
T4 = Water at 55^{o}C							
T4-20%load-1	2.990	0.374	**20.31%**	T4-20%Load-1	1.805	0.226	**51.89%**
T4-20%load-2	3.340	0.418	**10.98%**	T4-20%Load-2	2.615	0.327	**30.30%**
T4-40%load-1	2.930	0.366	**21.91%**	T4-40%Load-1	2.505	0.313	**33.24%**
T4-40%load-2	2.870	0.359	**23.51%**	T4-40%Load-2	2.960	0.370	**21.11%**
T4-60%load-1	3.400	0.425	**9.38%**	T4-60%Load-1	2.770	0.346	**26.17%**
T4-60%load-2	3.370	0.421	**10.18%**	T4-60%Load-2	2.760	0.345	**26.44%**
T4-80%load-1	2.840	0.355	**24.31%**	T4-80%Load-1	2.605	0.326	**30.57%**
T4-80%load-2	3.550	0.444	**5.38%**	T4-80%Load-2	2.940	0.368	**21.64%**

Table T15-1 Percentage decrease in tensile strength in T2 and T3 tanks samples with respect to time:

Test Name (1month)	**Peak Load (KN)**	**Tensile Strength (1 month) (GPa)**	**% decrease in strength (1month)**	**Test Name (2 months)**	**Peak Load (KN)**	**Tensile Strength (2 month) (GPa)**	**% decrease in strength (2 month)**
Before Test (avg value)	3.750	0.469					
T2 = NaOH at 45^{o}C							
T2-20%load-1	0.460	0.058	**86.74%**	T2-20%Load-1	0.380	0.047	**89.87%**
T2-20%load-2	0.568	0.071	**84.86%**	T2-20%Load-2	0.570	0.071	**84.81%**
T2-40%load-1	0.530	0.066	**85.87%**	T2-40%Load-1	0.570	0.071	**84.81%**
T2-40%load-2	0.600	0.075	**84.01%**	T2-40%load-2	0.285	0.036	**92.40%**
T2-60%load-1	0.520	0.065	**86.14%**	T2-60%load-1	0.380	0.047	**89.87%**
T2-60%load-2	0.540	0.068	**85.61%**	T2-60%load-2	0.475	0.059	**86.34%**
T2-80%load-1	0.615	0.077	**83.61%**	T2-80%load-1	0.208	0.026	**94.46%**
T2-80%load-2	0.500	0.063	**86.67%**	T2-80%load-2	0.285	0.036	**92.40%**
T3 = NaOH at 55^{o}C							
T3-20%load-1	0.430	0.054	**88.54%**	T3-20%Load-1	0.440	0.055	**88.27%**
T3-20%load-2	0.430	0.054	**88.54%**	T3-20%Load-2	0.380	0.047	**89.87%**
T3-40%load-1	0.310	0.039	**91.74%**	T3-40%Load-1	0.500	0.063	**86.67%**
T3-40%load-2	0.400	0.050	**89.34%**	T3-40%Load-2	0.320	0.040	**91.47%**
T3-60%load-1	0.350	0.044	**90.67%**	T3-60%Load-1	0.370	0.046	**90.14%**
T3-60%load-2	0.255	0.032	**93.20%**	T3-60%Load-2	0.195	0.024	**94.80%**
T3-80%load-1	0.195	0.024	**94.80%**	T3-80%Load-1	0.168	0.021	**95.52%**
T3-80%load-2	0.310	0.039	**91.74%**	T3-80%Load-2	0.300	0.038	**92.00%**

Graphical comparison of percentage decrease in tensile strength for various tanks**:**

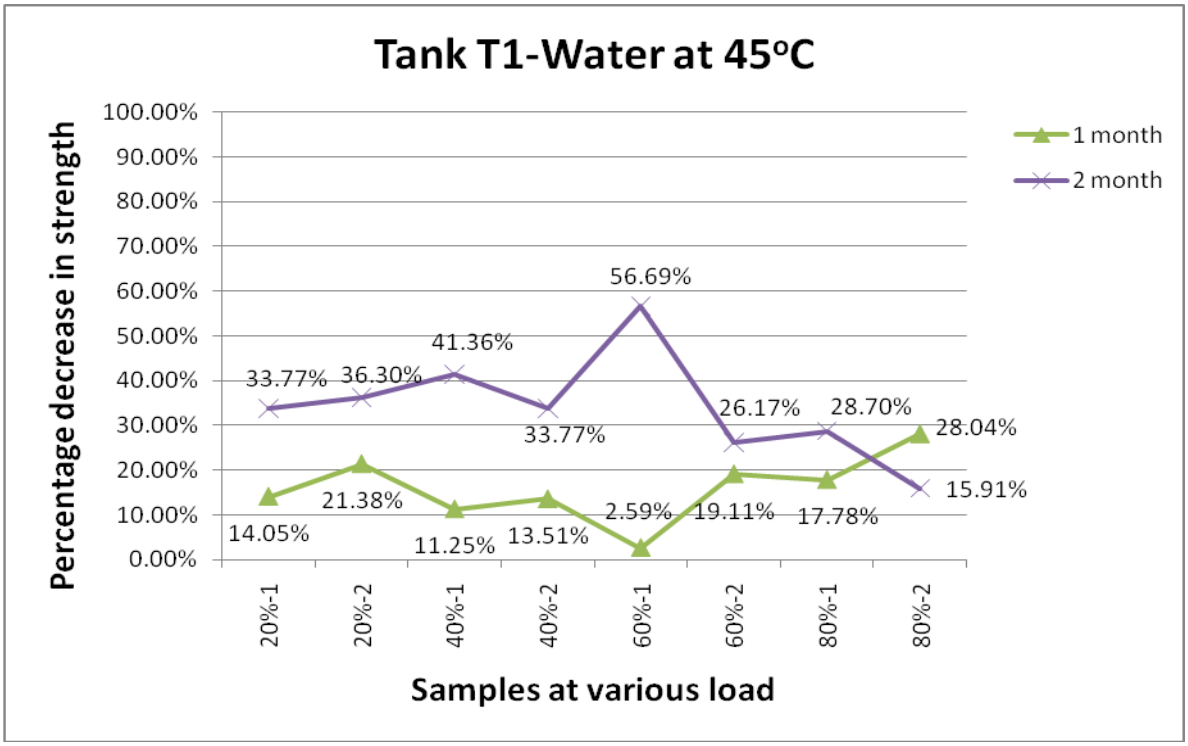

Fig. 6.164 Comparison of percentage decrease in tensile strength with respect to time in Tank T1

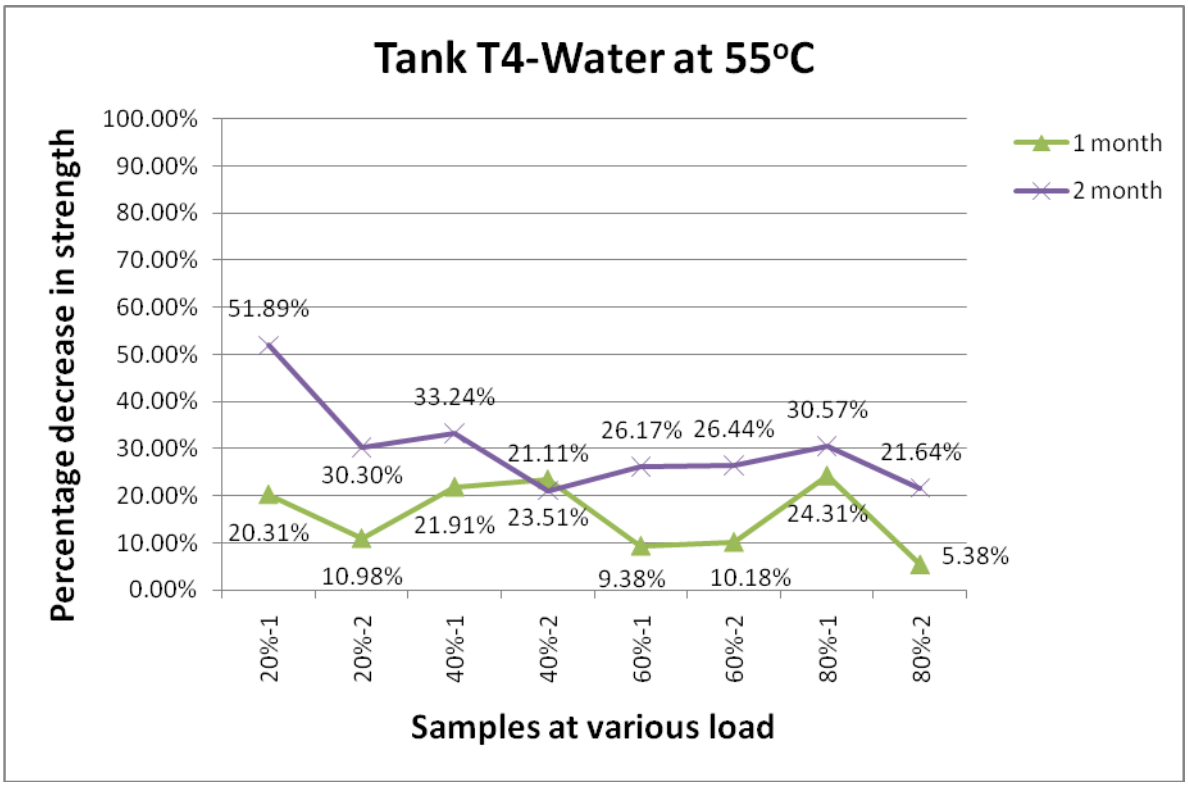

Fig. 6.165 Comparison of percentage decrease in tensile strength with respect to time in Tank T4

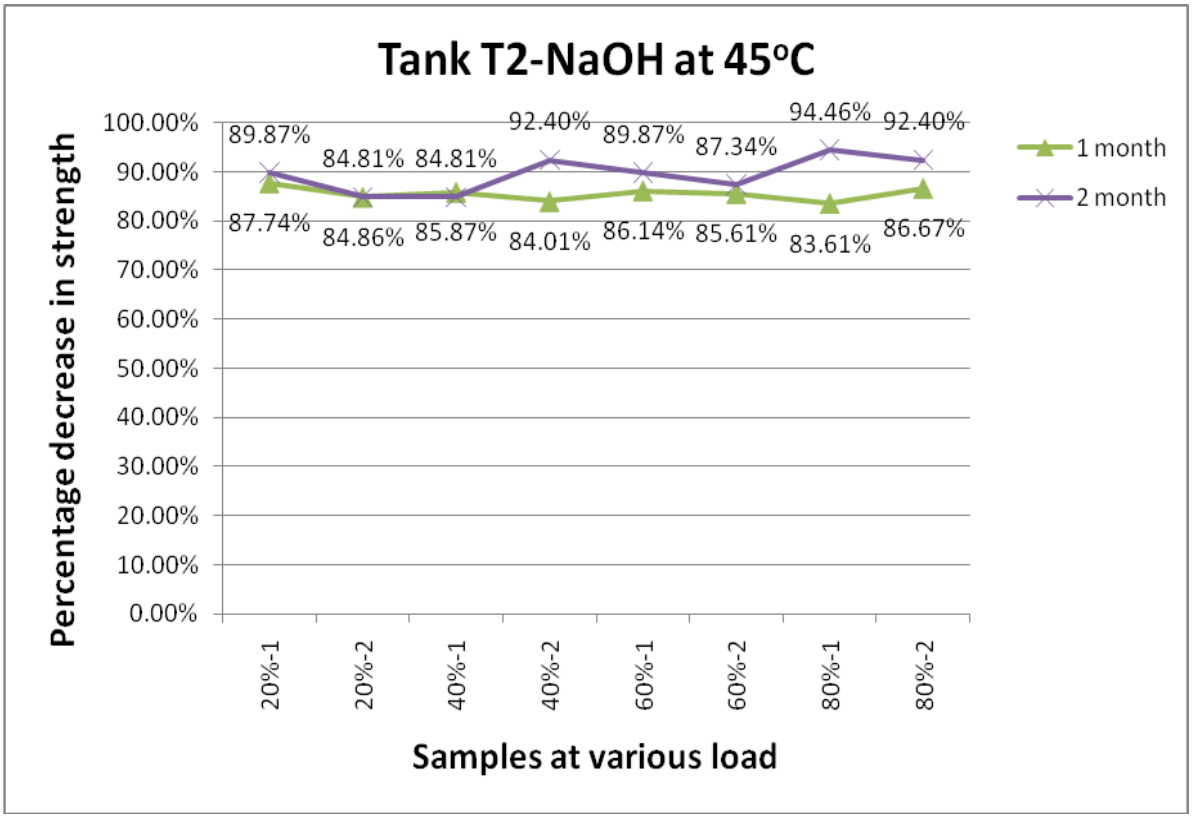

Fig. 6.166 Comparison of percentage decrease in tensile strength with respect to time in Tank T2

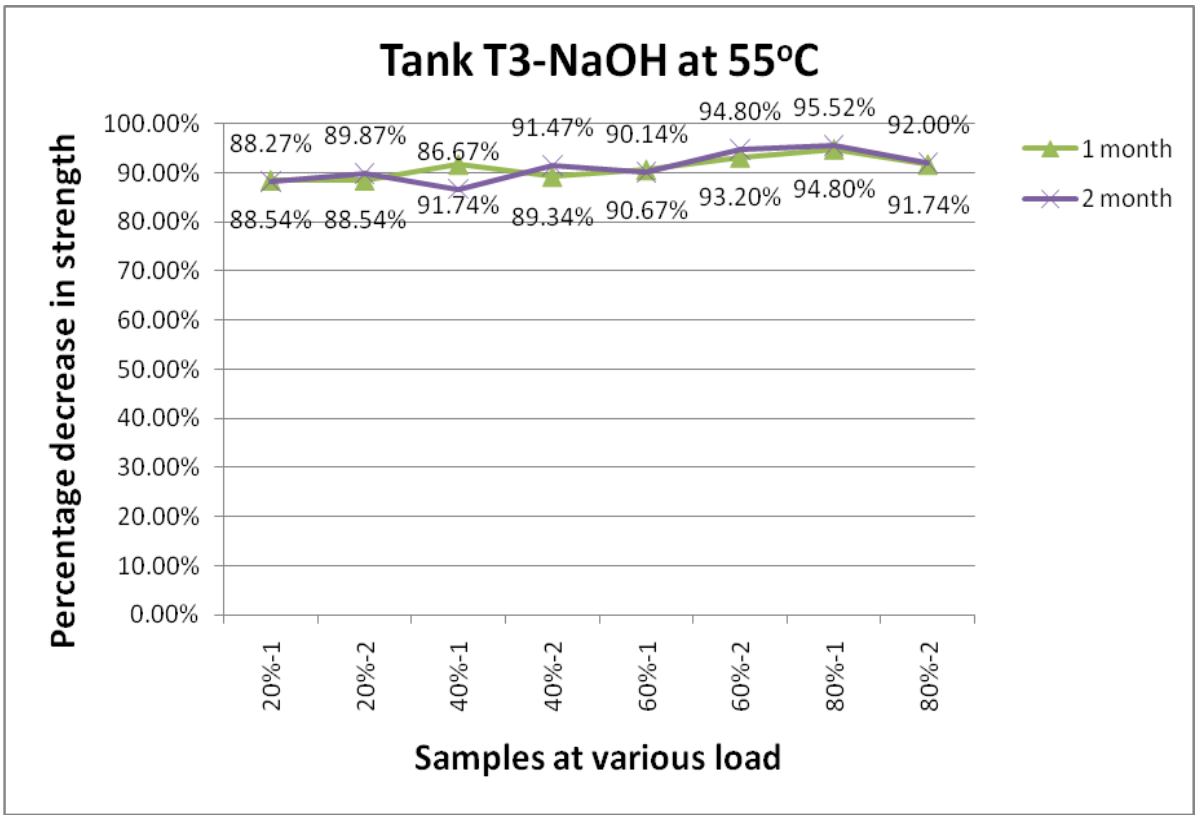

Fig. 6.167 Comparison of percentage decrease in tensile strength with respect to time in Tank T3

The trend of decrease in ultimate tensile strength is shown in Fig.6.164, Fig.6.165, Fig.6.166 and Fig.6.167 above. The tensile strength reduction in two T1 and T4 tanks seems to be nearly same after one and two with few exceptions. But when comparing the reduction in two tanks after one month with respect to reduction in two months there is noticeable change as we can seen that after one month the reduction is ranging from 10 to 25% mainly where as the reduction in two month seems to be between 25 to 45% mainly. Moving on to NaOH tanks there is large decrease in tensile strength ranging from 85 to 90% after one month. The strength seems to further decrease marginally after two months. Further it can also be noticed here that the decrease in ultimate tensile strength has gone up marginally in samples loaded at 80% comparing with other load samples. The effect of temperature change doesn't seem to have much effect on the tensile strength reduction.

The reason for decrease in ultimate tensile strength and change in percentage tensile strength seems to be the continuous degradation done by hygrothermal load which affected the epoxy and fibre strength. Further in NaOH tanks the reason for such large reduction is that epoxy has been subjected to chemical attack as well which had made it brittle and further supporting with SEM which also shows that epoxy has been deboned with fibre.

6.6.2 RESULTS FOR CHANGES IN COMPOSITION (BY EDX):

The comparisons of the elemental composition of all samples (after 1 and 2months) with respect to initial sample are as follows:

Table T16 Composition of samples after 1 and 2 months for water tanks

Tank Detail	Tank Name	% Loading	Time period	Weight Percentage of Elements (%)						
				Si	C	O	Mg	Al	Ca	Ti
Initial Sample				31.1	10.06	28.05	1.14	6.95	18.77	3.93
Water Tank (45°C)	T1	20%	1 month	26.55	15.49	31.31	2.21	5.96	16.64	0.84
			2 month	25.71	11.87	34.22	2.12	6.90	18.17	0.00
		40%	1 month	21.84	35.28	16.85	1.61	4.80	16.14	1.48
			2 month	26.61	9.15	36.96	1.77	5.54	16.97	0.00
		60%	1 month	25.16	26.01	22.24	1.01	5.57	16.96	1.05
			2 month	26.63	8.20	34.83	2.00	10.74	16.60	0.00
		80%	1 month	23.54	26.82	25.31	1.80	5.71	15.06	0.75
			2 month	28.61	6.33	36.57	1.85	6.97	16.67	0.00
Water Tank (55°C)	T4	20%	1 month	19.91	29.49	26.43	0.98	4.40	18.26	0.52
			2 month	30.93	11.74	32.11	1.75	6.40	16.07	0.00
		40%	1 month	8.13	55.41	12.97	0.62	1.53	20.02	1.32
			2 month	32.39	4.95	38.40	2.13	6.99	14.14	0.00
		60%	1 month	13.32	36.05	26.24	0.80	3.54	18.96	1.09
			2 month	34.34	6.88	26.42	1.70	6.11	22.55	0.00
		80%	1 month	18.52	39.68	25.45	1.06	4.44	10.34	0.51
			2 month	33.53	8.70	30.85	1.65	6.29	16.98	0.00

Table T16-1 Composition of samples after 1 and 2 months for NaOH tanks

Tank Detail	Tank Name	% Loading	Time period	Weight Percentage of Elements (%)						
				Si	C	O	Mg	Al	Ca	Ti
Initial Sample				31.10	10.06	28.05	1.14	6.95	18.77	3.93
NaOH Tank (45^{o}C)	T2	20%	1 month	16.72	44.45	19.84	0.75	3.84	12.77	0.63
			2 month	33.66	9.81	29.81	2.28	6.78	16.67	0.00
		40%	1 month	23.55	30.92	20.37	1.27	5.36	16.82	0.71
			2 month	34.04	10.10	26.62	1.80	8.67	16.76	0.00
		60%	1 month	19.90	39.38	22.76	0.90	4.95	11.66	0.45
			2 month	31.33	8.21	28.66	2.52	8.13	21.14	0.00
		80%	1 month	25.16	22.00	31.76	1.36	6.15	13.18	0.40
			2 month	33.75	6.98	30.02	0.65	8.60	18.99	0.00
NaOH Tank (55^{o}C)	T3	20%	1 month	23.18	30.38	26.62	1.15	5.64	12.55	0.49
			2 month	32.66	6.91	29.25	1.51	8.20	20.47	0.00
		40%	1 month	24.07	33.10	18.06	1.71	6.32	15.51	0.23
			2 month	33.92	8.28	28.63	0.57	6.43	21.18	0.00
		60%	1 month	19.58	36.25	26.08	0.96	4.35	11.10	0.68
			2 month	31.78	8.67	32.53	1.59	6.63	16.81	0.00
		80%	1 month	26.61	18.62	30.69	1.28	6.07	15.99	0.74
			2 month	33.45	4.92	30.58	2.58	8.62	19.85	0.00

Graphical comparison of the EDX results for various tanks:

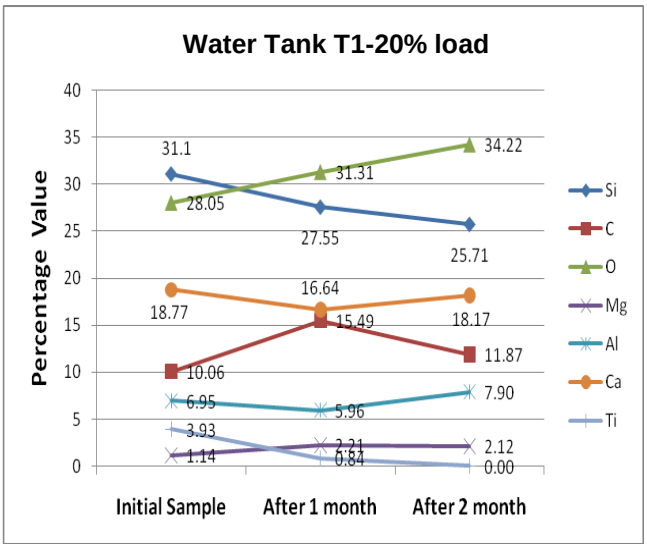

a)

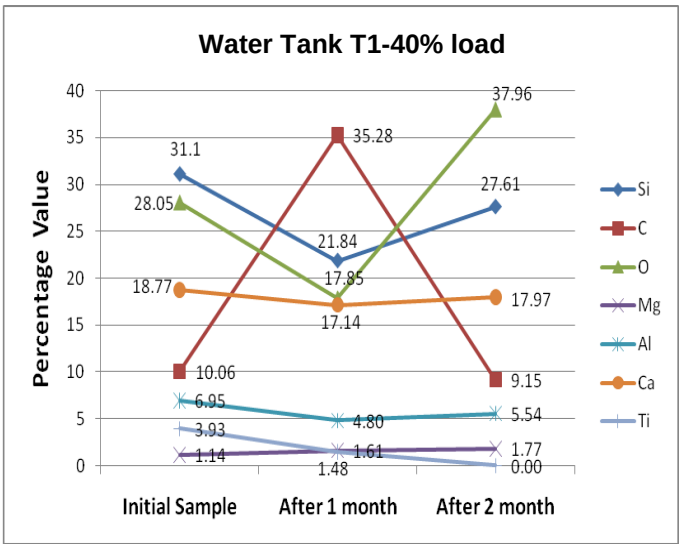

b)

Fig. 6.168 Comparison of composition after 1 and 2 months for T1 tank at (a) 20% (b) 40% load

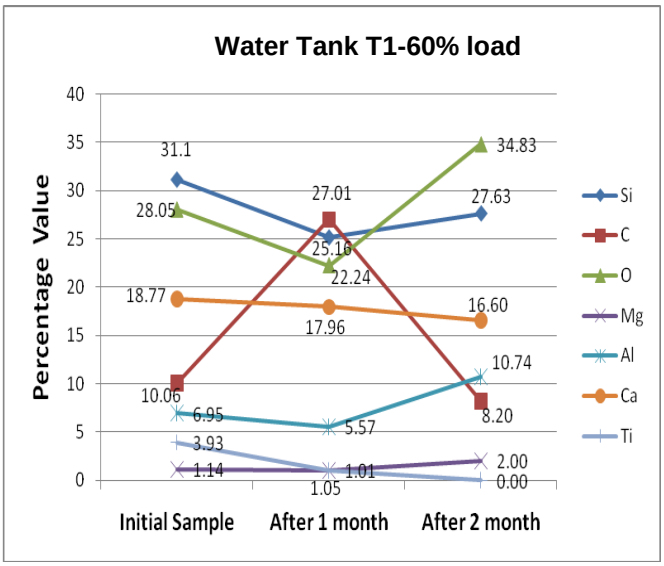

c)

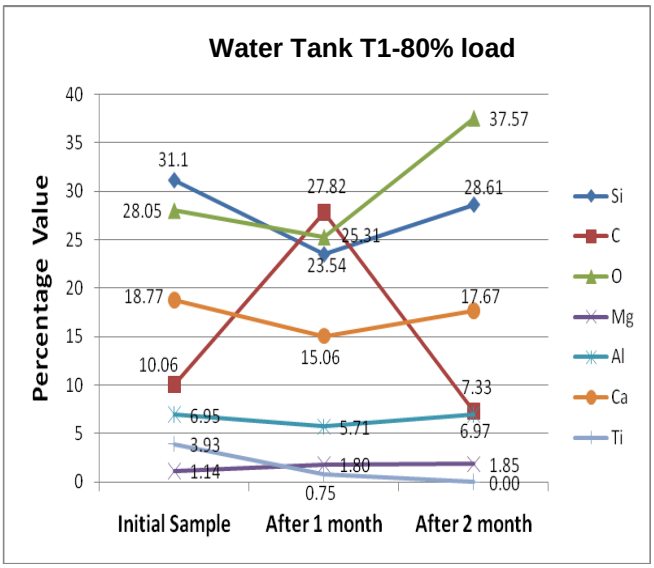

d)

Fig. 6.169 Comparison of composition after 1 and 2 months for T1 tank at (c) 60% (d) 80% load load

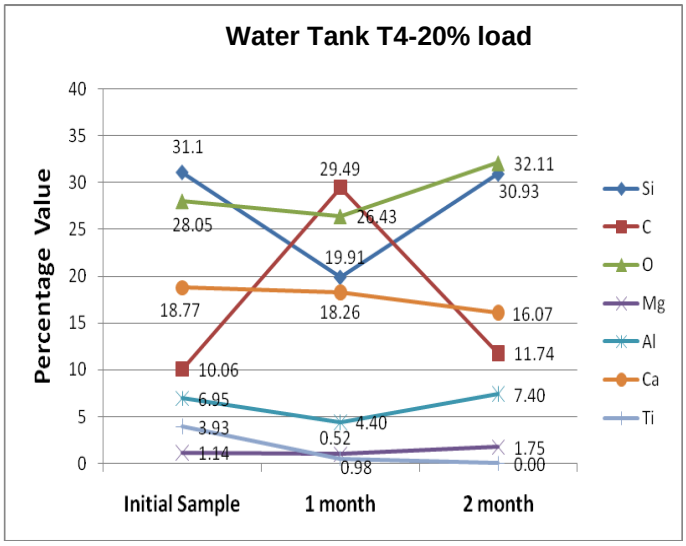

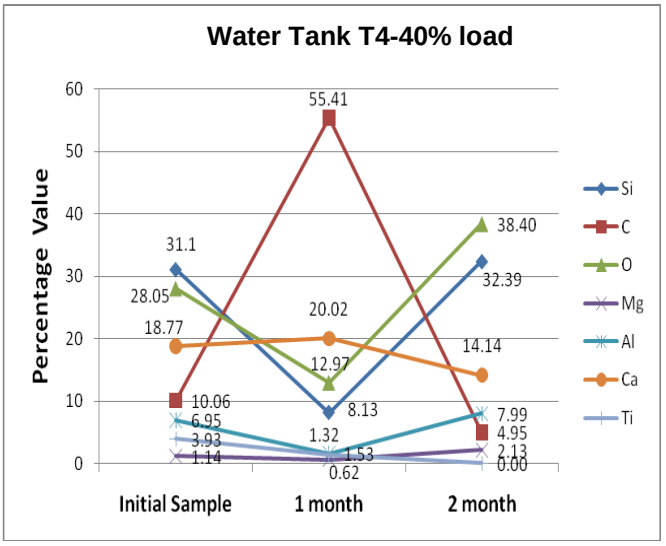

e) f)

Fig. 6.170 Comparison of composition of samples after 1 and 2 months for T4 tank at (e) 20% (f) 40% load

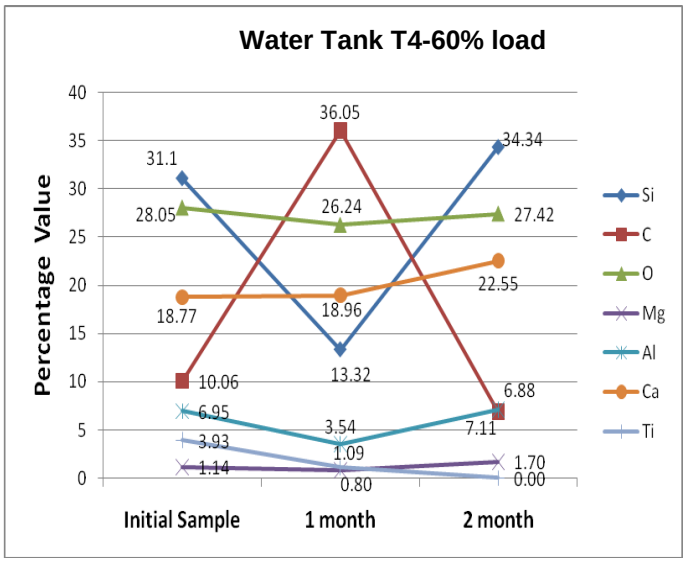

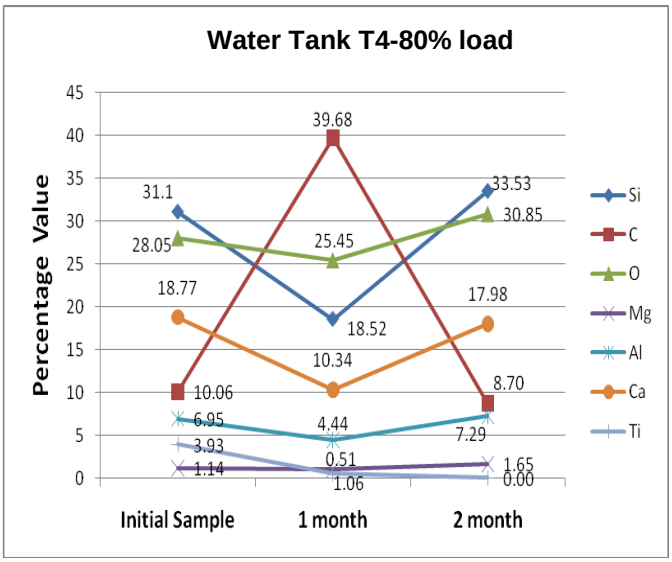

g) h)

Fig. 6.171 Comparison of composition of samples after 1 and 2 months for T4 tank at (g) 60% (h) 80% load

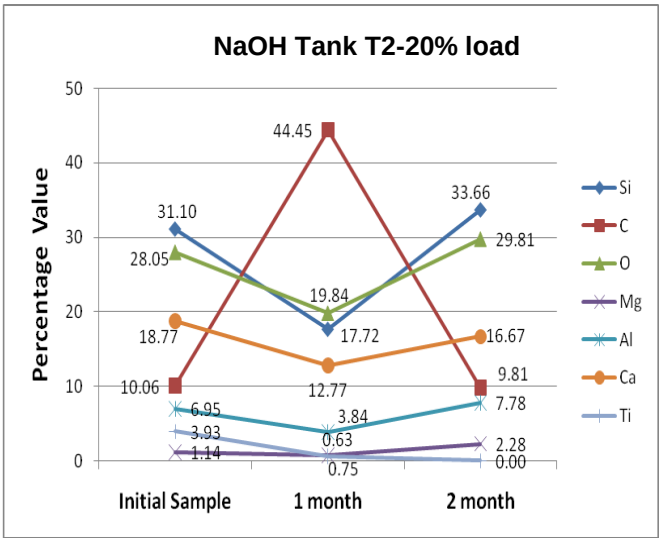

i)

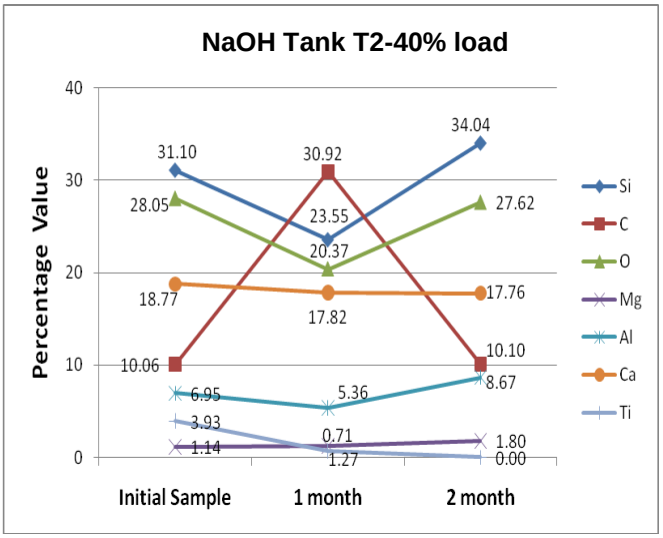

j)

Fig. 6.172 Comparison of composition of samples after 1 and 2 months for T2 tank at (i) 20% (j) 40% load

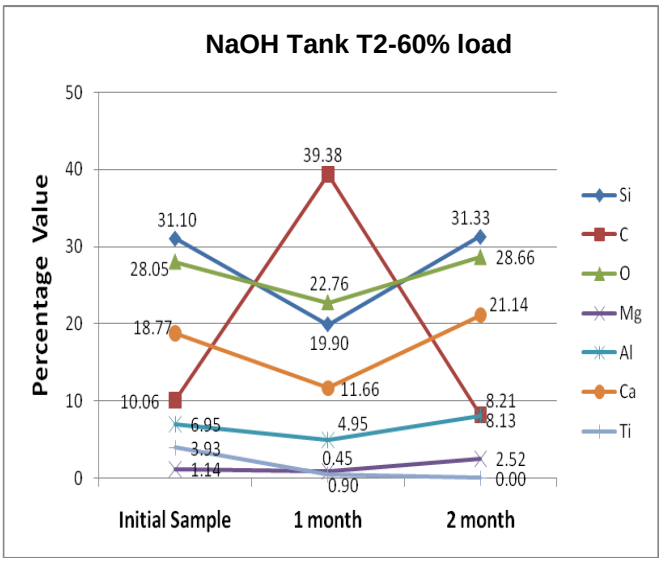

k)

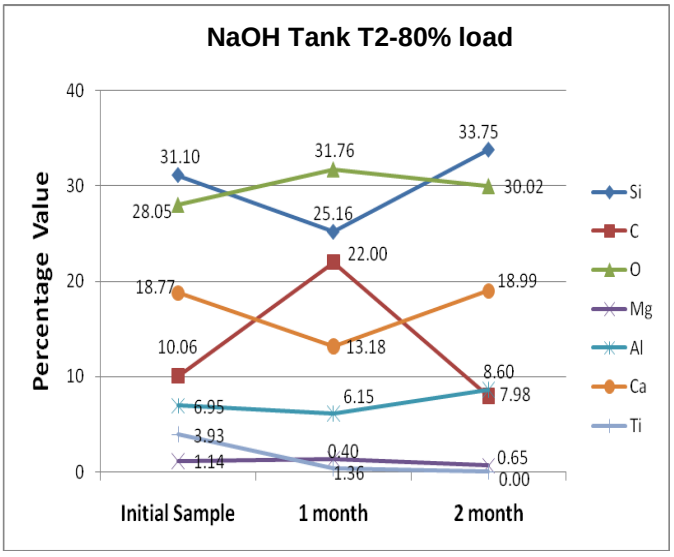

l)

Fig. 6.173 Comparison of composition of samples after 1 and 2 months for T2 tank at (k) 60% (l) 80% load

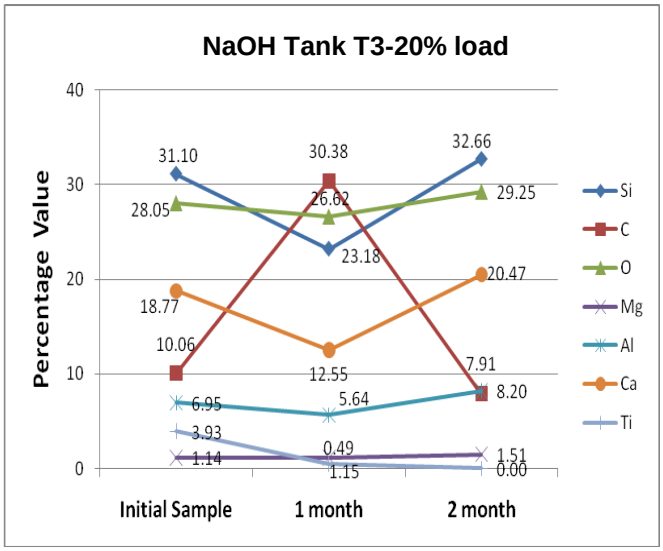

m)

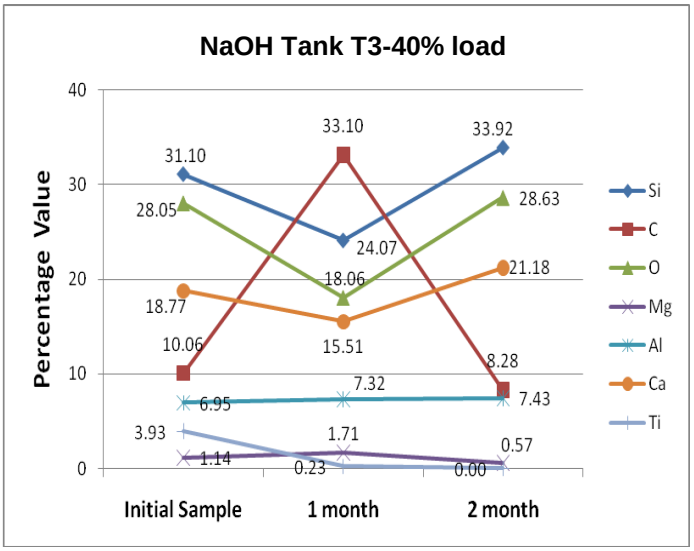

n)

Fig. 6.174 Comparison of composition of samples after 1 and 2 months for T3 tank at (m) 20% (n) 40% load

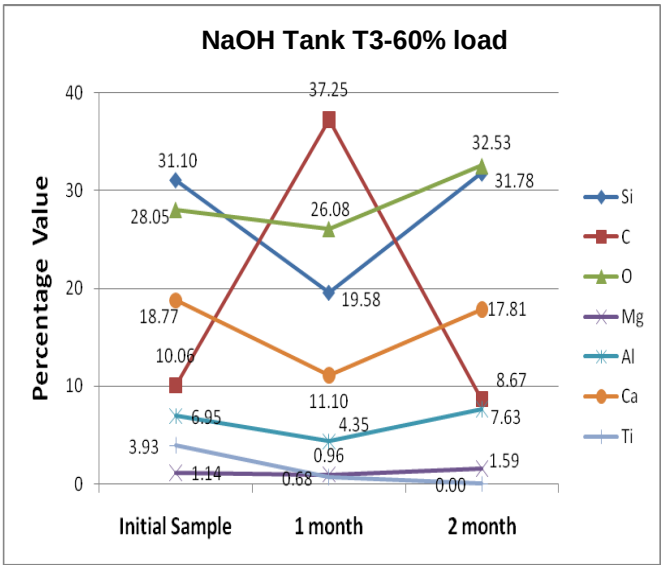

o)

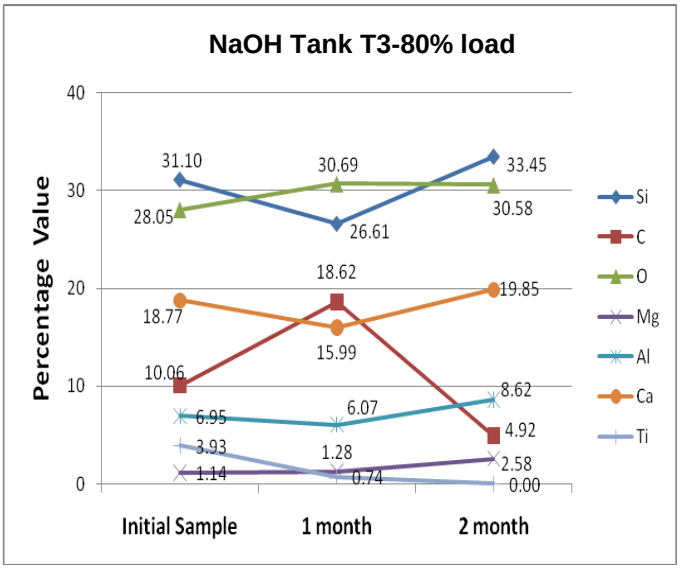

p)

Fig. 6.175 Comparison of composition of samples after 1 and 2 months for T3 tank at (o) 60% (p) 80% load

The compositional change in material is shown in Fig.6.168 to Fig.6.175. The silica content value has marginally decreased after 1 month in T1 tank but in second month it shows a considerable increase in same silica value. This trend seems to be happening with rest of other elements i.e. O, Mg, Al and Ca but the trend in C (carbon) value is increasing in first month and then decreasing in second month. The Ti which is present in first month is lost totally in second month. The T4 tank also shows the same trends as mentioned above. The percentage change is large in silica and carbon both after one and two months. Observing the NaOH tanks the trend here is also in consent with that of water tanks. The carbon is again increasing in first month and then decreasing in other month with increase in rest of the elements.

The carbon content increase in the fibre may be due to the carbon diffusion from the epoxy towards the fibre. The epoxy degradation is evident from the SEM images. In the second month however, further degradation of epoxy is observed with fibre pullout being a common phenomenon. This appears to have decreased the percentage of carbon being observed in the fibre.

6.6.3 AREA FRACTION AND CIRCULARITY RESULTS BY IMAGE ANALYSIS:

The Table T17 shows the percentage area fraction in fibre and epoxy in all tanks with respect to time

Table T17 Comparison of percentage area fraction of fibre and epoxy with respect to time

Tank Name	After 1 month		Initial		After 2 months	
	% Area fraction		% Area fraction		% Area fraction	
	Epoxy	Fibre	Epoxy	Fibre	Epoxy	Fibre
T1-20% load	42.21	57.20	37.886	61.765	46.707	48.187
T1-40% load	43.13	56.11			59.186	40.03
T1-60% load	25.33	74.17			55.063	44.427
T1-80% load	41.90	57.41			49.811	49.863
T2-20% load	43.54	55.60			55.311	40.306
T2-40% load	46.76	52.58			50.372	48.784
T2-60% load	40.49	58.33			72.31	23.278
T2-80% load	42.89	55.98			61.121	36.825
T3-20% load	42.97	54.35			56.37	43.012
T3-40% load	27.57	70.93			45.727	53.752
T3-60% load	20.53	78.37			44.773	54.525
T3-80% load	21.58	71.10			40.471	59.137
T4-20%load	31.71	64.10			57.184	42.203
T4-40% load	41.99	57.32			45.203	54.266
T4-60% load	43.63	55.97			47.641	51.477
T4-80% load	37.36	61.20			50.551	48.771

The Table T18 shows the maximum and minimum diameter of fibre and circularity ratio in tanks with respect to time.

Table T18 Comparison diameter of fibre and circularity ratio with respect to time

Tank Name	1 month			2 month		
	Max Dia of fibre (mm)	Smaller Dia(mm)	Circularity ratio*	Max Dia of fibre (mm)	Smaller Dia (mm)	Circularity ratio*
T1-20%	0.015	0.015	1.000	0.014	0.014	1.000
T1-40%	0.013	0.013	1.000	0.012	0.011	0.917
T1-60%	0.014	0.014	1.000	0.016	0.016	1.000
T1-80%	0.016	0.016	1.000	0.017	0.017	1.000
T2-20%	0.013	0.012	0.923	0.014	0.013	0.929
T2-40%	0.012	0.011	0.917	0.012	0.012	1.000
T2-60%	0.014	0.014	1.000	0.013	0.012	0.923
T2-80%	0.015	0.014	0.933	0.015	0.014	0.933
T3-20%	0.014	0.014	1.000	0.017	0.017	1.000
T3-40%	0.012	0.011	0.917	0.016	0.015	0.938
T3-60%	0.016	0.015	0.938	0.014	0.014	1.000
T3-80%	0.014	0.013	0.929	0.014	0.014	1.000
T4-20%	0.015	0.015	1.000	0.013	0.013	1.000
T4-40%	0.013	0.013	1.000	0.014	0.014	1.000
T4-60%	0.014	0.014	1.000	0.013	0.011	0.846
T4-80%	0.012	0.012	1.000	0.014	0.014	1.000

*Circularity ratio = $\frac{\text{Minimum fibre diameter}}{\text{Maximum fibre diameter}}$

The graphical comparison of the results obtained from the analysis of the above images:

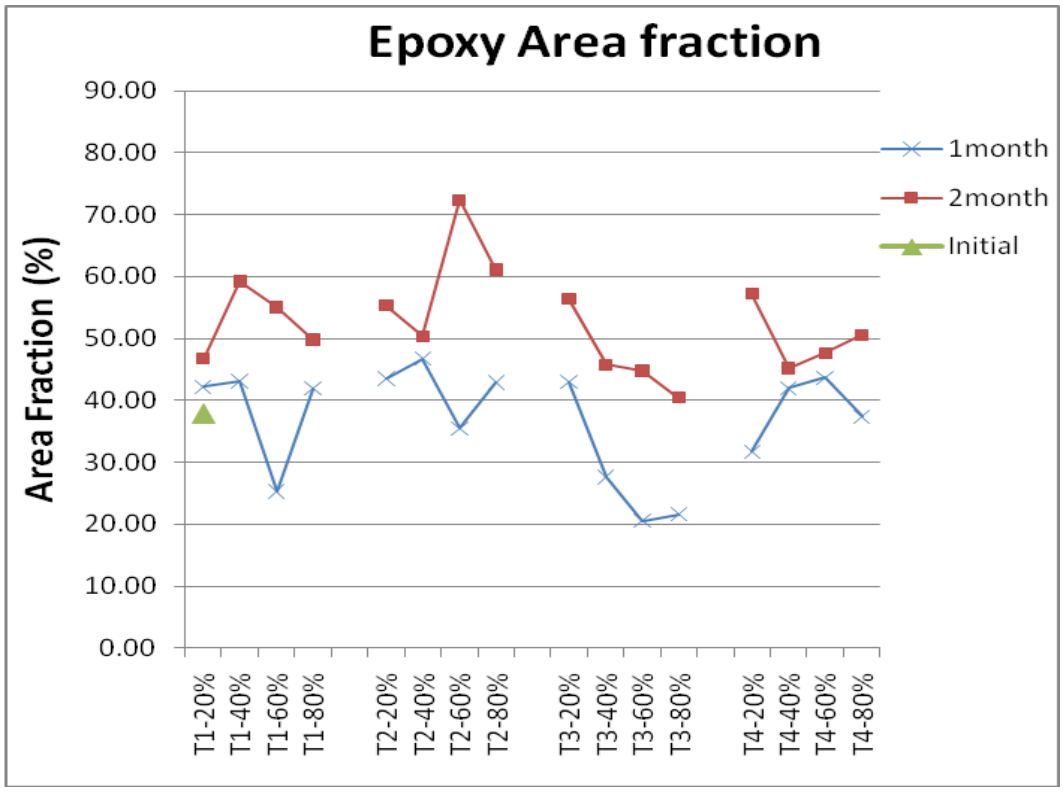

Fig.6.176 Comparison of Epoxy area fraction with respect to time

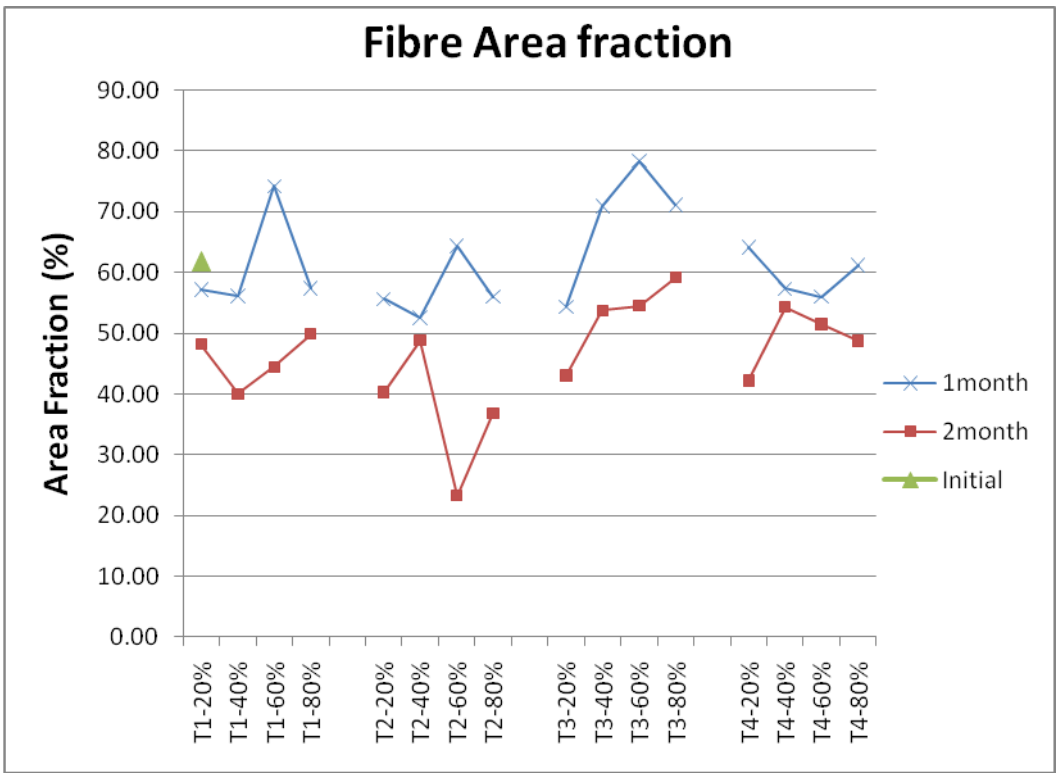

Fig.6.177 Comparison of Fibre area fraction with respect to time

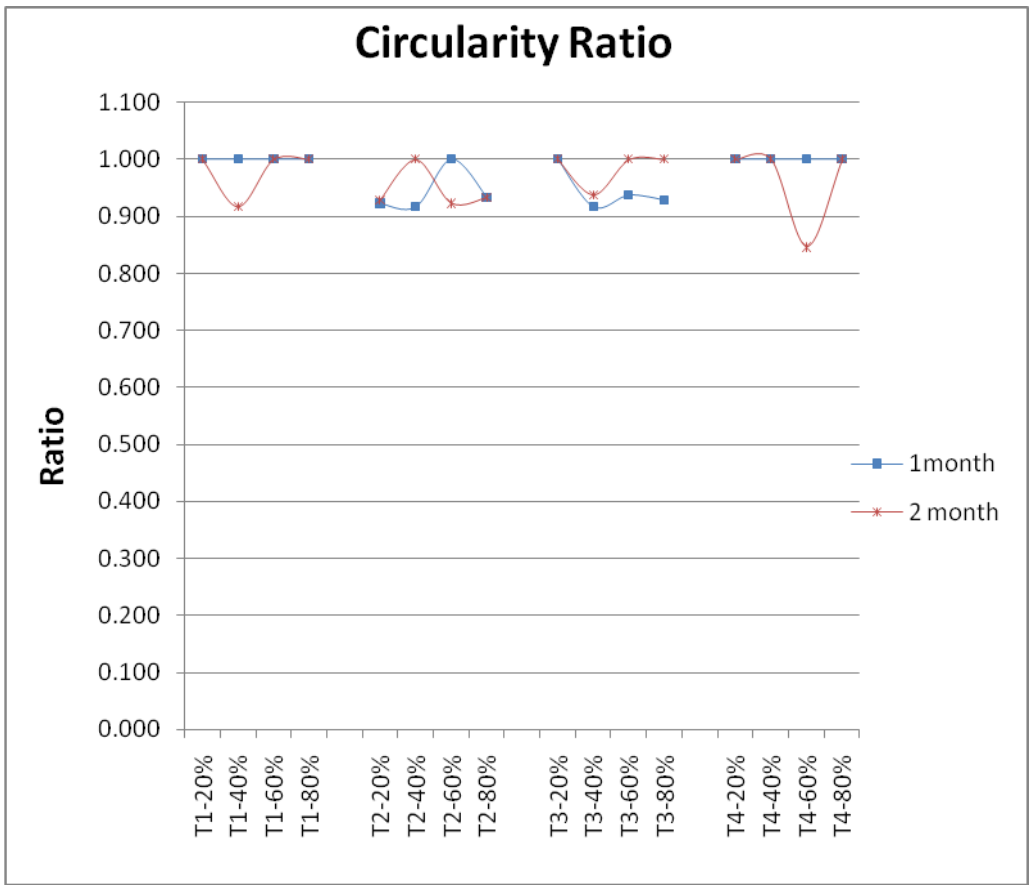

Fig.6.178 Comparison of Circularity Ratio with respect to time

The area fraction of samples is compared in Fig.6.176 for epoxy and Fig.6.177 for fibres. From comparison of epoxy fractions it is clearly seen that it is increasing with time as there is considerable increase after two month compared to one month. But the trend is seen to be opposite in fibre fraction comparison. Here the fibre fraction is increasing in first month and decreased in second month. All the samples loaded at different value shows the same trend when compared between one and two month. The samples in NaOH tanks have shown more increase in epoxy area fraction after two months compared to one month and similarly more decrease in fibre fraction when comparing to that of water tanks.

The reason for such a trend seems to be that fibre in total area is degrading with heat and moisture attack and epoxy seems to have expanded with above effect which obviously leaves more area for epoxy as compared to fibre. In NaOH tank as seen in SEM images the fibre is also been eaten up at periphery which further supports more loss of fibre leaving more area for epoxy in the composite cross section.

The Circularity ratio (Fig.6.178) values seems to have gone downwards from a ratio of 1.0 especially in NaOH tanks, with more downwards trend with increasing time. The reason for such a trend is eating up of fibre by the NaOH attack leading to change in shape with most damage on outer circumference of fibres.

6.6.4 RESULTS OF PERCENTAGE WEIGHT GAIN BY SAMPLES:

The following tables T19, T19-1 shows the details of the percentage weight gain in samples with respect to time at each loading percentage:

Table T19 Percentage weight gain in samples of Water Tank T1 and T4

Sample No	% Loading of U.T.L.	Initial Weight (gms)	Weight after 1 month (gms)	Weight Difference (gms)	% weight gain (1month)	Weight after 2 months (gms)	Weight Difference (gms)	% weight gain* (2month)
Tank T1								
1	20%	28.214	28.687	0.473	1.7%	-		
2	20%	29.967	30.489	0.522	1.7%	-		
3	20%	28.023	-			28.994	0.971	3.5%
4	20%	27.545	-			28.860	1.315	4.8%
1	40%	29.345	29.867	0.522	1.8%	-		
2	40%	25.987	26.410	0.423	1.6%	-		
3	40%	28.102	-			29.406	1.304	4.6%
4	40%	26.134	-			27.440	1.306	5.0%
1	60%	27.034	27.467	0.433	1.6%	-		
2	60%	28.960	29.498	0.538	1.9%	-		
3	60%	28.457	-			29.847	1.390	4.9%
4	60%	28.450	-			29.976	1.526	5.4%
1	80%	29.387	30.123	0.736	2.5%	-		
2	80%	30.389	31.005	0.616	2.0%	-		
3	80%	25.234	-			26.584	1.350	5.3%
4	80%	31.476	-			32.860	1.384	4.4%
Tank T4								
1	20%	30.387	30.897	0.510	1.7%	-		
2	20%	26.554	27.256	0.702	2.6%	-		
3	20%	28.789	-			29.872	1.083	3.8%
4	20%	31.123	-			32.317	1.194	3.8%
1	40%	28.554	29.113	0.559	2.0%	-		
2	40%	30.123	30.887	0.764	2.5%	-		
3	40%	31.002	-			32.642	1.640	5.3%
4	40%	28.145	-			29.821	1.676	6.0%
1	60%	29.143	29.564	0.421	1.4%	-		
2	60%	29.354	29.987	0.633	2.2%	-		
3	60%	29.562	-			30.589	1.027	3.5%
4	60%	28.281	-			29.583	1.302	4.6%
1	80%	30.456	31.123	0.667	2.2%	-		
2	80%	29.245	29.689	0.444	1.5%	-		
3	80%	29.231	-			30.698	1.467	5.0%
4	80%	29.502	-			30.798	1.296	4.4%

Table T19-1 Percentage weight gain in samples of NaOH Tank T2 and T3

Sample No.	% Loading of U.T.L.	Initial Weight (gms)	Weight after 1 month (gms)	Weight Difference (gms)	Weight addition (of fibre) gms	New weight difference (gms)	% weight gain* (1month)
Tank T2							
1	20%	27.878	28.342	0.464	1.010	1.474	5.3%
2	20%	32.456	32.876	0.420	1.010	1.430	4.4%
1	40%	28.234	28.618	0.384	1.468	1.852	6.6%
2	40%	30.189	30.545	0.356	1.468	1.824	6.0%
1	60%	26.456	26.950	0.494	1.583	2.077	7.8%
2	60%	26.344	26.887	0.543	1.583	2.126	8.1%
1	80%	25.510	25.921	0.411	1.823	2.234	8.8%
2	80%	24.693	25.005	0.312	1.823	2.135	8.6%
Tank T3							
1	20%	30.245	30.587	0.342	1.645	1.987	6.6%
2	20%	31.706	32.100	0.394	1.645	2.039	6.4%
1	40%	26.598	26.967	0.369	2.001	2.370	8.9%
2	40%	27.559	27.987	0.428	2.001	2.429	8.8%
1	60%	27.464	28.007	0.543	1.912	2.455	8.9%
2	60%	28.688	29.124	0.436	1.912	2.348	8.2%
1	80%	29.354	29.658	0.304	2.115	2.419	8.2%
2	80%	30.867	31.454	0.587	2.115	2.702	8.8%
Sample No.	**% Loading of U.T.L.**	**Initial Weight (gms)**	**Weight after 2 months (gms)**	**Weight Difference (gms)**	**Weight addition (of fibre) gms**	**New weight difference (gms)**	**% weight gain* (2 month)**
Tank T2							
3	20%	25.124	25.862	0.738	2.294	3.032	12.1%
4	20%	29.187	29.889	0.702	2.294	2.996	10.3%
3	40%	31.987	32.614	0.627	3.125	3.752	11.7%
4	40%	25.188	25.724	0.536	3.125	3.661	14.5%
3	60%	29.965	30.598	0.633	3.824	4.457	14.9%
4	60%	26.943	27.502	0.559	3.824	4.383	16.3%
3	80%	25.187	25.892	0.705	3.815	4.520	17.9%
4	80%	25.486	26.105	0.619	3.815	4.434	17.4%
Tank T3							
3	20%	27.015	27.740	0.725	3.340	4.065	15.0%
4	20%	27.956	28.810	0.854	3.340	4.194	15.0%
3	40%	29.043	29.936	0.893	3.988	4.881	16.8%
4	40%	30.987	31.901	0.914	3.988	4.902	15.8%
3	60%	26.005	26.982	0.977	3.977	4.954	19.0%
4	60%	32.998	33.781	0.783	3.977	4.760	14.4%
3	80%	26.566	27.484	0.918	4.012	4.930	18.6%
4	80%	29.488	30.951	1.463	4.012	5.475	18.6%

* The time variation of percentage weight gain (w_t) can be measured as:

$$w_t = \frac{W(t) - W_0}{W_0} \times 100$$

Here $W(t)$ is the total weight after time t

W_0 is the reference dry weight of the specimen before immersion in medium.

The graphical comparisons of the percentage weight gain by various samples are:

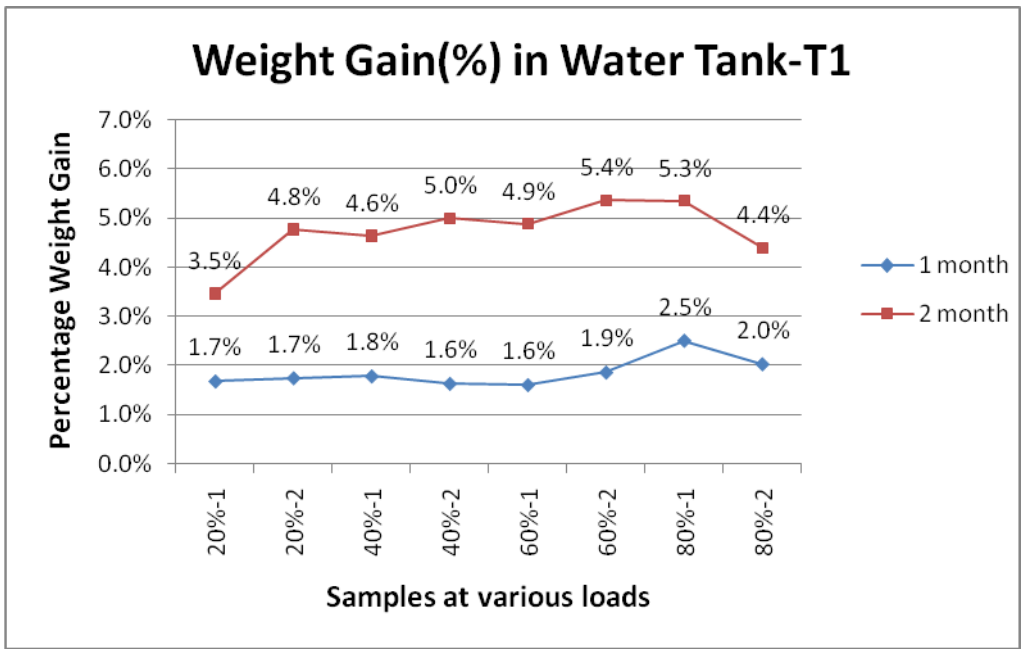

Fig. 6.179 Comparison of percentage weight gain in tank T1 with respect to time at various loads

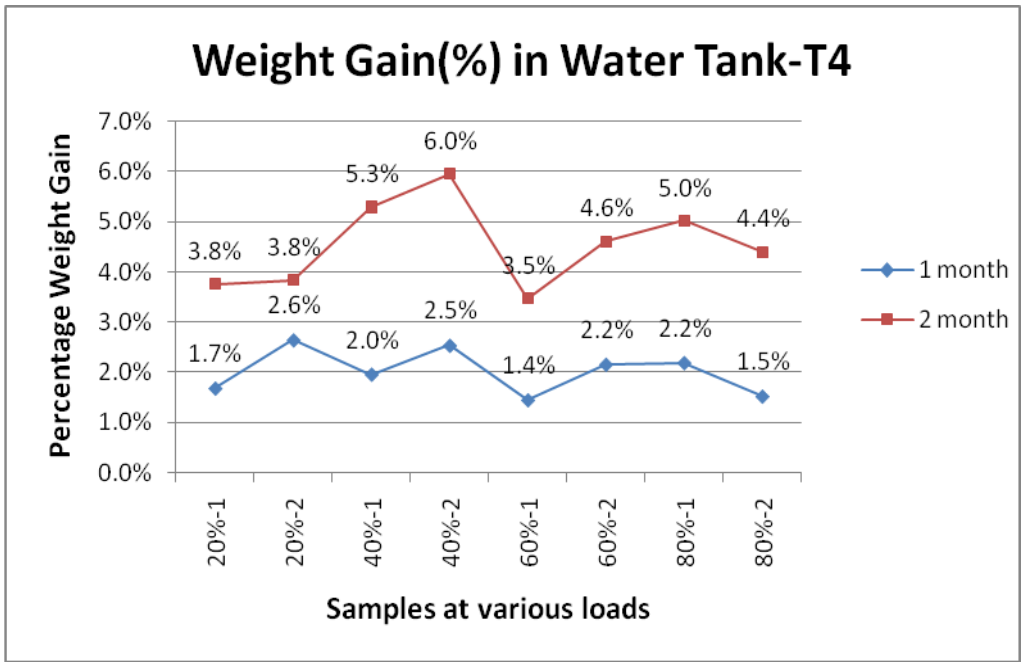

Fig. 6.180 Comparison of percentage weight gain in tank T4 with respect to time at various loads

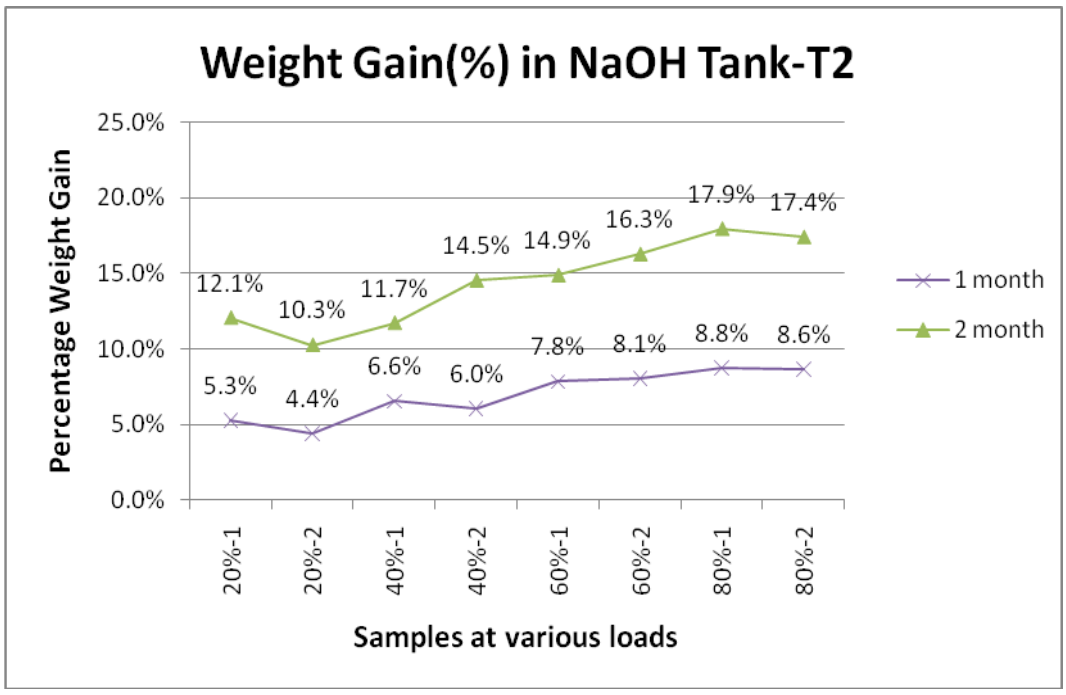

Fig. 6.181 Comparison of percentage weight gain in tank T2 with respect to time at various loads

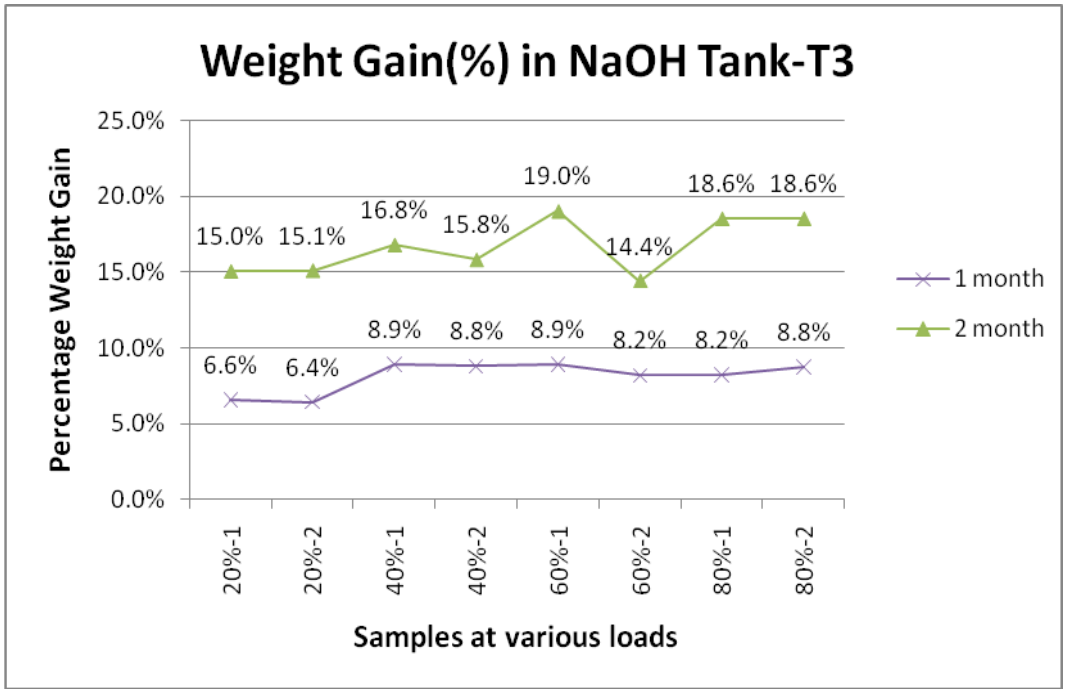

Fig. 6.182 Comparison of percentage weight gain in tank T3 with respect to time at various loads

The percentage weight gain (of moisture) was compared for various tanks in Fig.6.179 to Fig.6.182. It could be easily noticed that in water tanks the percentage weight gain is increasing with respect to time indicating that more moisture is absorbed after two months comparing to first month in almost all the samples with few exceptions. There was marginal increase in weight gain of samples at 55^{o}C temperature (see Fig.6.180) as compared to samples at 45^{o}C (Fig.6.179).In case of NaOH tanks the percentage weight gain was also higher in second month and also it was higher with respect to water tanks in both the months. The average weight gain in water tank was 4.73% and 4.54% in Tank T1 and T4 respectively. But in NaOH tanks average values were 14.38% and 16.67% in Tank T2 and T3 respectively.

The reason for increase in percentage weight gain is obvious in both tanks as with time the pores of epoxy will loosen due to given hygrothermal load giving way to moisture. But in case of NaOH tanks the weight gain was higher due to chemical attack on the fibre periphery as seen in SEM images, creating more voids to hold moisture.

CHAPTER 7 CLOSURE

7.1 CONCLUSION:

From the experiment conducted following conclusions have been obtained:

1) The reduction in tensile strength is considerably large (about 85 to 90%) in the almost all the samples immersed in the aqueous NaOH tank as compared to the initial samples tensile strength. This trend of reduction is on higher side in samples loaded at 60% and 80% of U.T.L. While there is marginal reduction in the strength of the samples immersed in water as compared to initial samples. The trend of reduction in water bath is as per expectation, which shows 10-20% reduction in first month and 30-40% reduction in second month. The SEM images also backup these results showing damage done to fibre especially in samples immersed in aqueous NaOH.

2) To further investigate the reason for reduction in strength a compositional change is taken into consideration by performing E.D.X. on damaged samples. The trend shows a decrease in almost all the elements like Silica, Oxygen, Magnesium, Aluminium and Calcium with exception in carbon percentage which has gone up considerably in first month in all the samples under study comparing to initial values.

In second month the trend has been totally reversed to that of first month showing an upward trend in all the elements mentioned earlier and with decrease in carbon percentage by about 20%.

3) The area fraction of the fibre and epoxy are analysed using image analysis. The results showed an increase in area fraction of the epoxy with increasing time showing a marked increase in second month in all the sample of both water and aqueous NaOH tank. Similarly the result of fibre area fraction shows a decreasing trend with time with marked decrease in second month. This indicates that epoxy is expanding covering more area with fibre degradation and pullout leading to decrease in fibre in same area.

4) The change in circularity ratio is seen more pronounced in the fibres of samples immersed in aqueous NaOH which can be noticed easily in SEM image of samples. The chemical attack on periphery of fibres by NaOH leads to change in shape. Thus change in circularity ratio is evident in case of aqueous NaOH samples but some samples immersed in water tank had also shown chipping of an edge completely with rest of periphery in quite a circular shape.

5) The percentage weight gain showed an increasing trend with time as expected both in samples immersed in water and aqueous NaOH tank. The weight gain is slightly more in samples at 55^{o}C compared to samples at 45^{o}C. But the trend in aqueous NaOH tank showed a larger weight gain than that in the water tank.

7.2 SCOPE OF FUTURE WORK:

1) The composite material with induced crack can be taken to study the effect of pre-damaged composite materials.

2) The duration of current experiment can be increased to see the effect in long term.

3) There is lot of scope of improvement in finite element modelling to simulate the results with more accuracy and study effect of various parameters with respect to time.

4) The strength of alkaline aqueous solution can be varied to see the change in chemical attack on composite.

5) By changing the fibre orientation and number of plies we can compare the change in results with respect to current experimentation.

REFERENCES

[1] www.whitebuffalobeadsandstones.com & www.ia.ucsb.edu

[2] www.wikipedia.com/Composite material.html

[3] www.structsource.com/pdf/composite.pdf

[4] www.emba.uvm.edu/iatridis/me257/Introduction.html

[5] www.engr.sjsu.edu/sgleixner/PRIME/FRP.pdf

[6] www.autospeed.com/composites.html

[7]ww.engineer.tamuk.edu/departments/ieen/faculty/DrLPeel/Courses/Meen3344/Powerpoint_Files/ Chapter_16_avi.ppt

[8] American Institute of Aeronautics and Astronautics- Effects of Glass Fabric and Laminate Construction on the Fatigue of Resin Infused Blade Materials by Daniel D. Samborsky and John F. Mandell

[9] A.Mukherjee, S.J. Arwikar (ACI Structural Journal) Title No. 102-S82 [2006]-Performance of externally bonded GFRP sheets on concrete in tropical environments Part II: Micro structural tests.

[10] The University of Oklahoma-Design of composite-material plates for maximum uniaxial compressive buckling load by Timothy L.Chen and Charles W. Bert

[11] www.basf-cc.co.in

[12] www.asme.org- Modelling the Transport of Low-Molecular-Weight penetrates within Polymer Matrix Composites (David A. Bond, Paul A. Smith)

[13] A.Mukherjee, S.J. Arwikar (ACI Structural Journal) Title No. 102-S76 [2006]-Performance of externally bonded GFRP sheets on concrete in tropical environments Part I: Structural scale tests.

[14] Abhijit Mukherjee and S. J. Arwikar [2007]-Performance of Glass Fibre-Reinforced Polymer Reinforcing Bars in Tropical Environments-Part I: Structural Scale Tests.

[15] Abhijit Mukherjee and S. J. Arwikar [2007]-Performance of Glass Fibre-Reinforced Polymer Reinforcing Bars in Tropical Environments-Part II: Micro structural Tests.

[16] Pavankiran Vaddadi, Raman P. Singh [2003]-Transient hygrothermal stresses in fibre reinforced composites a heterogeneous characterization approach.

[17] Pavankiran Vaddadi, Raman P. Singh [2002]-Inverse analysis for transient moisture diffusion through fibre-reinforced composites.

[18] Samit Roy , Kenneth M. Liechti [2005]-Characterization and modelling of strain assisted diffusion in an epoxy adhesive layer.

[19] Pavankiran Vaddadi , Raman P. Singh [2007]-Interlaminar fatigue crack growth of cross-ply composites under thermal cycles.

[20] E. Ahci , R. Talreja [2006]-Characterization of viscoelasticity and damage in high temperature polymer matrix composites.

[21] Zheng-Ming Huang [2000]-Simulation of the mechanical properties of fibrous composites by the bridging micromechanics model.

[22] Ashcroft, I. A., Abdel Wahab, M. M., and Crocombe, A. D. [2003]-Predicting degradation in bonded composite joints using a semi-coupled finite element method.

[23] Asp, L. E. [1997]-The effects of moisture and temperature on the interlaminar delamination toughness of a carbon/ epoxy composite.

[24] V.Alvarez & A.Vazquez [2005]-Effect of Hygrothermal History on Water and Mechanical Properties of Glass/Vinylester Composites**.**

[25] Benkhedda, A., Tounsi, A., and Adda bedia, E. A. [2007]-Effect of temperature and humidity on transient hygrothermal stresses during moisture desorption in laminated composite plates.

[26] Botelho, E. C., Pardini, L. C., and Rezende, M. C. [2006]-Hygrothermal effects on the shear properties of carbon fibre/epoxy composites.

[27] Leon L. Mishnaevsky Jr and Siegfried Schmauder [2001]-Continuum mesomechanical finite element modelling in materials development.

[28] Leon L. Mishnaevsky Jr. [2004]-Three-dimensional numerical testing of microstructures of particle reinforced composites.

[29] Leon Mishnaevsky Jr. and Povl Brøndsted [2007]-Micromechanisms of damage in unidirectional fibre reinforced composites with ductile matrix: computational analysis.

[30] www.selecindia.com/products.php?category=30

[31]www.ab.com/industrialcontrols/products/relays_timers_and_temp_controllers/solid-state_relays.html

[32] Abaqus User Manual-Getting started with Abaqus-Chapter3-Page3-4

[33] Fibre Reinforced Composites (Materials, manufacturing and design), third edition- by PK Mallick, Publisher- CRC Press